



**IAN JORDAAN  
AND ASSOCIATES**

# **Investigation of Molikpaq 1986 Ice Loading Events & Evaluation of Load Measuring Devices**

## **FINAL REPORT: APPENDICES**

### **Submitted to:**

**Canadian Hydraulics Centre  
National Research Council of  
Canada  
Ottawa, ON  
Canada K1A 0R6**

### **By:**

**Ian Jordaan and Associates  
Inc.  
7 East Middle Battery Road  
St. John's, NL  
Canada A1A 1A3**

**January 14, 2010**

## **Contents of Appendix**

<b>Item</b>	<b>Page Number</b>
<b>Appendix IJA – A:</b> Practical Formulation of Design Load Calculation	2
<b>Appendix IJA – B:</b> Analysis of Subevents as Defined by Brian Wright	5
<b>Appendix IJA – C:</b> Preliminary Geotechnical Overview of 1986 Molikpaq Response (C-CORE)	156
<b>Appendix IJA – C:</b> C-CORE Technical Memorandum	242
<b>Appendix IJA – D:</b> Response to C-CORE Report “Preliminary Geotechnical Overview of 1986 Molikpaq Response” by Kevin Hewitt	248

## **Appendix IJA - A**

### **Practical Formulation of Design Load Calculation**

Submitted by Ian Jordaan

## **Values of Parameters for Probabilistic Model**

In previous work, results from the Molikpaq experience were proposed for use in design (IJA C-CORE internal work). This should be considered in conjunction with Figure 1-1. The table below shows a result that has been proposed for preliminary design. The values have been corrected for panels that were found to not register load and for ice thickness that extends below the lower panels. Each ice event (impact) in Figure 1-1 will have a different mean and standard deviation, sampled from distributions derived from the values below.

The work introduced the concept of probabilistic averaging. In essence, random variations in pressure occur across the face of the structure and the total global load is the sum (integral) of these pressures. Since the Medof and strain gauge sensors provide estimates of loads only on a certain fraction of the total area (about 10%), there will be much more statistical variation over these small areas than over the entire structure face. The technique of probabilistic averaging corrects for this effect by estimating the standard deviation of global loads rather than using the value obtained from the local (10%) area covered by the panels.

**Table: Inputs for Pressure Distribution Proposed for Preliminary Analysis based on Molikpaq Data**

Event Date Event Number	Average Pressure over Panels* <sup>1</sup> (MPa)			PA Std* <sup>1</sup>
	Mean	Std	PA Std* <sup>1</sup>	
7 Jan 1986	1	0.119	0.050	0.034
6 Feb 1986	2	0.239	0.165	0.095
7 Feb 1986	3	0.260	0.174	0.089
7 Feb 1986	4	0.398	0.137	0.093
8 Feb 1986	5	0.312	0.235	0.121
8 Feb 1986	6	0.224	0.141	0.073
17 Feb 1986	7	0.397	0.109	0.074
28 Feb 1986	8	0.413	0.214	0.146
22 May 1986	9	0.269	0.099	0.067
22 May 1986	10	0.249	0.162	0.110
2 Jun 1986	11	0.458	0.177	0.079
2 Jun 1986	12	0.323	0.124	0.064
10 Nov 1985	13	0.170	0.139	0.062
27 Nov 1985	14	0.251	0.133	0.068
16 Dec 1985	15	0.291	0.163	0.084
12 May 1986	16	0.355	0.158	0.107
7 Mar 1986	17	0.201	0.094	0.048
7 Mar 1986	18	0.126	0.087	0.045
8 Mar 1986	19	0.142	0.149	0.077
8 Mar 1986	20	0.429	0.145	0.075
8 Mar 1986	21	0.044	0.020	0.009
8 Mar 1986	22	0.107	0.010	0.005
25 Mar 1986	23	0.185	0.092	0.063
12 Apr 1986	24	0.207	0.182	0.081
12 Apr 1986	25	0.315	0.184	0.082
12 Apr 1986	26	0.227	0.096	0.043
	Mean	0.257	0.132	0.073
	Std	0.108	0.054	0.031

<sup>1</sup> Pressure-averaged standard deviation

## **Appendix IJA - B**

### **Analysis of Sub Events as Defined by Brian Wright**

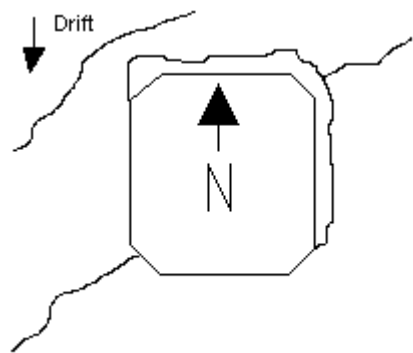
Submitted by Ian Jordaan & Associates Inc.

## Table of Contents

<b>March 25, 1986 – f603251302.....</b>	<b>7</b>
<b>April 12 – f604121101 .....</b>	<b>14</b>
Event ID – 14 - 1.....	21
Event ID – 14 - 3.....	24
<b>April 12 – f604121201 .....</b>	<b>27</b>
Event ID – 15 - A - 1 .....	34
Event ID – 15 - A - 2 .....	37
Event ID – 15 - A - 3 .....	40
Event ID – 15 - A - 4 .....	43
Event ID – 15 - A - 5 .....	46
Event ID – 15 - A - 6 .....	49
Event ID – 15 - A - 8 .....	52
<b>April 12 – f60412140A .....</b>	<b>55</b>
Event ID – 15 - B - 1.....	62
<b>May 12 – f605120301 .....</b>	<b>65</b>
Event ID – 16 - 2.....	73
Event ID – 16 - 4.....	76
Event ID – 16 - 5.....	79
<b>May 22 – f605220801 .....</b>	<b>82</b>
Event ID – 17 - 1.....	89
Event ID – 17 - 3.....	92
<b>May 22 – f605221301 .....</b>	<b>95</b>
Event ID – 18 – 1 .....	102
Event ID – 18 – 2 .....	105
Event ID – 18 – 4 .....	108
Event ID – 18 – 5 .....	111
Event ID – 18 – 6 .....	114
<b>June 2 – f606021301 .....</b>	<b>117</b>
Event ID – 19 – 1 .....	124
Event ID – 19 – 2 .....	127
Event ID – 19 – 4 .....	130
Event ID – 19 – 5 .....	133
Event ID – 19 – 7 .....	136
Event ID – 19 – 8 .....	139
<b>June 2 – f606022201 .....</b>	<b>142</b>
Event ID – 20 – 1 .....	149
Event ID – 20 – 2 .....	152



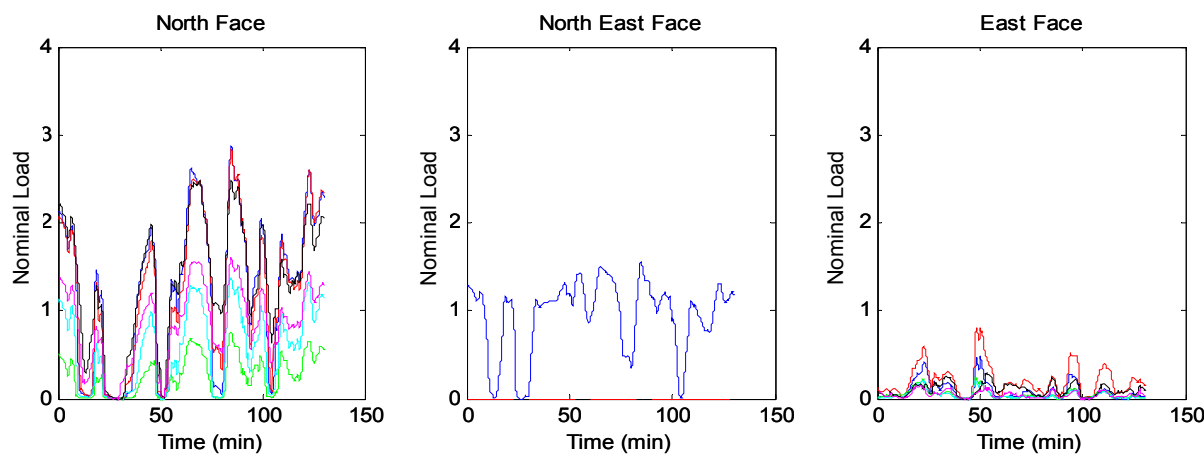
**MARCH 25, 1986 – F603251302**  
**Event ID – 8**  
**Creep Event**  
**Ice Thickness: 3.5m**



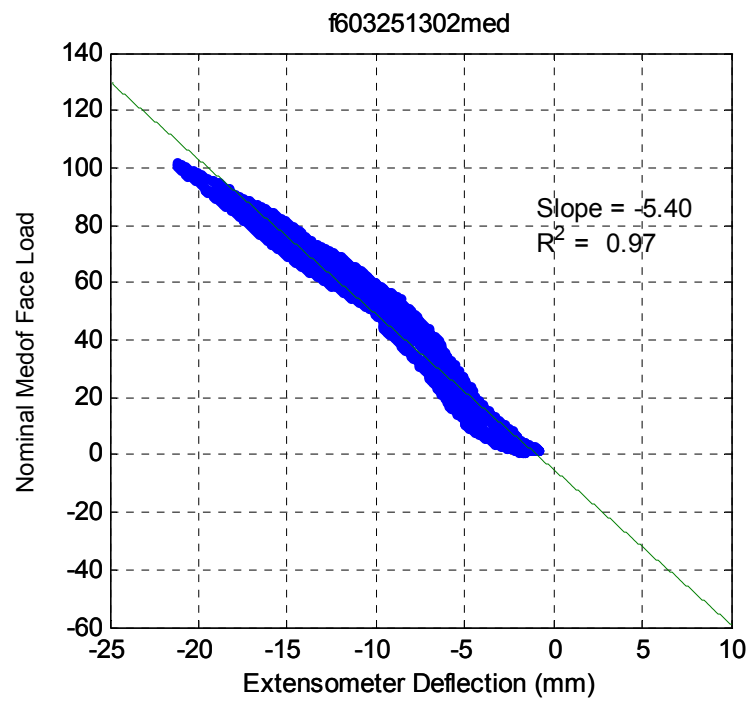
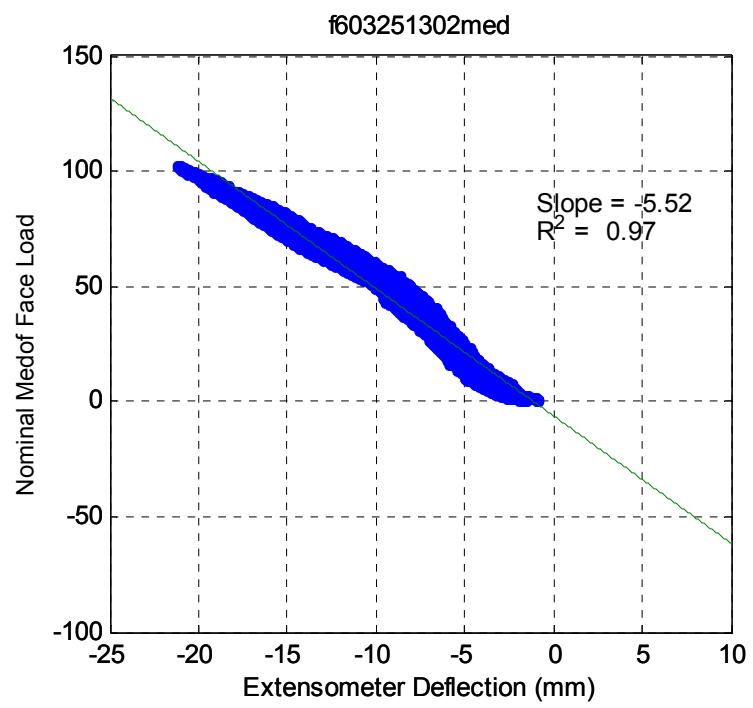
#### **Dynamac Event Description**

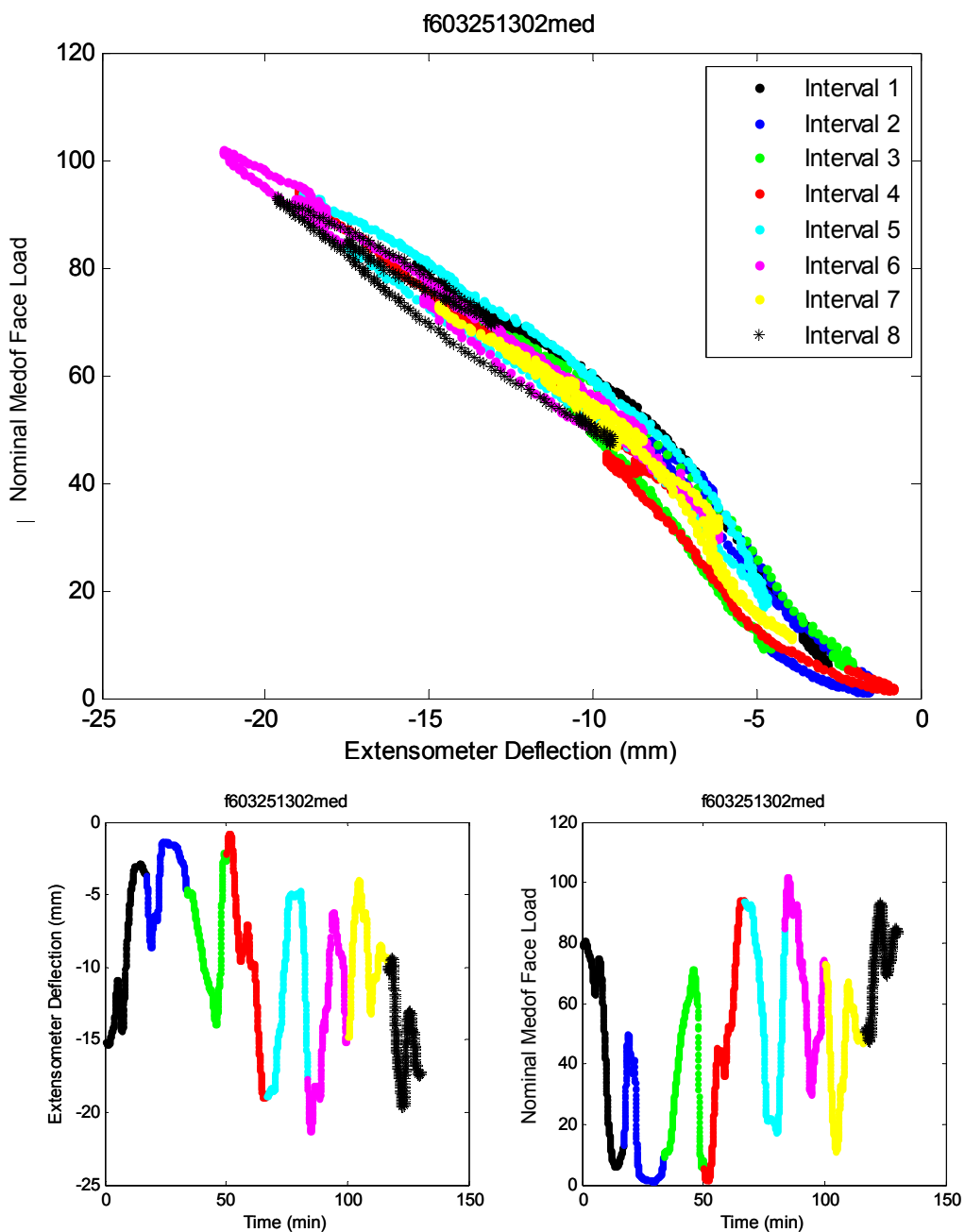
After 3 weeks of stationary ice, the multi-year ice in the vicinity of the Molikpaq began to slowly creep towards the south, thereby simultaneously loading the N, NW & NE faces. The ice drift speed was estimated at < 1 m/hr.

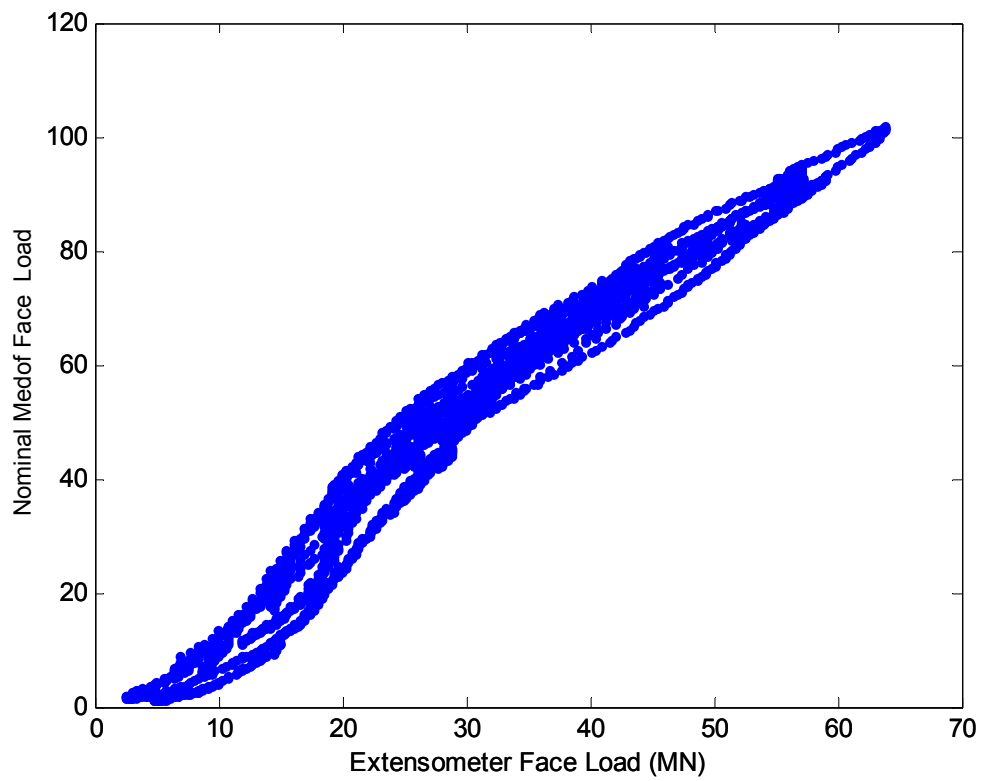
Note: The Bottom panel shows no loading during this event.



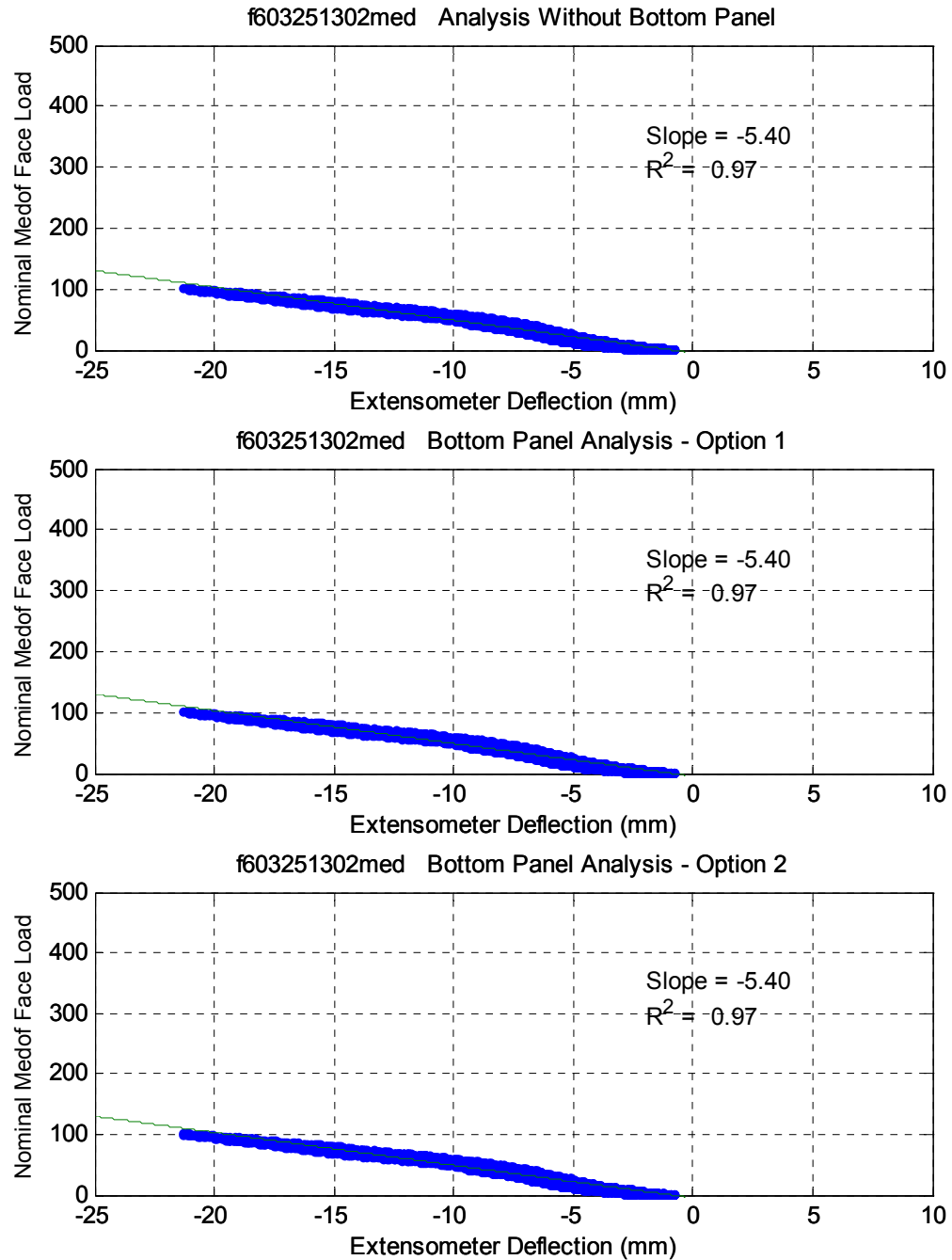
<i>Event ID</i>	<i>Date</i>	<i>Fast File</i>	<i>Segment</i>	<i>Time Period</i>	<i>Failure Mode</i>	<i>Panel Groups</i>	<i>Spacing of Groups</i>
2	25-Mar (C)	F603251305	full file	13:50:10-16:00:08	SLW	N1, N2 & N3	≈ 40m



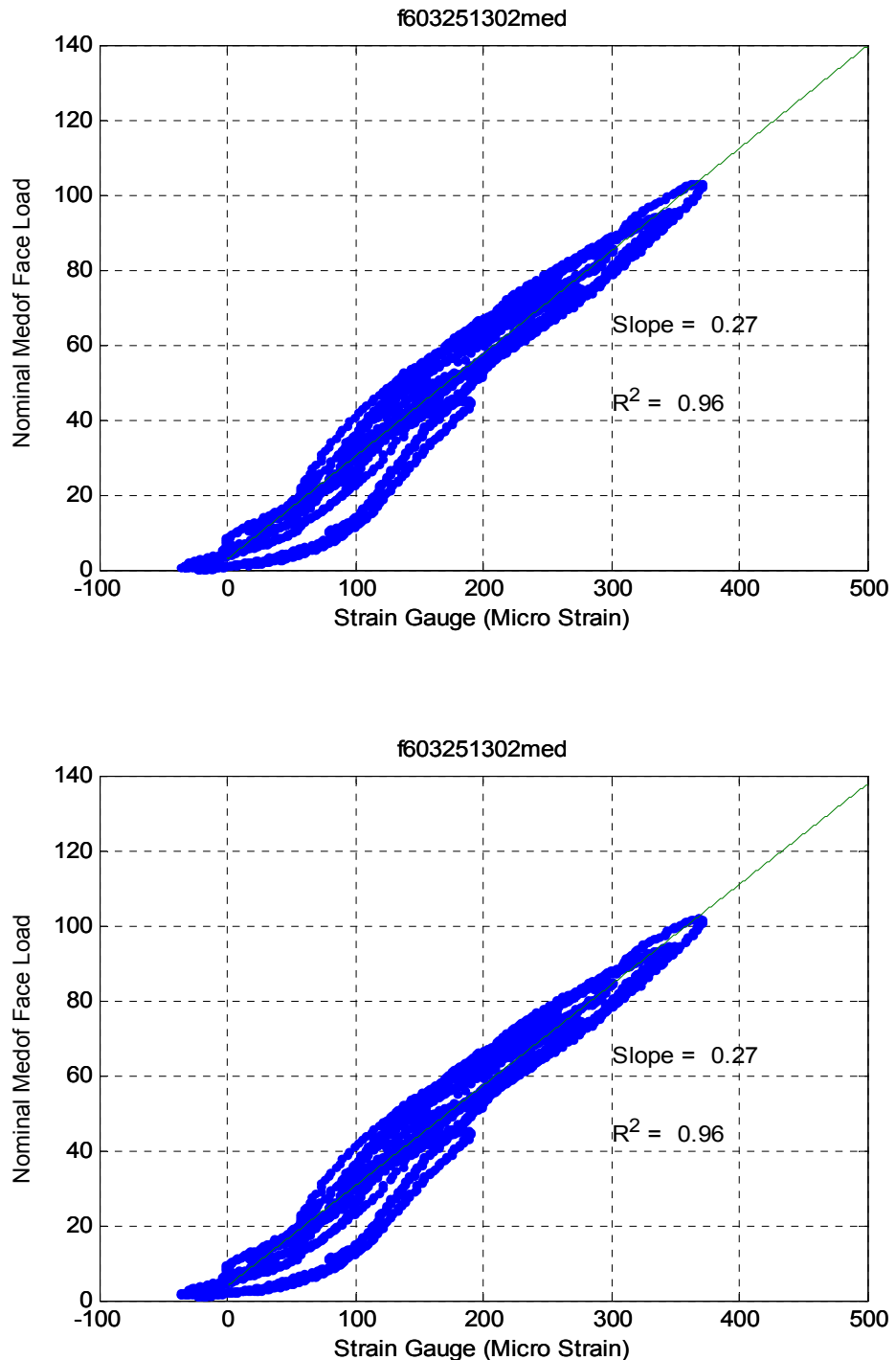




### Lower Panel Analysis



## Strain Gauge Results

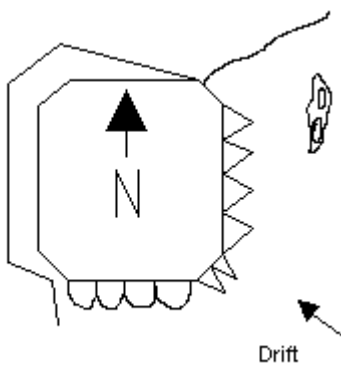


**APRIL 12 – F604121101**

**Event ID – 14**

**Crushing Event**

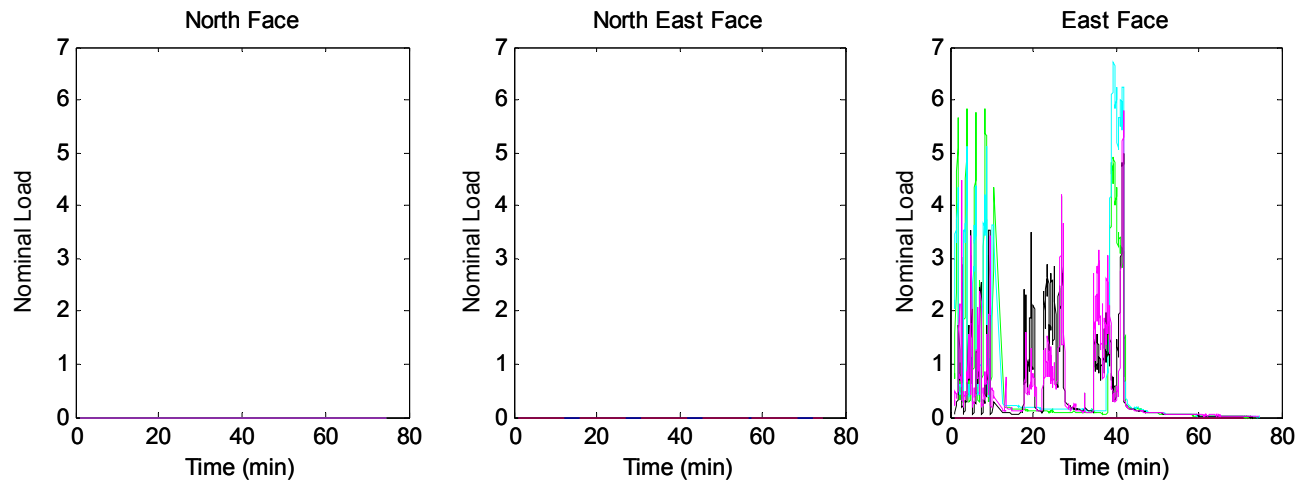
**Ice Thickness: 3.3m**



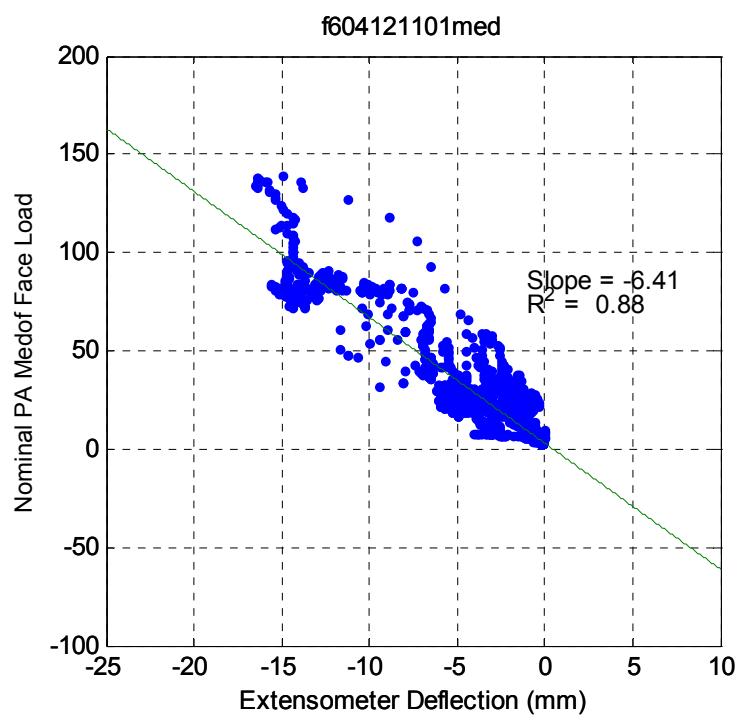
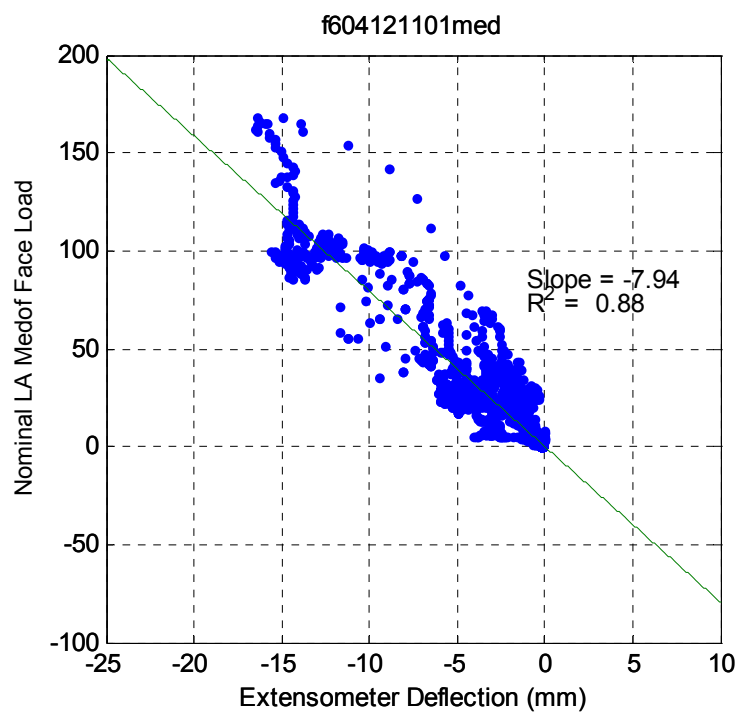
### **Dynamac Event Description**

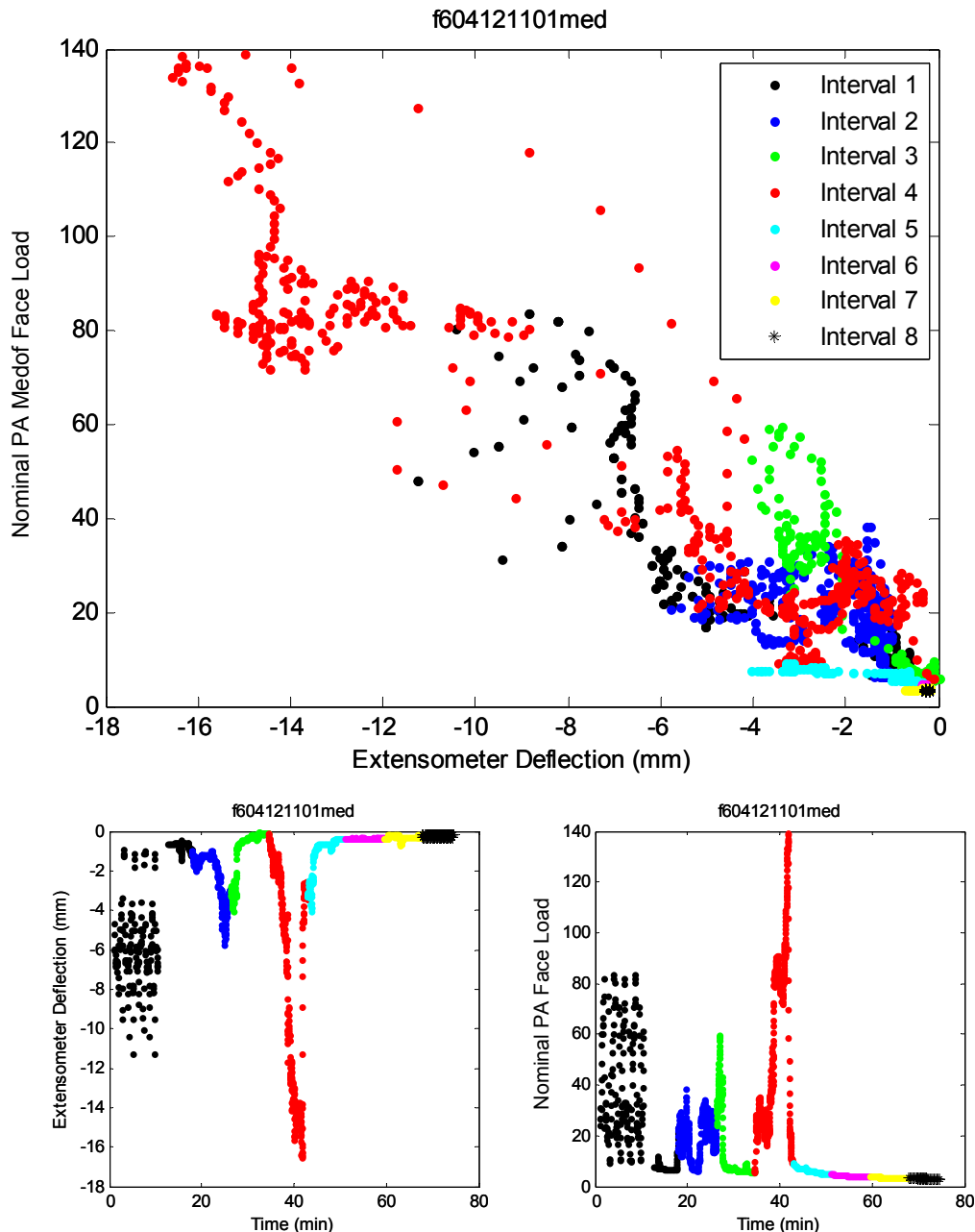
The Molikpaq contacted multi-year ice on the S, SE & E faces resulting in extrusion-collapse cycles.

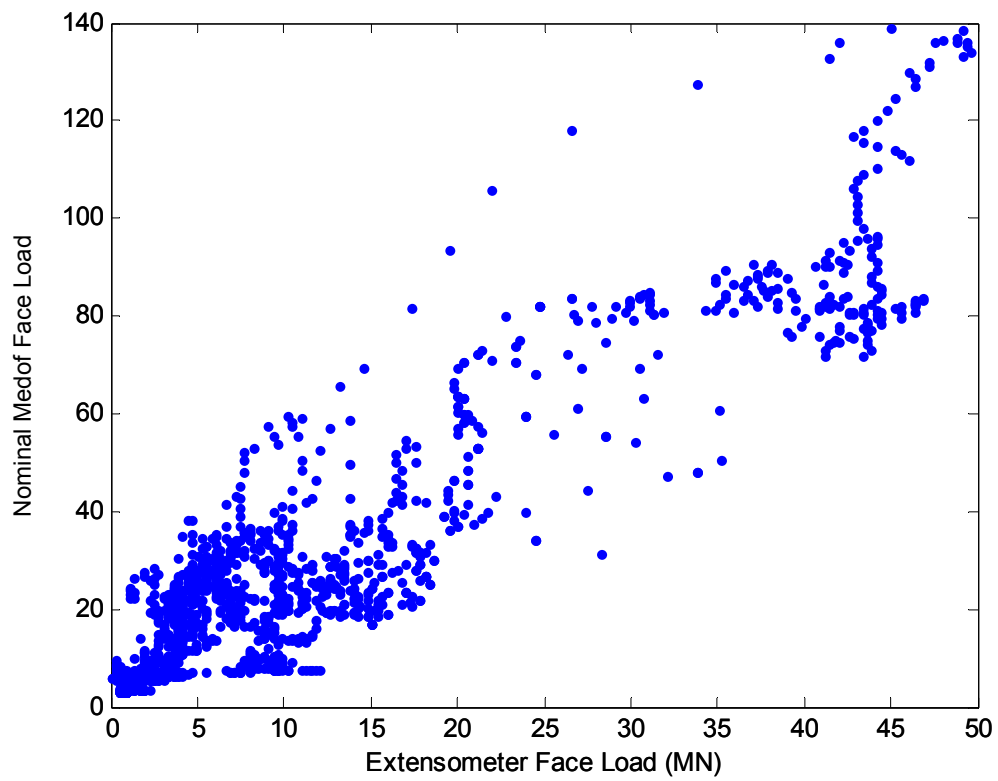
Note: The Bottom panel shows no loading during this event.



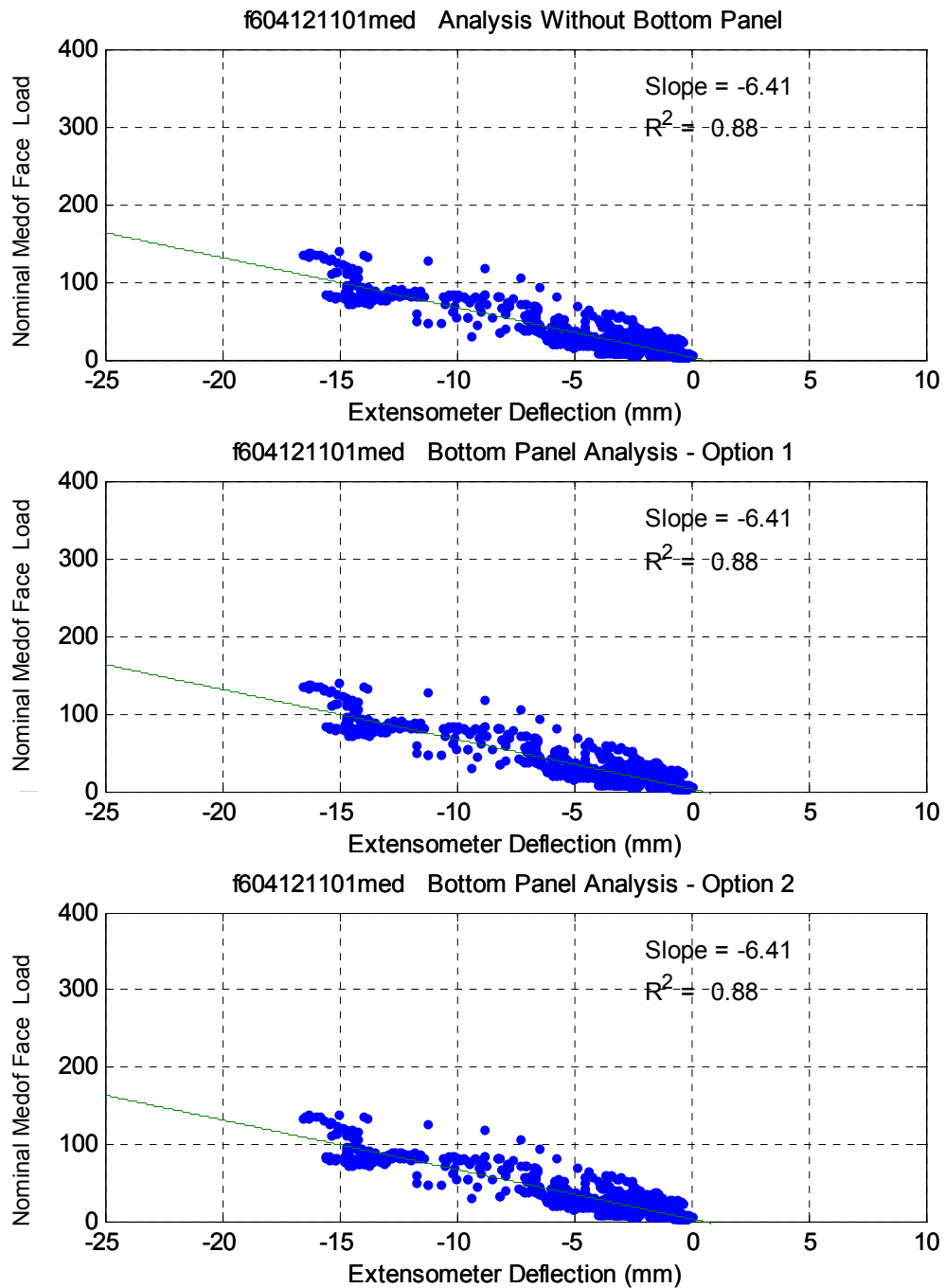
<i>Event ID</i>	<i>Date</i>	<i>Fast File</i>	<i>Segment</i>	<i>Time Period</i>	<i>Failure Mode</i>	<i>Panel Groups</i>	<i>Spacing of Groups</i>
14	12-Apr (C)	F604121101	full file	11:16:02 – 12:29:31	CC, CR, MM & SLW	N1, N2 & N3	≈ 40m
14-1			1	11:16:02 – 11:24:51	CC	E2 & E3	≈ 20m
14-2			2	11:24:52 – 11:52:48	SLD & MM	E3	< 20m
14-3			3	11:52:49 – 11:57:12	CR	E2	< 20m
14-4			4	11:57:13 – 12:29:31	SLD	E1, E2 & E3	≈ 40m



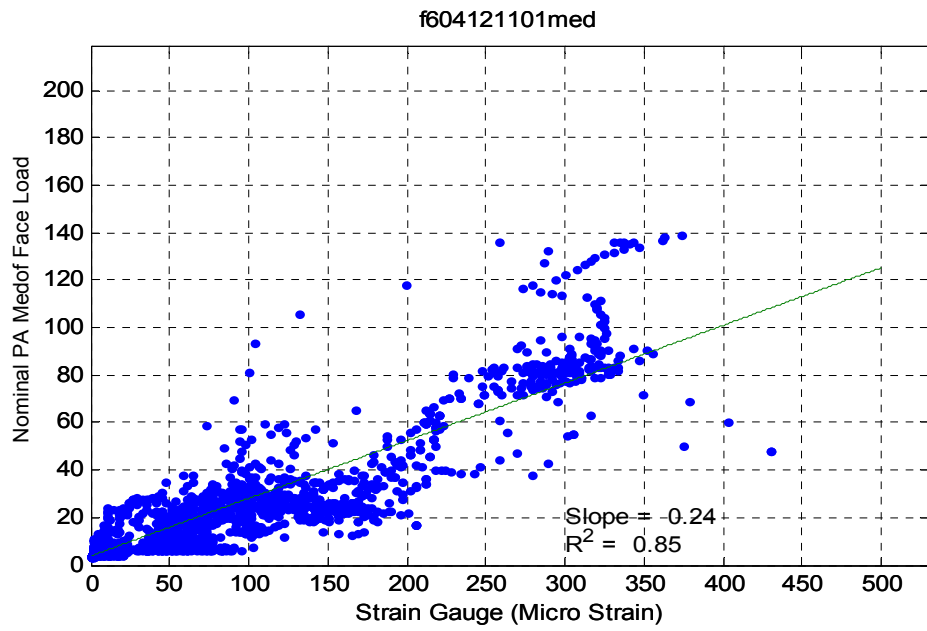
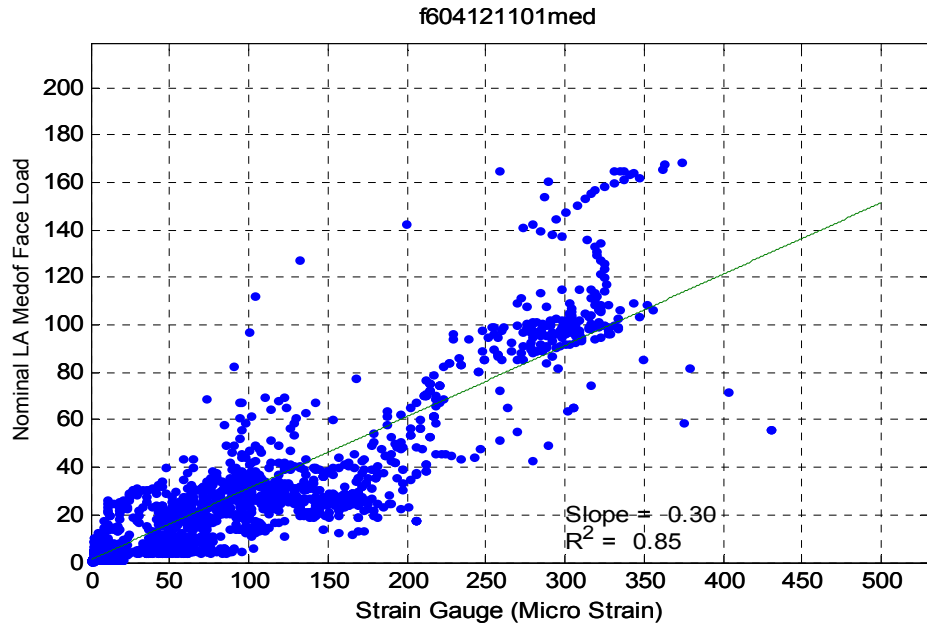




## Bottom Panel Analysis

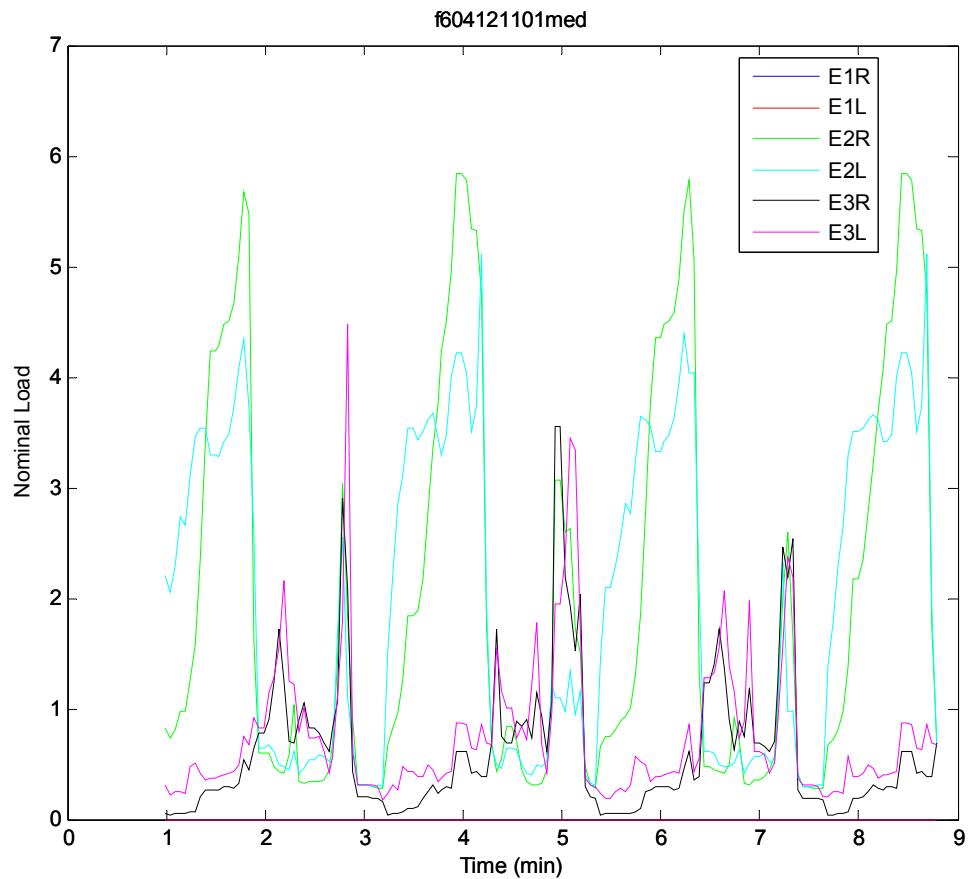


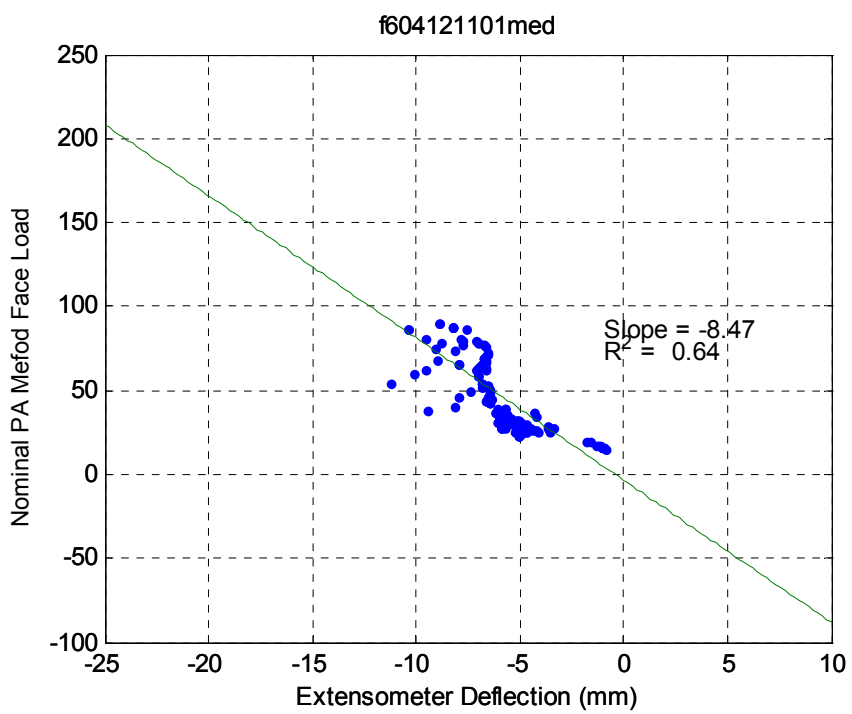
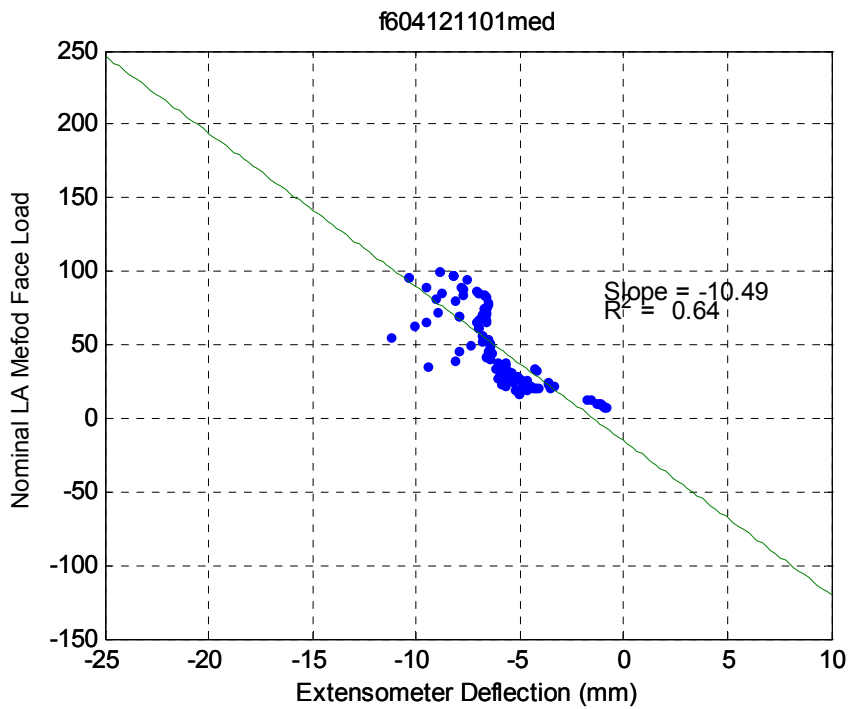
## Strain Gauge Results

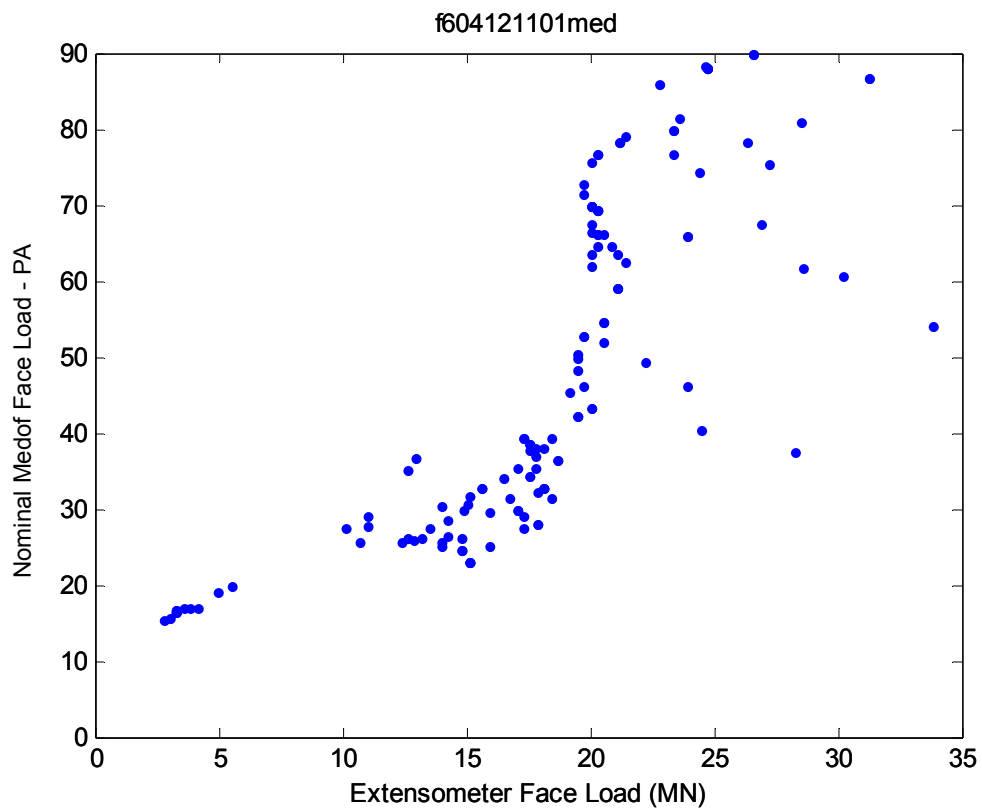


**April 12 – f604121101**  
**1.1 Event ID – 14 - 1**

**Cyclic Crushing**

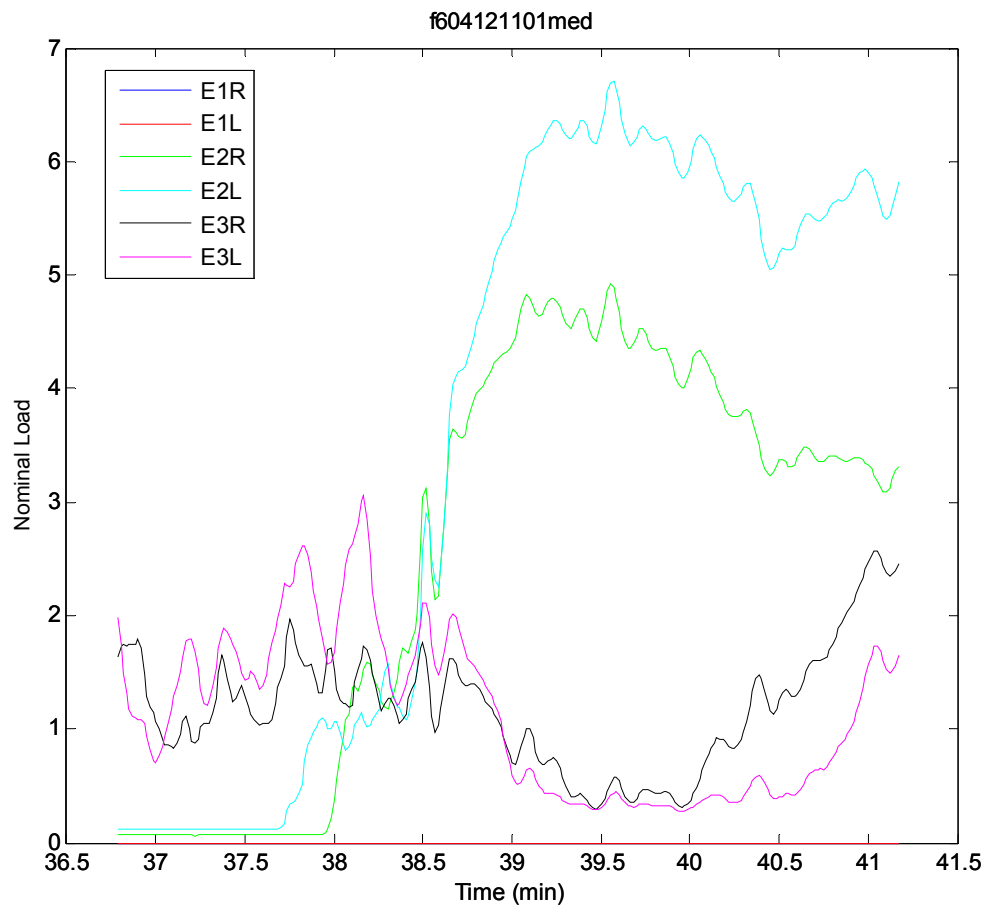


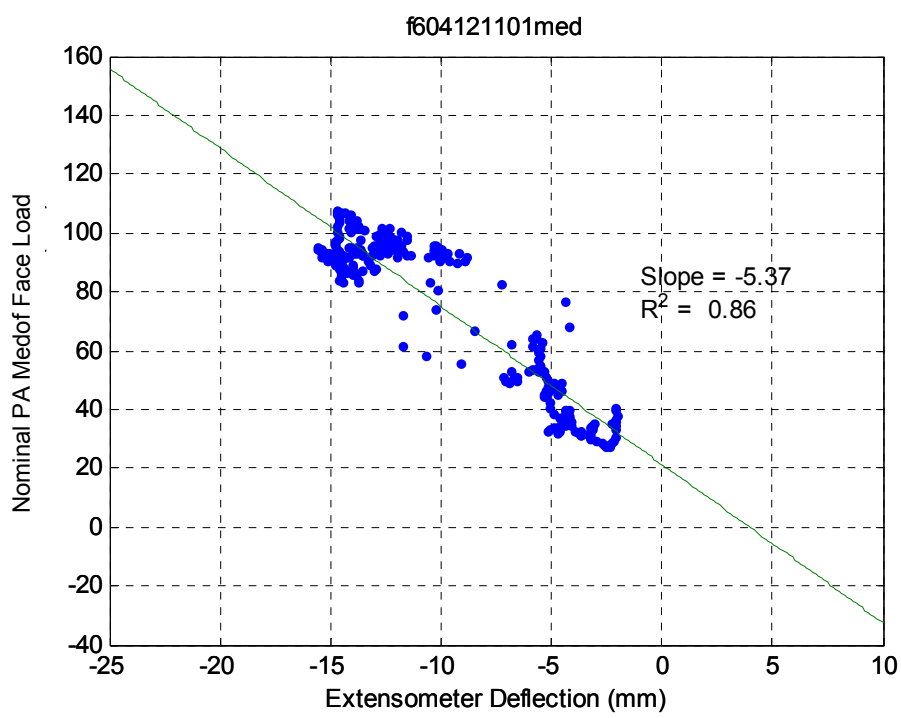
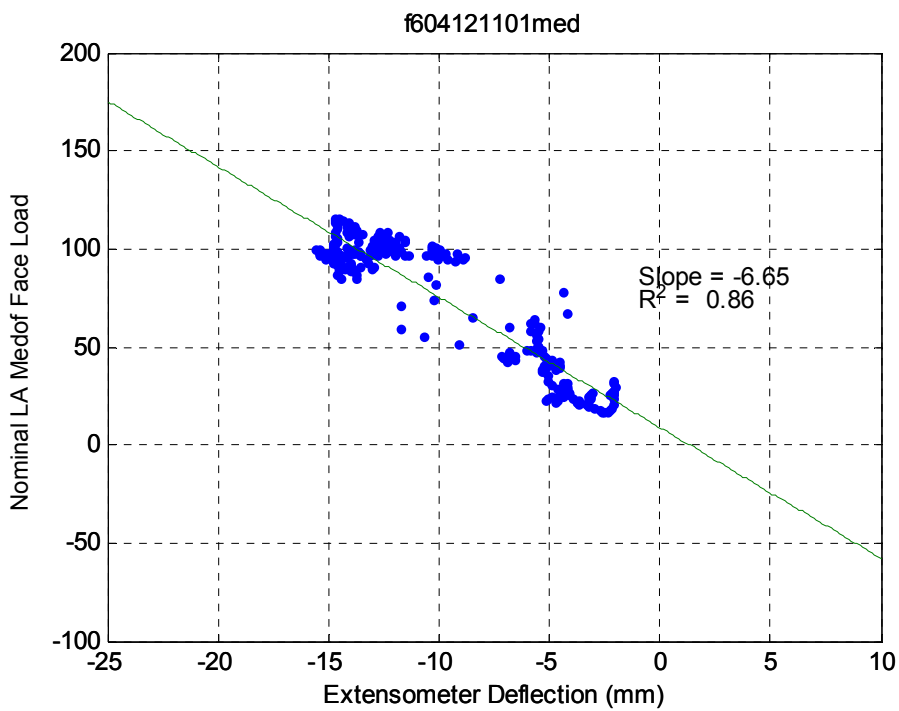


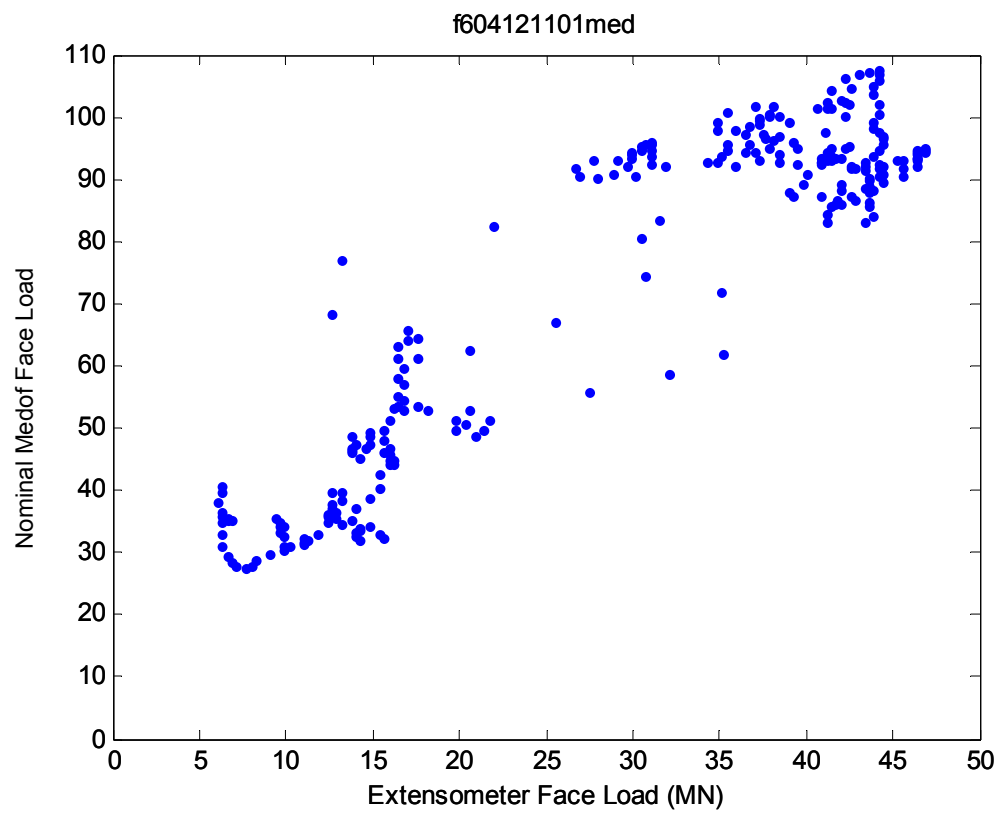


**April 12 – f604121101**  
**1.2 Event ID – 14 - 3**

### Crushing

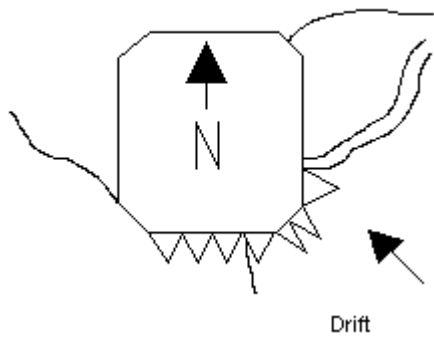






**2 APRIL 12 – F604121201**

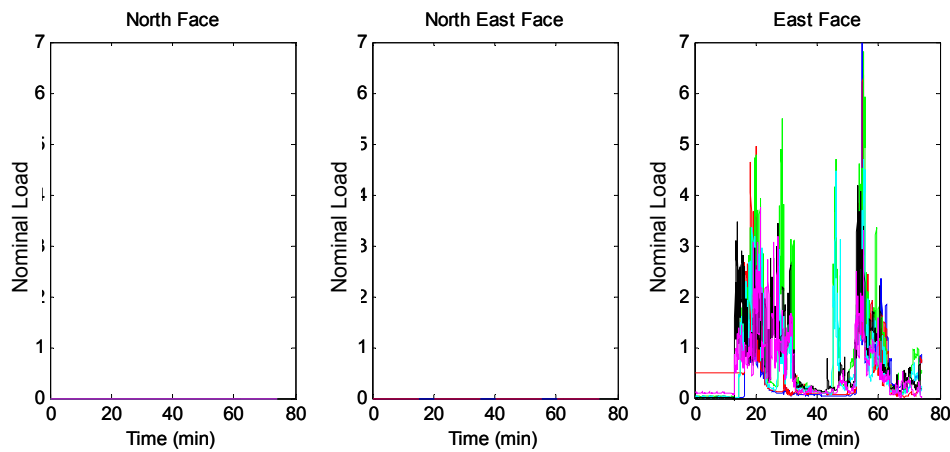
**Event ID – 15 – A**  
**Crushing**  
**Ice Thickness: 3.5m**



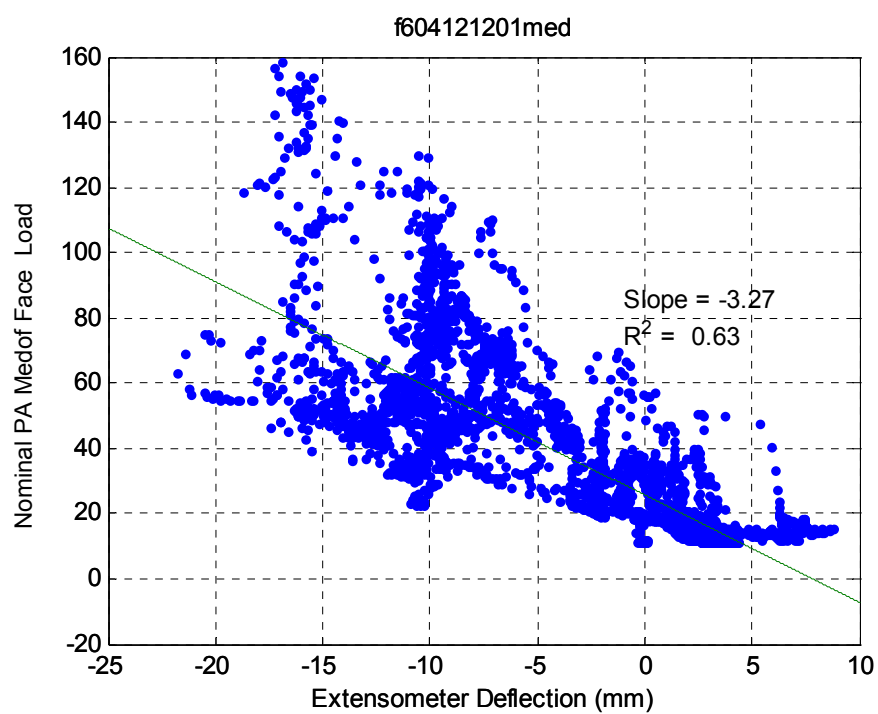
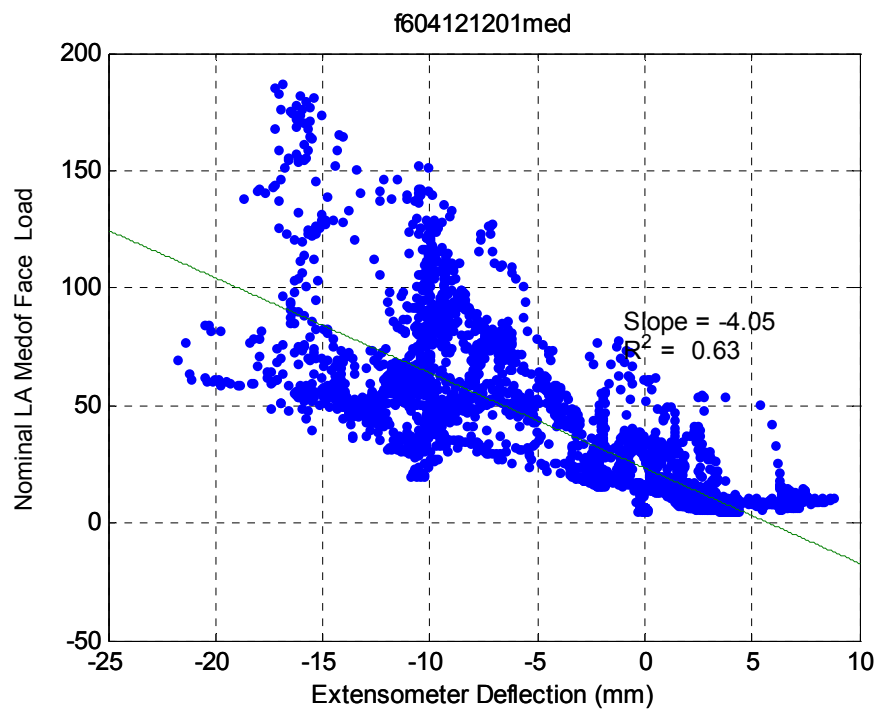
### **Dynamac Event Description**

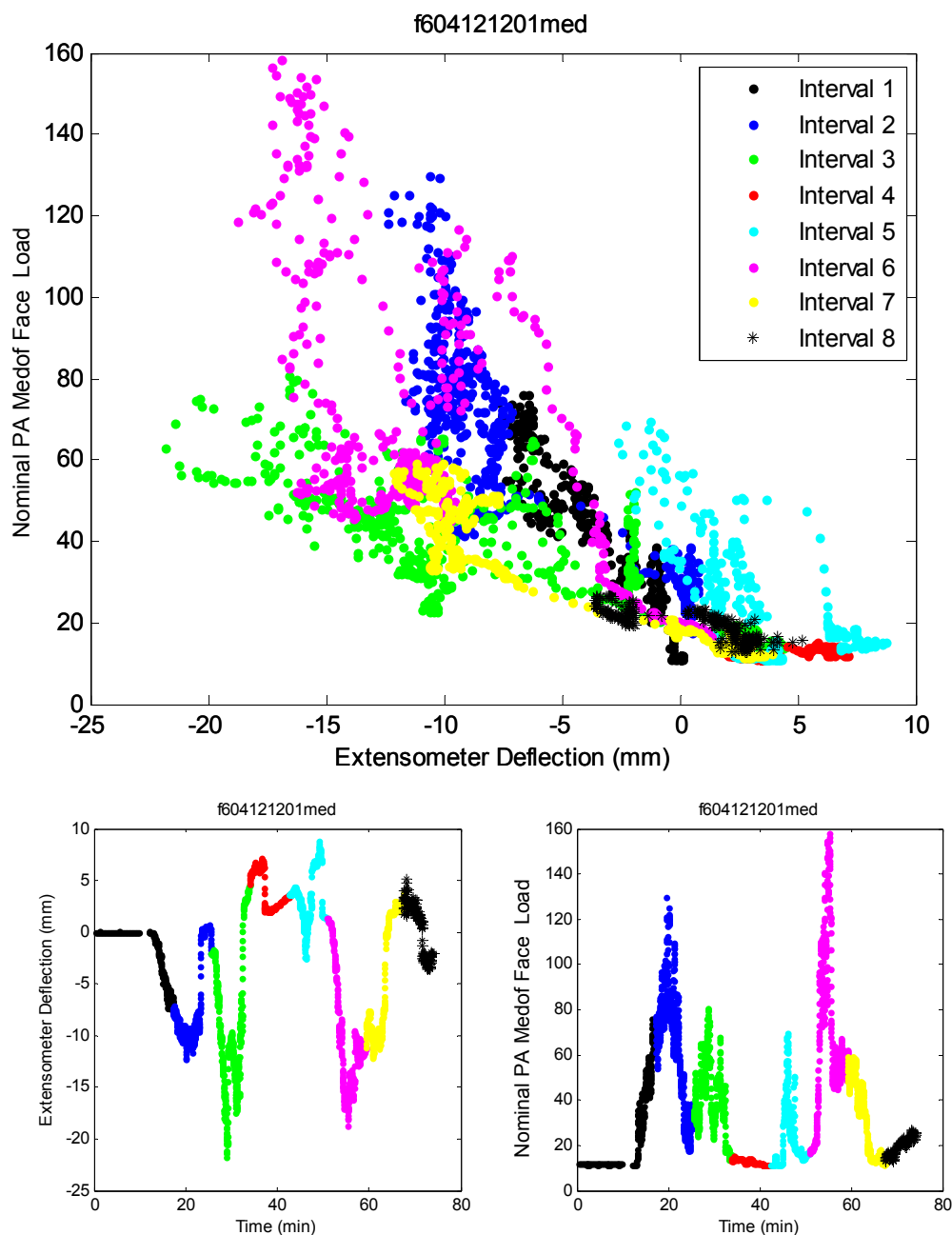
The Molikpaq contacted multi-year ice on the S, SE & E faces resulting in extrusion-collapse cycles.

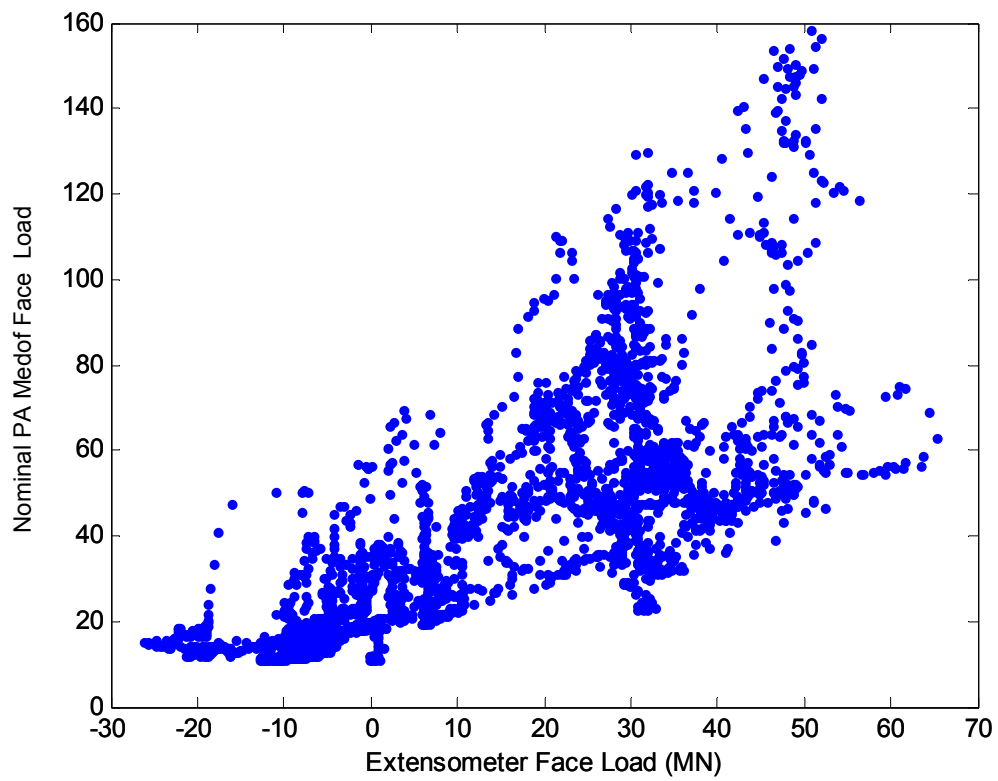
Note: The Bottom panel is loaded during this event. Some modeling of the effect of the bottom panel is required.



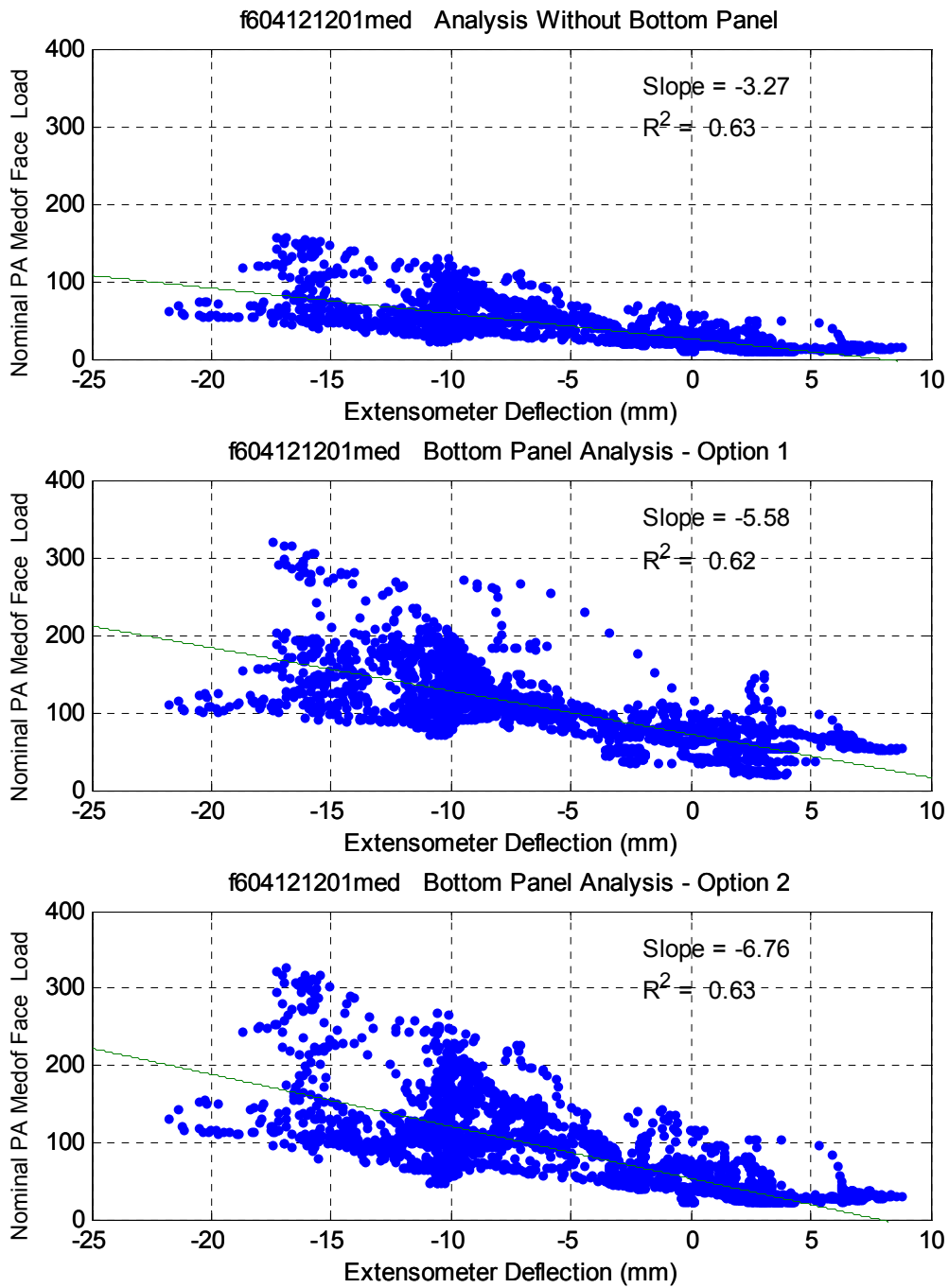
<i>Event ID</i>	<i>Date</i>	<i>Fast File</i>	<i>Segment</i>	<i>Time Period</i>	<i>Failure Mode</i>	<i>Panel Groups</i>	<i>Spacing of Groups</i>
15A	12-Apr (C)	F604121201	full file	13:00:07 – 14:01:04	CR, M & SLD	E1, E2 & E3	≈ 40m
15A-1			1	13:00:07 – 13:01:32	CR	E3	< 20m
15A-2			2	13:01:33 – 13:03:11	CR	E2 & E3	≈ 20m
15A-3			3	13:03:12 – 13:08:46	CR	E1, E2 & E3	≈ 40m
15A-4			4	13:08:47 – 13:10:43	CR	E2 & E3	≈ 20m
15A-5			5	13:10:44 – 13:14:57	CR	E3	< 20m
15A-6			6	13:14:58 – 13:19:25	CR	E2 & E3	≈ 20m
15A-7			7	13:19:26 – 13:42:30	SLD	E1, E2 & E3	≈ 40m
15A-8			8	13:42:31 – 13:50:15	CR	E2 & E3	≈ 20m
15A-9			9	13:50:16 – 14:01:04	SLD & MM	E1, E2 & E3	≈ 40m



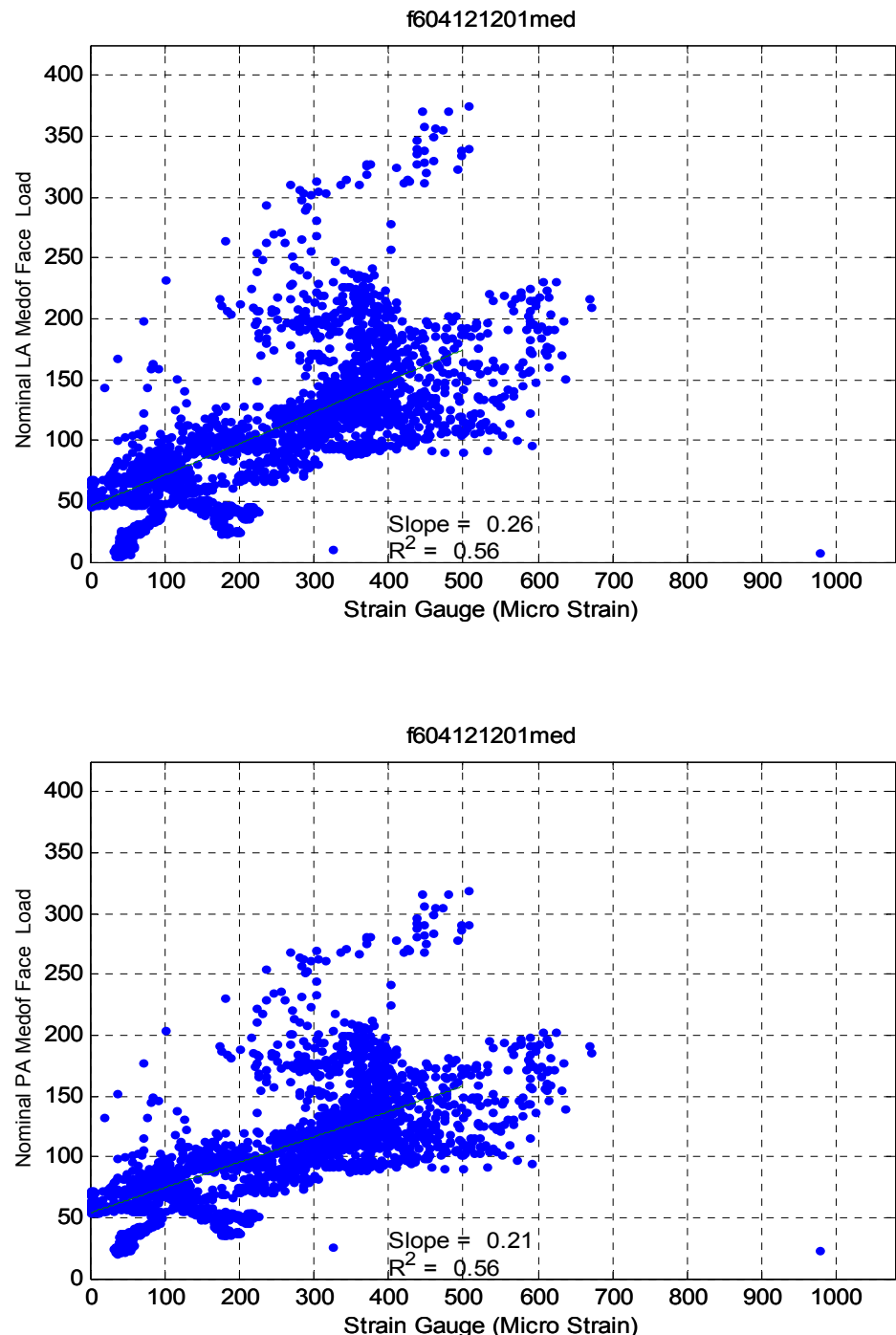




## Analysis of Bottom Panel



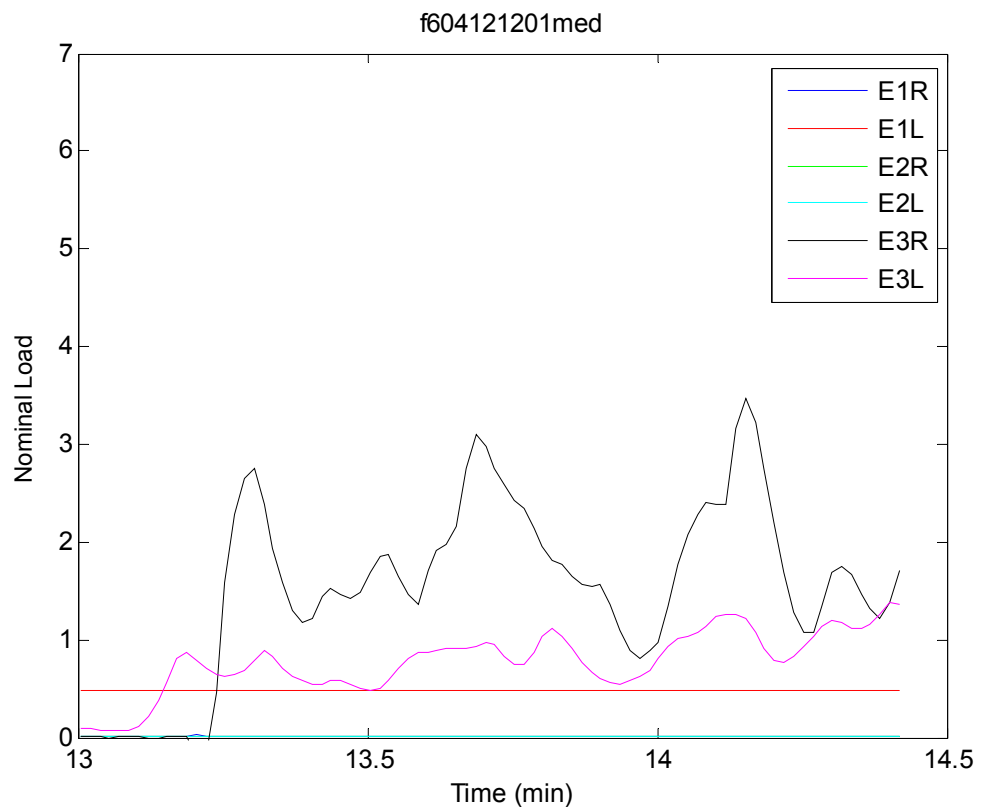
## Strain Gauge Results

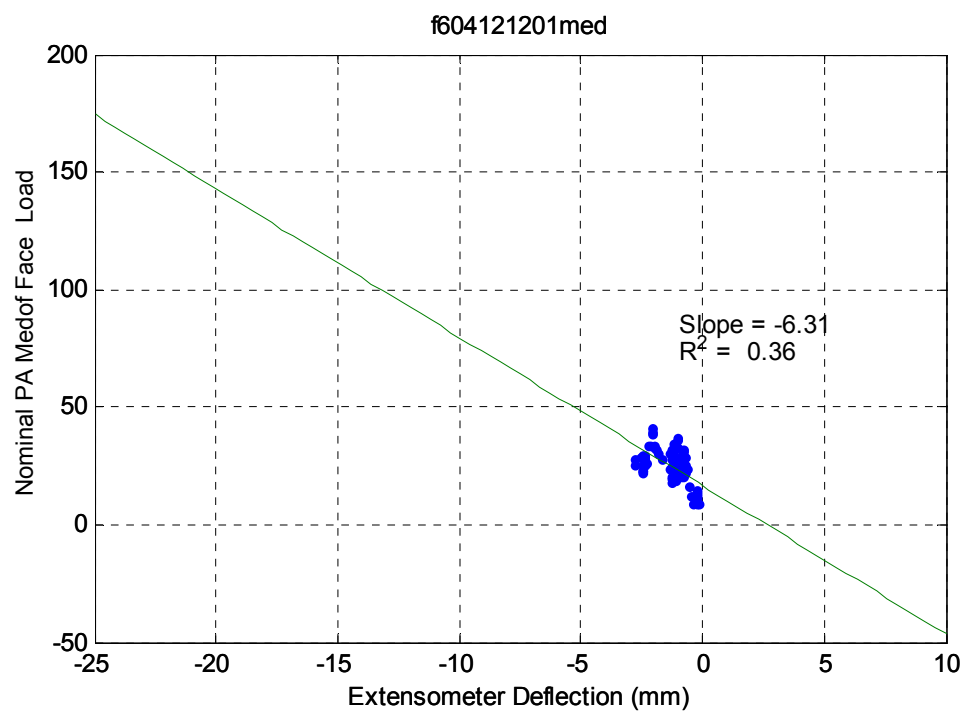
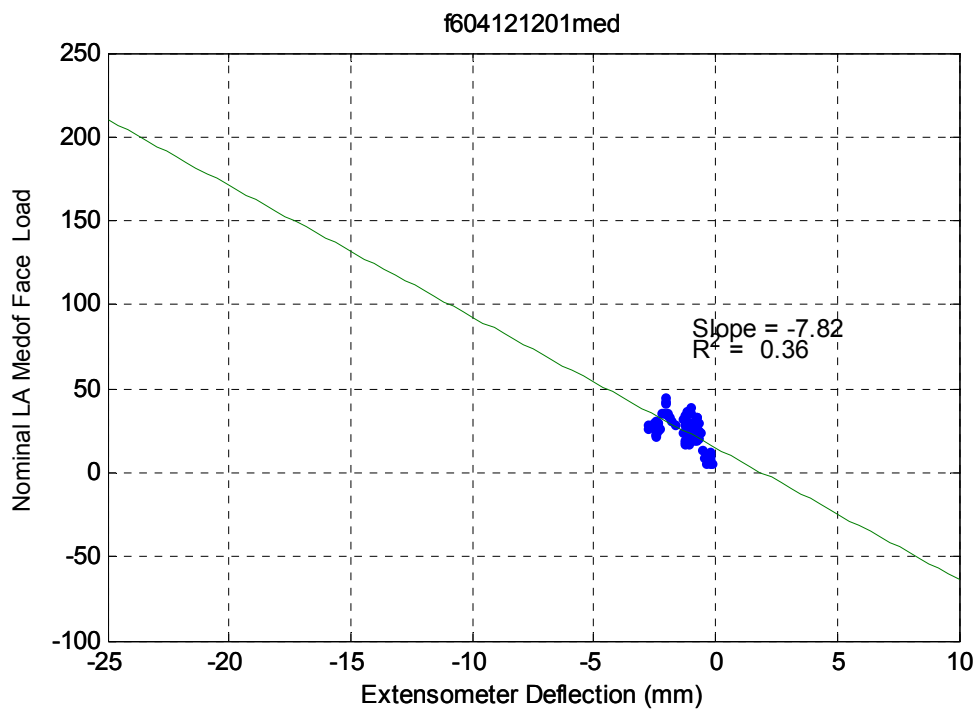


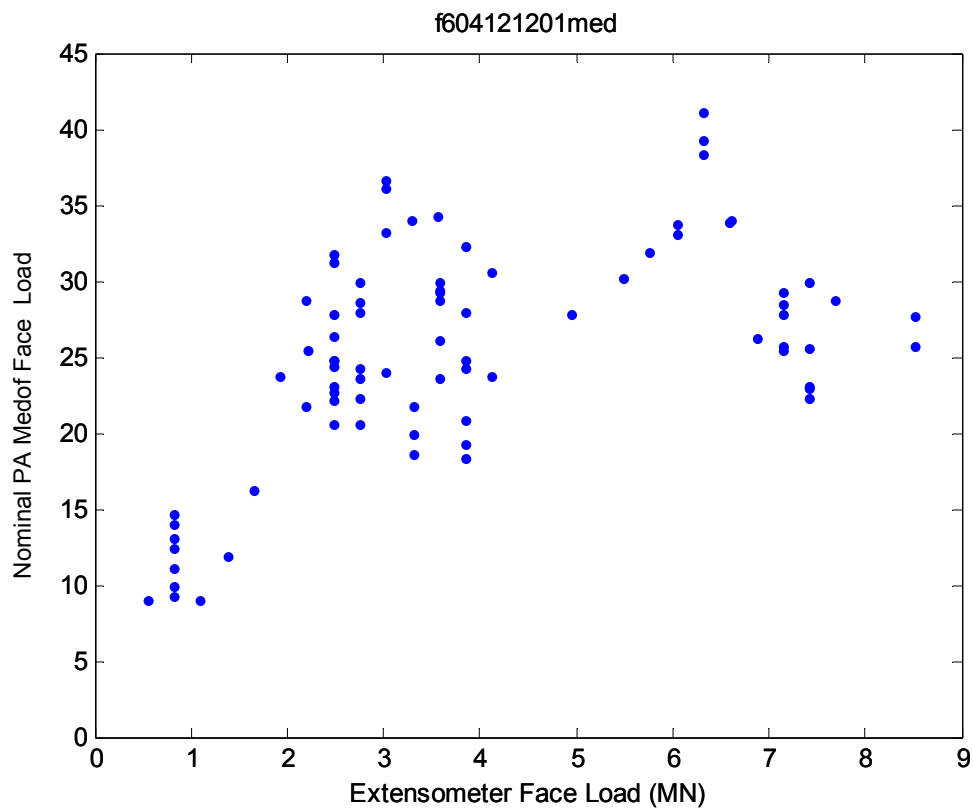
**April 12 – f604121201**

**2.1 Event ID – 15 - A - 1**

### **Crushing**

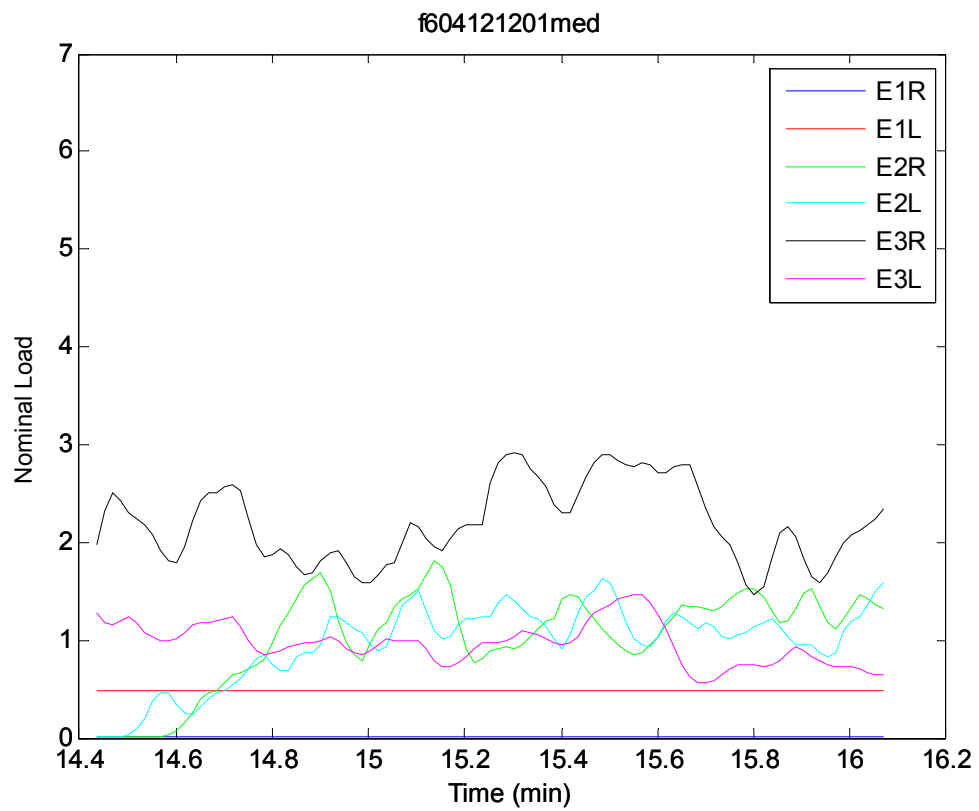


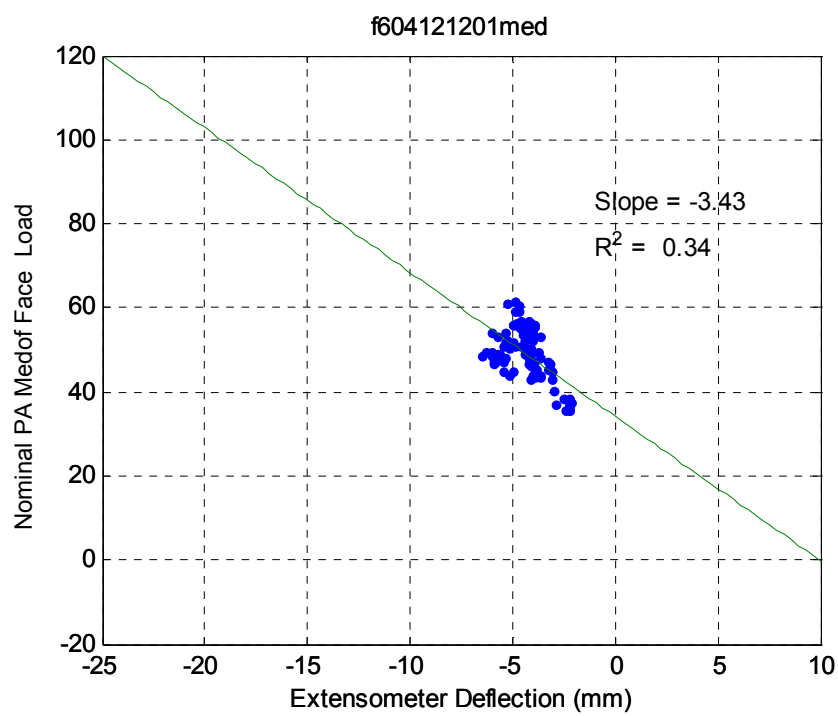
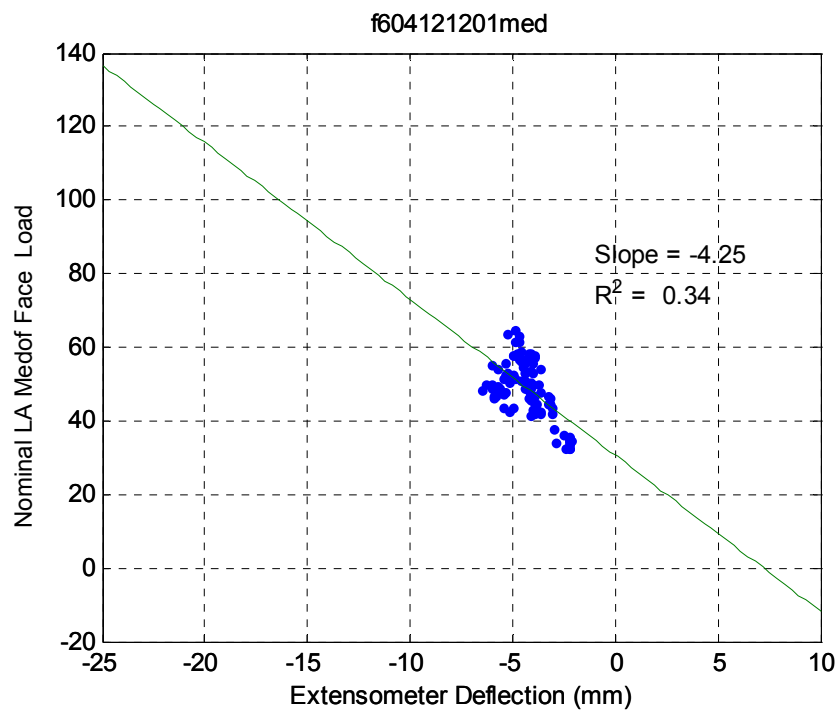


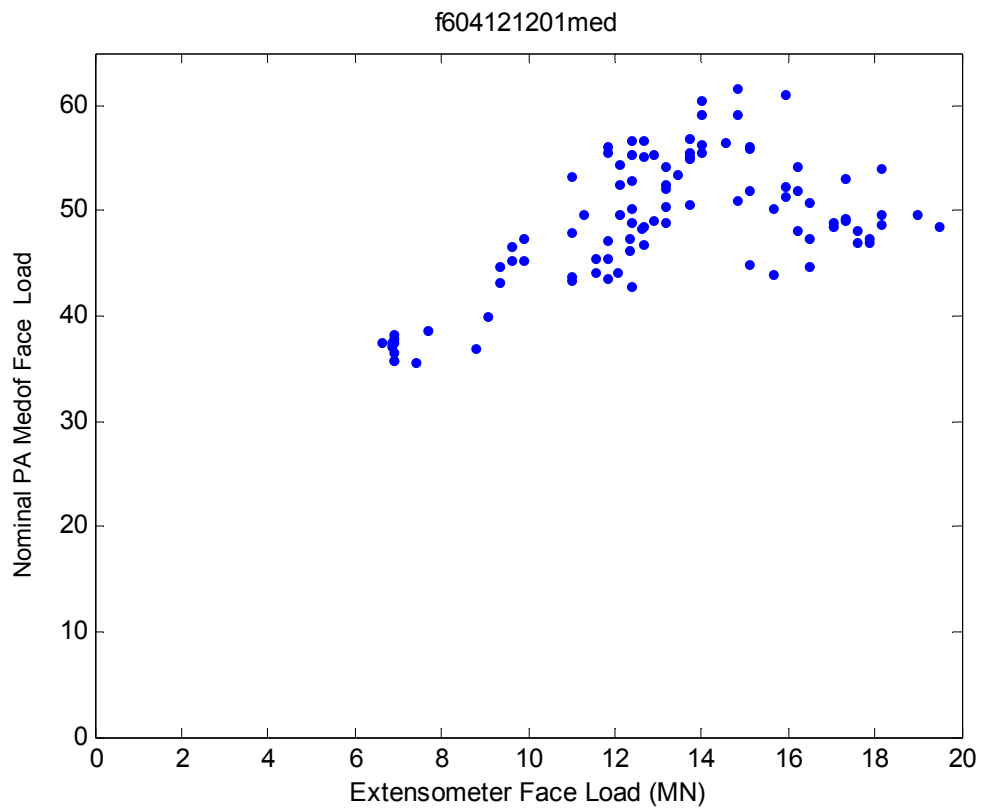


**April 12 – f604121201**  
**2.2 Event ID – 15 - A - 2**

### Crushing

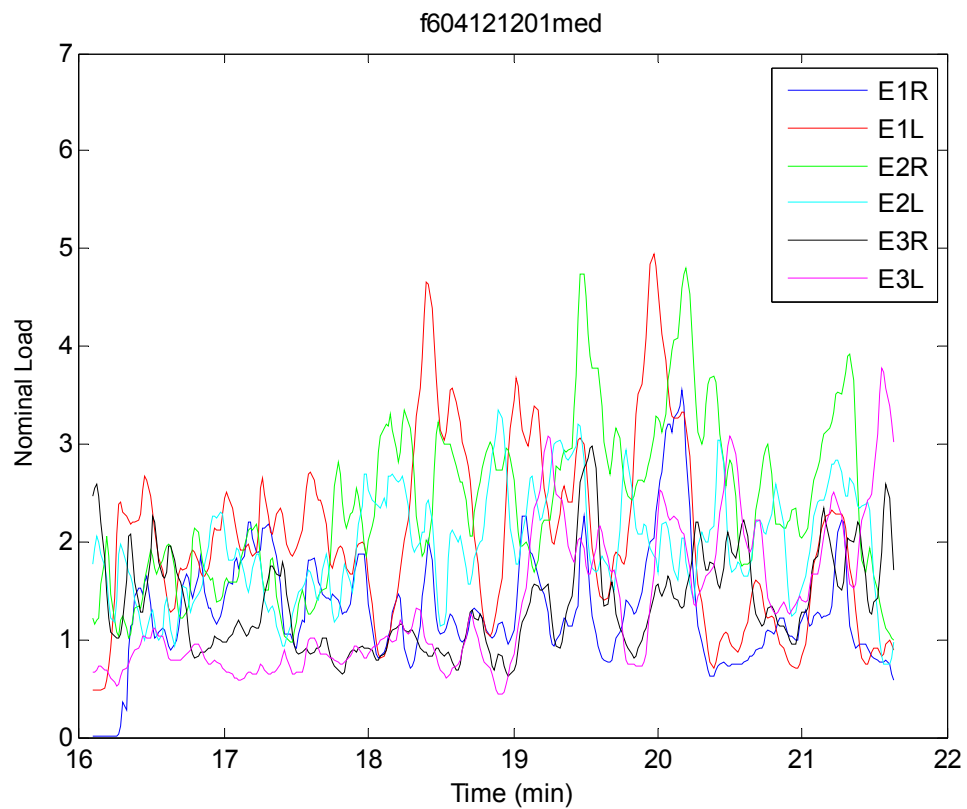


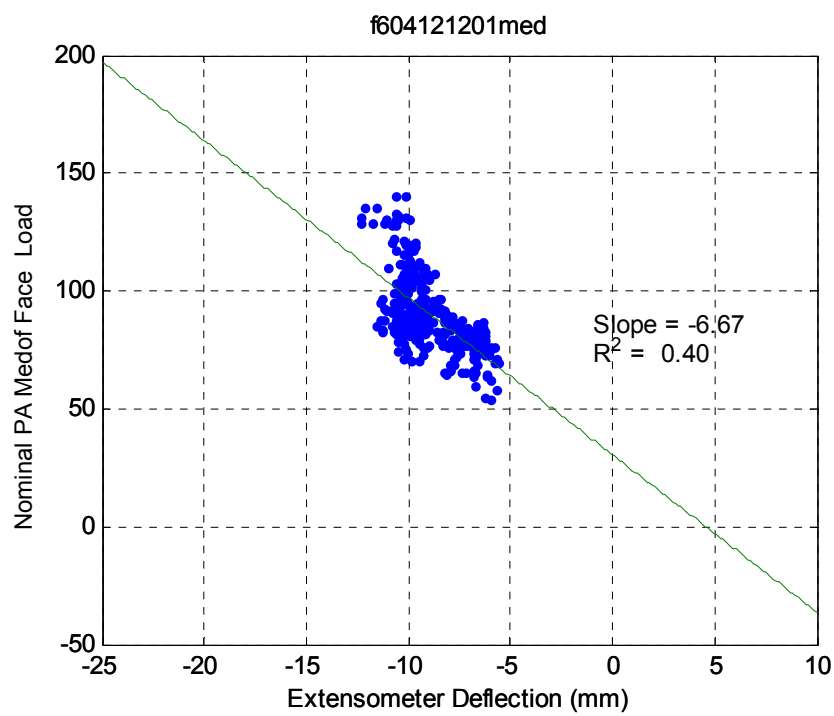
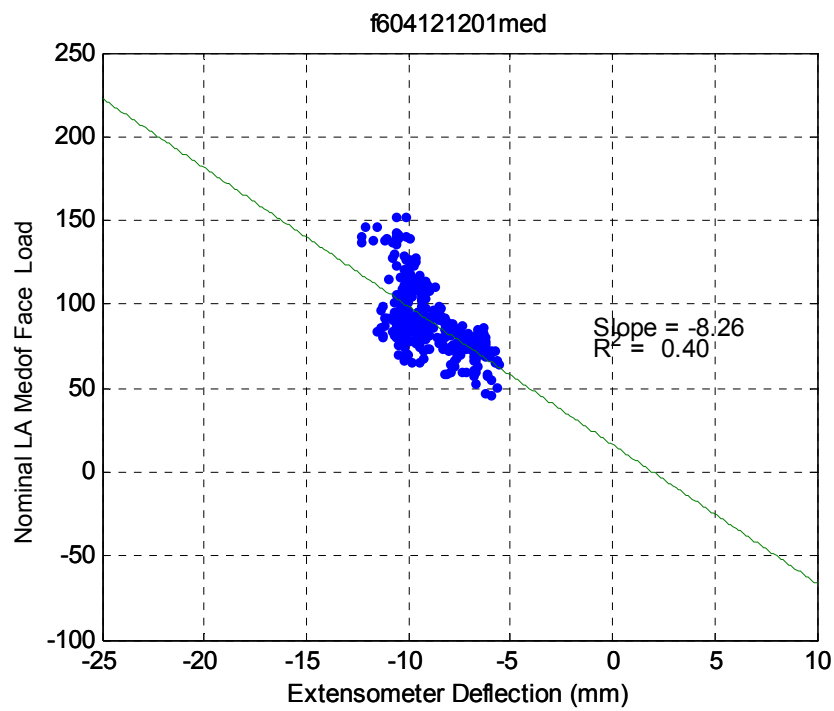


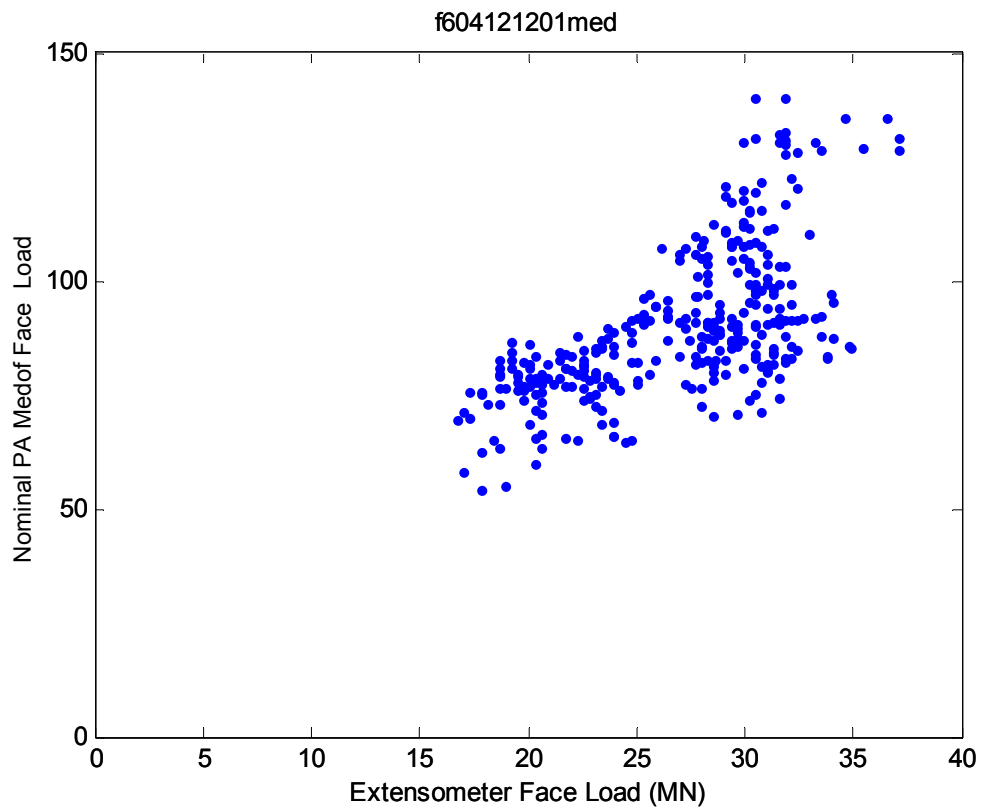


**April 12 – f604121201**  
**2.3 Event ID – 15 - A - 3**

**Crushing**

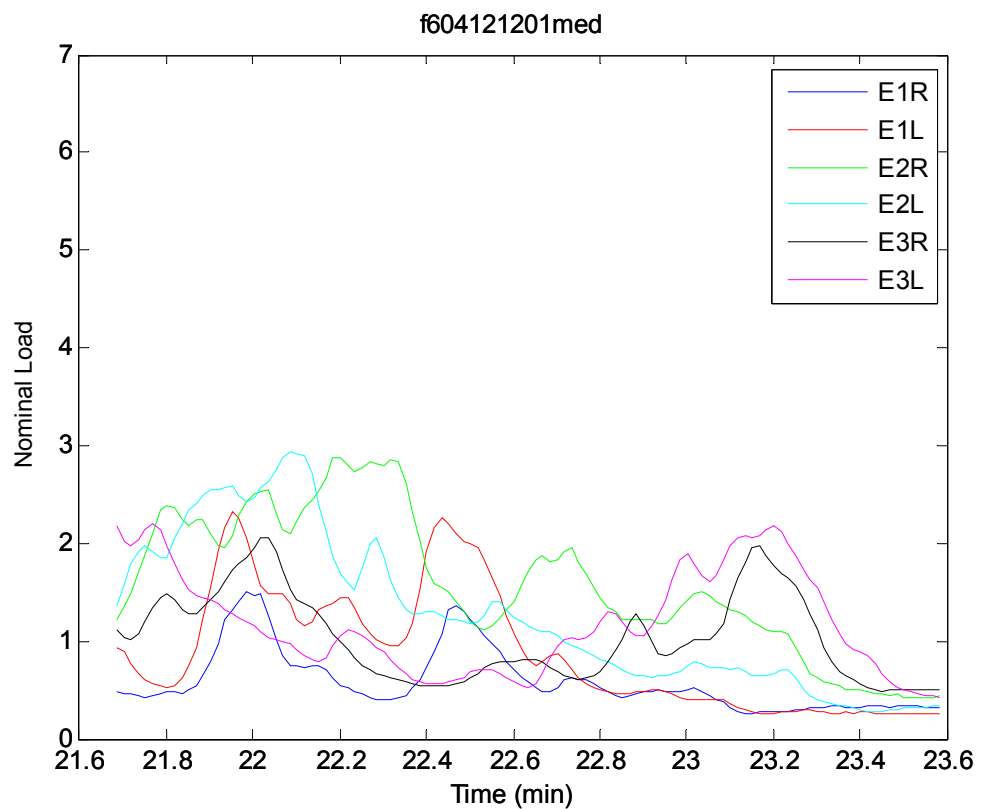


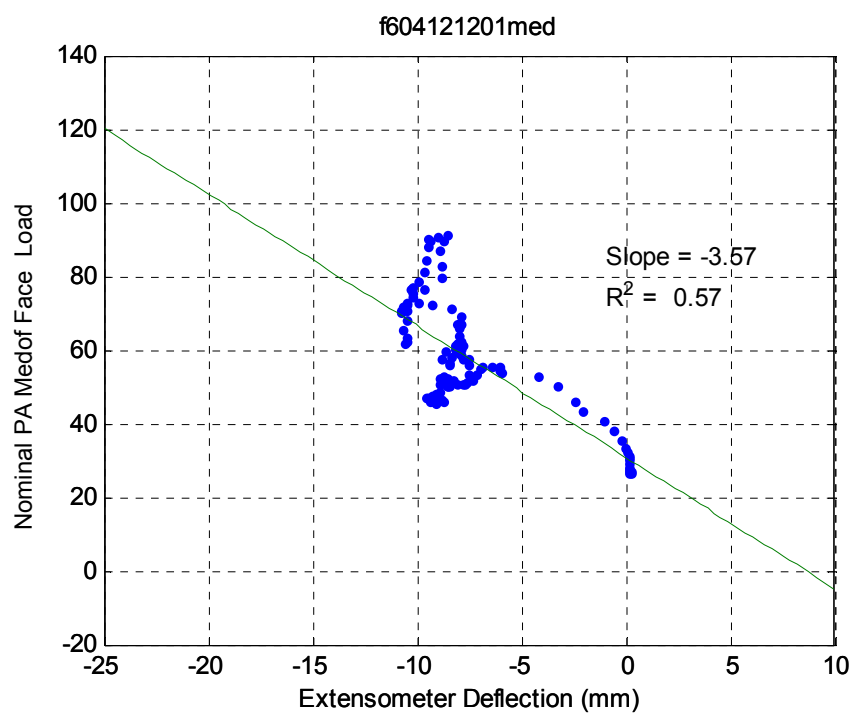
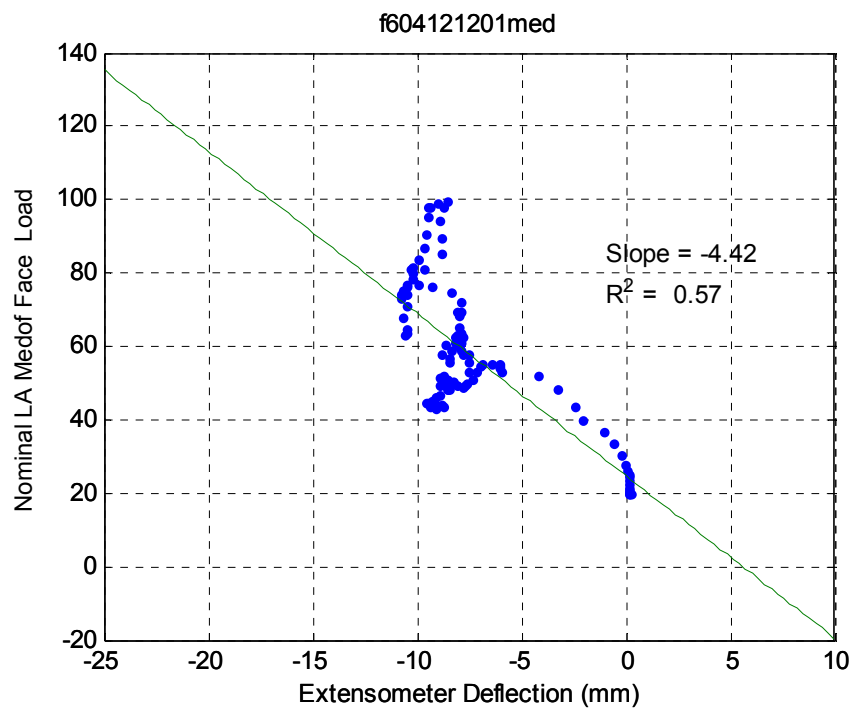


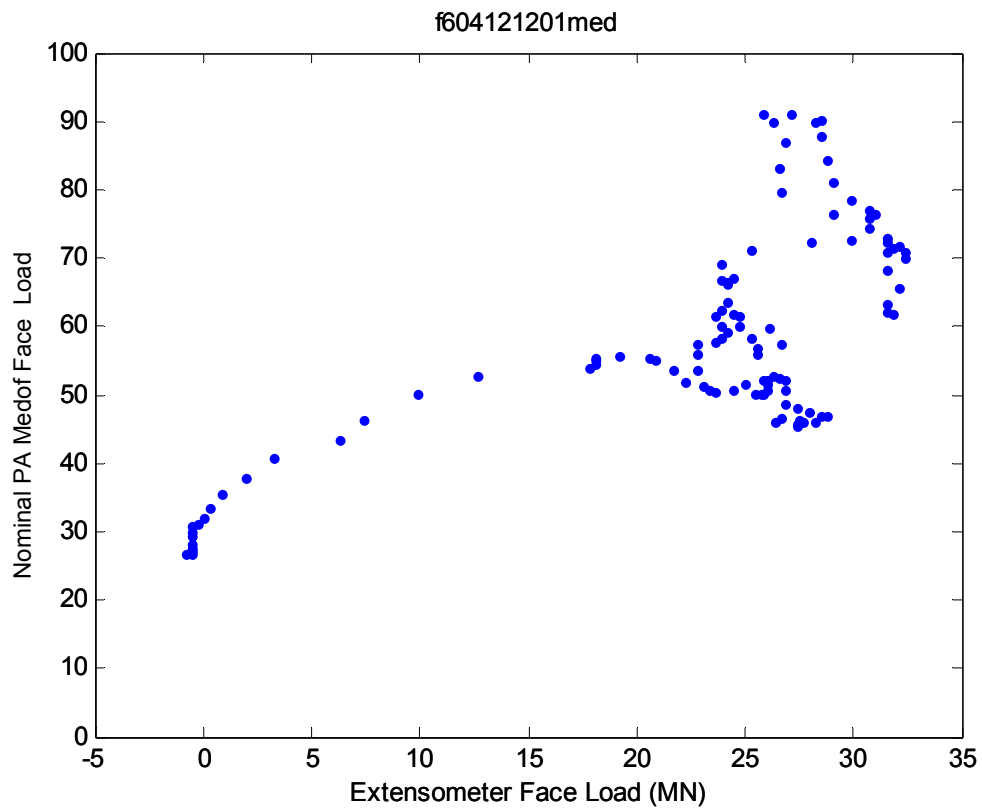


**April 12 – f604121201**  
**2.4 Event ID – 15 - A - 4**

**Crushing**

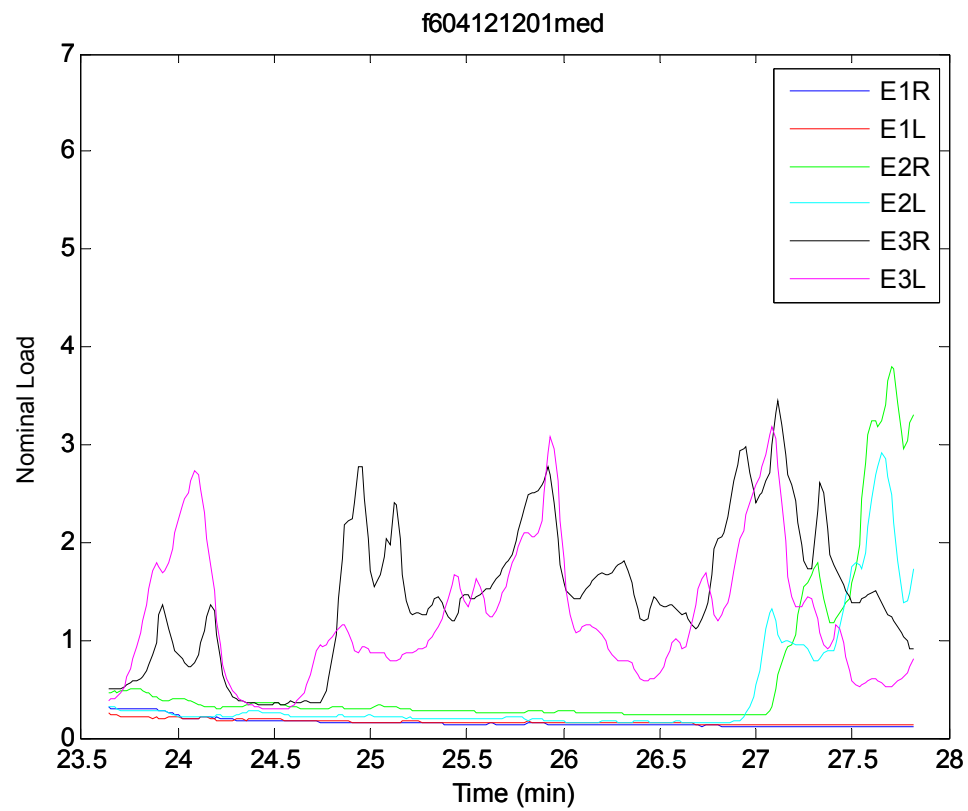


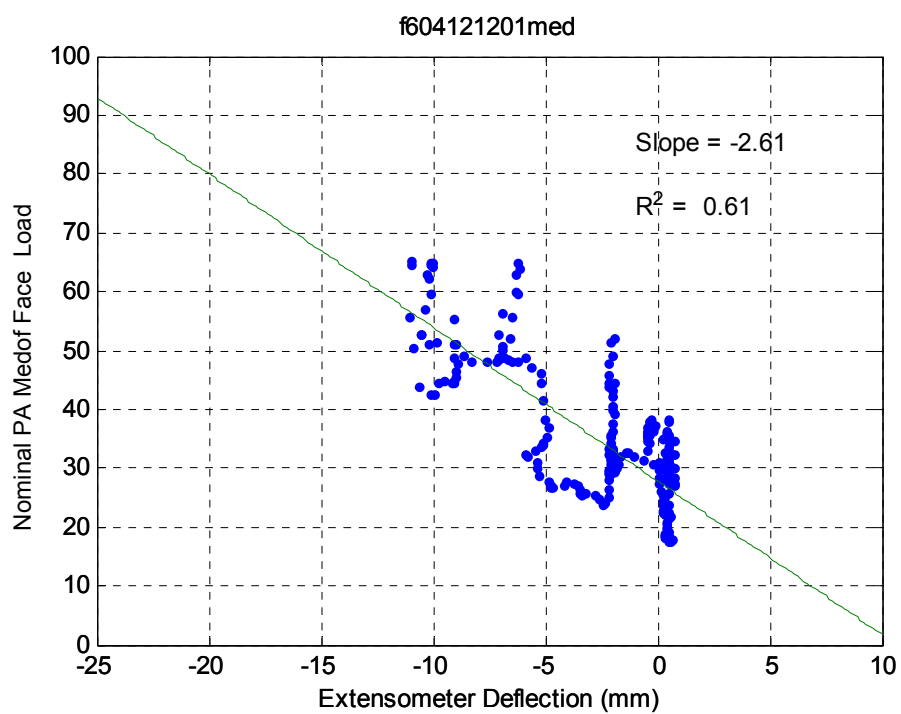
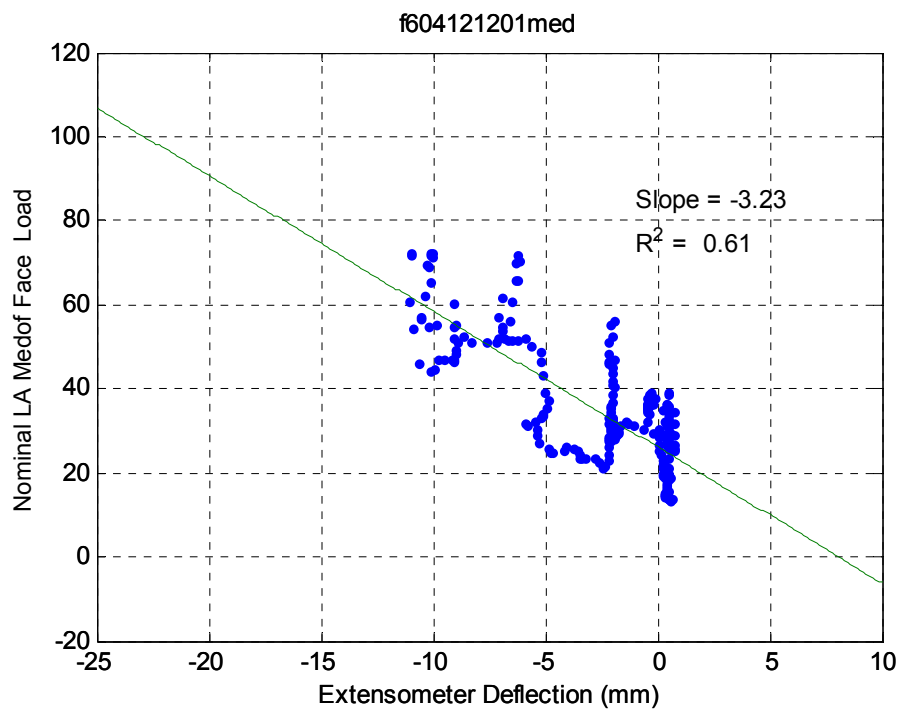


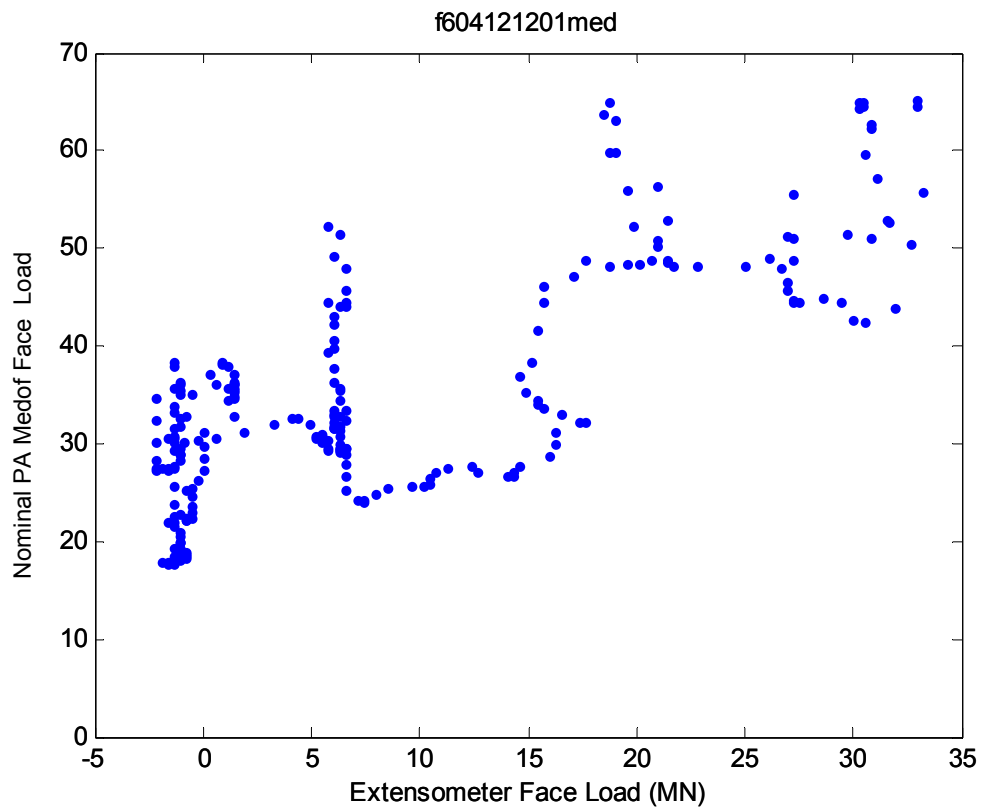


**April 12 – f604121201**  
2.5    *Event ID – 15 - A - 5*

### Crushing

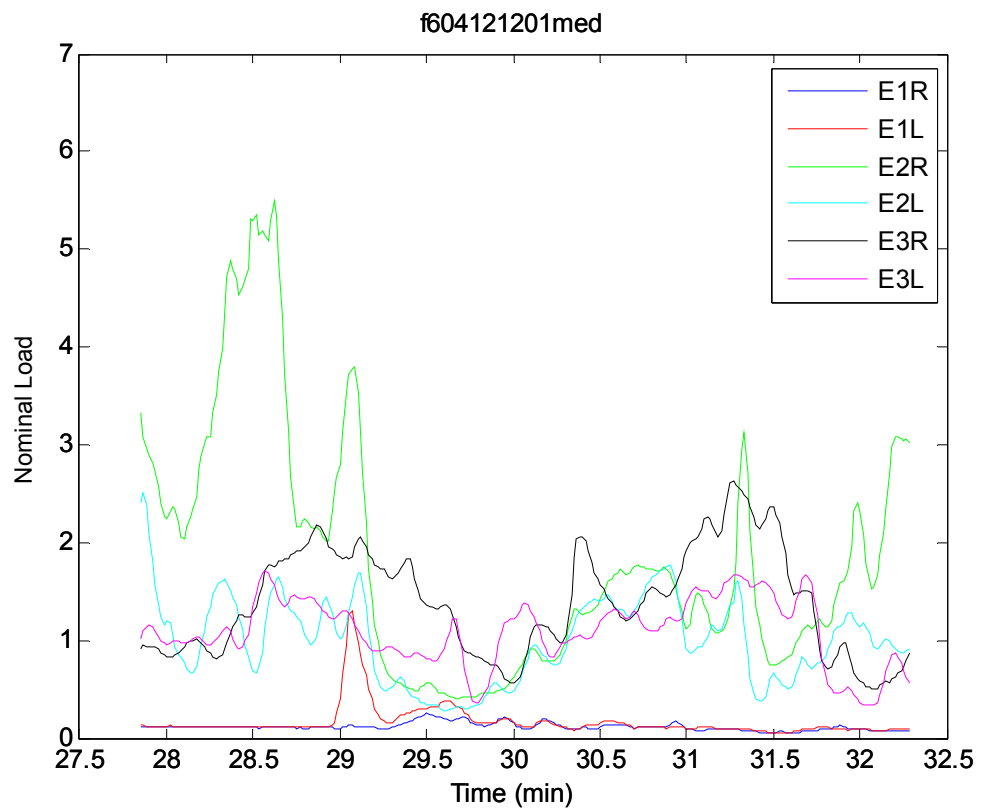


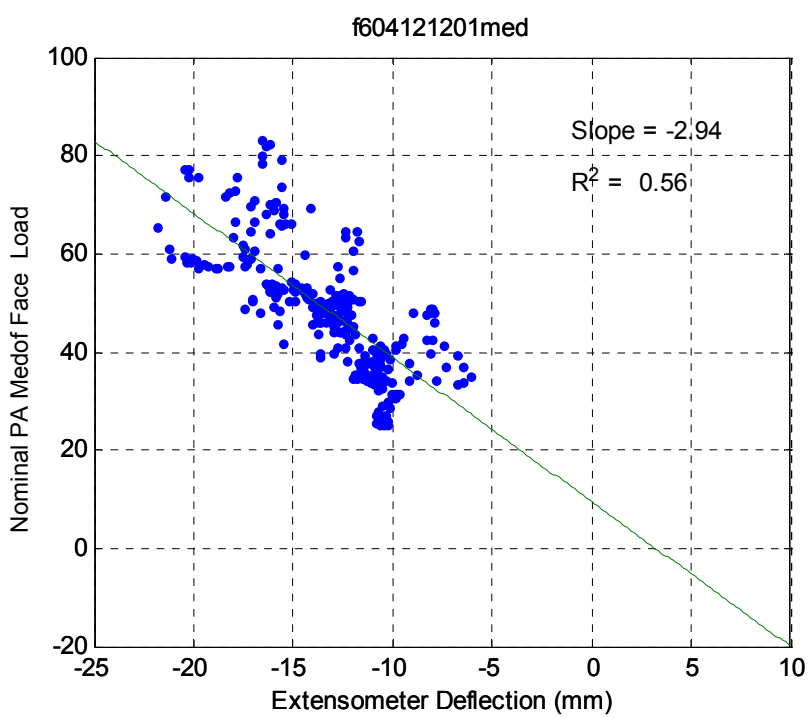
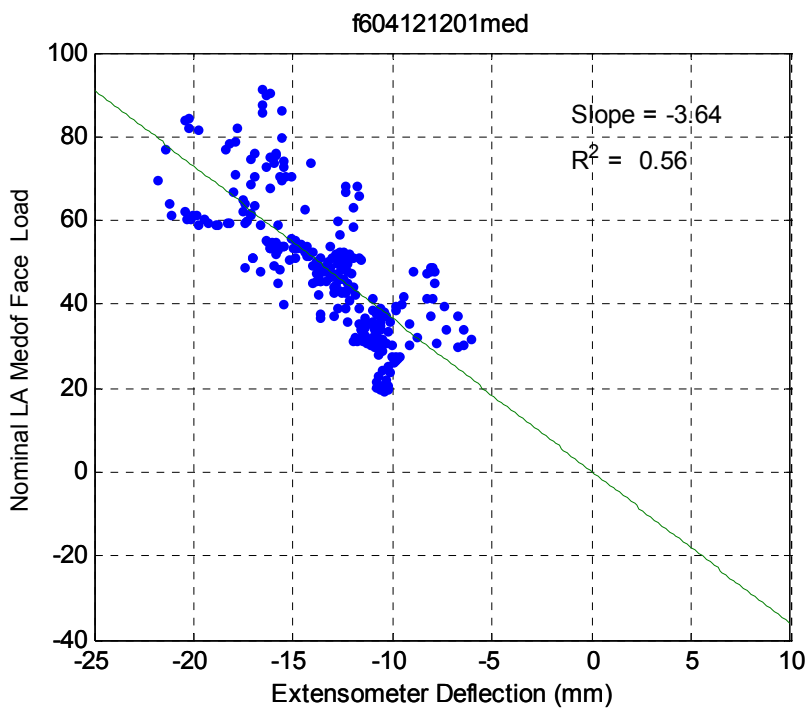


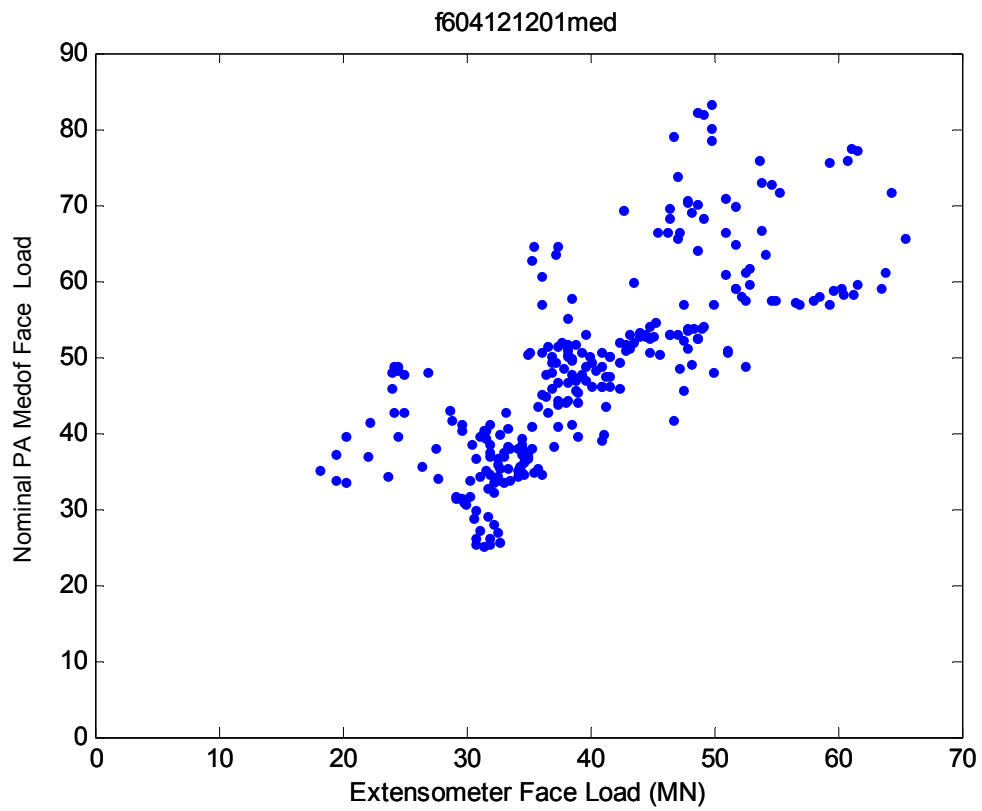


**April 12 – f604121201**  
**2.6 Event ID – 15 - A - 6**

**Crushing**

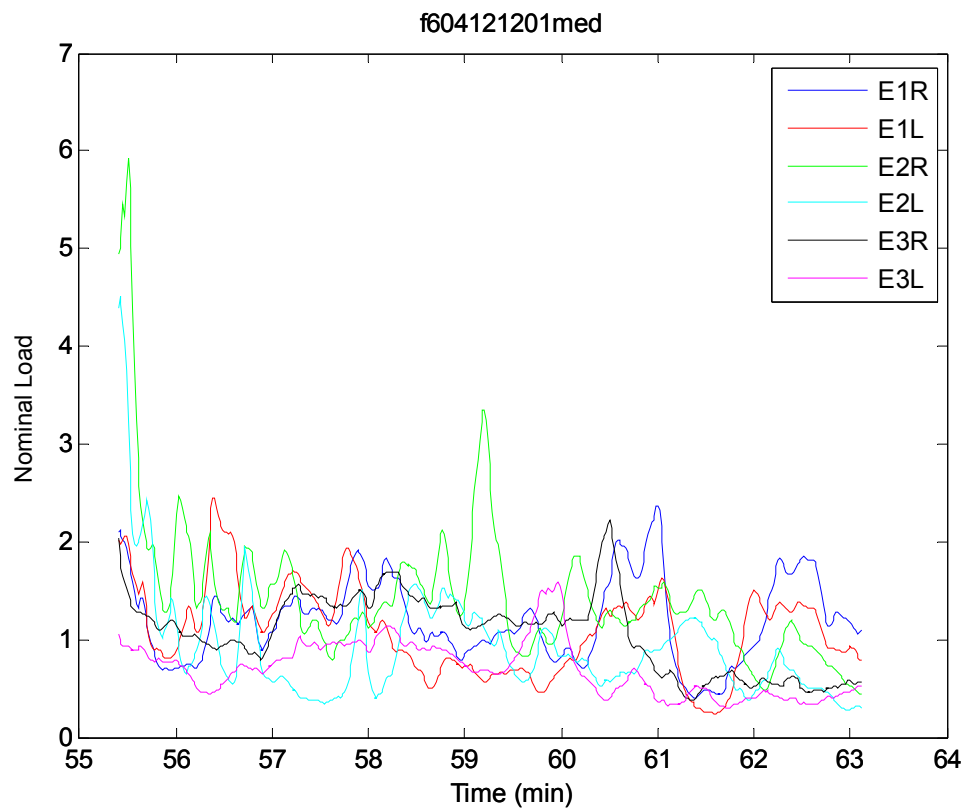


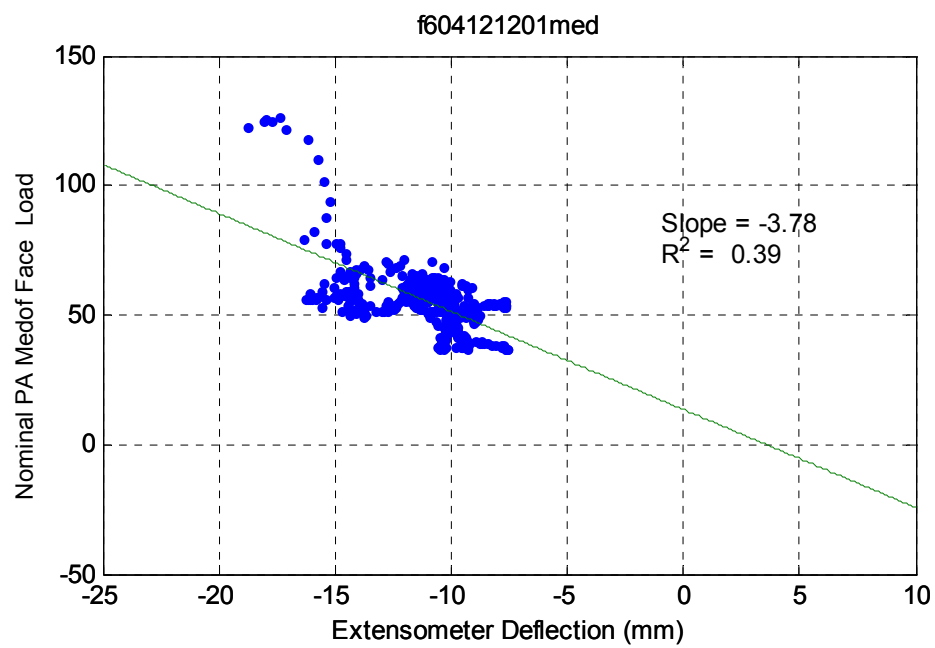
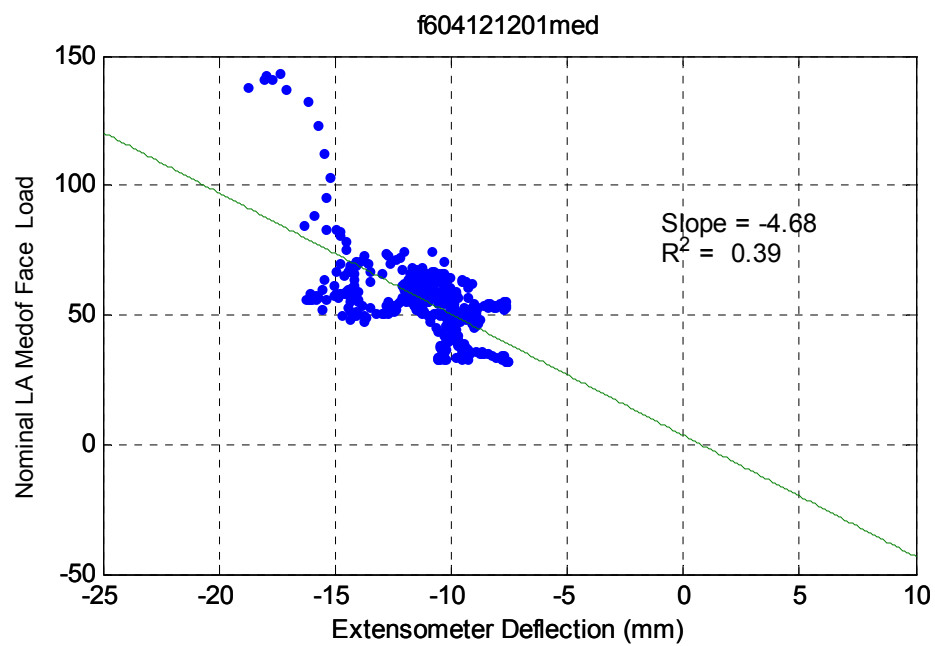


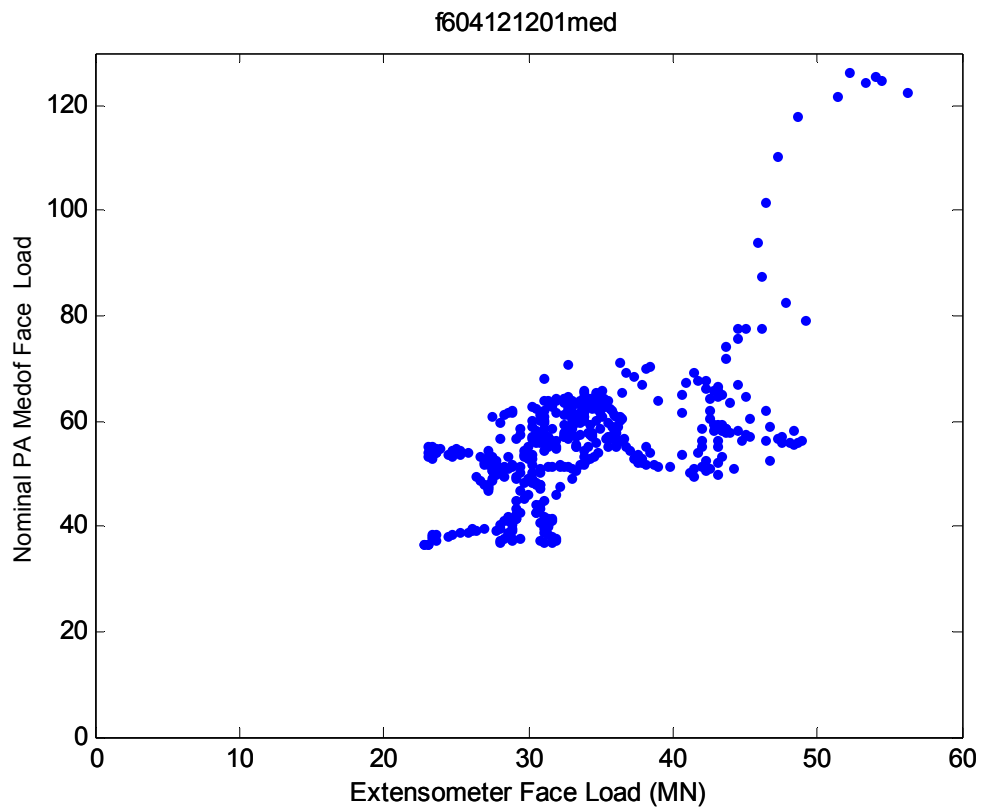


**April 12 – f604121201**  
**2.7 Event ID – 15 - A - 8**

### Crushing

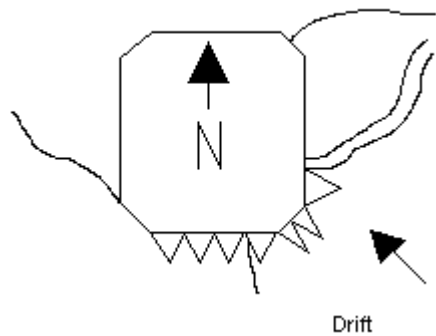






### 3 APRIL 12 – F60412140A

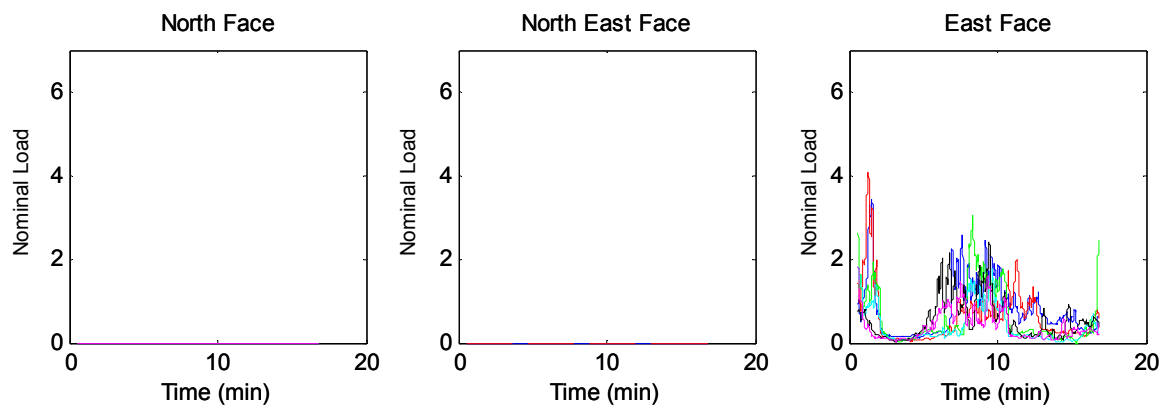
**Event ID – 15 – B**  
**Crushing**  
**Ice Thickness: 5.9m**



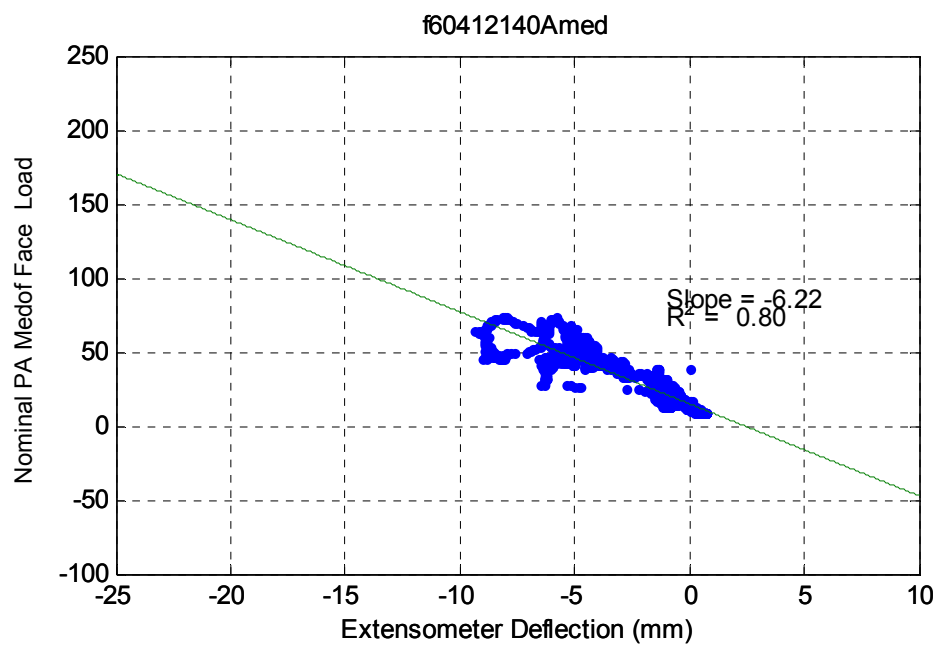
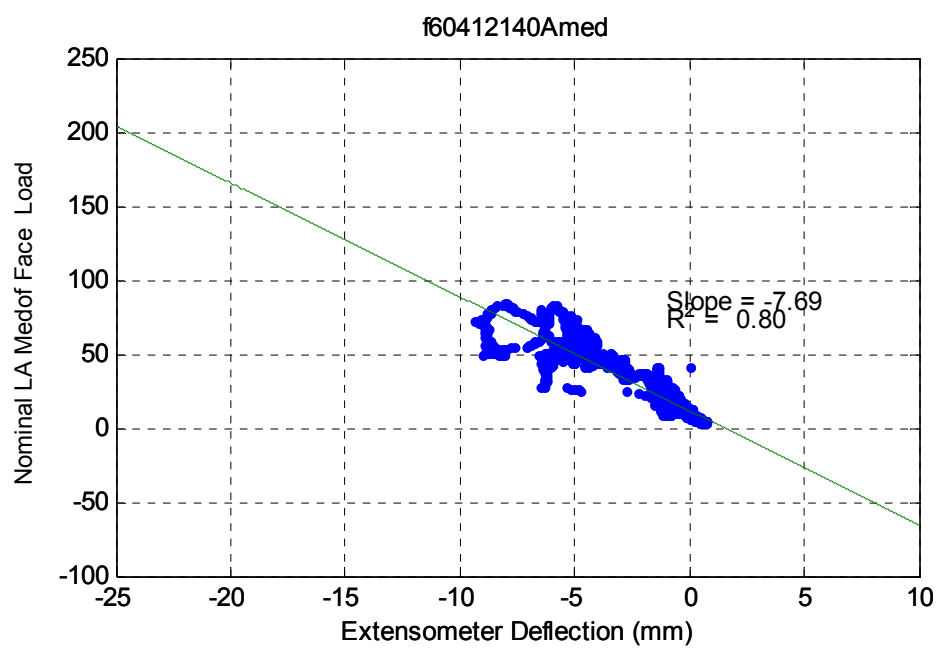
#### Dynamac Event Description

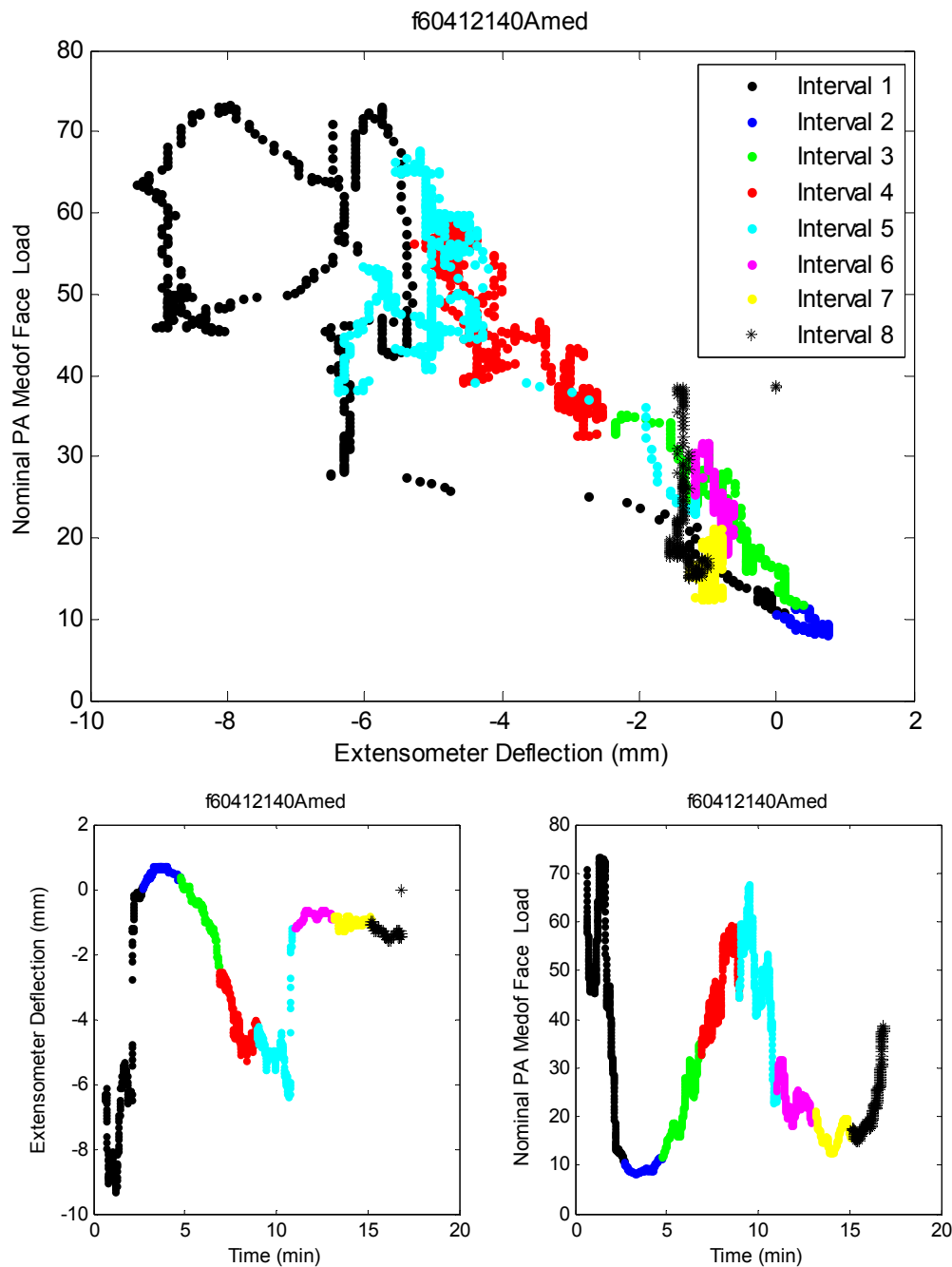
The Molikpaq contacted multi-year ice on the S, SE & E faces resulting in extrusion-collapse cycles.

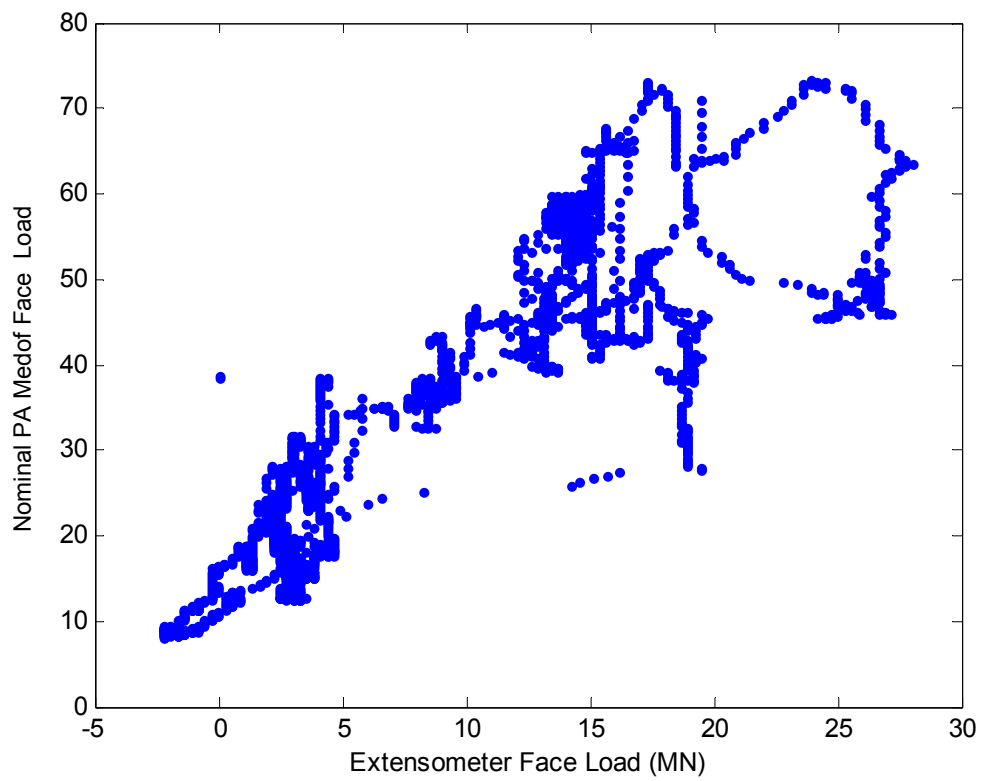
Note: The Bottom panel is loaded during this event. Some modeling of the effect of the bottom panel is required.



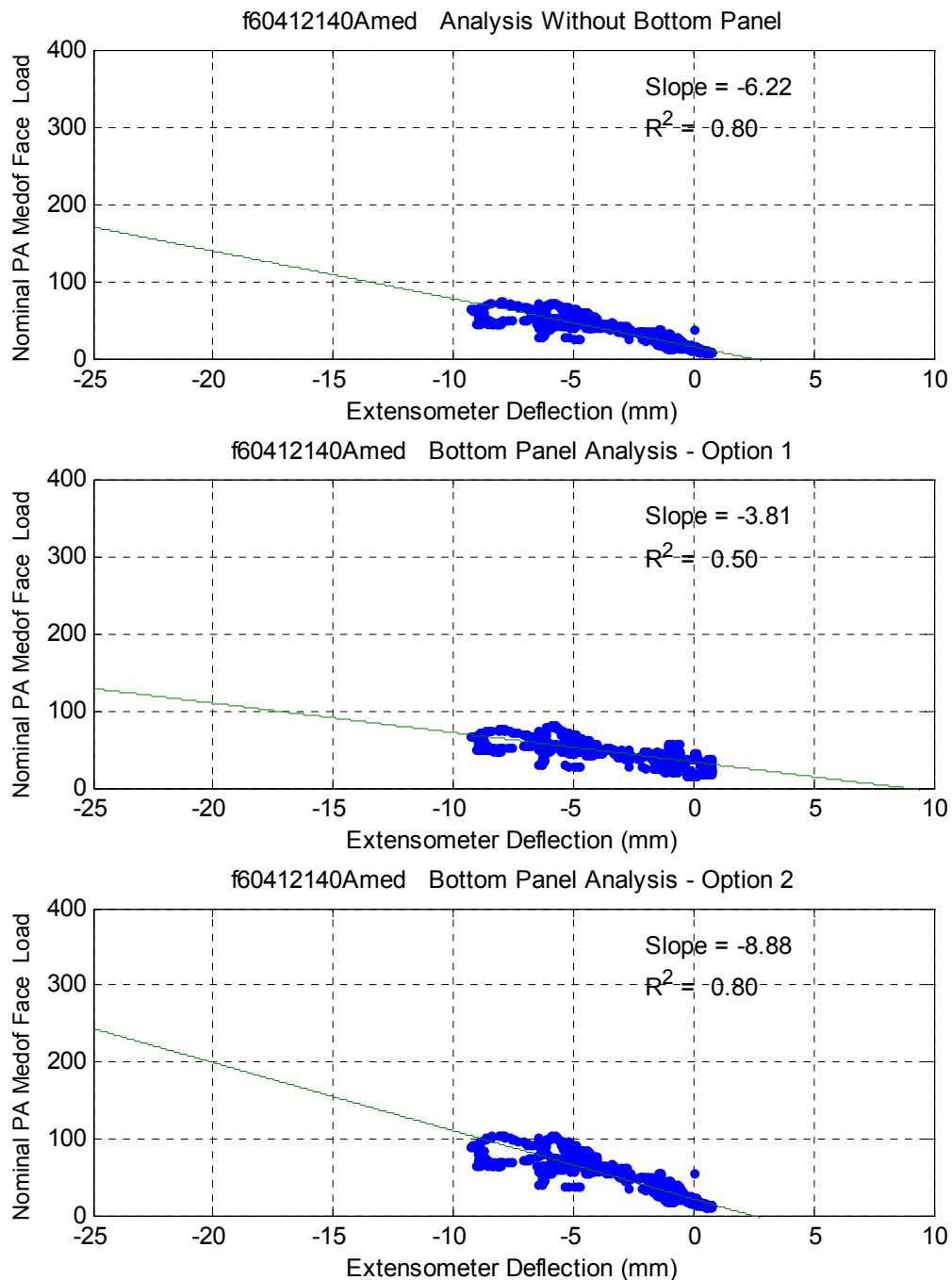
<i>Event ID</i>	<i>Date</i>	<i>Fast File</i>	<i>Segment</i>	<i>Time Period</i>	<i>Failure Mode</i>	<i>Panel Groups</i>	<i>Spacing of Groups</i>
15B	12-Apr (C)	F60412140A	full file	14:19:35 – 14:35:31	CR & MM	E1, E2 & E3	≈ 40m
15B-1			1	14:19:35 – 14:20:56	CR	E1 & E2	≈ 20m
15B-2			2	14:20:57 – 14:35:31	MM	E1, E2 & E3	≈ 40m



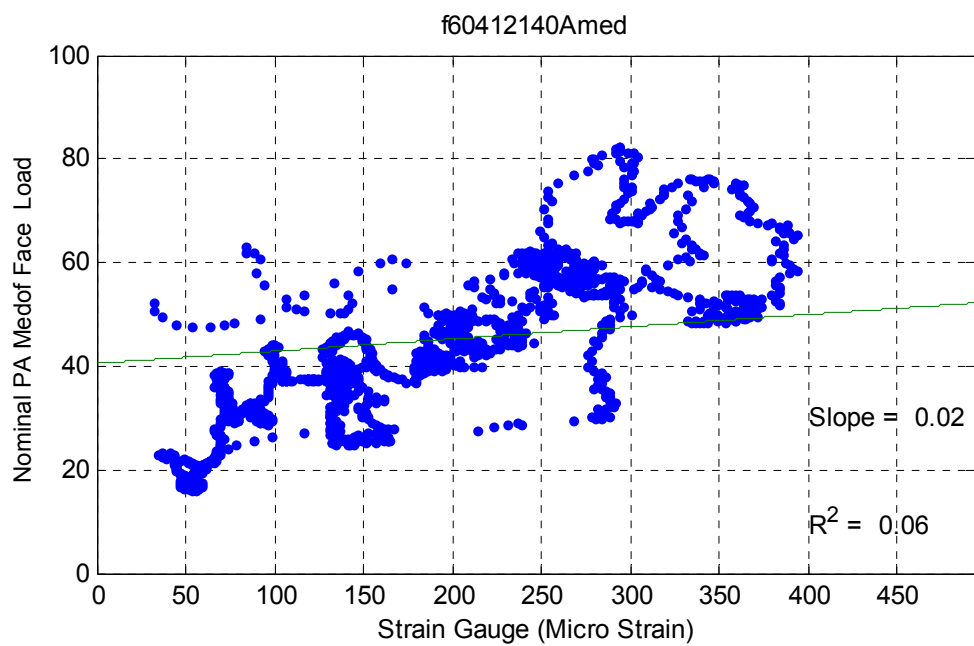
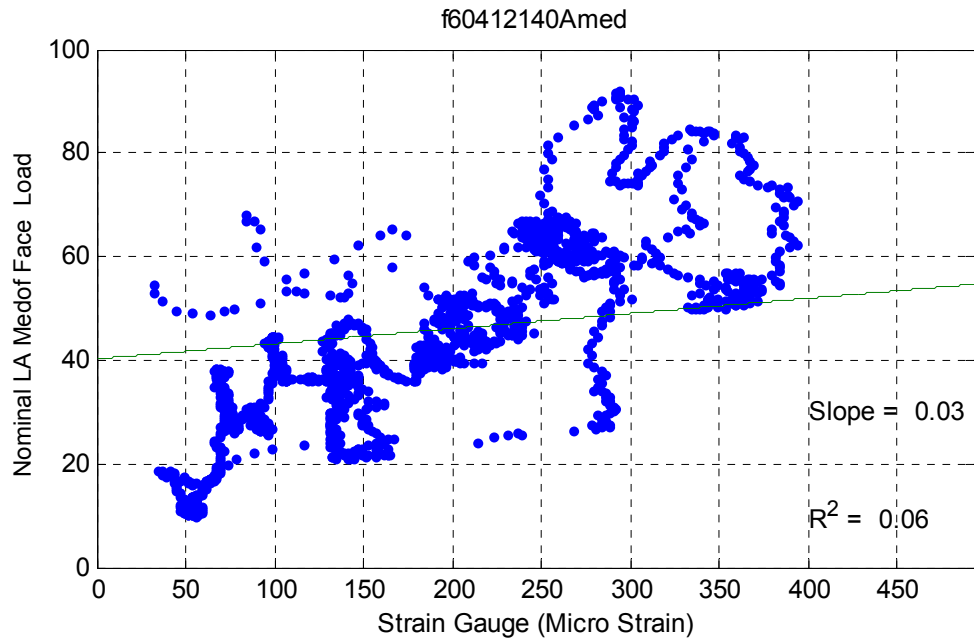




## Analysis of Bottom Panel



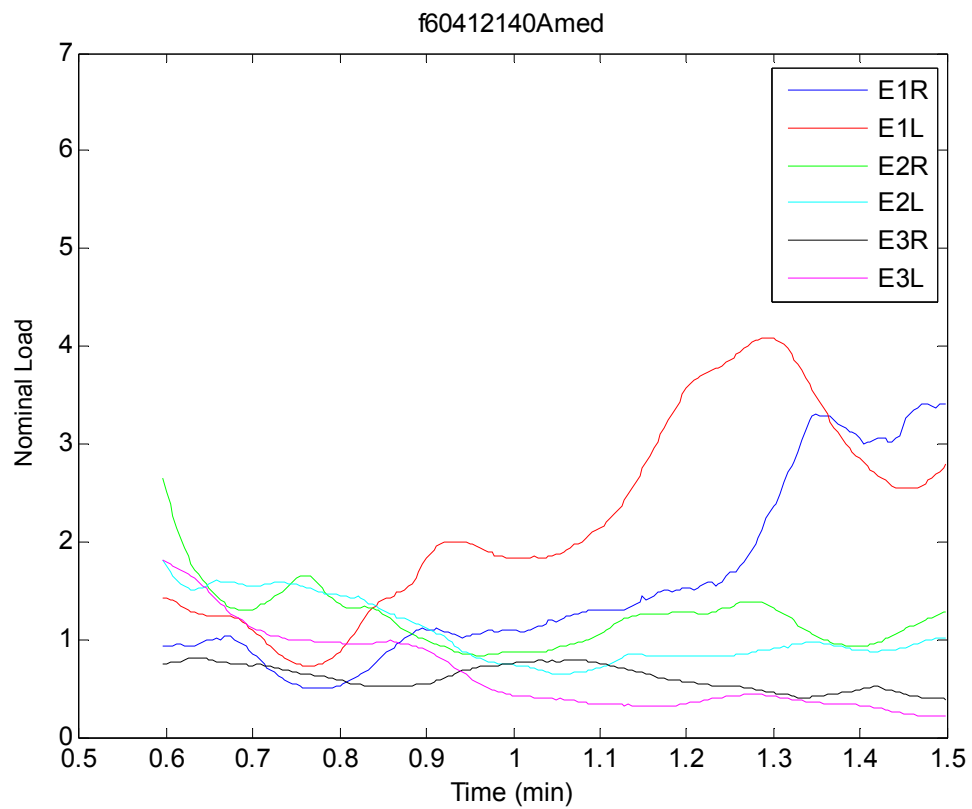
## Strain Gauge Results

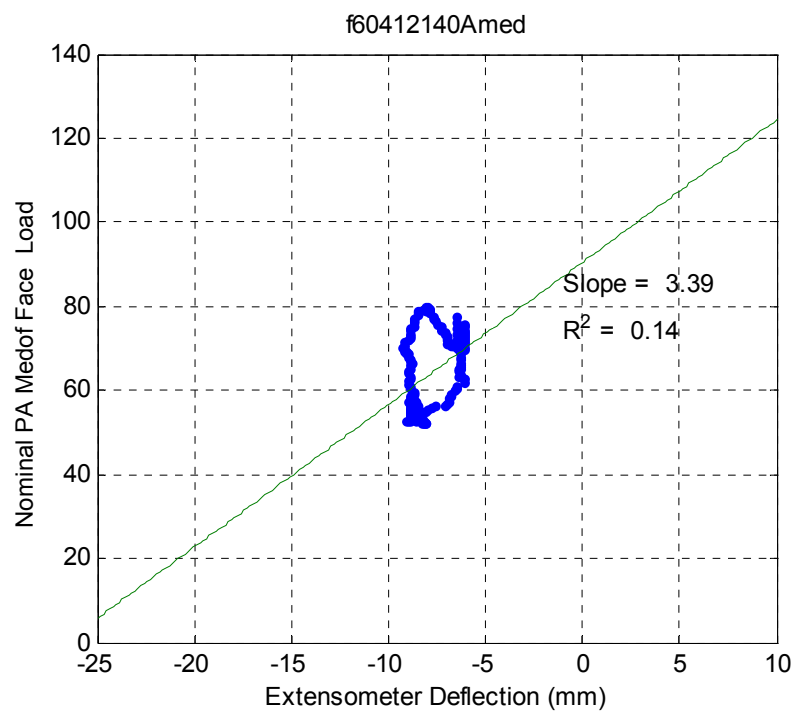
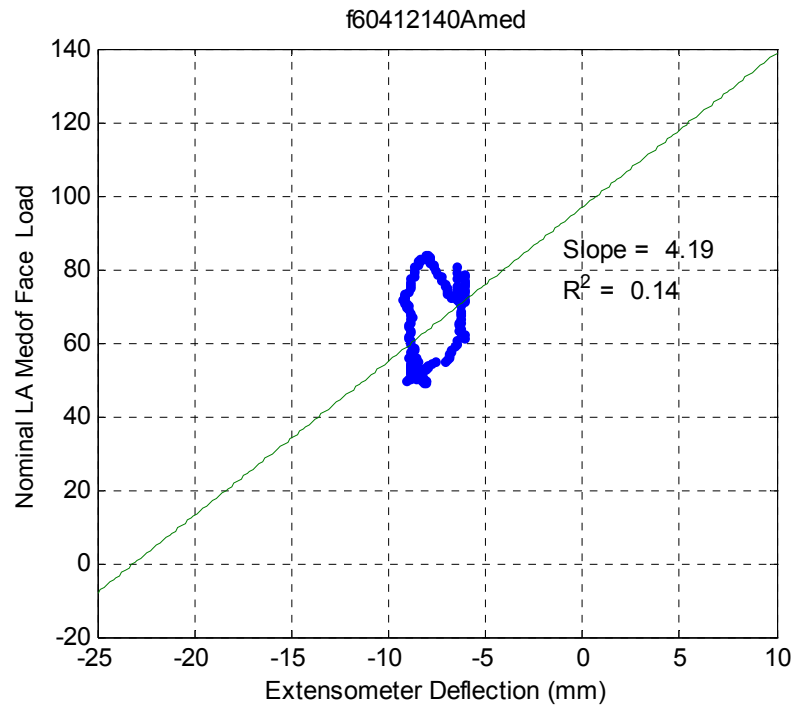


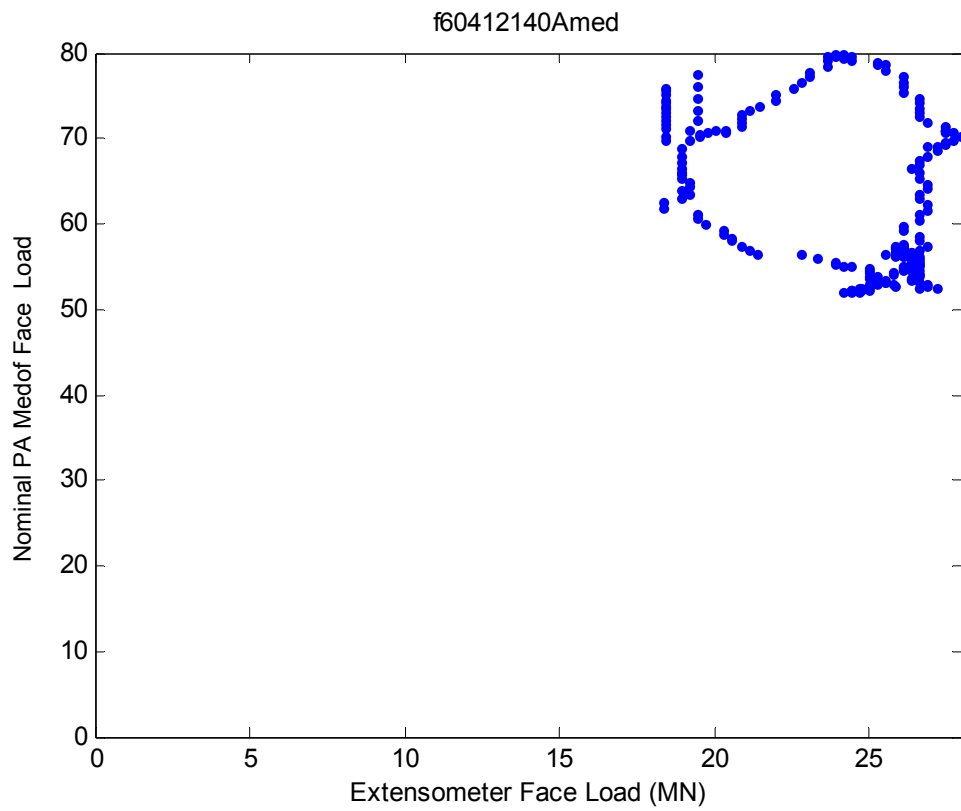
**April 12 – f60412140A**

**3.1 Event ID – 15 - B - 1**

**Crushing**

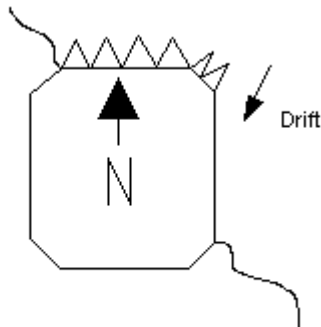






## 4 MAY 12 – F605120301

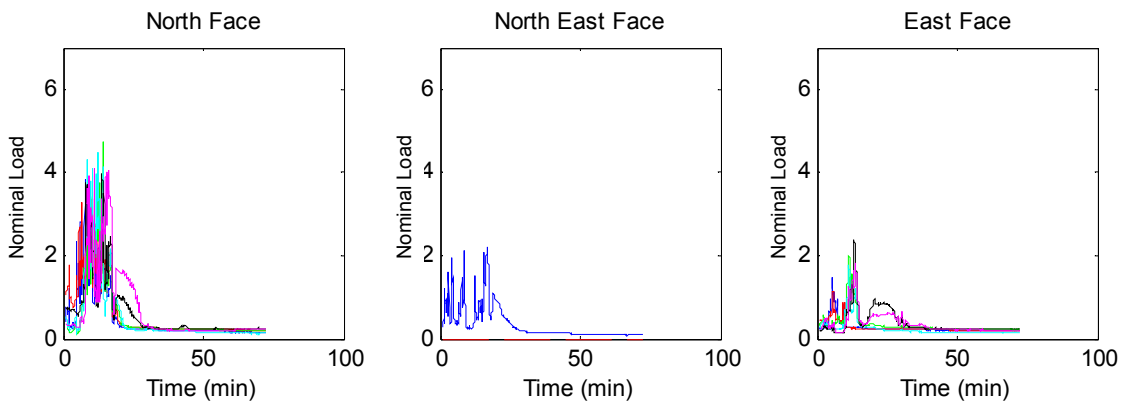
**Event ID – 16**  
**Crushing**  
**Ice Thickness: 2.5m**



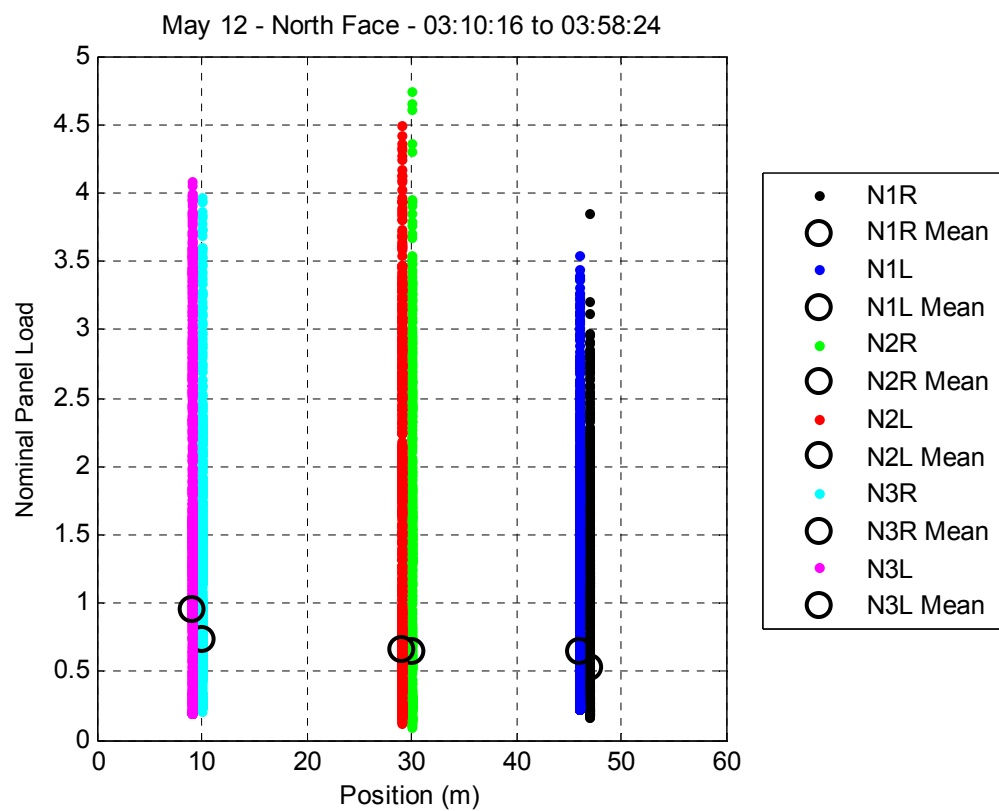
### Dynamac Event Description

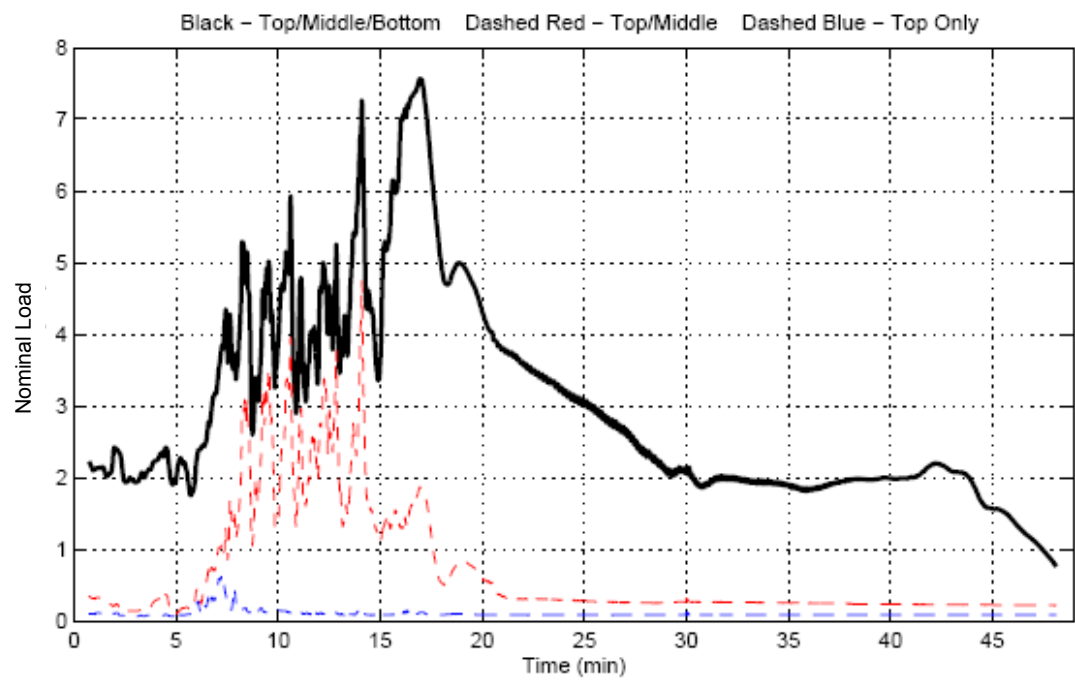
A large floe (4nm x 8nm) of thick 1<sup>st</sup> year ice (with large multi-year inclusions) impacted the Molikpaq. Initial contact was made on the E corner of the N face and the NE face. From the moment of impact, the floe seemed to start decelerating. As its speed reduced, vibrations increased; caused largely by "hammering" movement of the floe. The frequency decreased and the amplitude increased as the drift dropped.

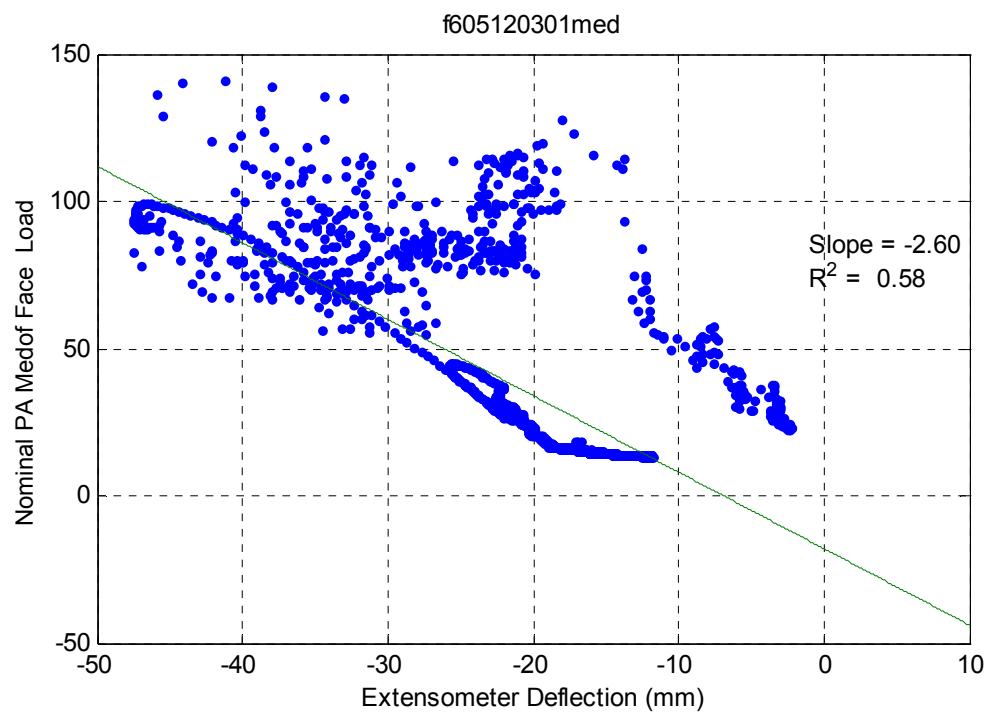
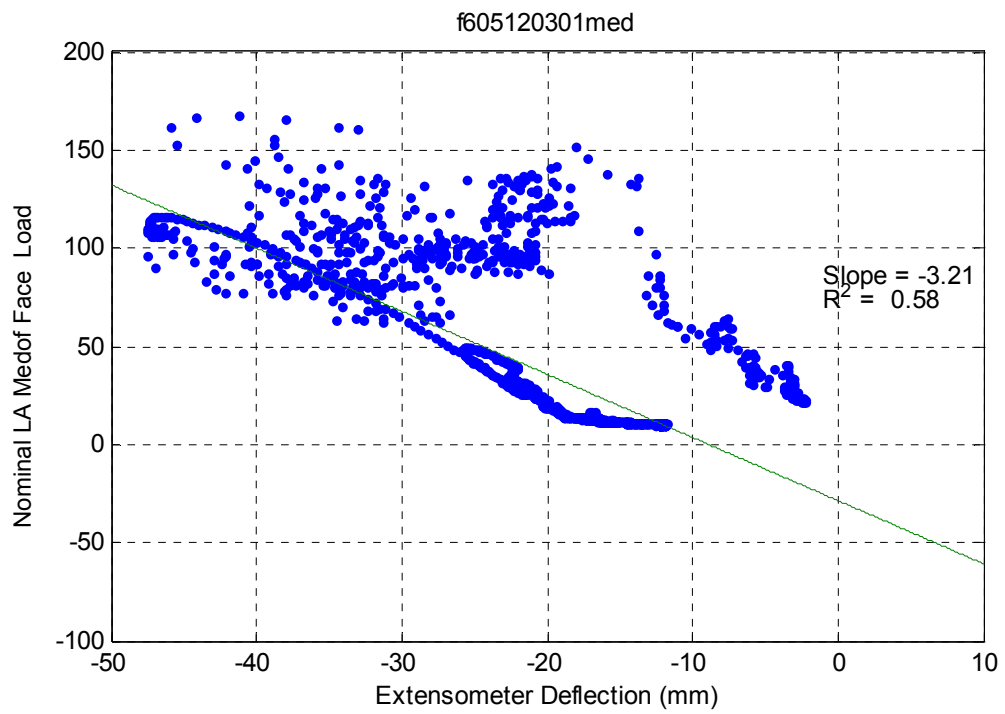
Note: The Bottom panel is loaded during this event. Some modeling of the effect of the bottom panel is required.

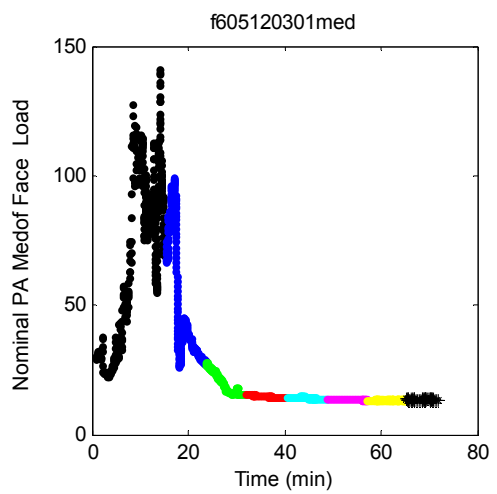
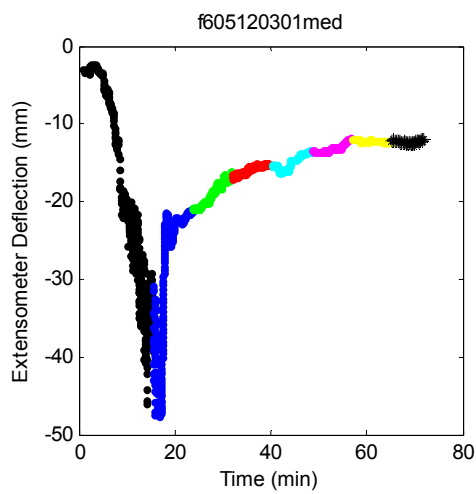
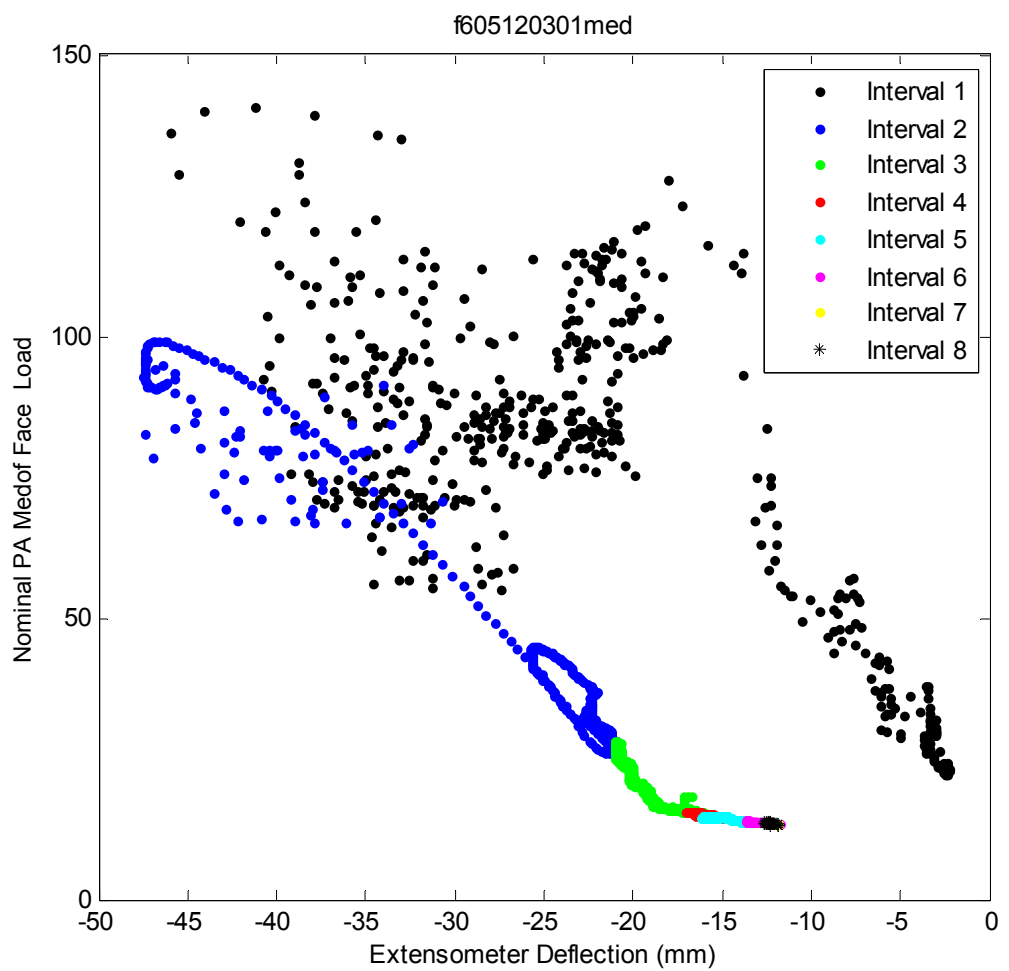


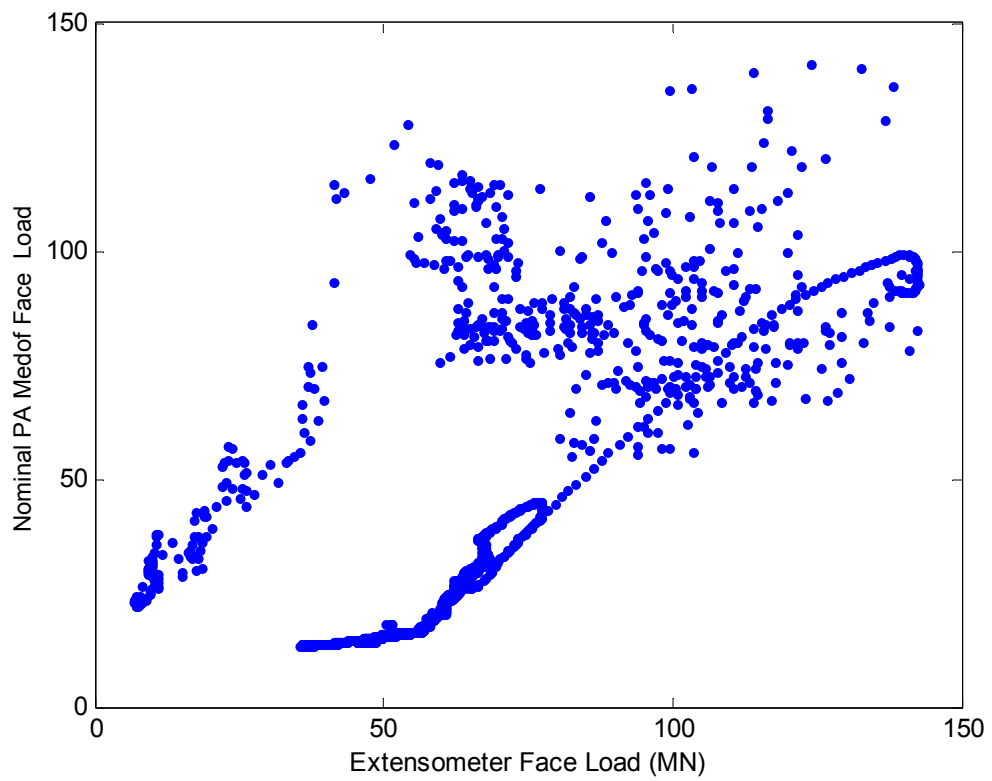
<i>Event ID</i>	<i>Date</i>	<i>Fast File</i>	<i>Segment</i>	<i>Time Period</i>	<i>Failure Mode</i>	<i>Panel Groups</i>	<i>Spacing of Groups</i>
16	12-May (C)	F605120301	Full file	03:10:16 – 03:58:24	CR, MM & SLW	N1, N2 & N3	≈ 40m
16-1			1	03:10:16 – 03:16:28	MM	N1, N2 & N3	≈ 40m
16-2			2	03:16:29 – 03:19:28	CR	N1, N2 & N3	≈ 40m
16-3			3	03:19:29 – 03:22:23	MM	N1, N2 & N3	≈ 40m
16-4			4	03:22:24 – 03:27:33	CR	N1, N2 & N3	≈ 40m
16-5			5	03:27:34 – 03:58:24	SLW	N1, N2 & N3	≈ 40m



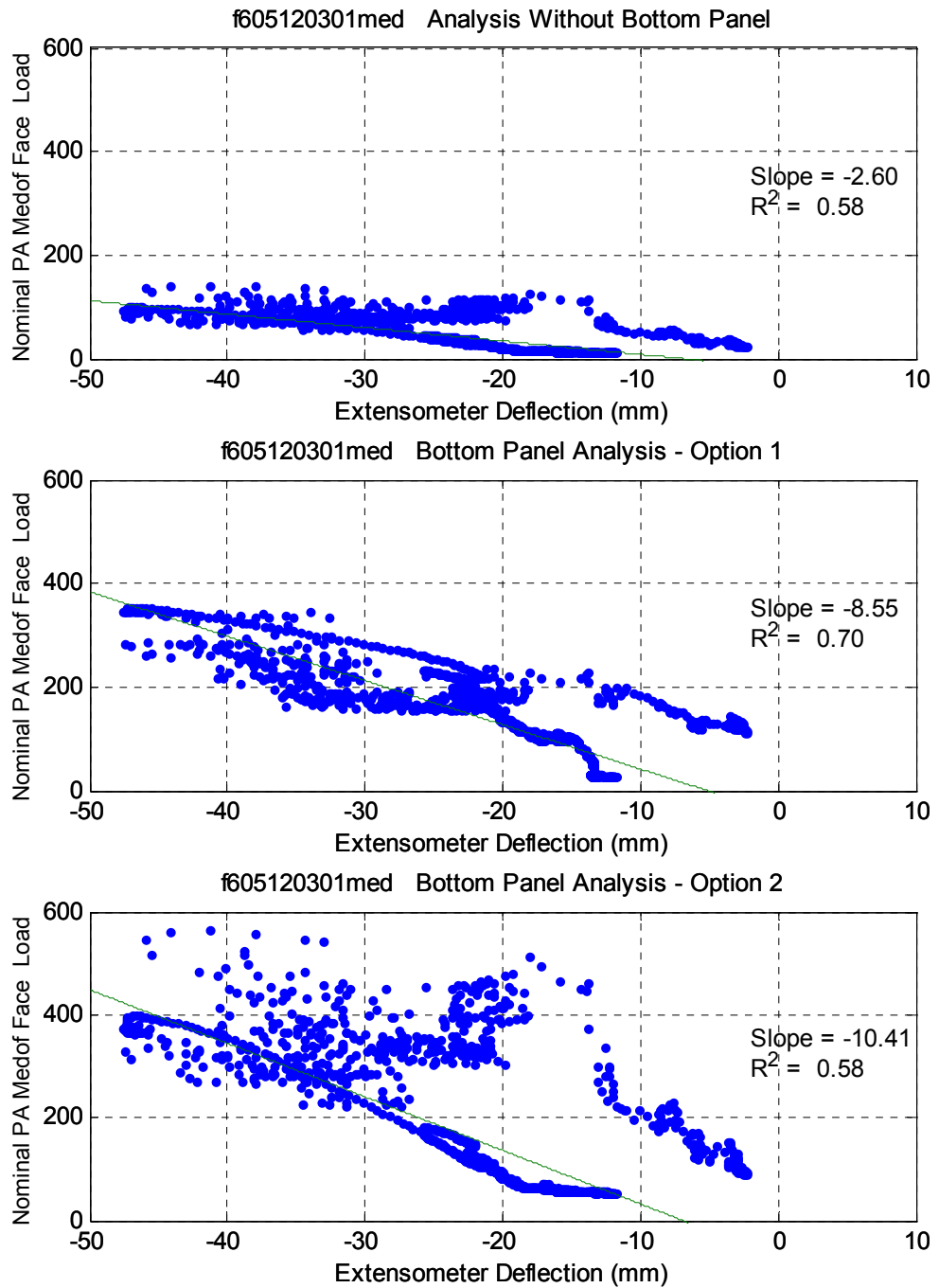




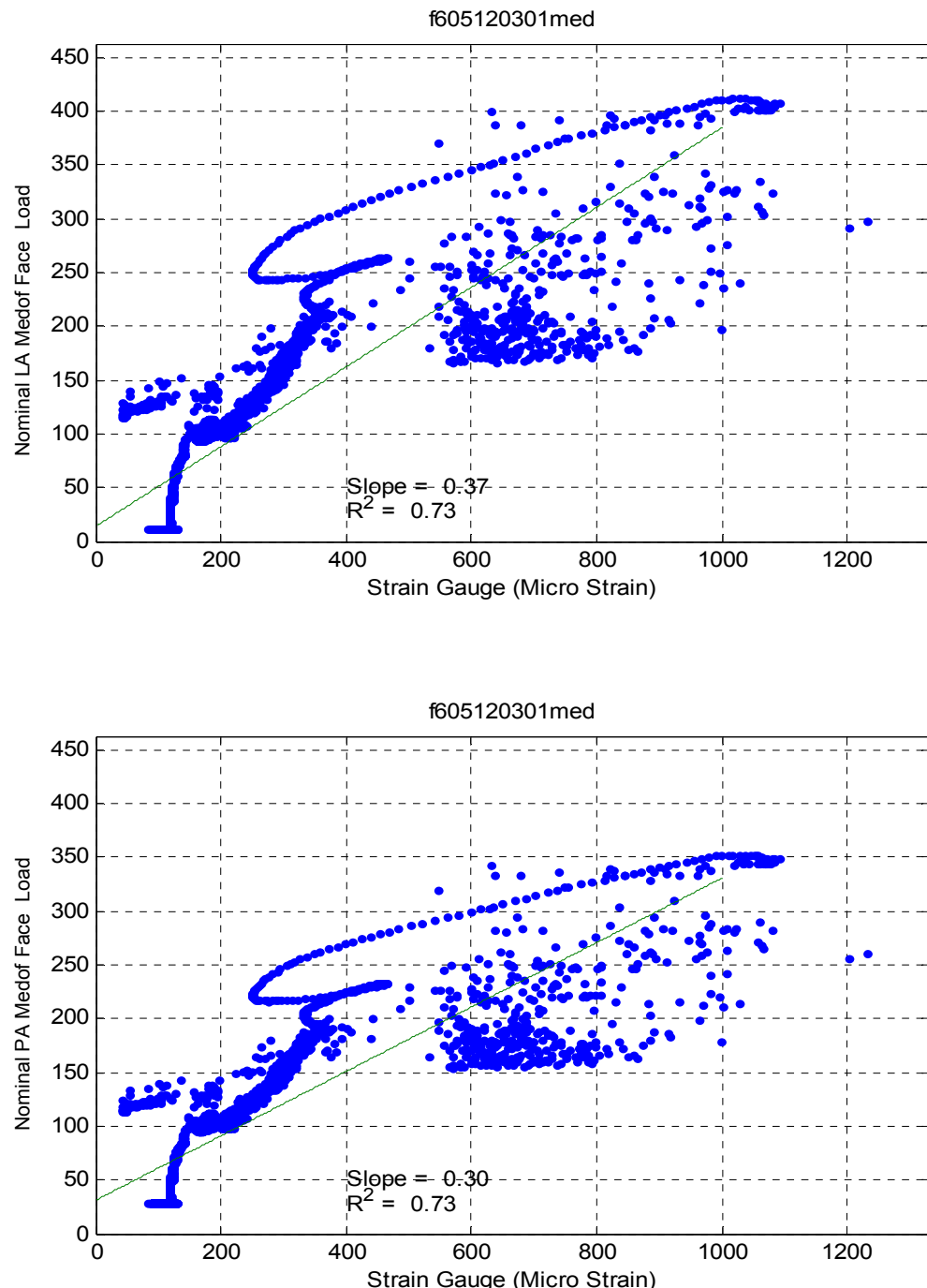




## Bottom Panel Analysis

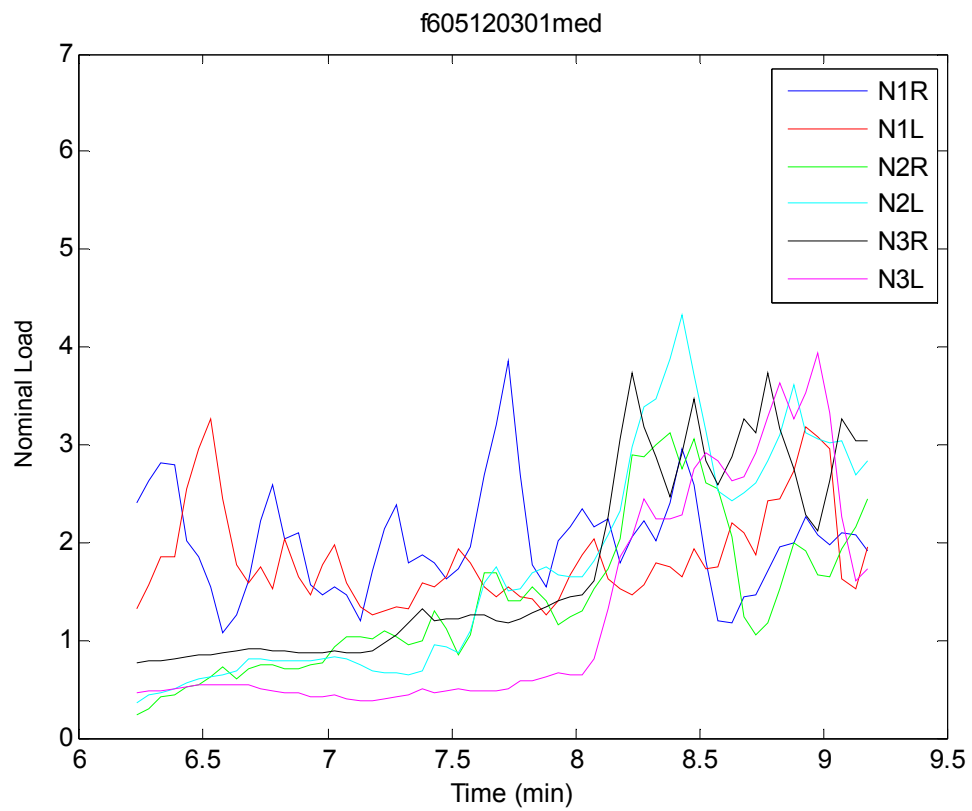


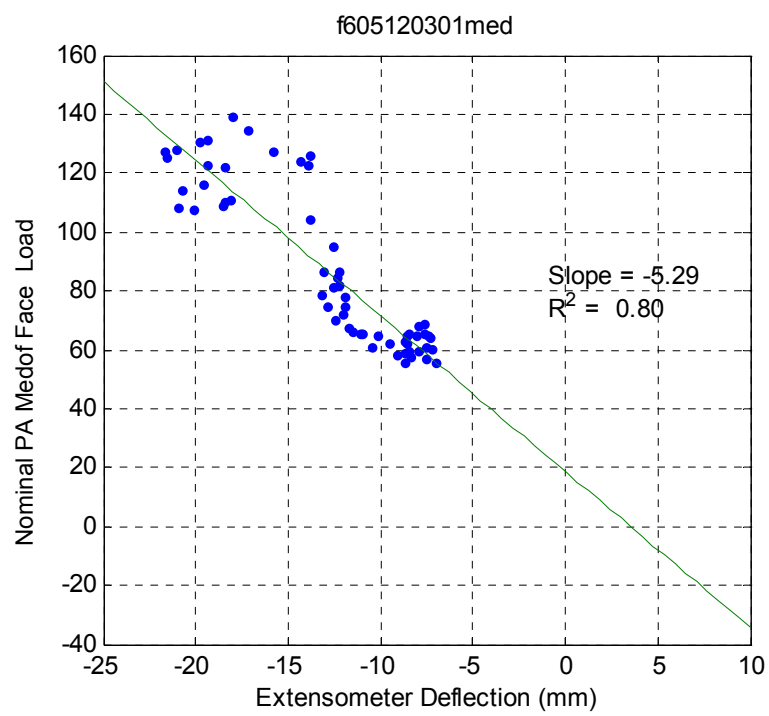
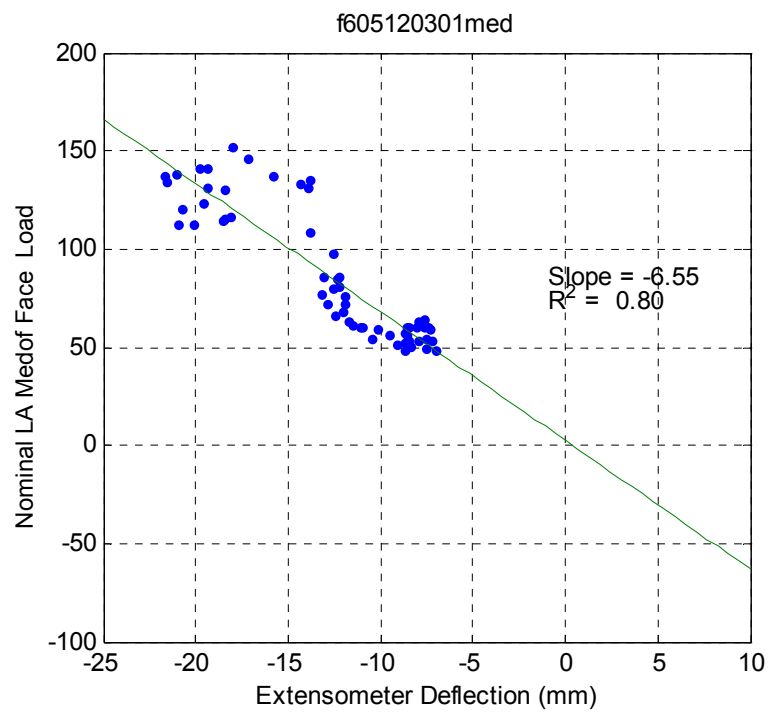
## Strain Gauge Results

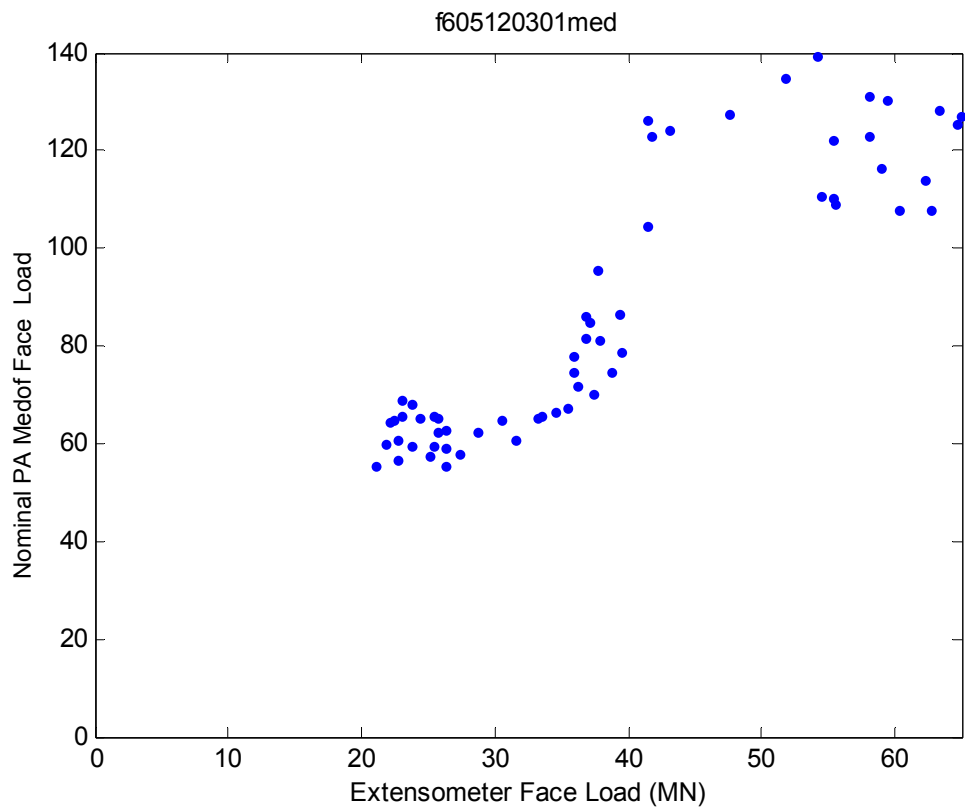


**May 12 – f605120301**  
**4.1 Event ID – 16 - 2**

**Crushing**

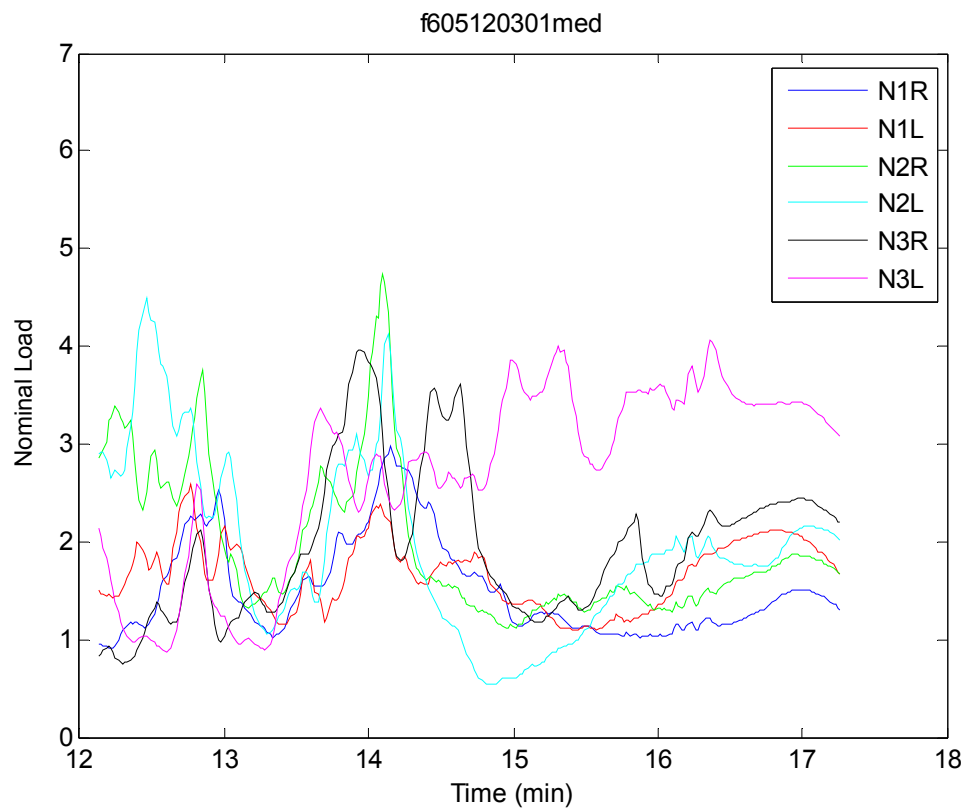


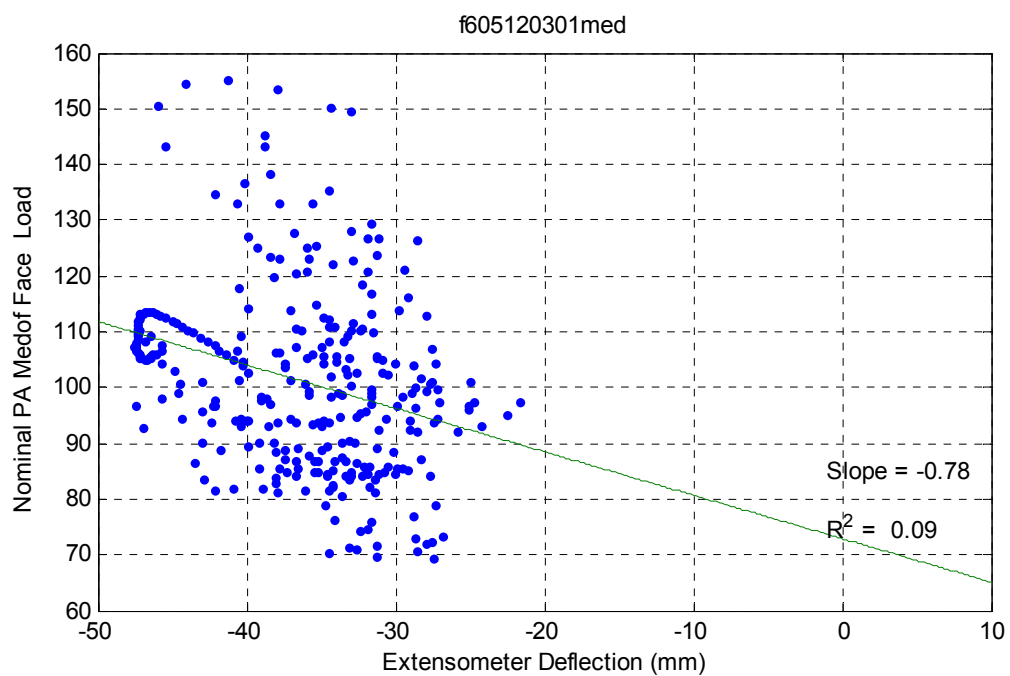
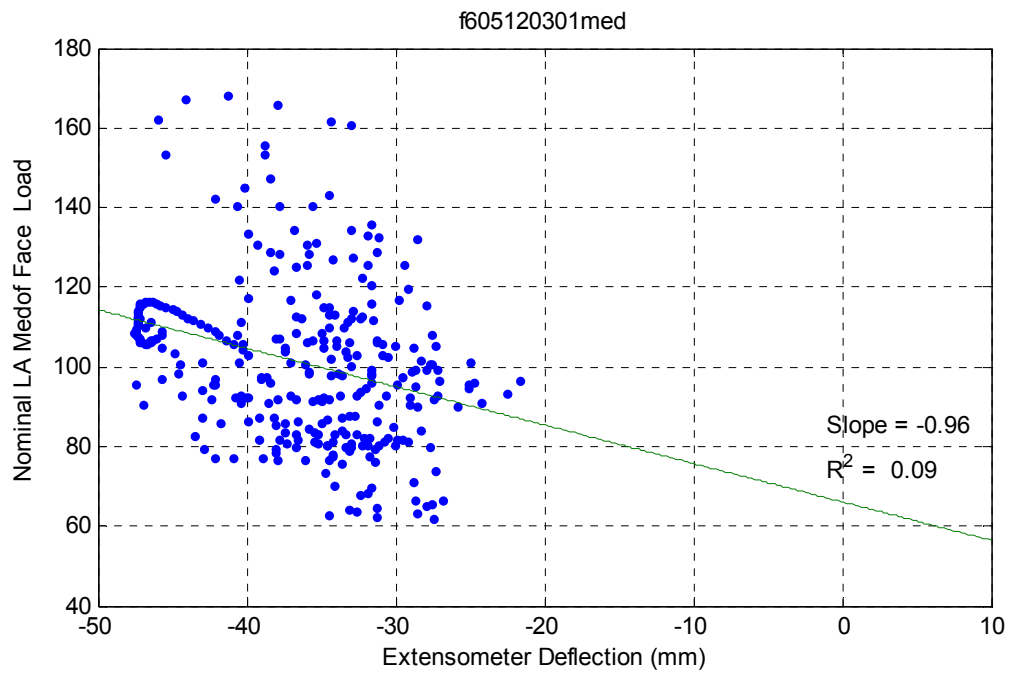


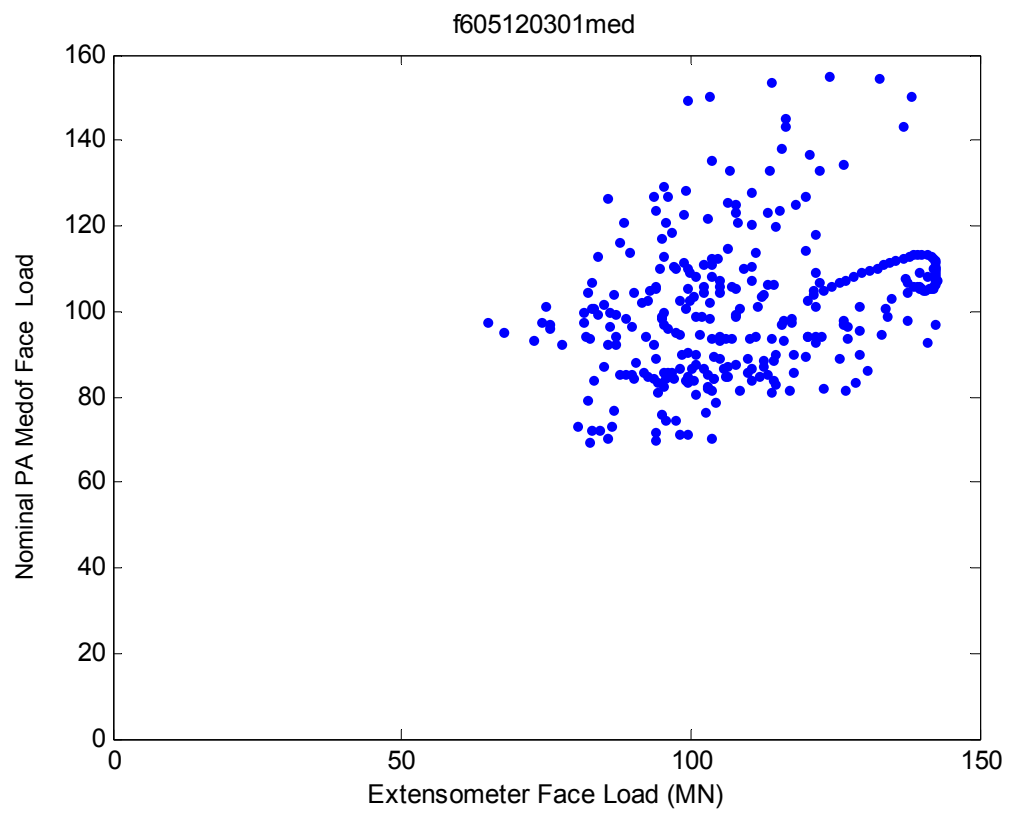


**May 12 – f605120301**  
**4.2 Event ID – 16 - 4**

**Crushing**

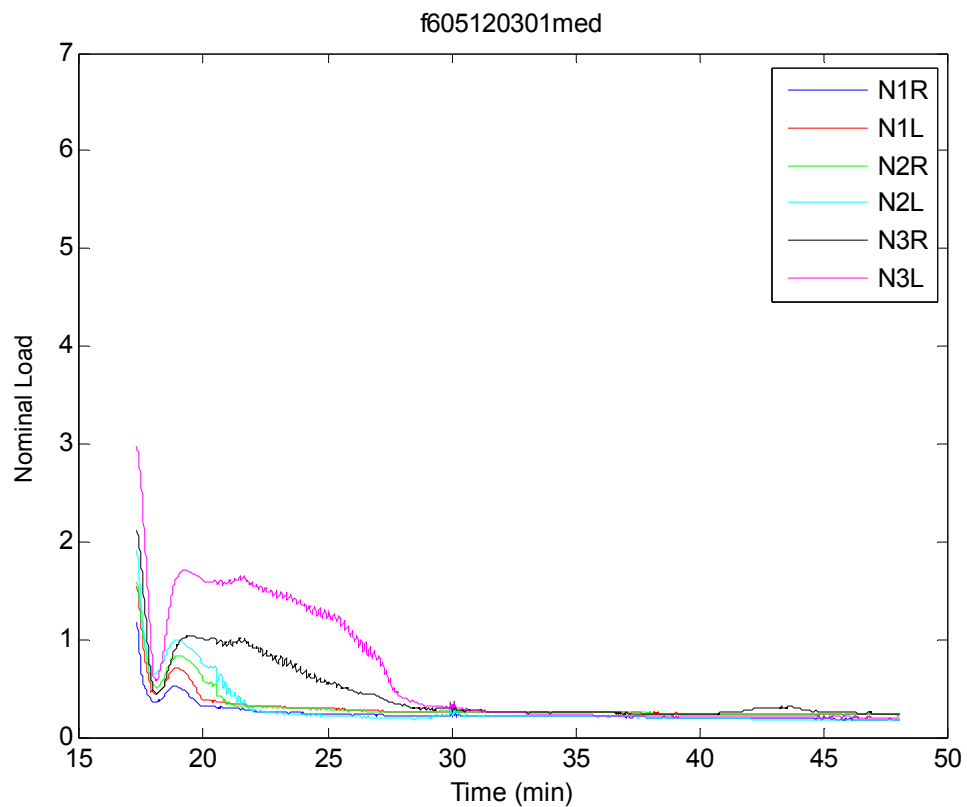


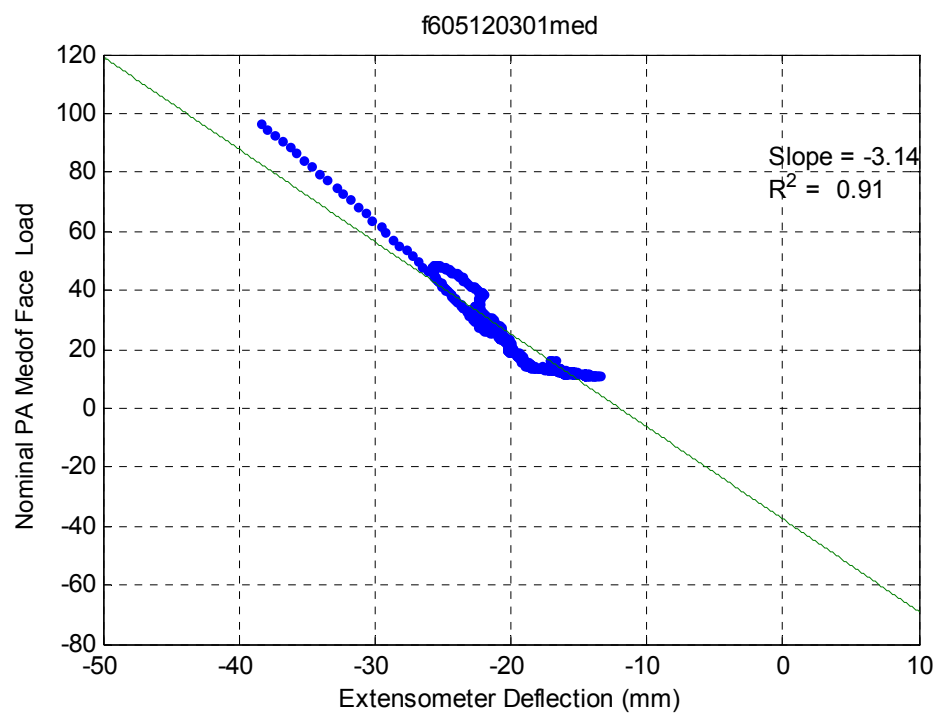
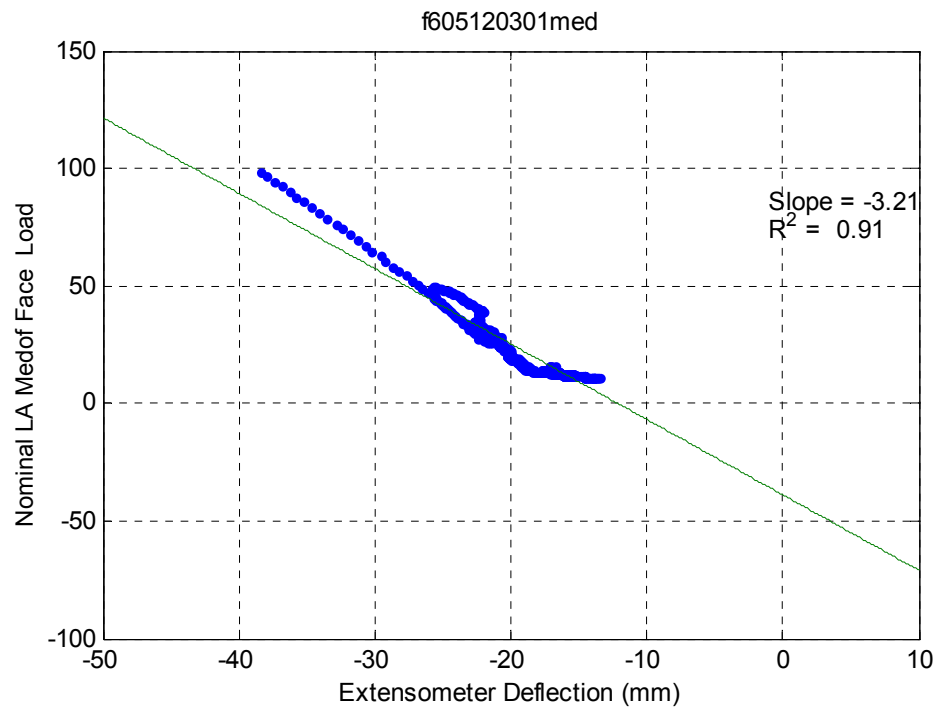


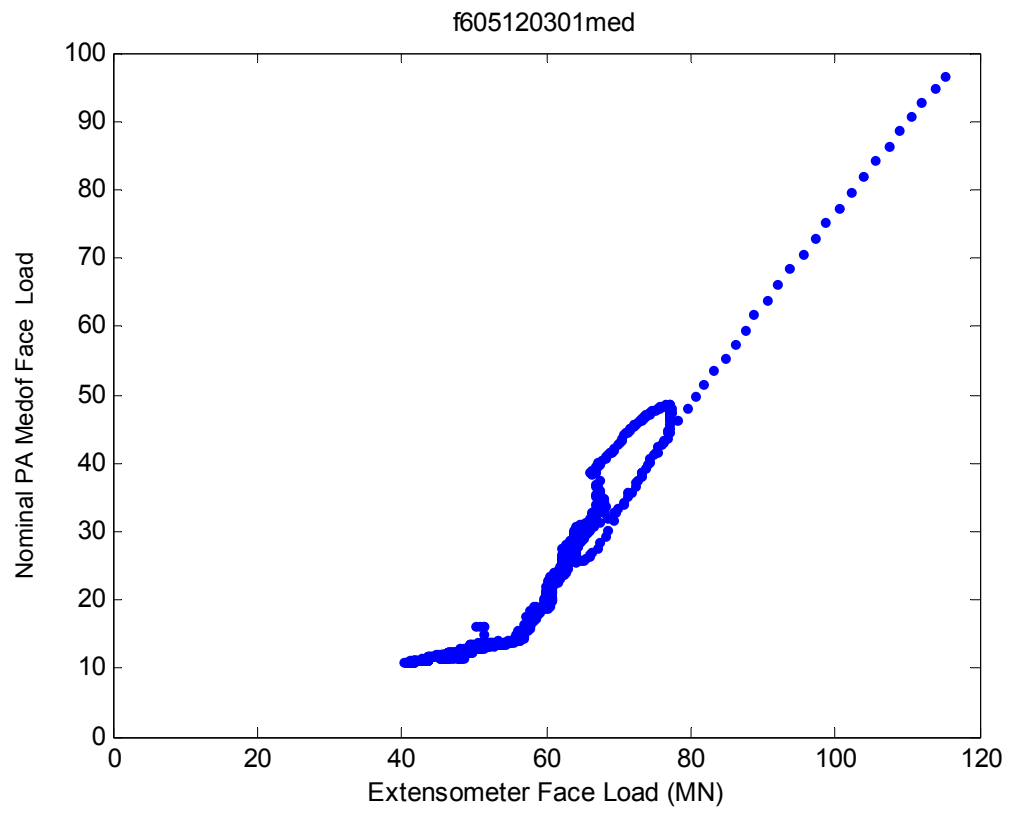


**May 12 – f605120301**  
**4.3 Event ID – 16 - 5**

**Creep**





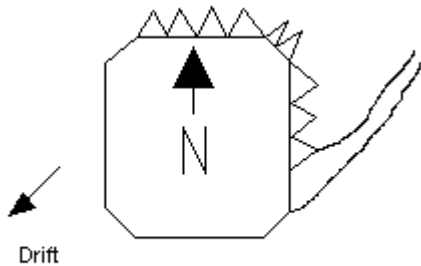


## 5 MAY 22 – F605220801

**Event ID – 17**

**Creep**

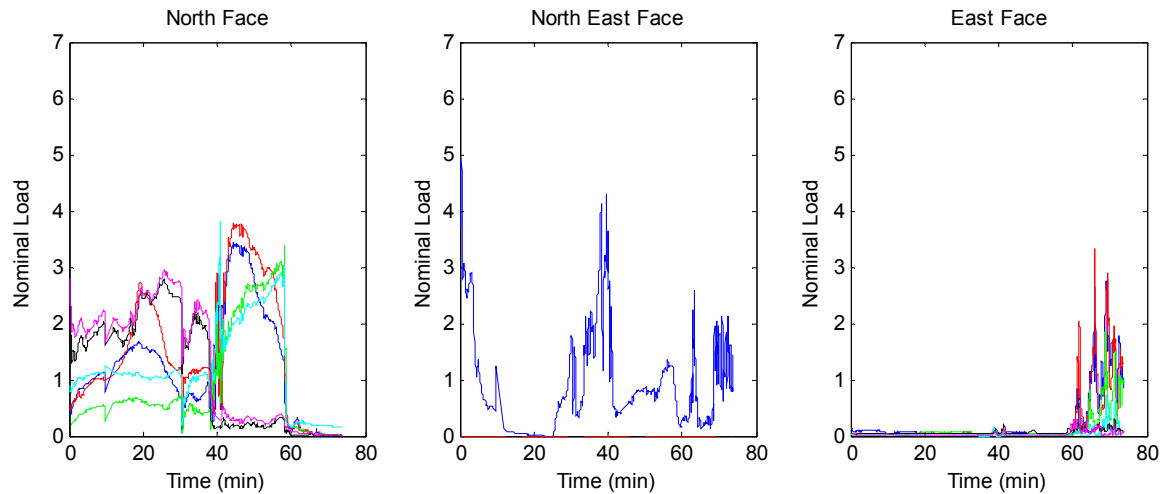
**Ice Thickness: 2.5m**



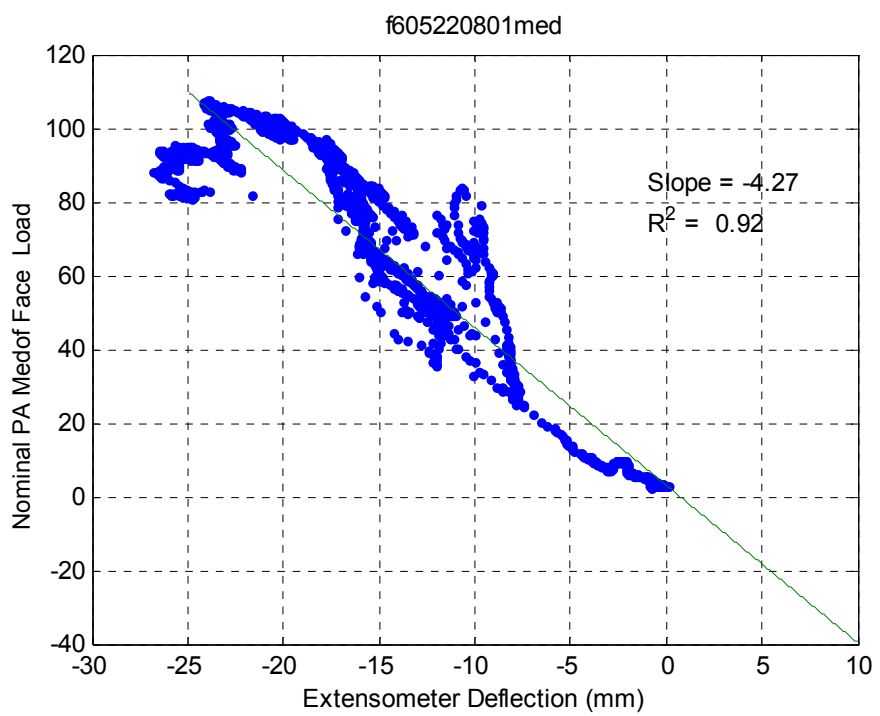
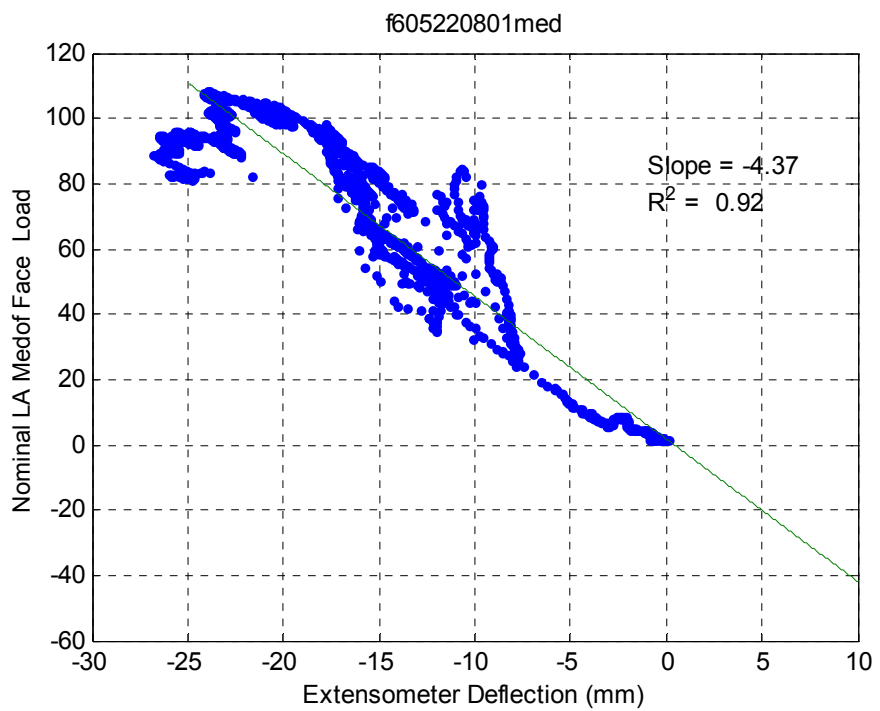
### Dynamac event Description

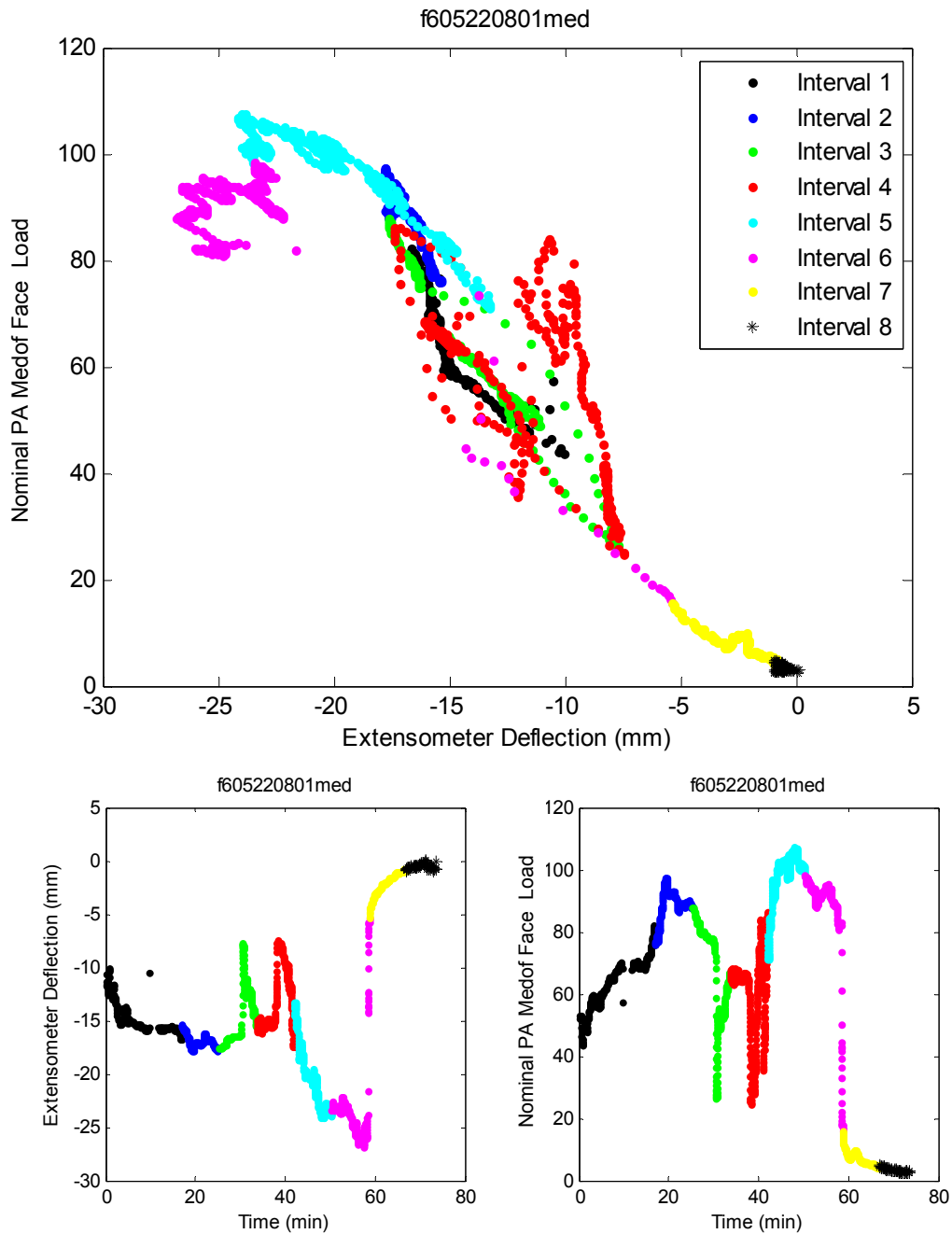
Creep loading from thick FY ice on the N & NE faces caused failure through crushing. As the ice sheet continued to drift, the leading edge started to contact the E face resulting in crushing and substantial sliding toward the south.

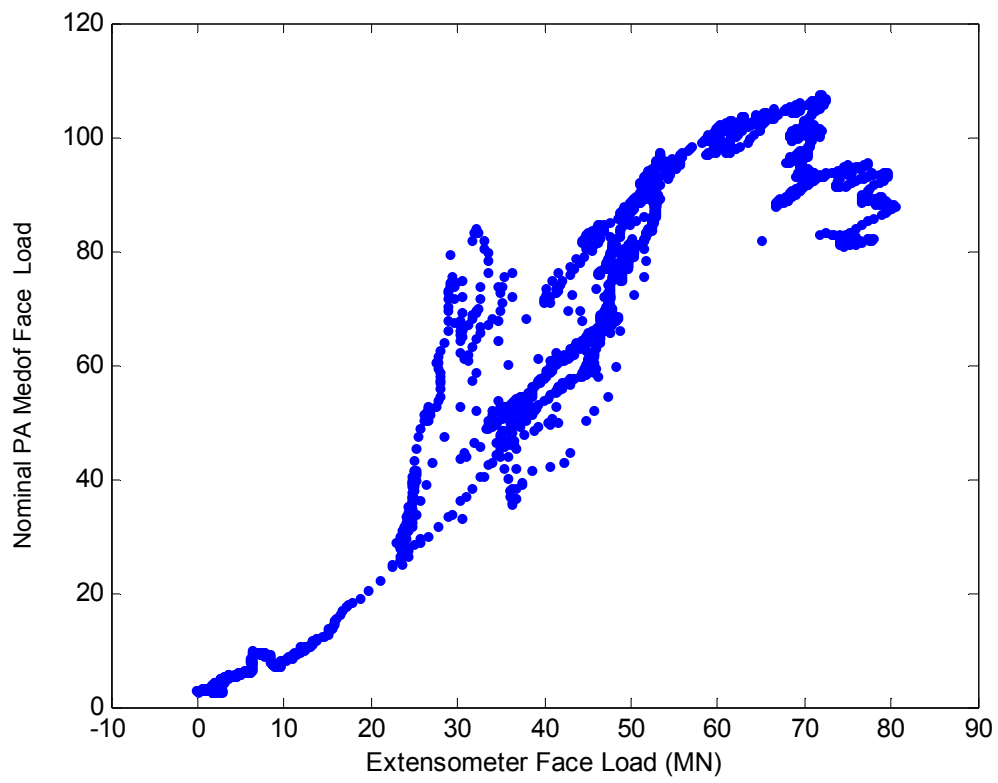
Note: The Bottom panel is loaded during this event. Some modeling of the effect of the bottom panel is required.



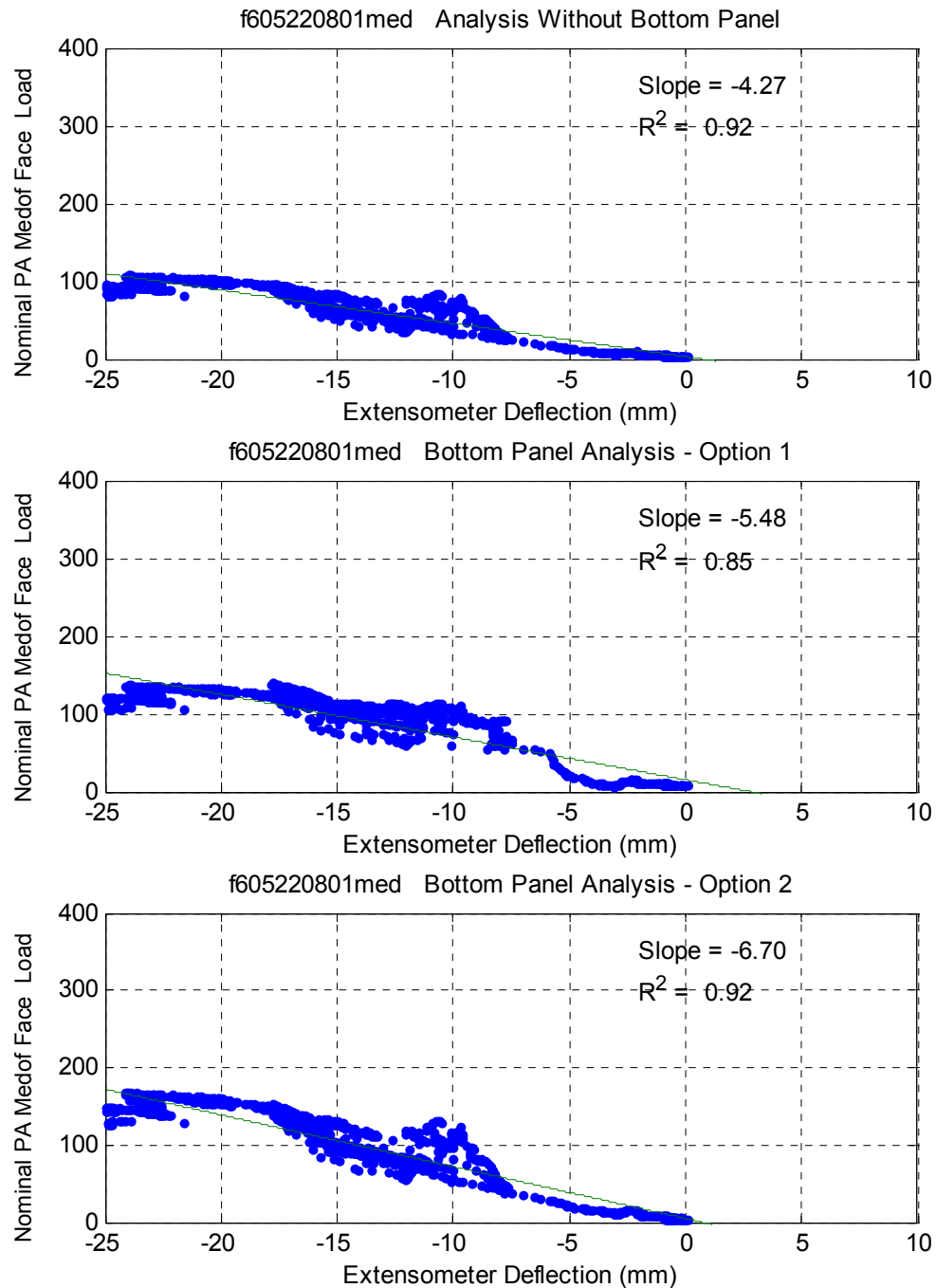
<i>Event ID</i>	<i>Date</i>	<i>Fast File</i>	<i>Segment</i>	<i>Time Period</i>	<i>Failure Mode</i>	<i>Panel Groups</i>	<i>Spacing of Groups</i>
17	22-May (C)	F605220801	full file	08:39:23 – 09:50:27	SLW & MM	N1, N2 & N3	≈ 40m
17-1			1	08:39:23 – 09:16:56	SLW	N1, N2 & N3	≈ 40m
17-2			2	09:16:57 – 09:21:25	MM	N1, N2 & N3	≈ 40m
17-3			3	09:21:26 – 09:29:50	SLW	N1, N2 & N3	≈ 40m



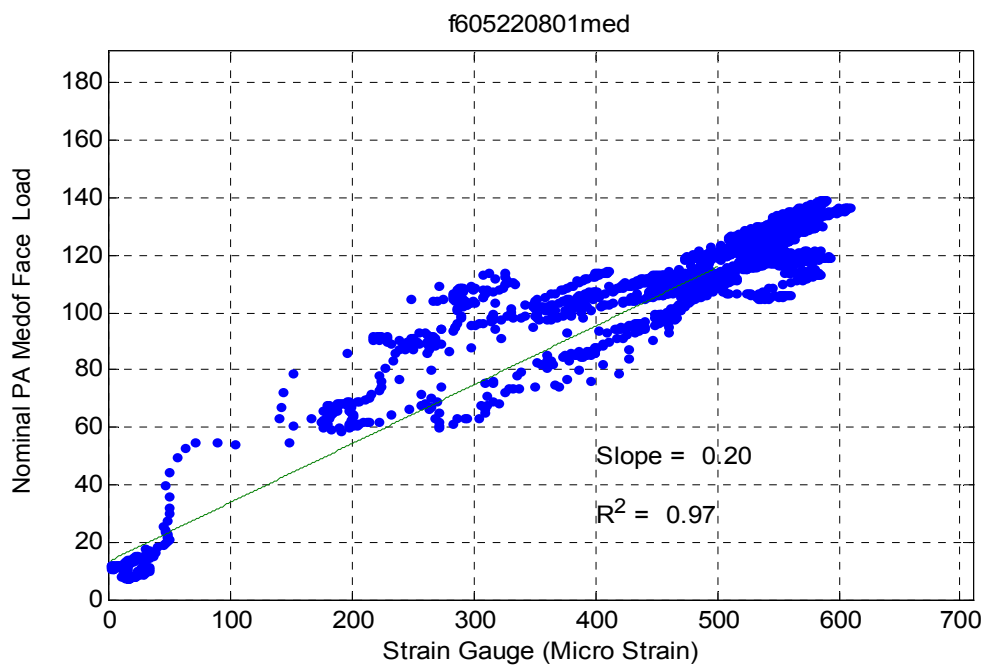
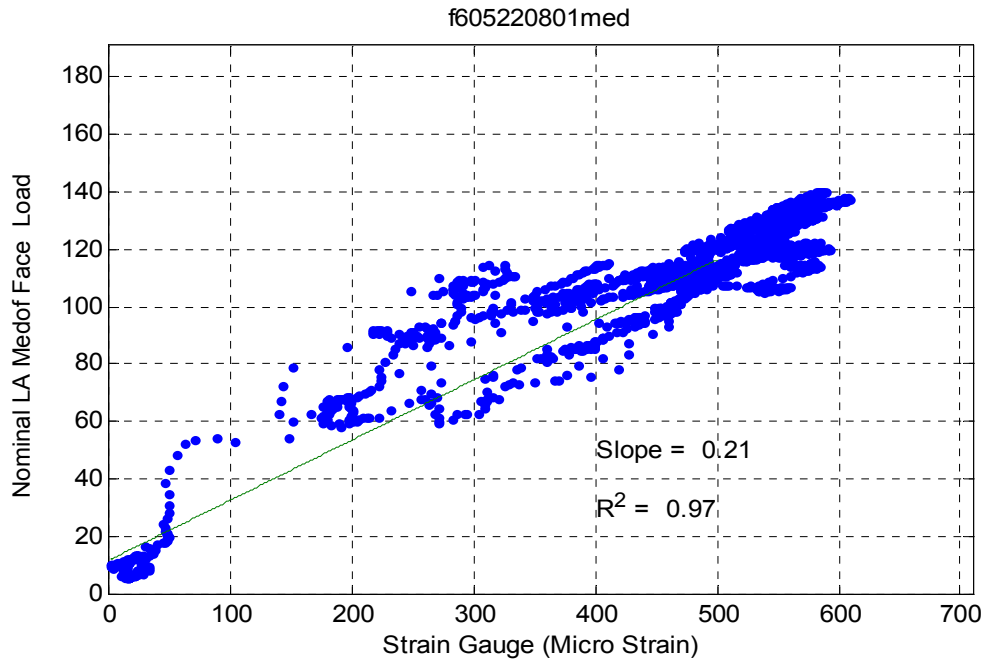




## Bottom Panel Analysis

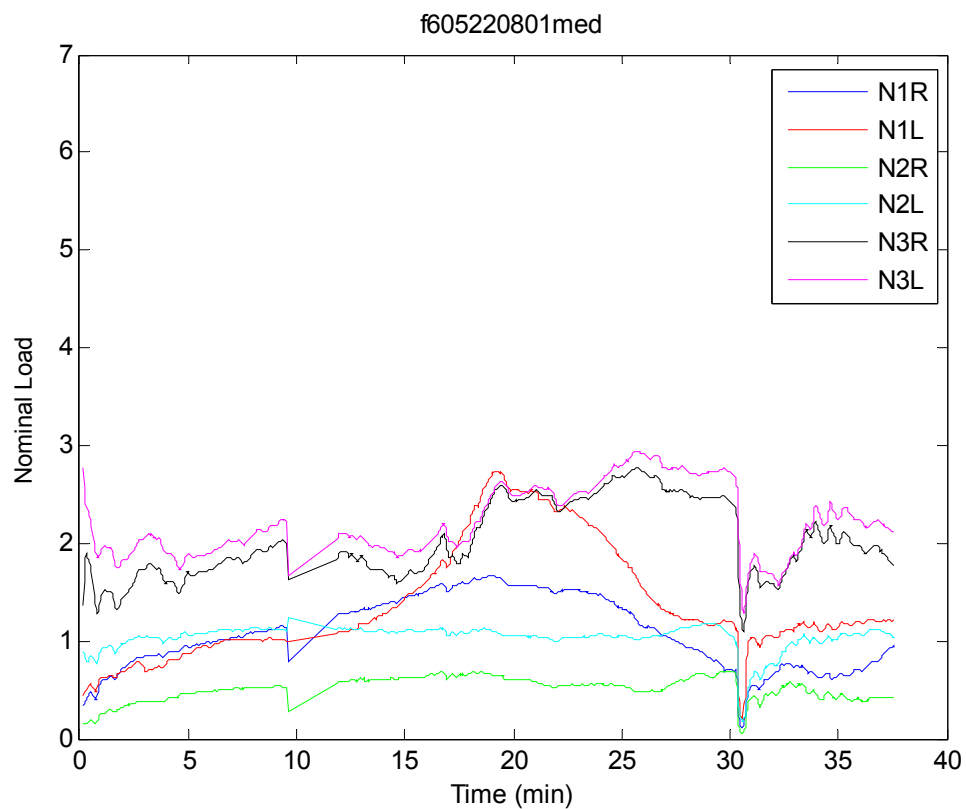


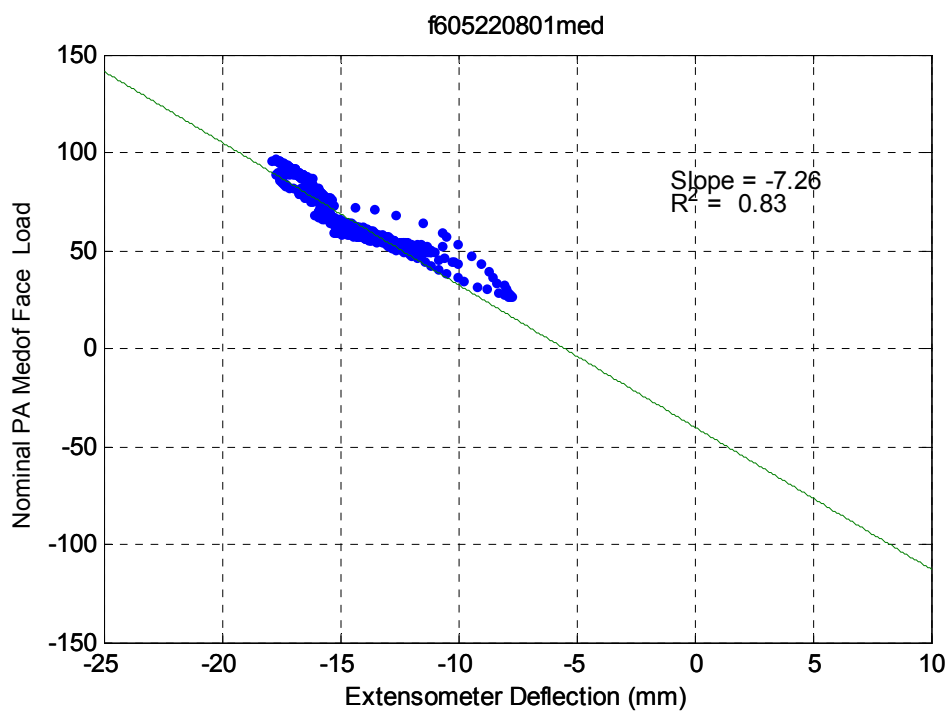
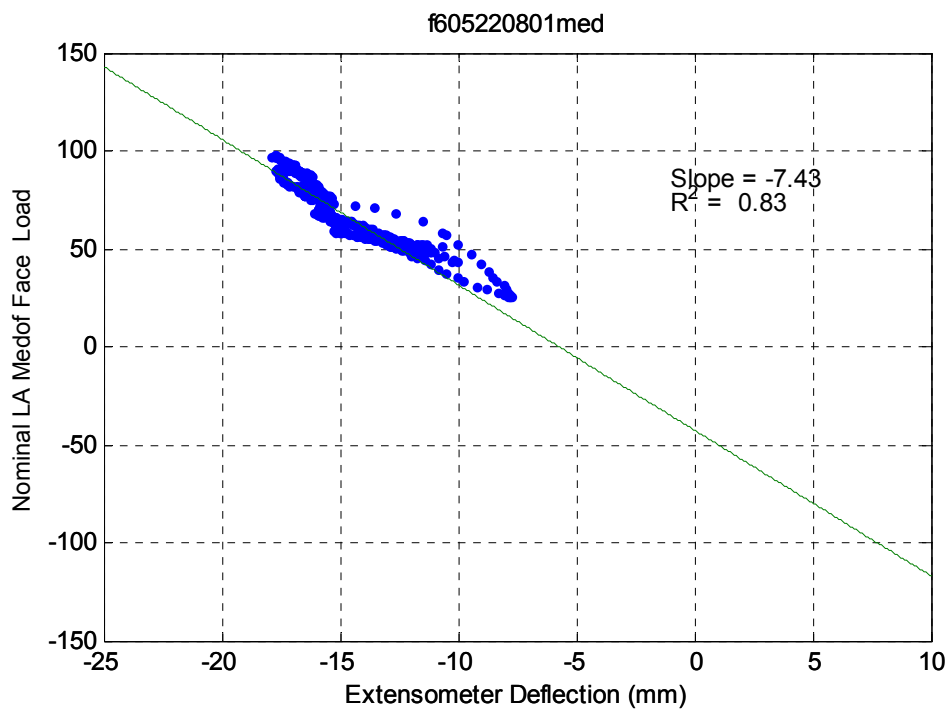
## Strain Gauge Results

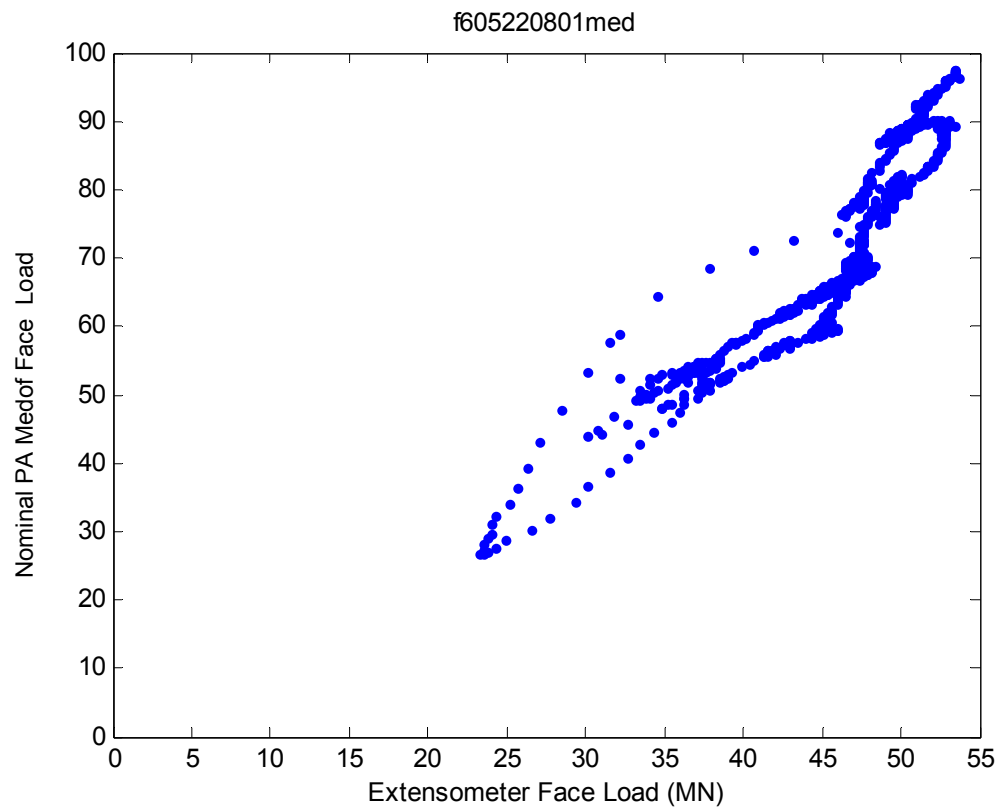


**May 22 – f605220801**  
**5.1 Event ID – 17 - 1**

Creep

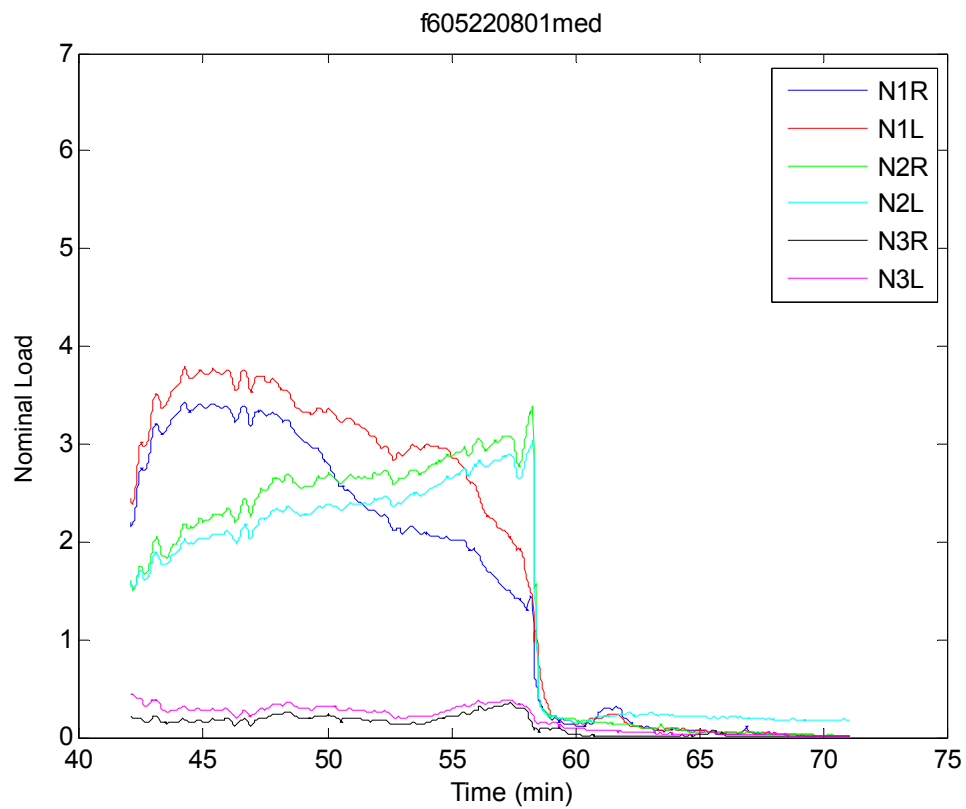


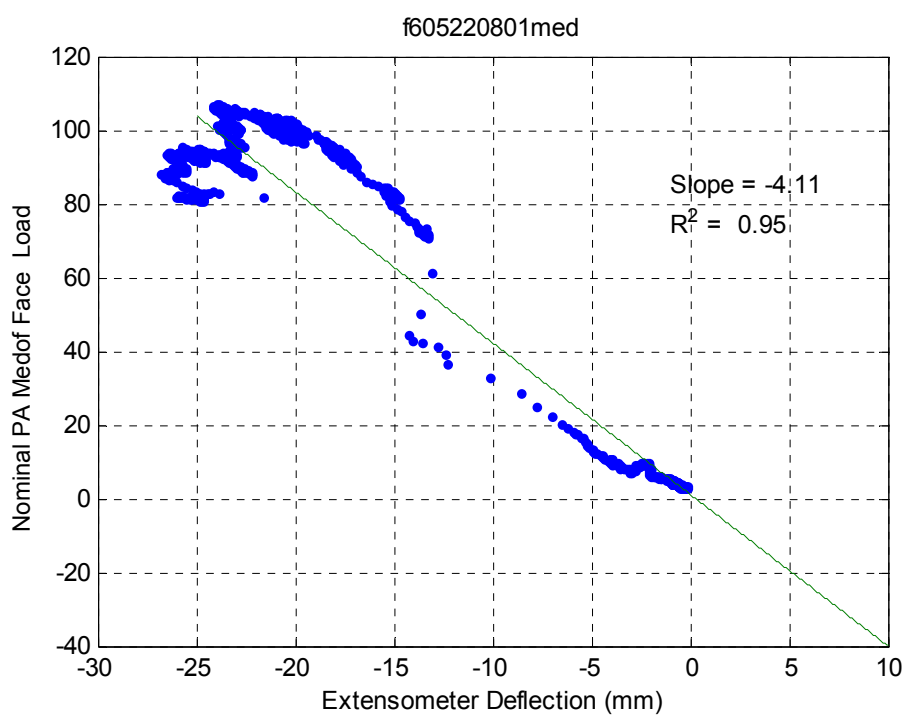
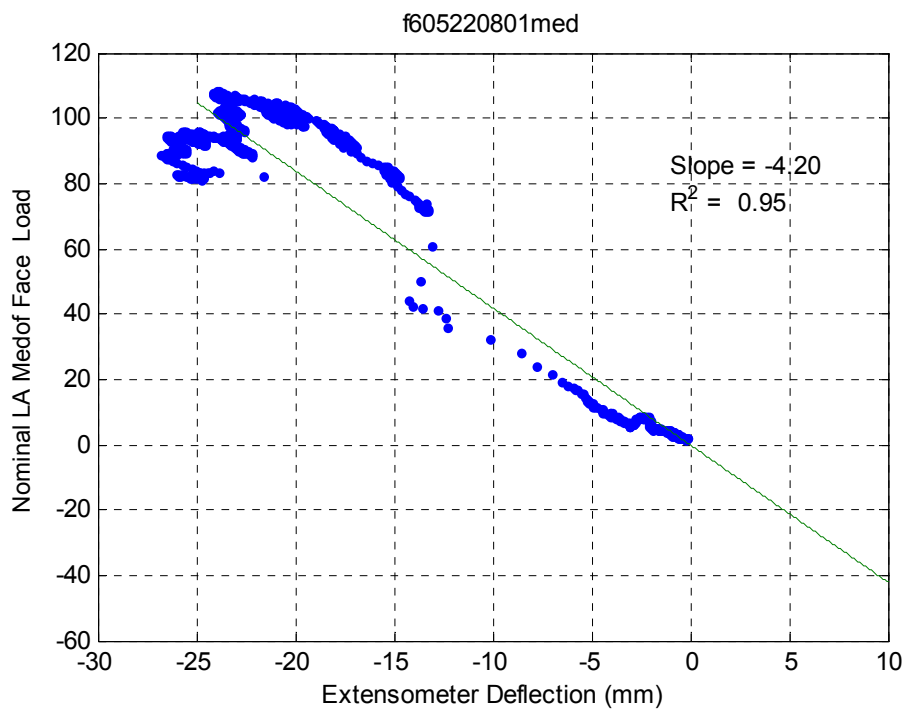


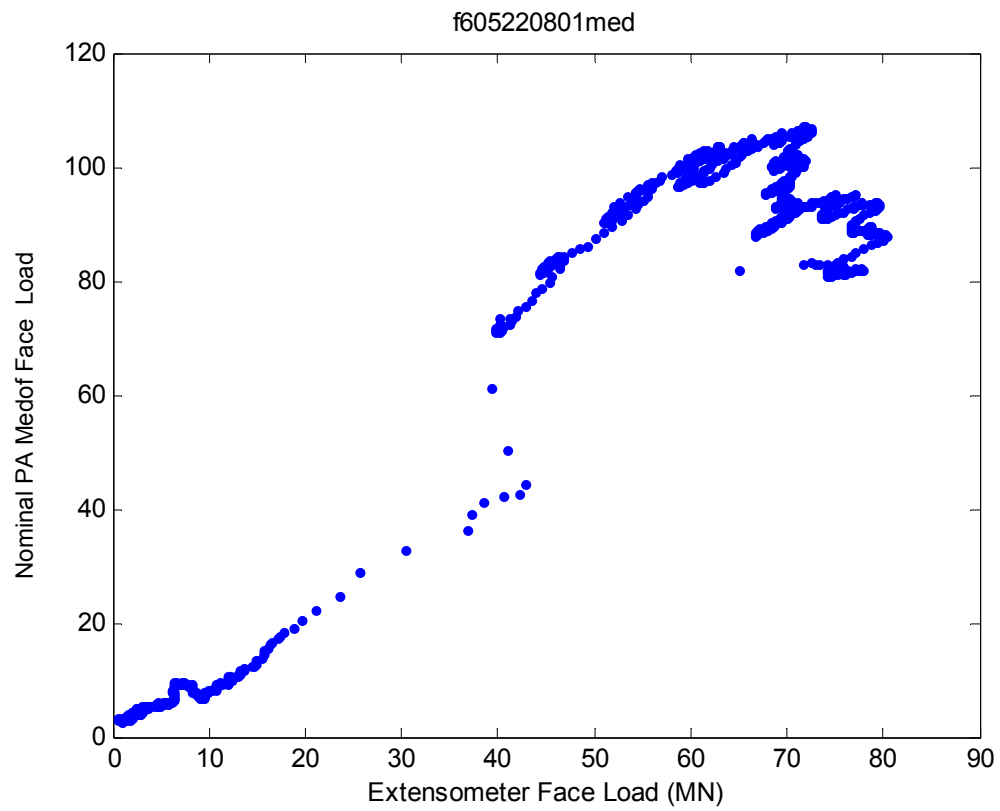


**May 22 – f605220801**  
**5.2 Event ID – 17 - 3**

Creep





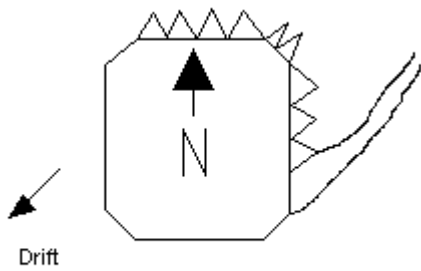


**6 MAY 22 – F605221301**

**Event ID – 18**

**Crushing**

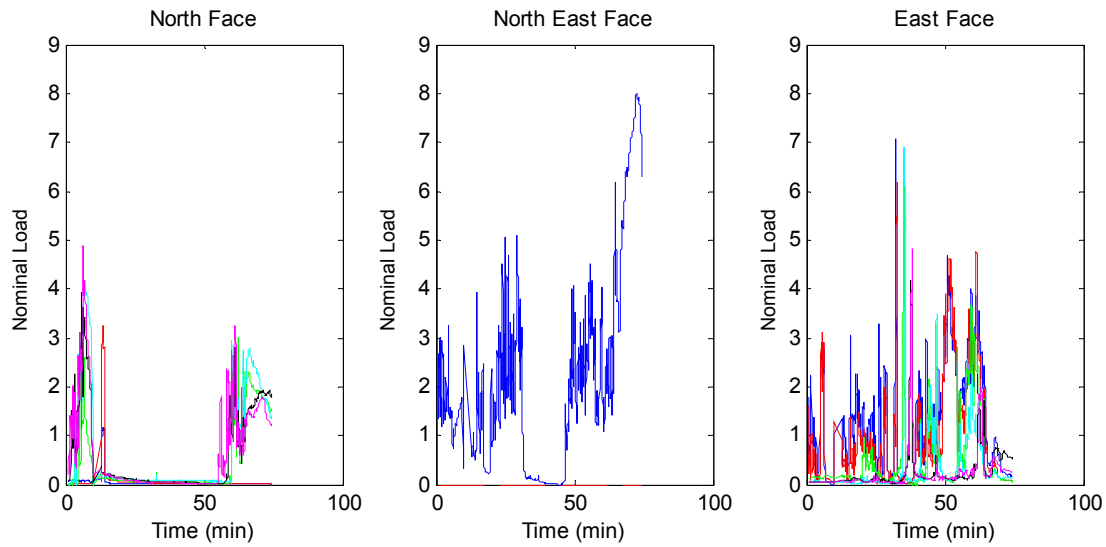
**Ice Thickness: 2.5m**



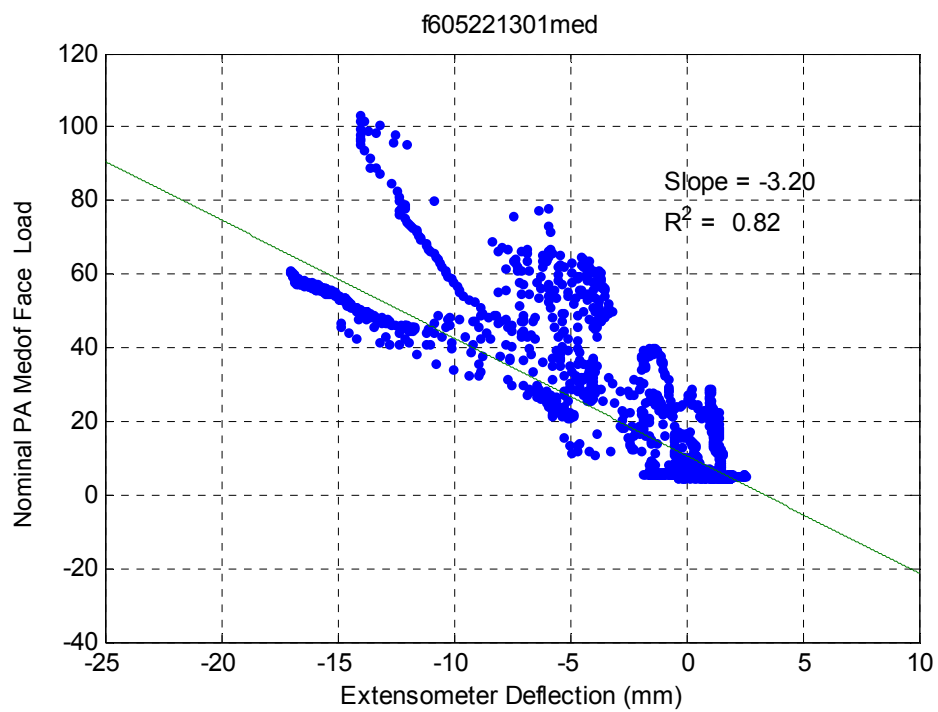
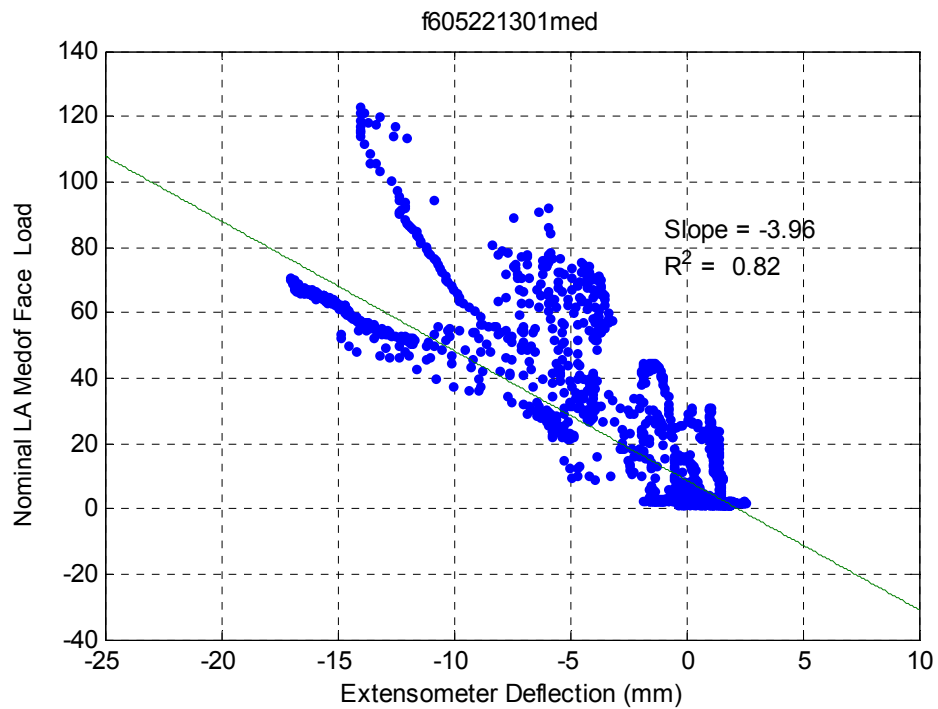
**Dynamac Event Description**

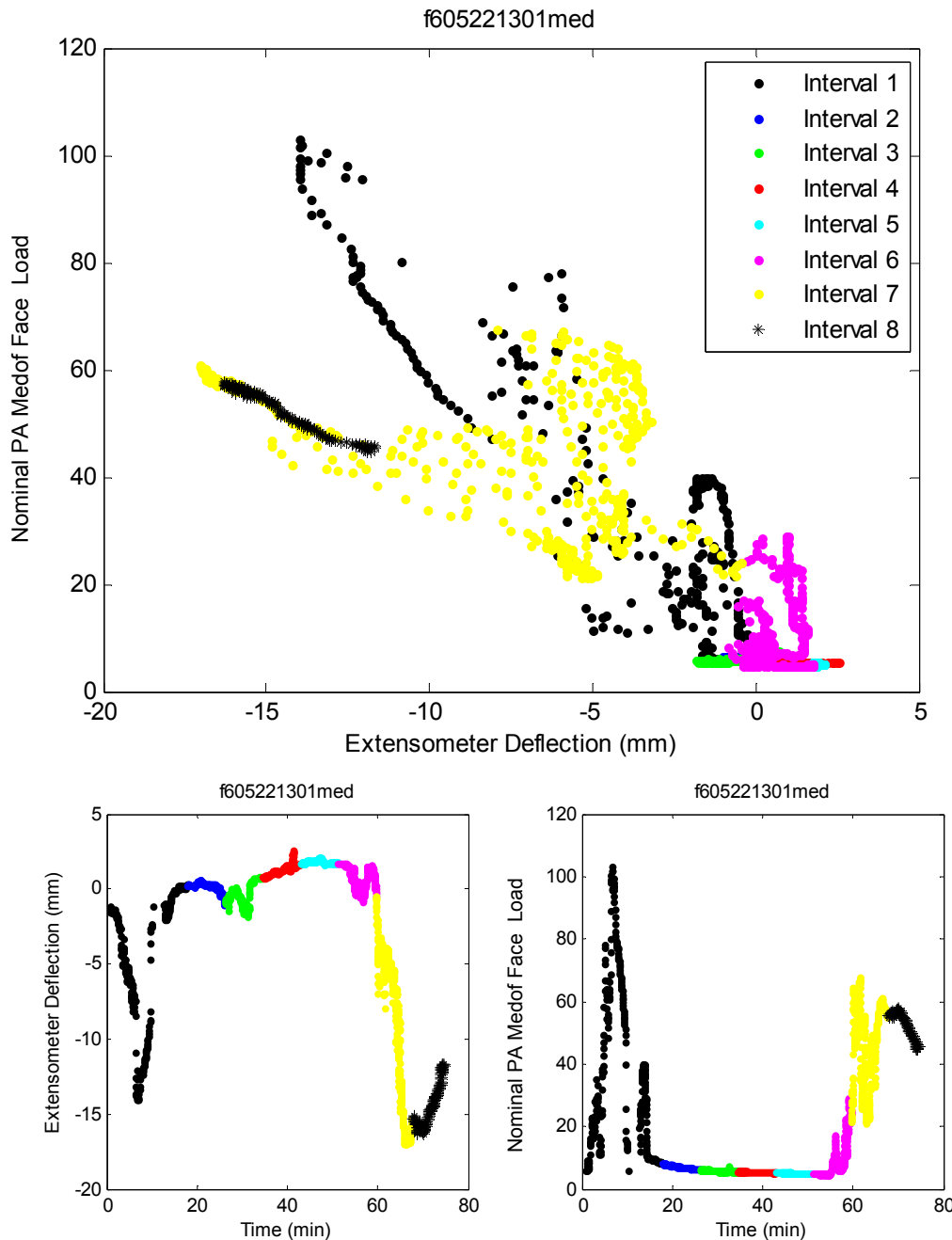
Thick first year ice failed in crushing against the NE caisson face. The western portion of the floe remained stationary while the eastern part crushed and slid along the east face. The western portion began to move again resulting in crushing along the NE face and continued crushing on the E face.

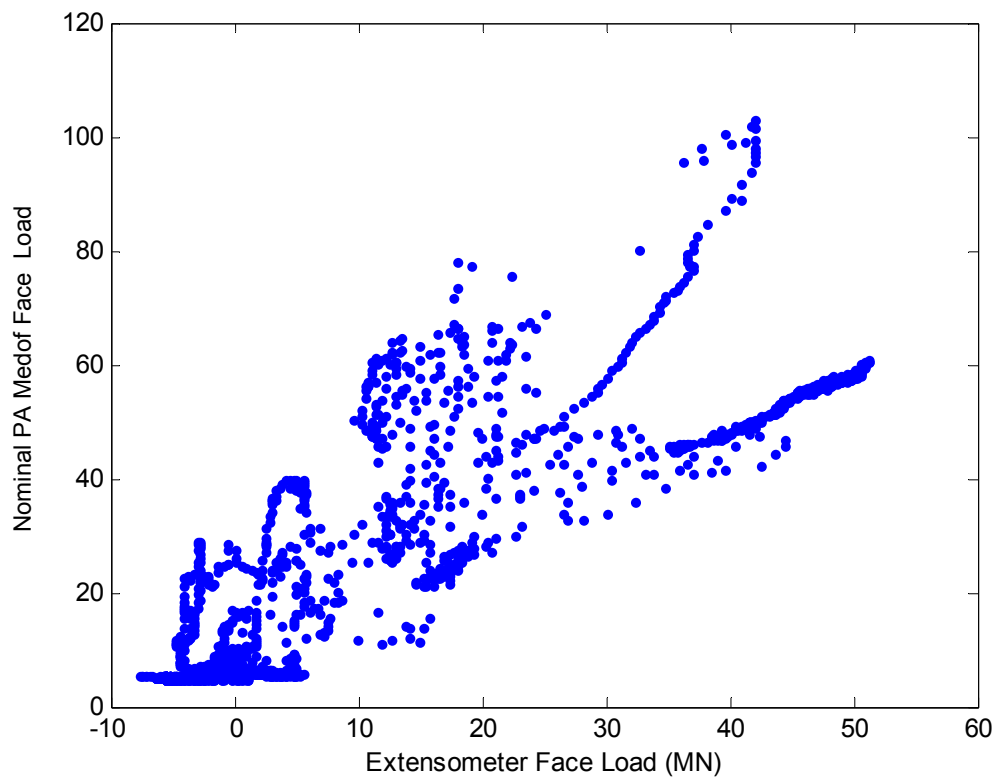
Note: The Bottom panel is loaded during this event. Some modeling of the effect of the bottom panel is required.



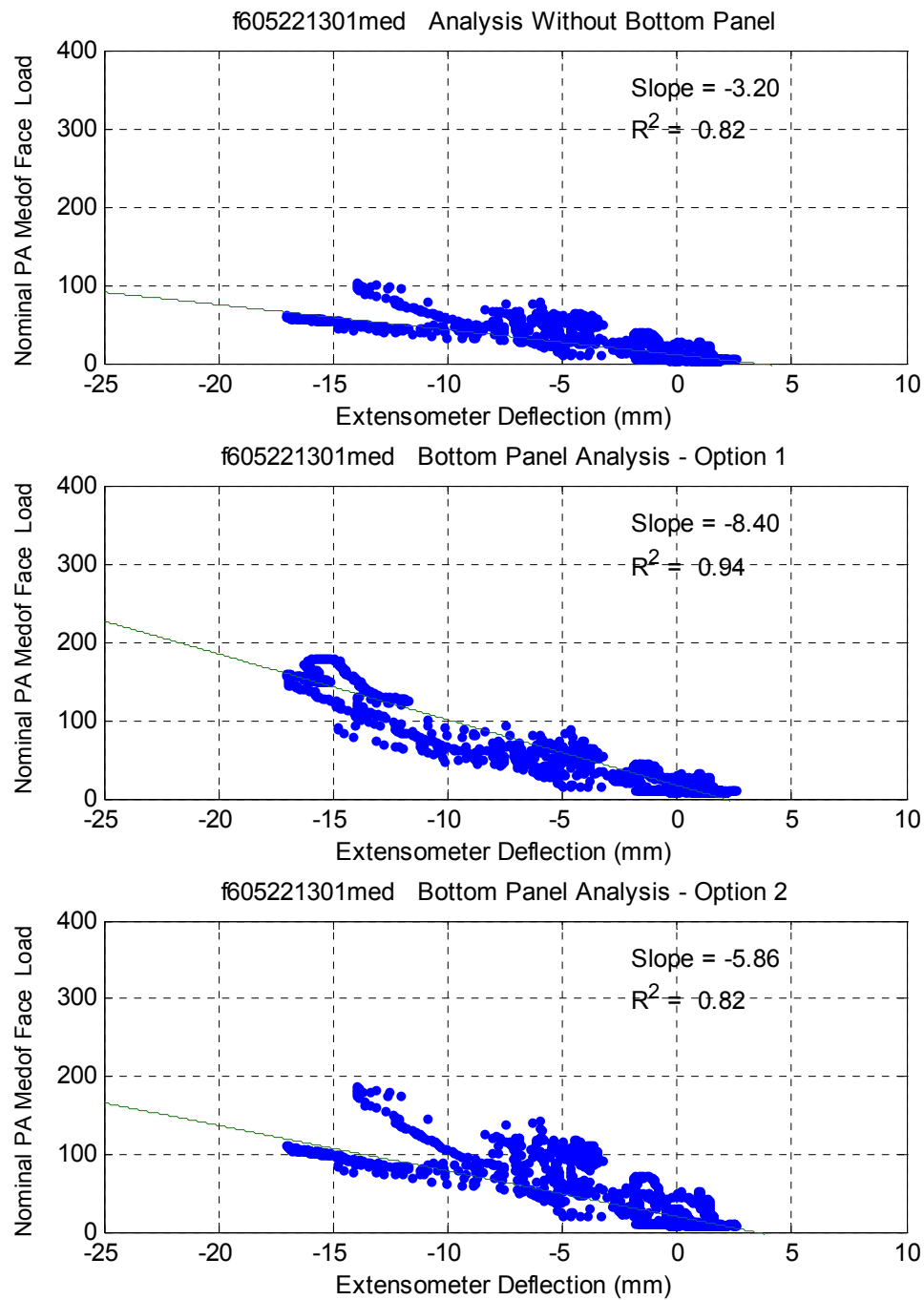
<i>Event ID</i>	<i>Date</i>	<i>Fast File</i>	<i>Segment</i>	<i>Time Period</i>	<i>Failure Mode</i>	<i>Panel Groups</i>	<i>Spacing of Groups</i>
18	22-May (C)	F605221301	full file	13:58:07 – 15:11:32	CR, SLD & SLW	N1, N2 & N3	≈ 40m
18-1			1	13:58:07 – 14:01:04	CR	N3	< 20m
18-2			2	14:01:05 – 14:06:43	CR	N2 & N3	≈ 20m
18-3			3	14:06:44 – 14:54:50	SLD	N1, N2 & N3	≈ 40m
18-4			4	14:54:51 – 14:56:54	CR	N3	< 20m
18-5			5	14:56:55 – 15:01:58	CR	N2 & N3	≈ 20m
18-6			6	15:01:59 – 15:11:32	SLW	N2 & N3	≈ 20m



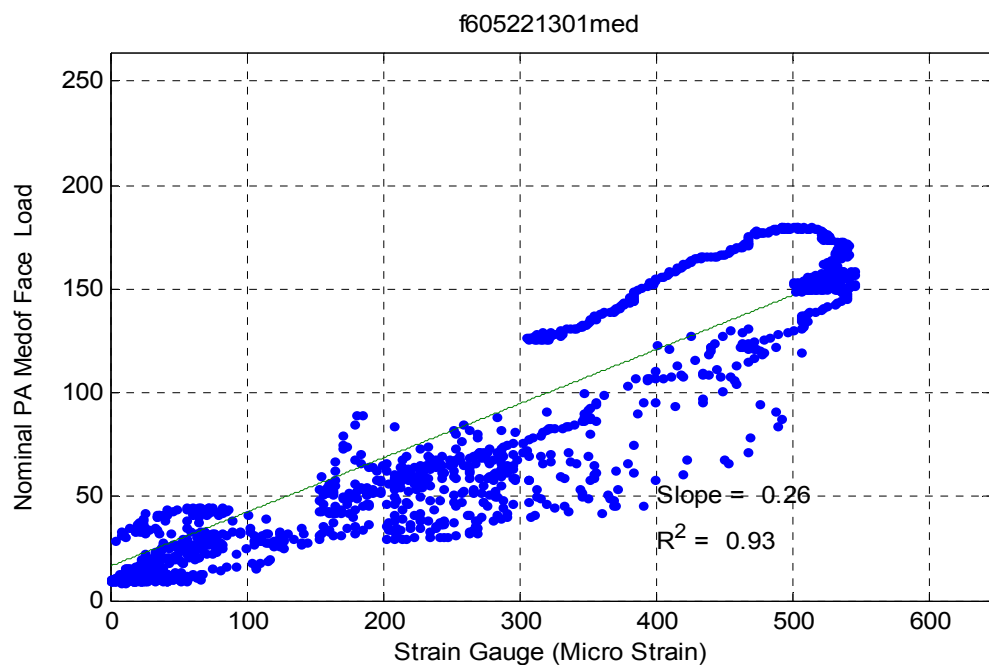
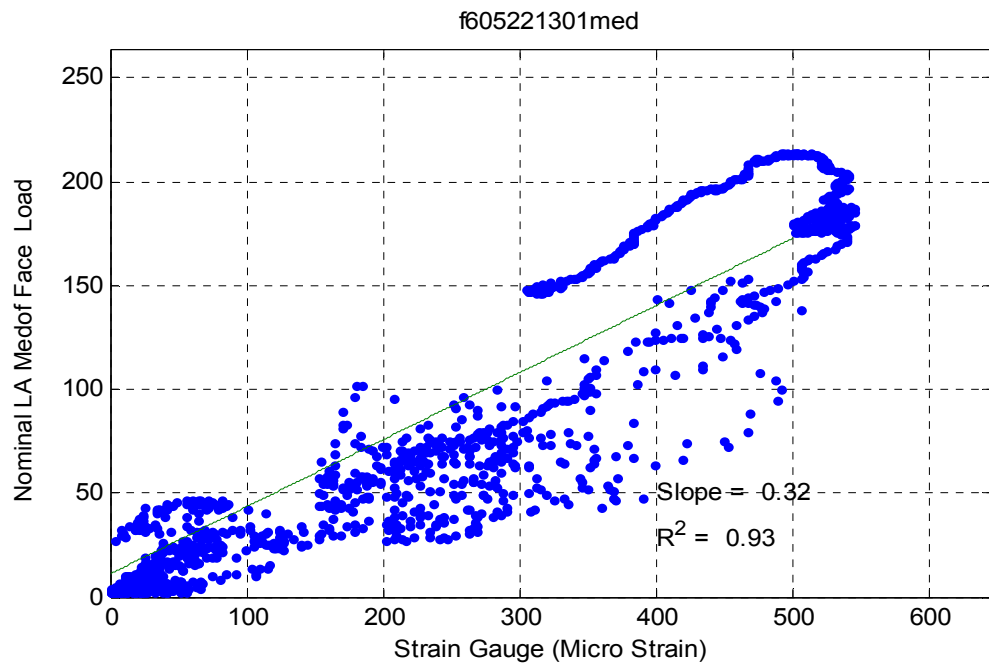




## **Bottom Panel Analysis**

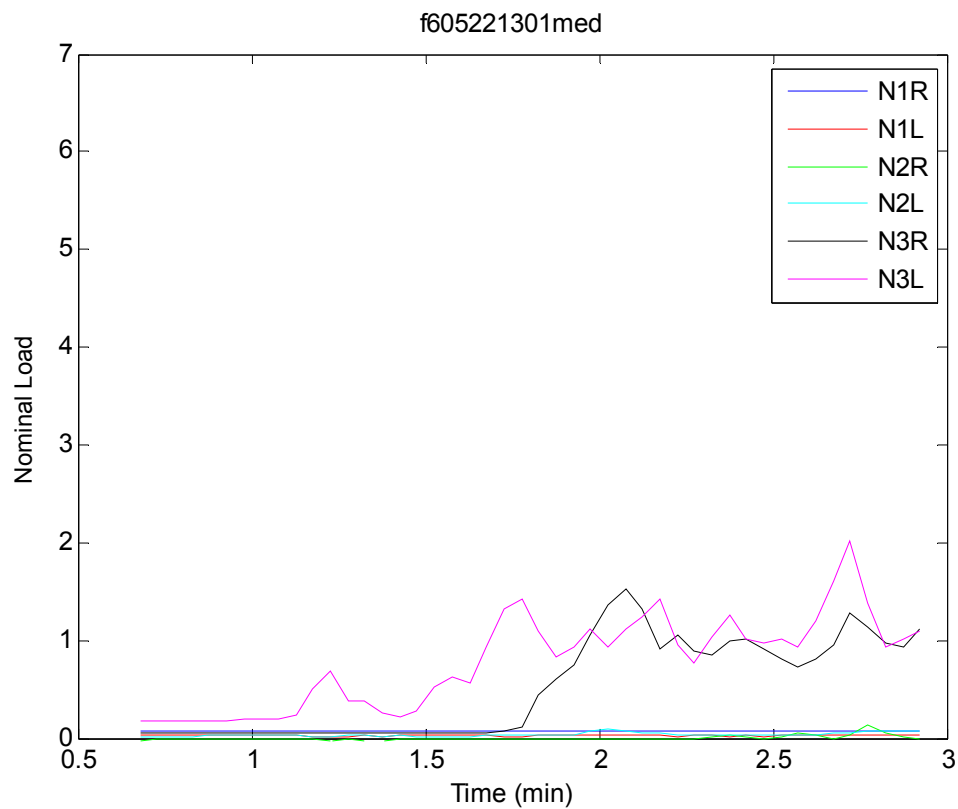


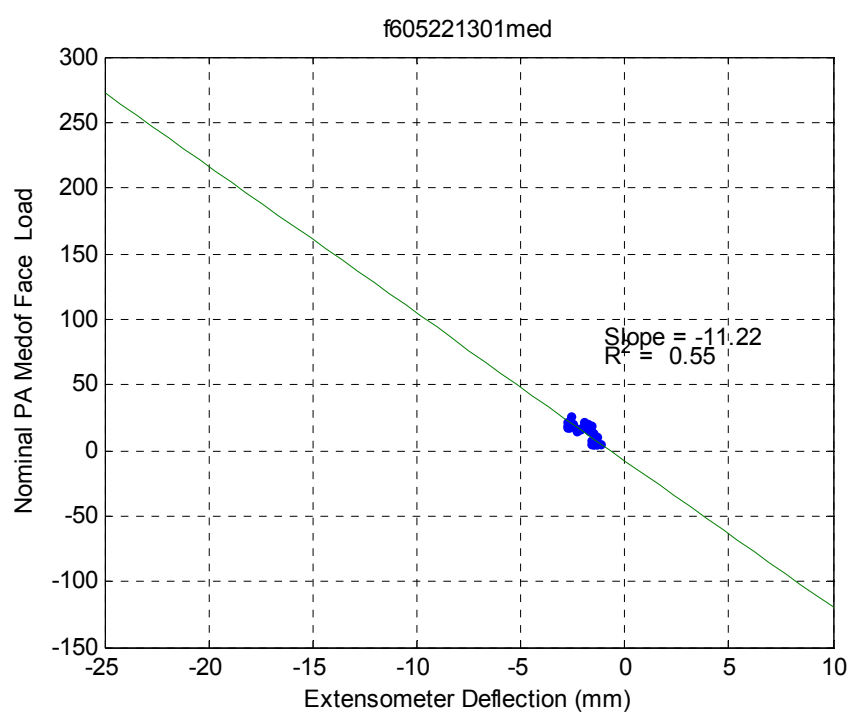
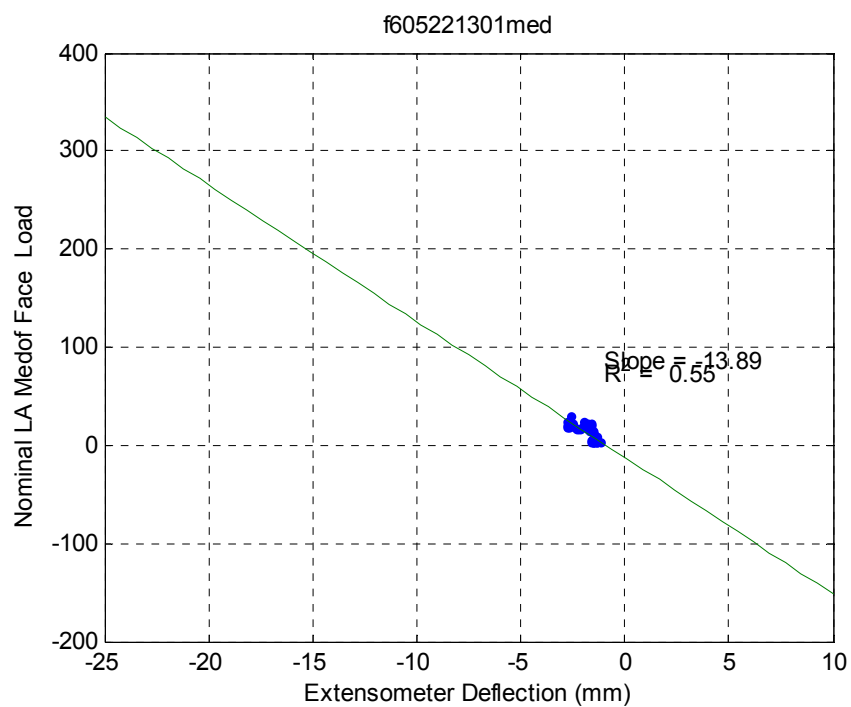
## Strain Gauge Results

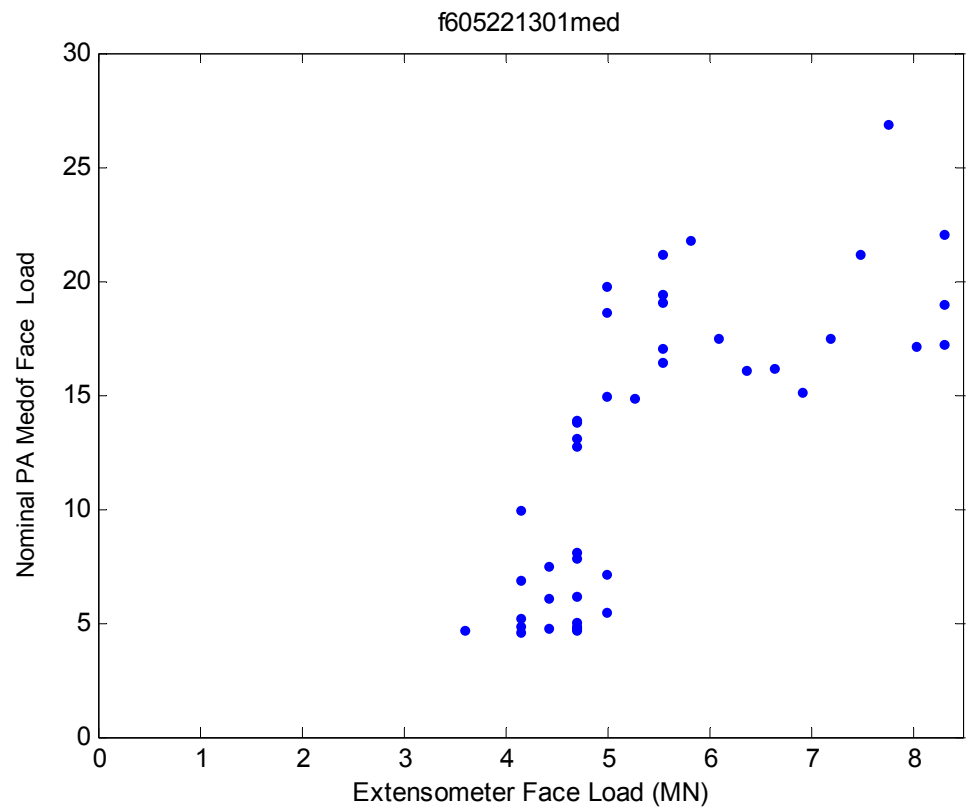


**May 22 – f605221301**  
**6.1 Event ID – 18 – 1**

### Crushing

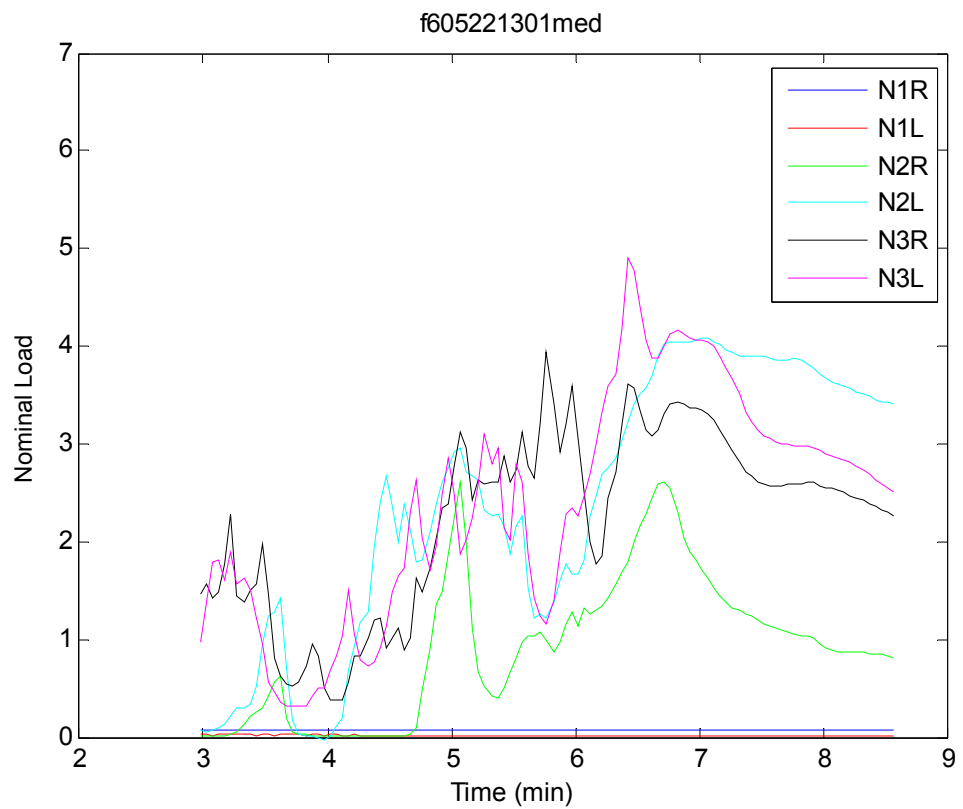


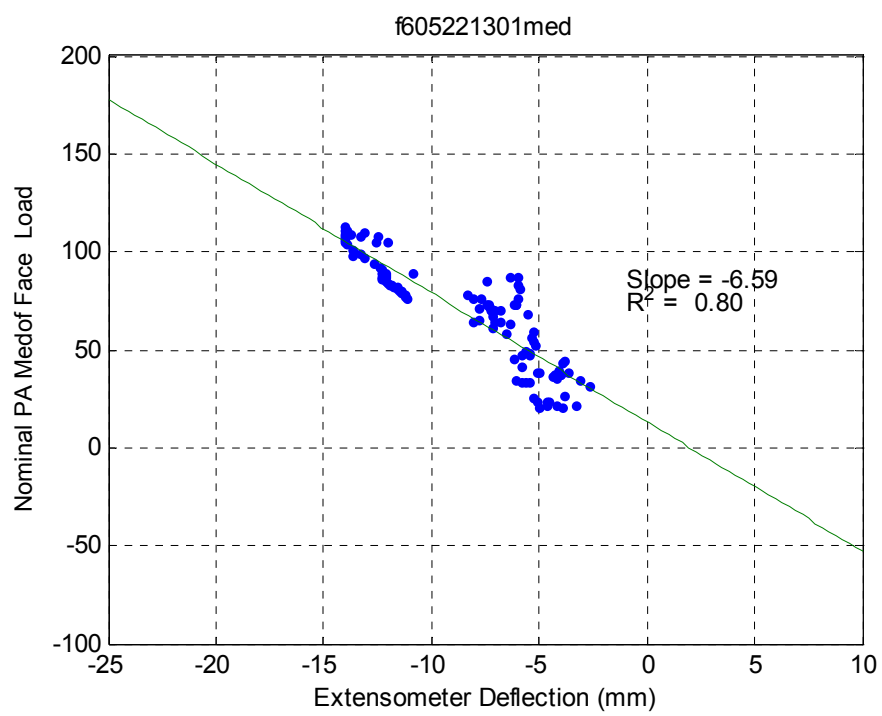
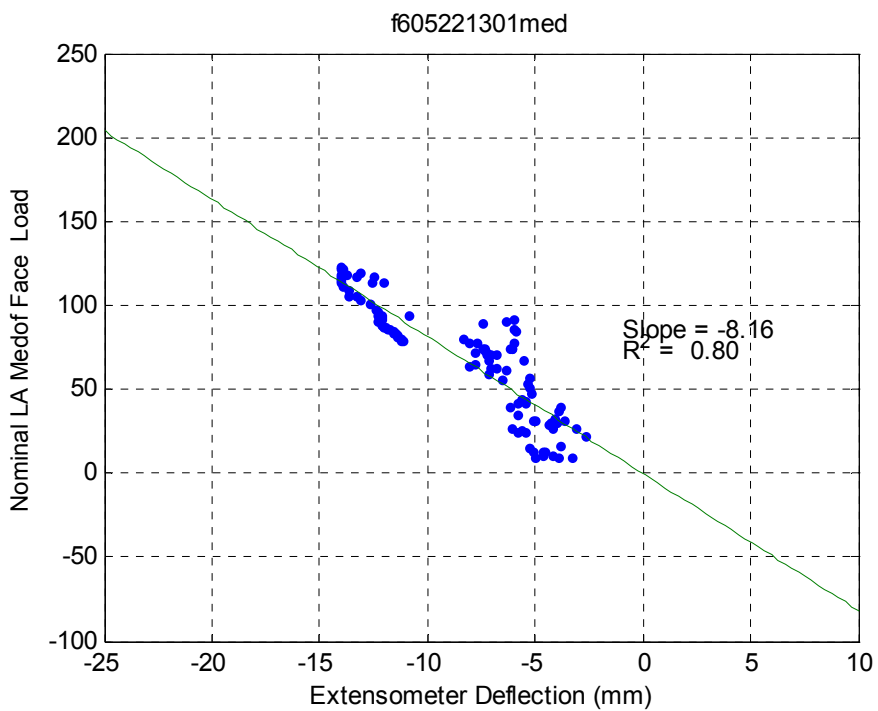


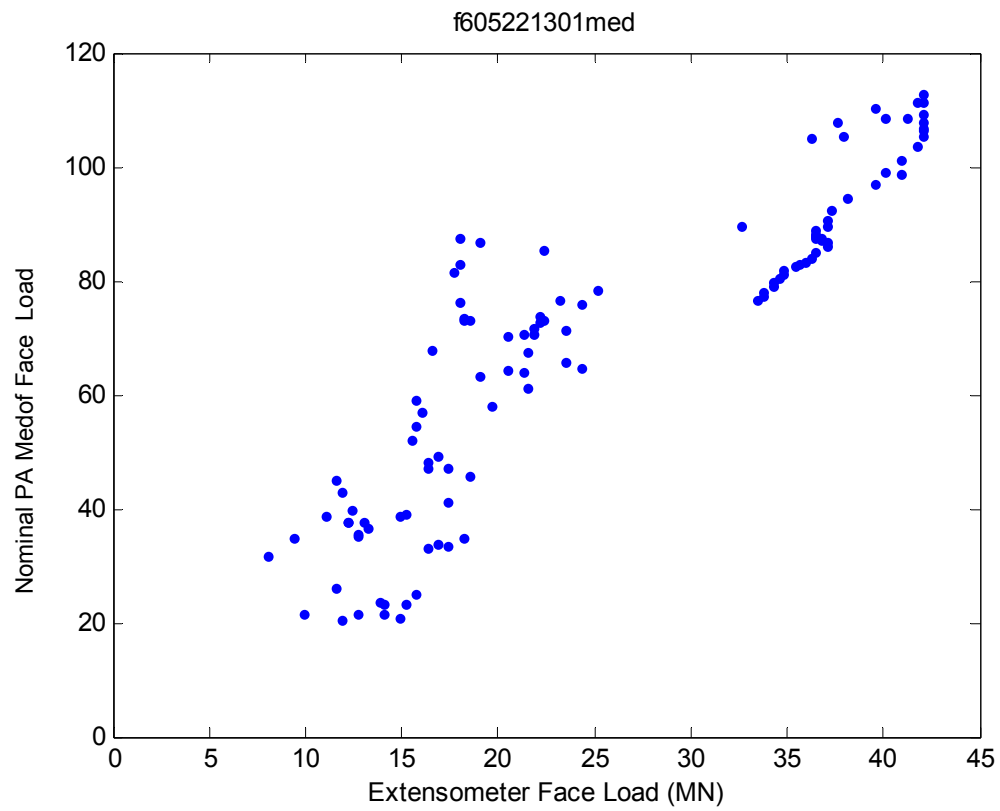


**May 22 – f605221301**  
**6.2 Event ID – 18 – 2**

**Crushing**

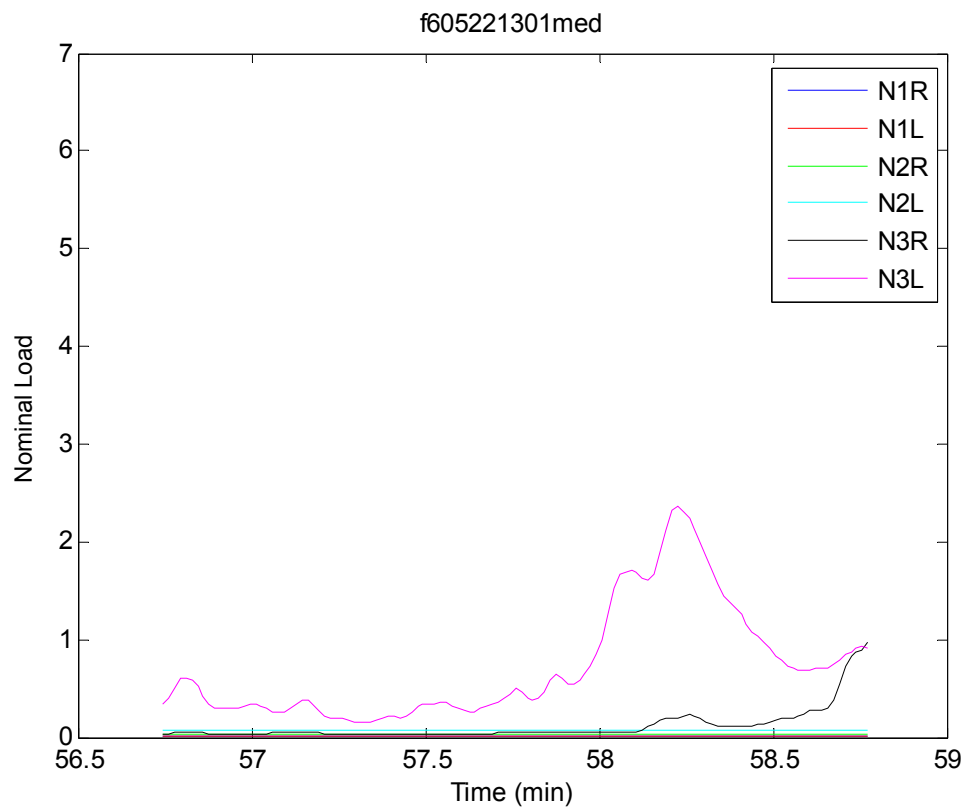


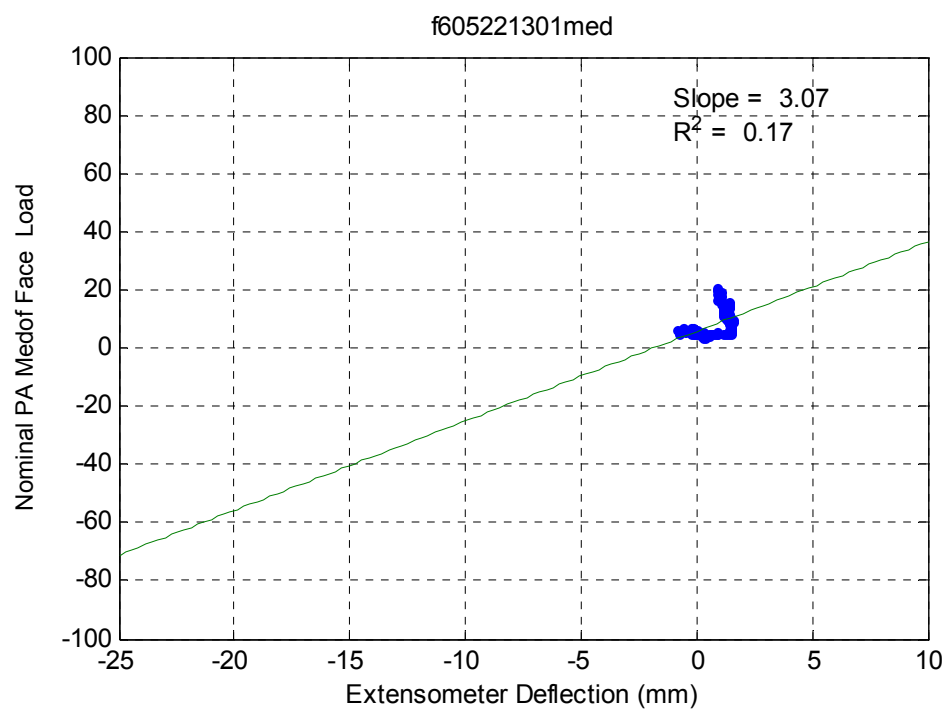
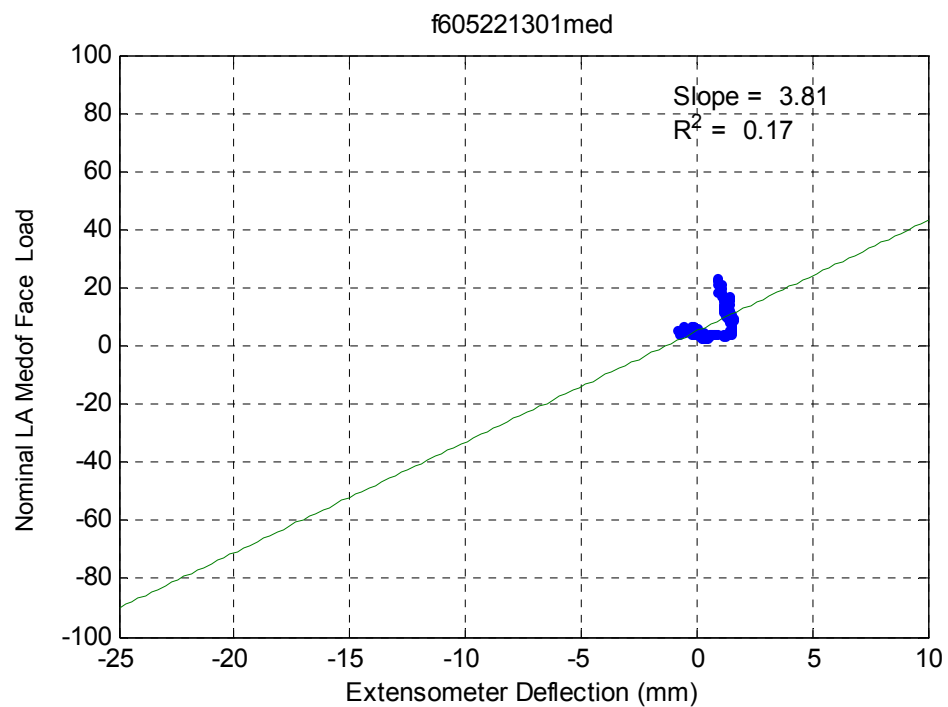


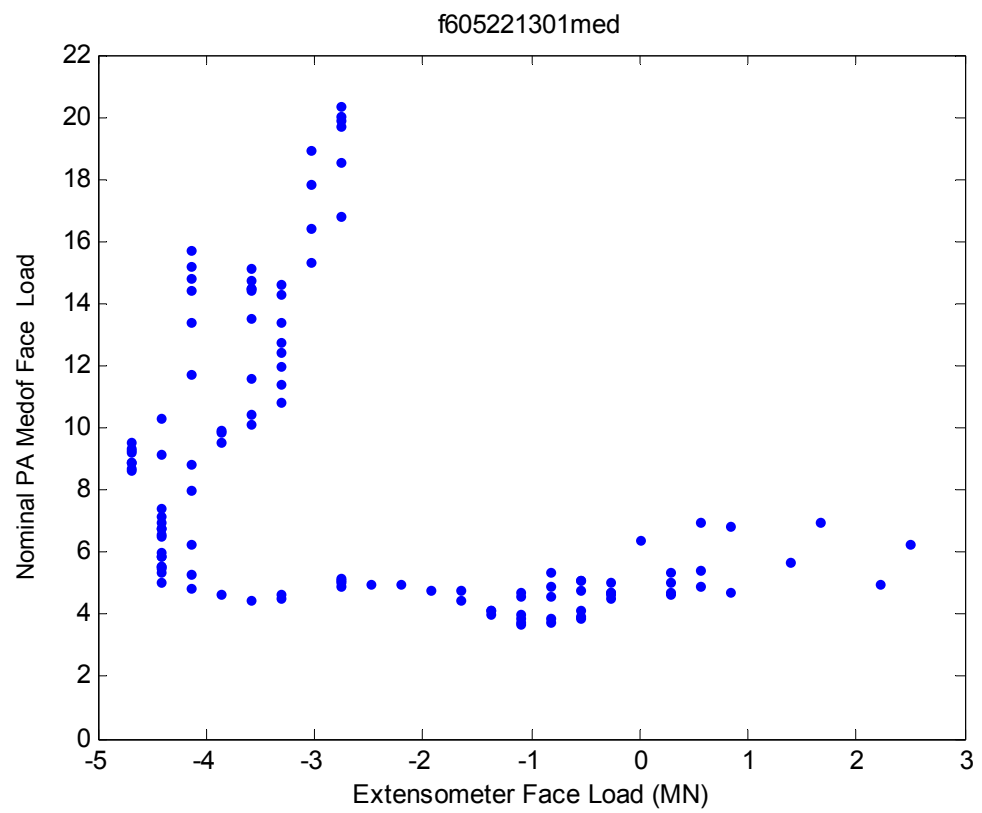


**May 22 – f605221301**  
**6.3 Event ID – 18 – 4**

### Crushing

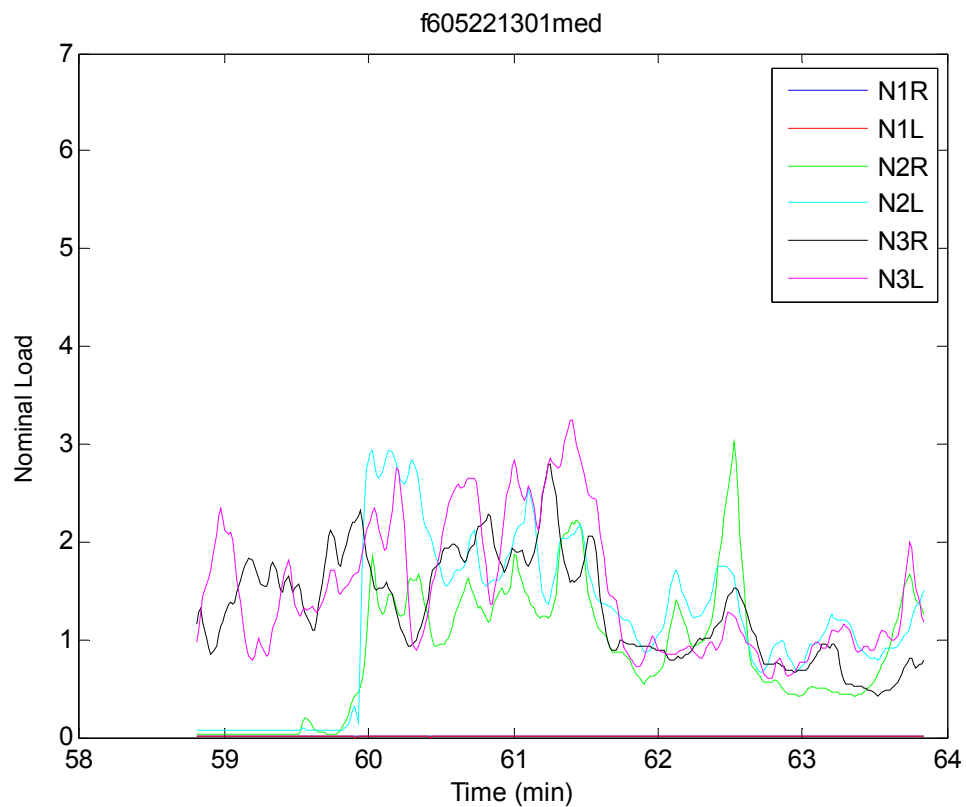


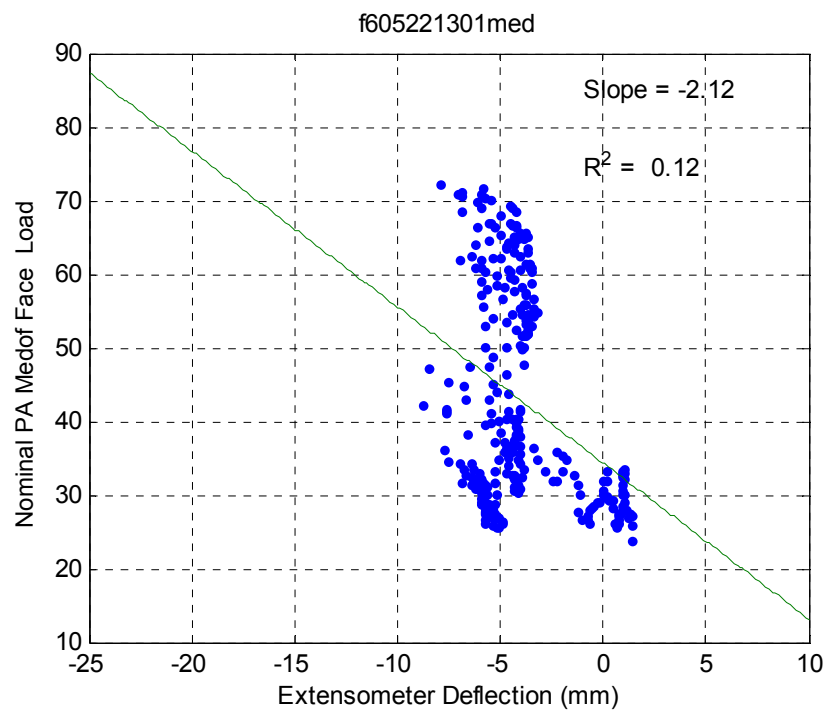
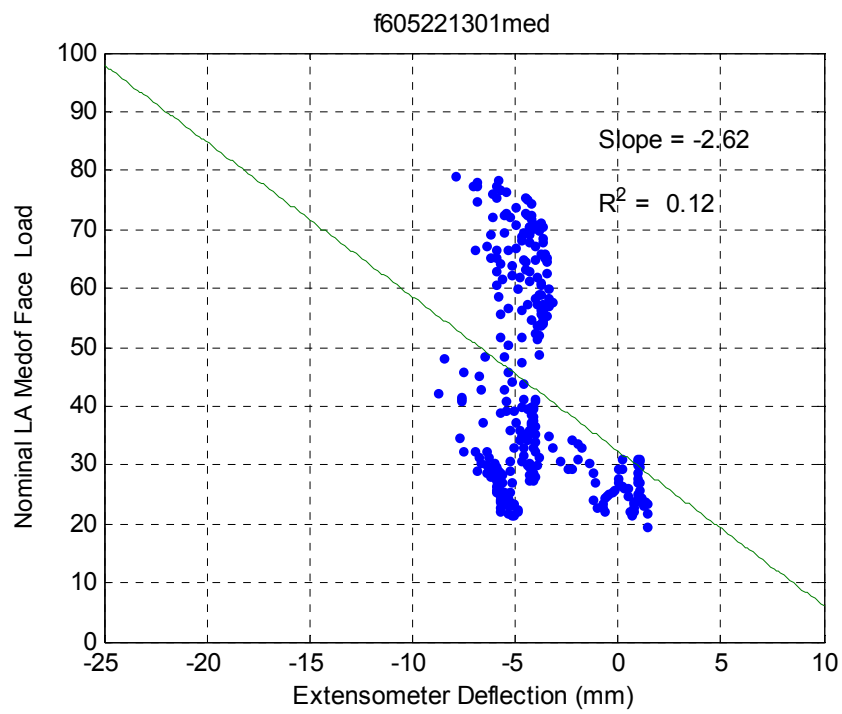


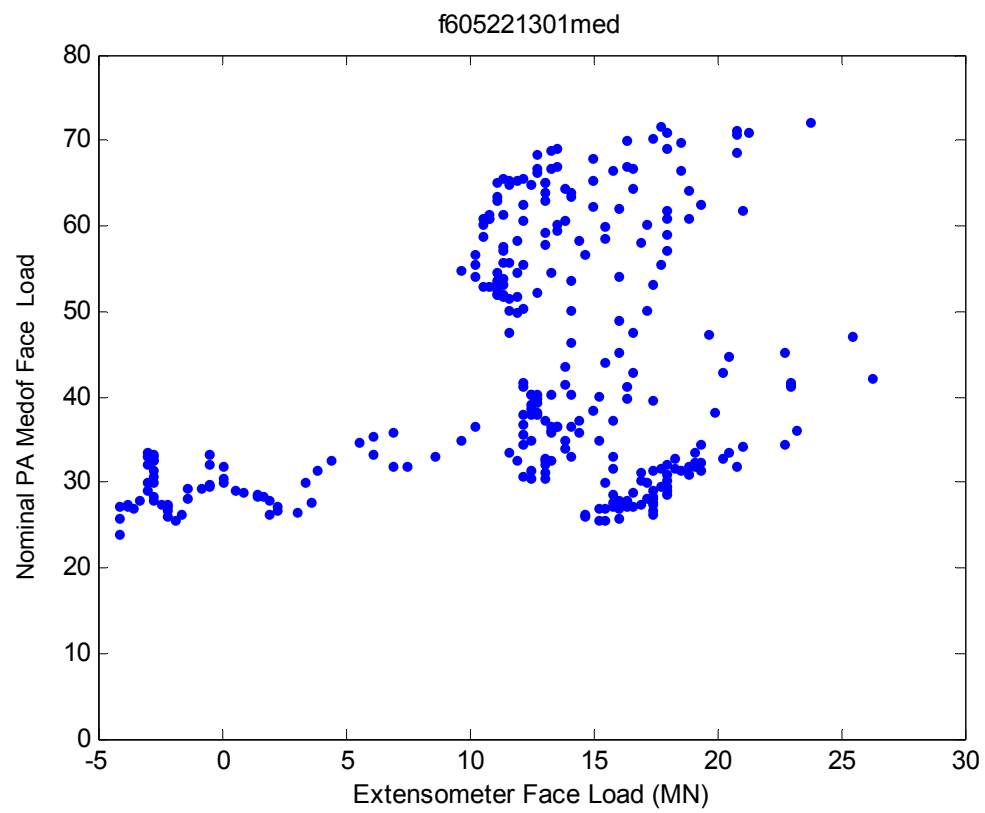


**May 22 – f605221301**  
**6.4 Event ID – 18 – 5**

**Crushing**

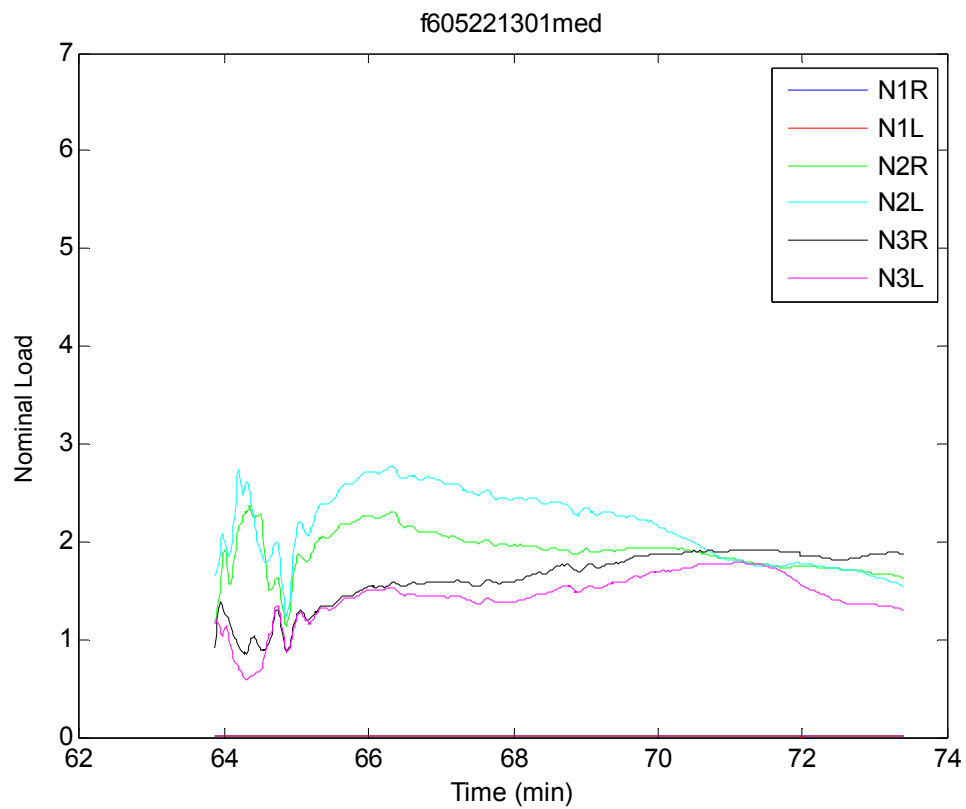


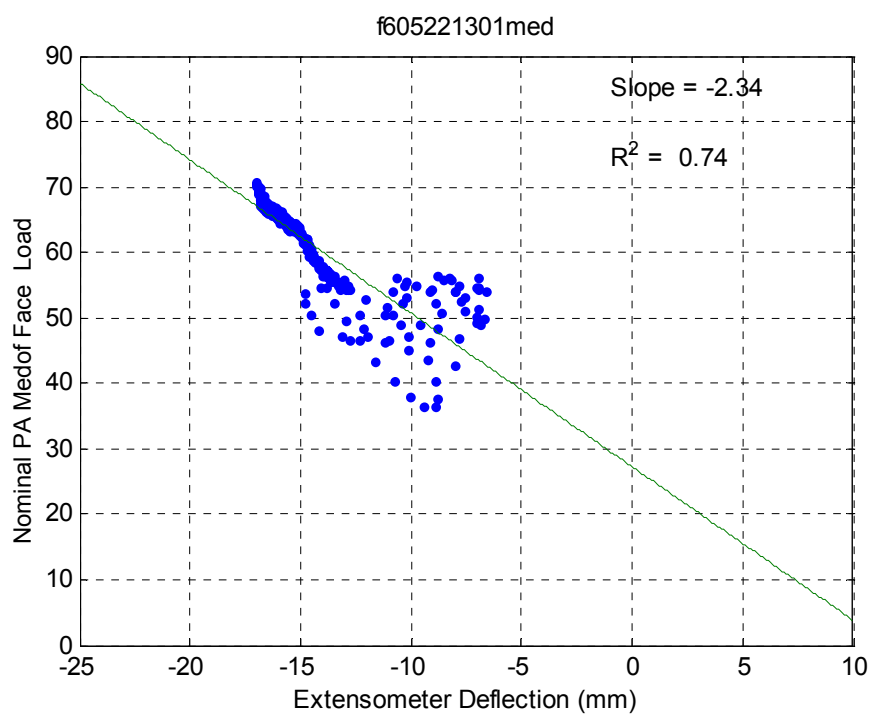
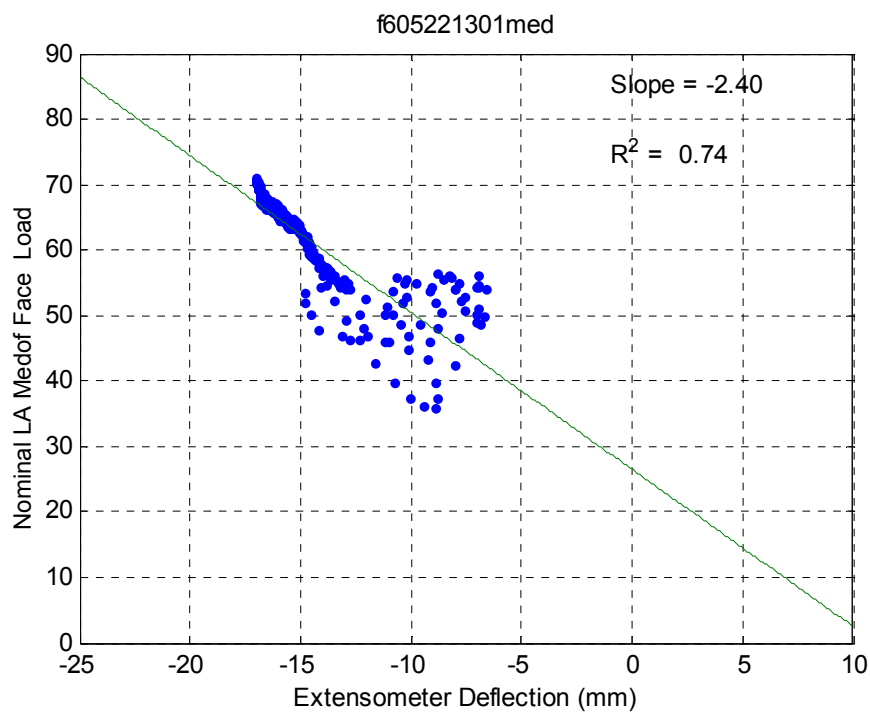


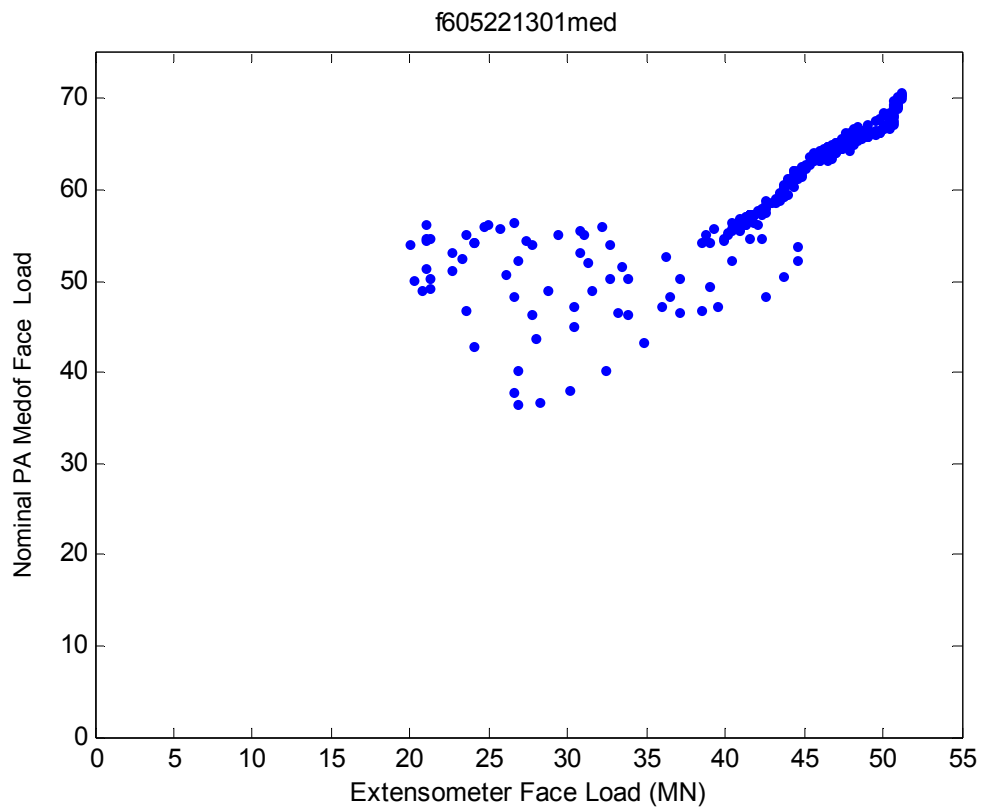


**May 22 – f605221301**  
**6.5 Event ID – 18 – 6**

### Creep





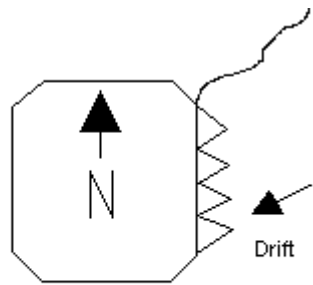


## 7 JUNE 2 – F606021301

### Event ID – 19

Crushing

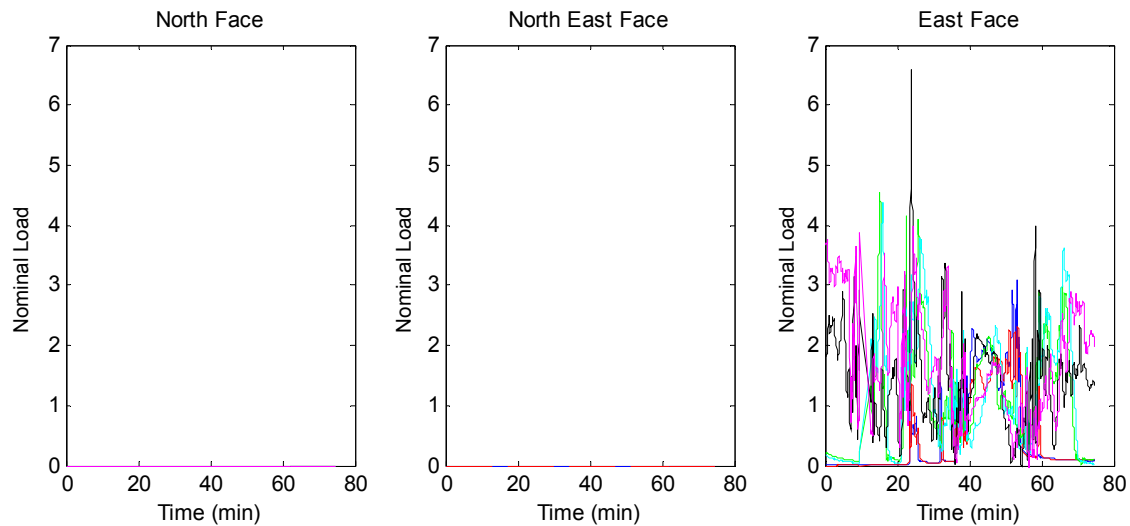
Ice Thickness: 2m



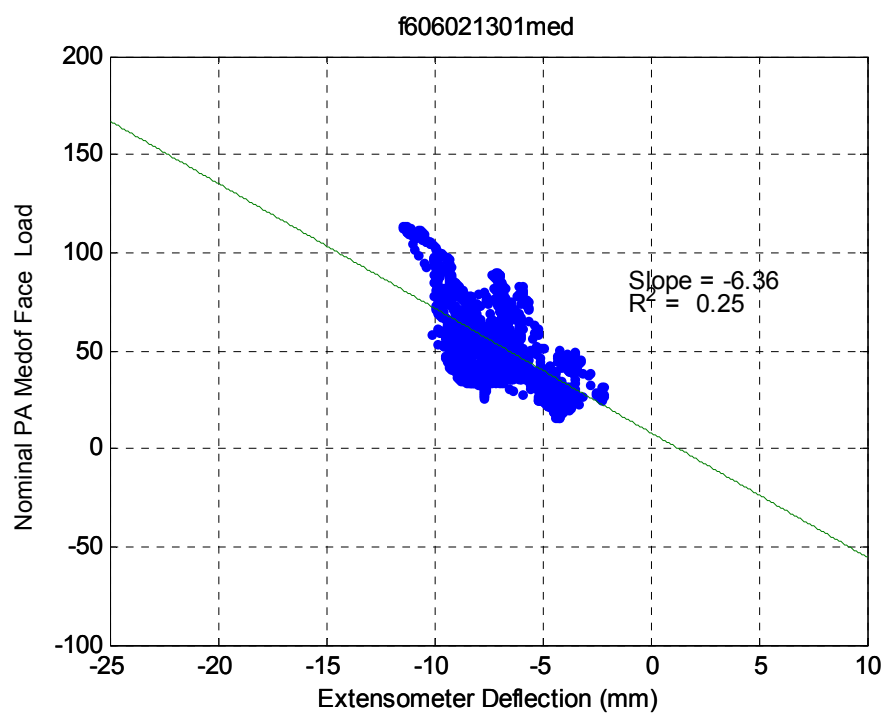
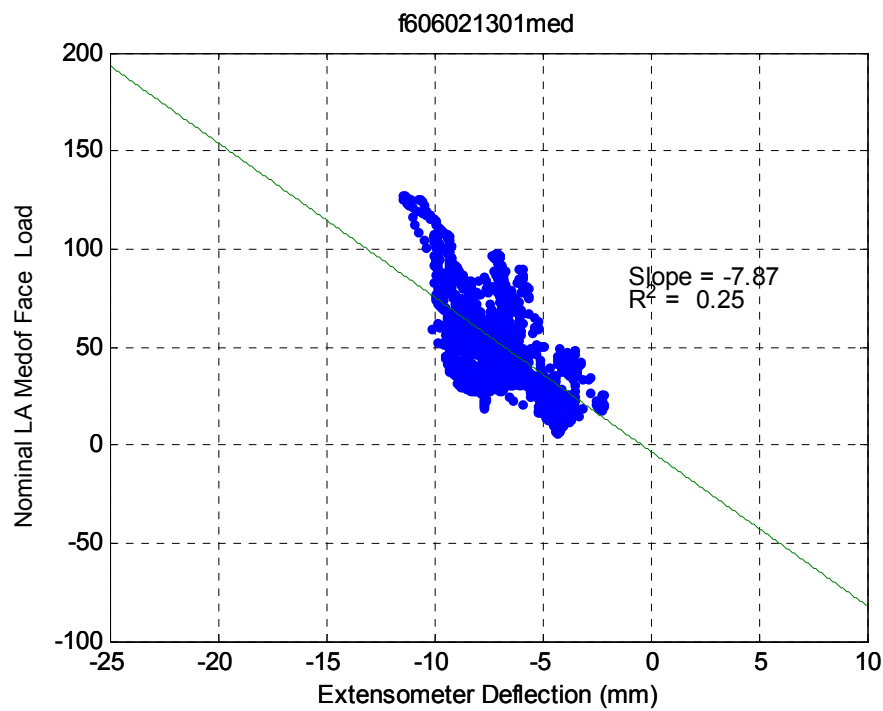
### Dynamac Event Description

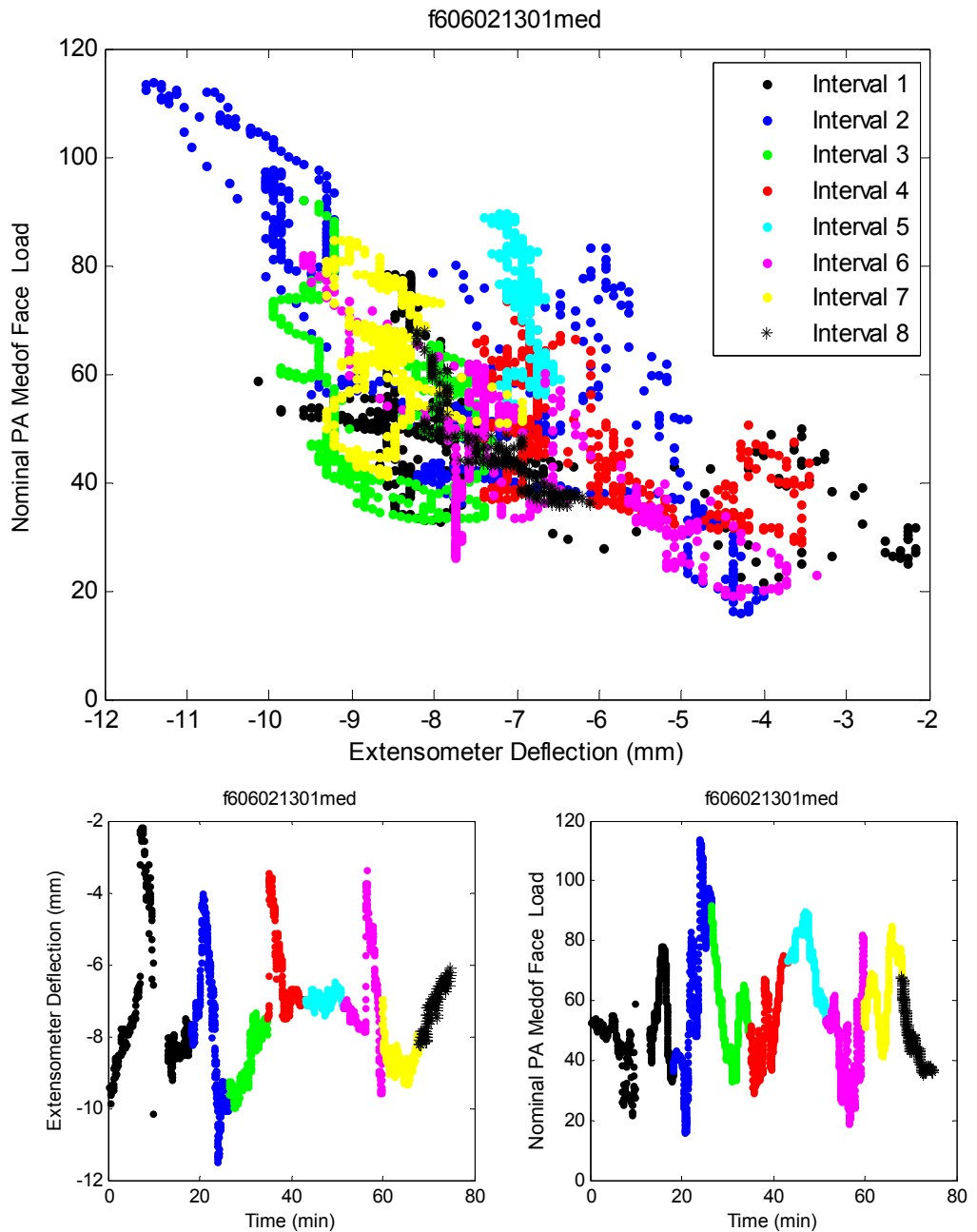
A vast floe comprising 8/10 thick and medium first year ice with 2/10 medium multi-year inclusions impacted the Molikpaq. The interaction involved creep loading, crushing and sliding on the E face.

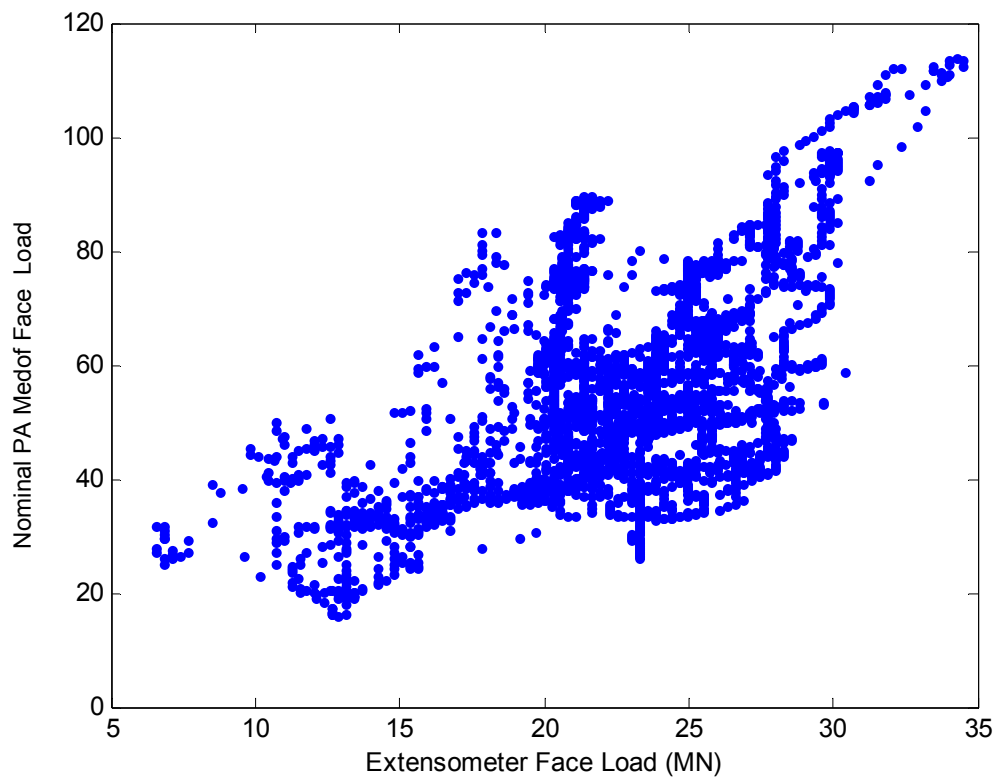
Note: The Bottom panel is loaded during this event. Some modeling of the effect of the bottom panel is required.



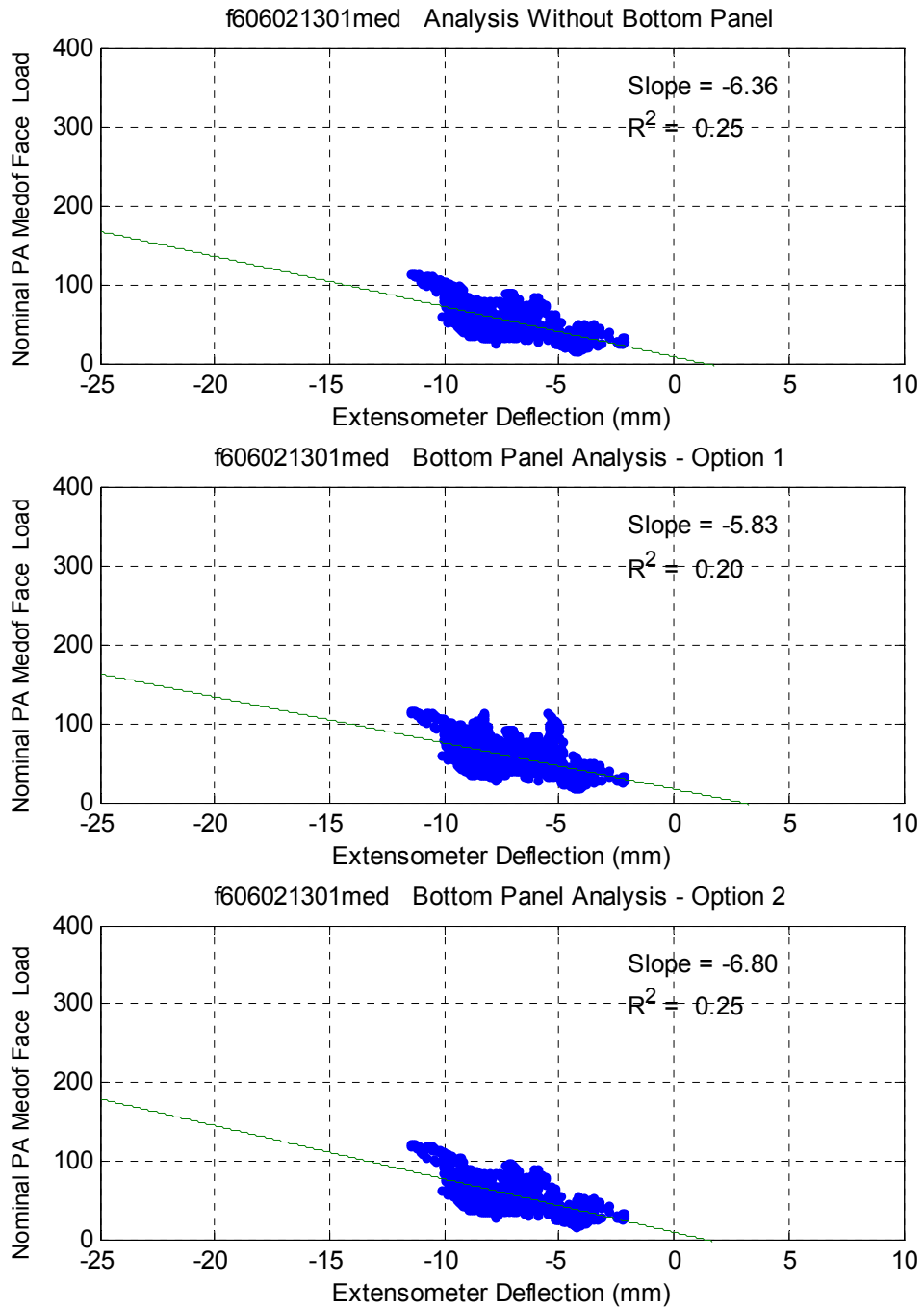
<i>Event ID</i>	<i>Date</i>	<i>Fast File</i>	<i>Segment</i>	<i>Time Period</i>	<i>Failure Mode</i>	<i>Panel Groups</i>	<i>Spacing of Groups</i>
19	2-Jun (C)	F606021301	full file	13:02:26 – 14:16:45	CR, MM, SLW & SLD	E1, E2 & E3	≈ 40m
19-1			1	13:02:26 – 13:11:30	SLW	E3	< 20m
19-2			2	13:11:31 – 13:32:05	CR	E2 & E3	≈ 20m
19-3			3	13:32:06 – 13:41:08	SLD & MM	E1, E2 & E3	≈ 40m
19-4			4	13:41:09 – 13:51:53	CR	E1, E2 & E3	≈ 40m
19-5			5	13:51:54 – 13:55:09	CR	E1 & E2	≈ 20m
19-6			6	13:55:10 – 13:58:04	SLD	E1, E2 & E3	≈ 40m
19-7			7	13:58:05 – 14:10:16	CR	E2 & E3	≈ 20m
19-8			8	14:10:17 – 14:16:45	CR	E3	< 20m



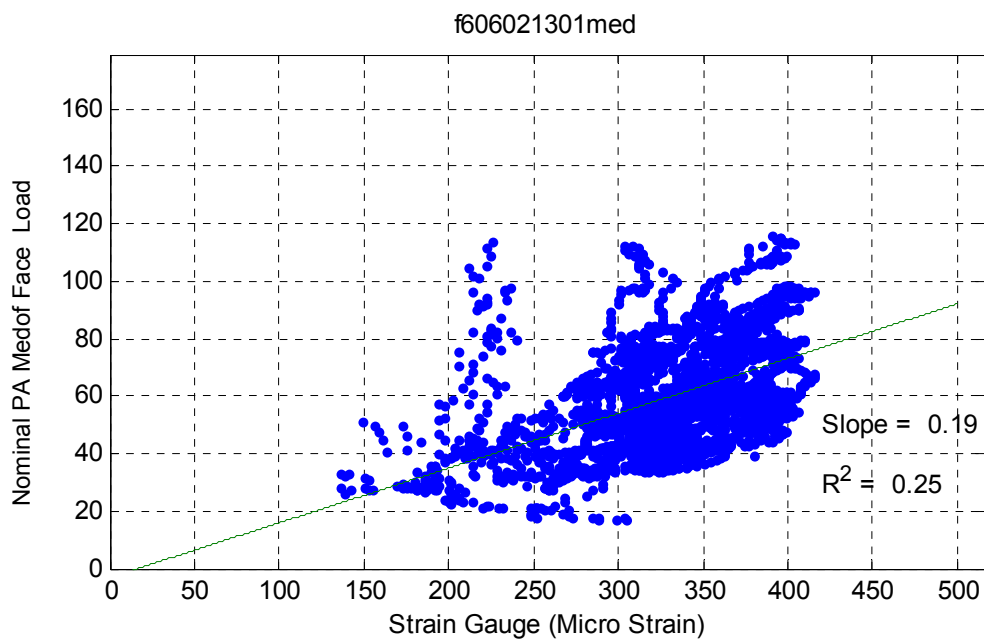
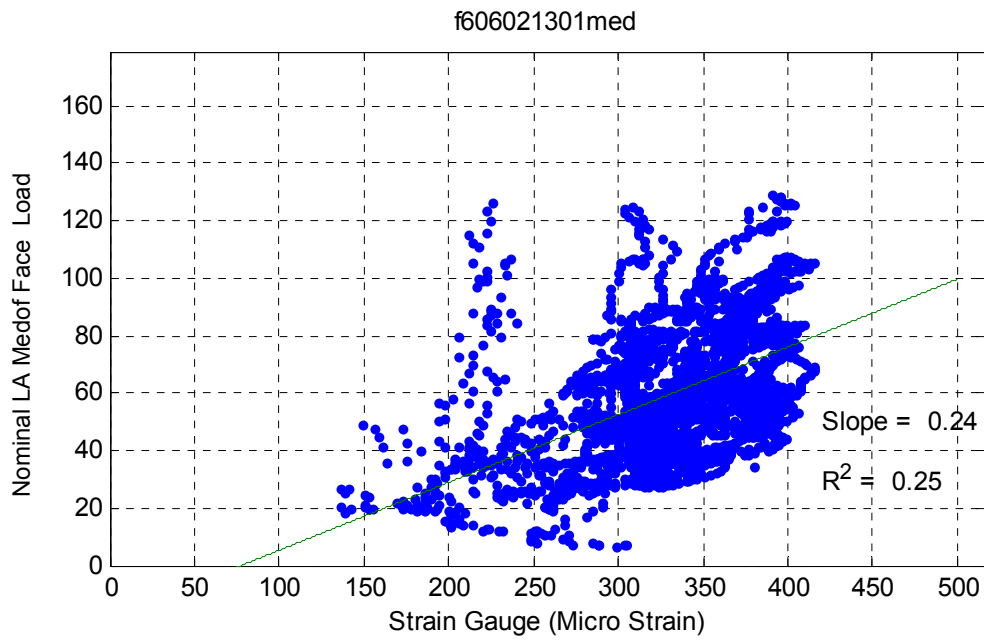




### Bottom Panel Analysis



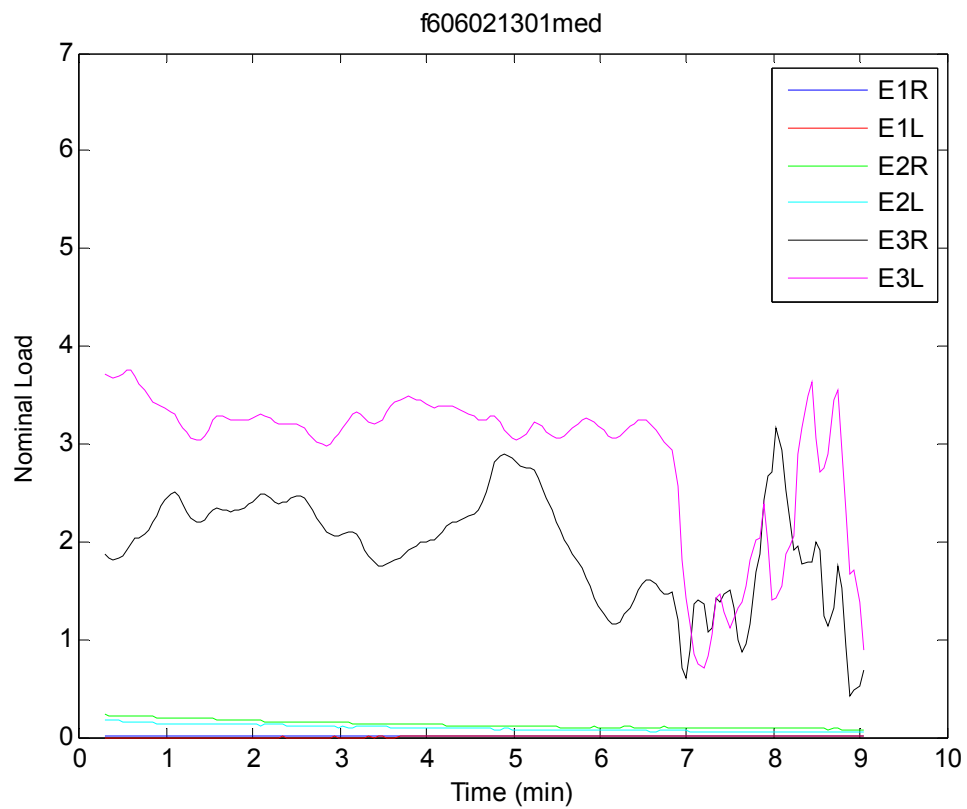
## Strain Gauge Results

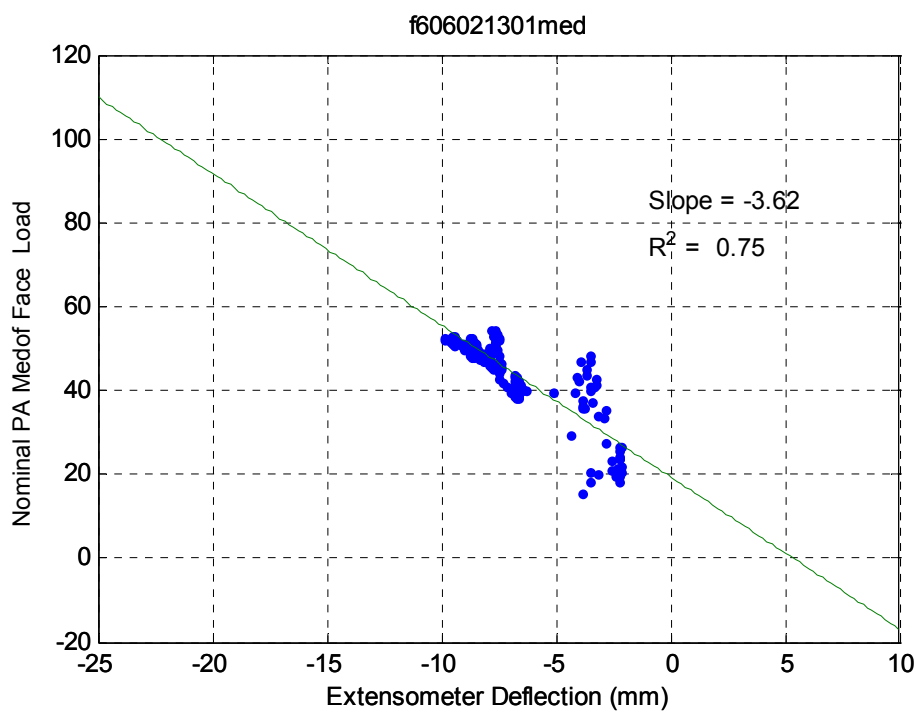
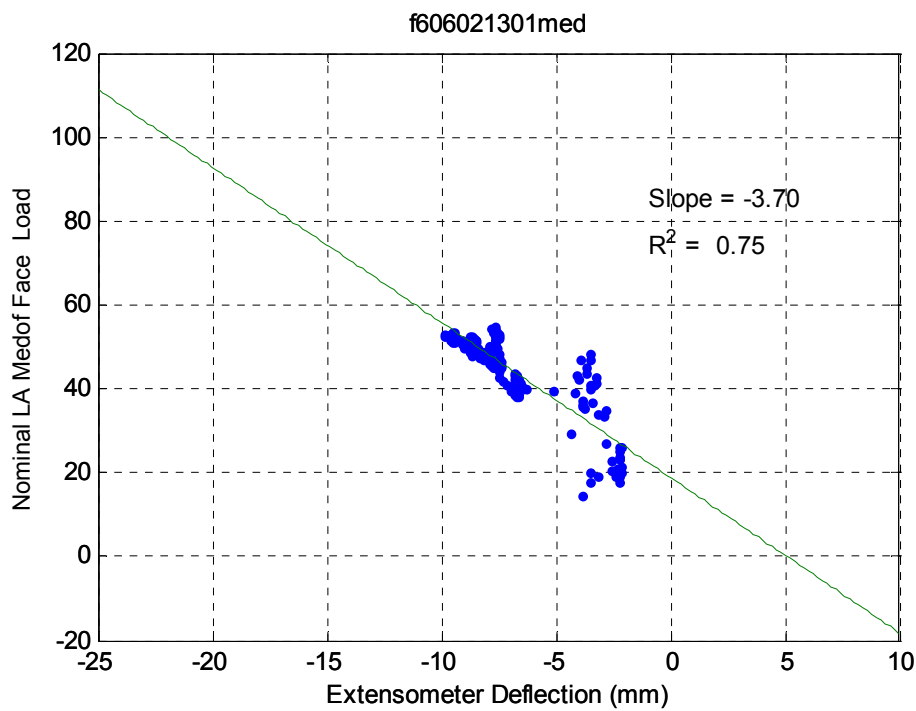


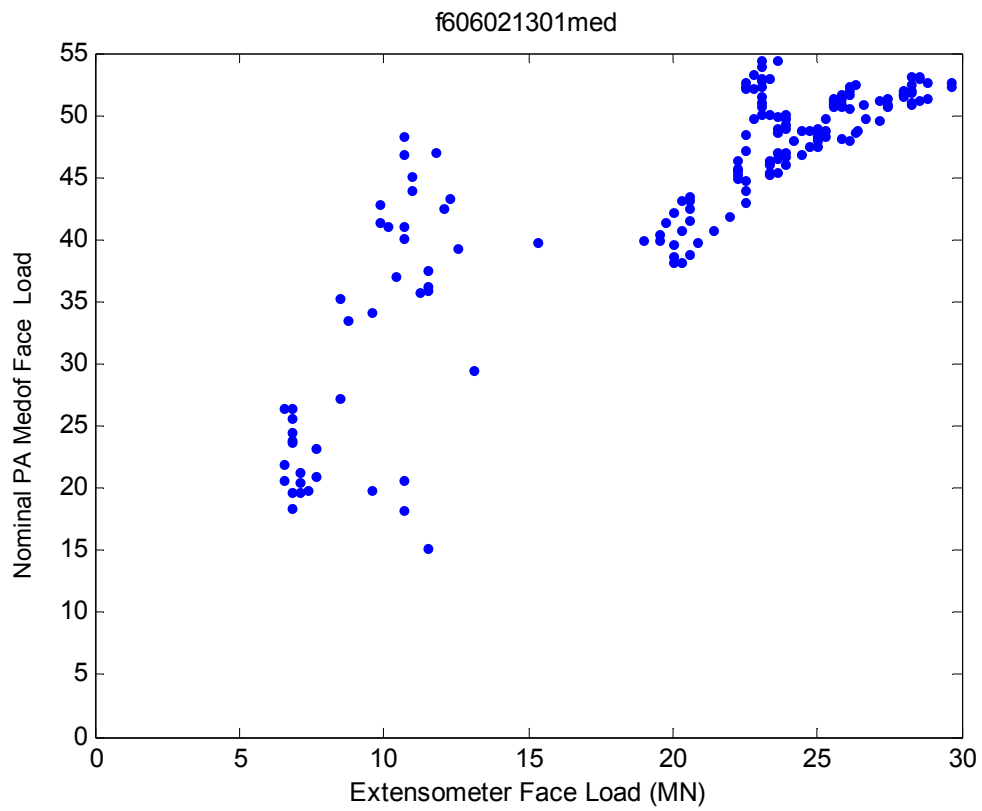
**June 2 – f606021301**

**7.1 Event ID – 19 – 1**

### Creep



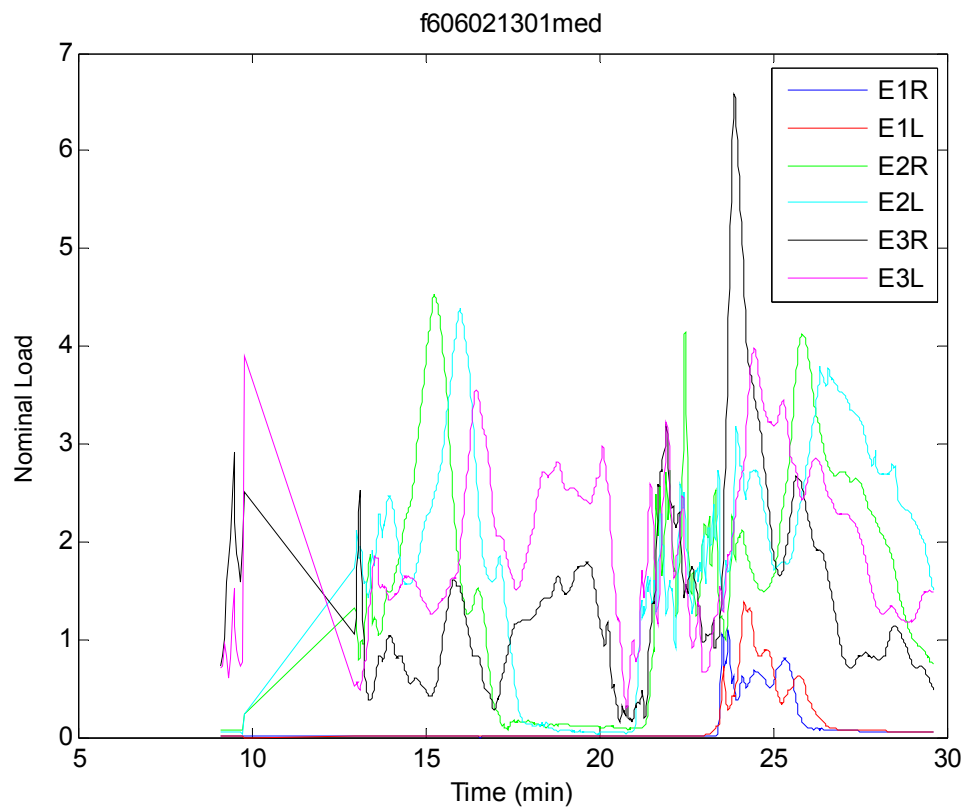


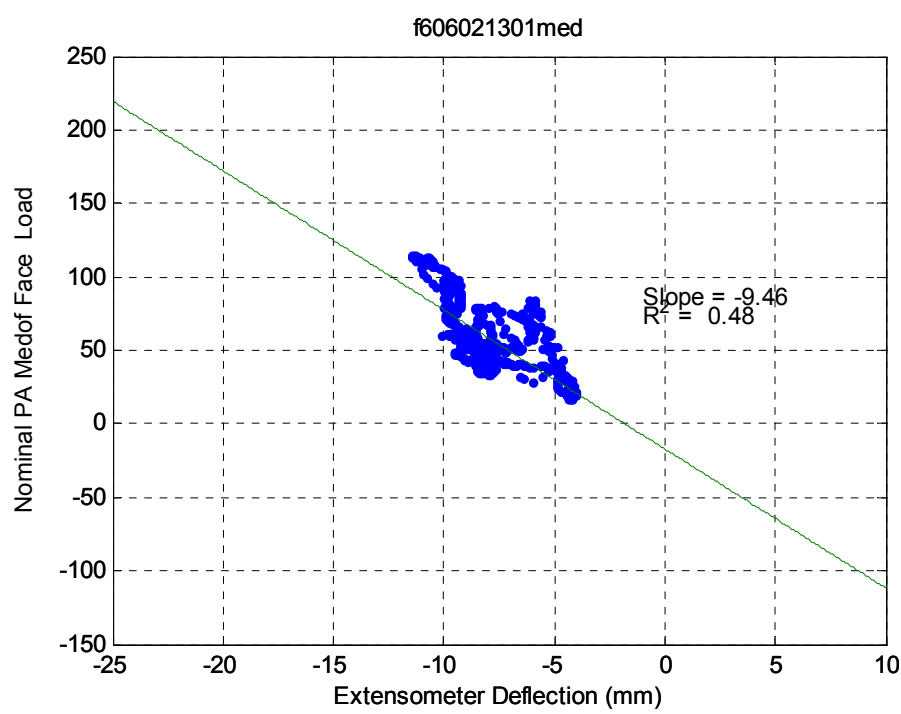
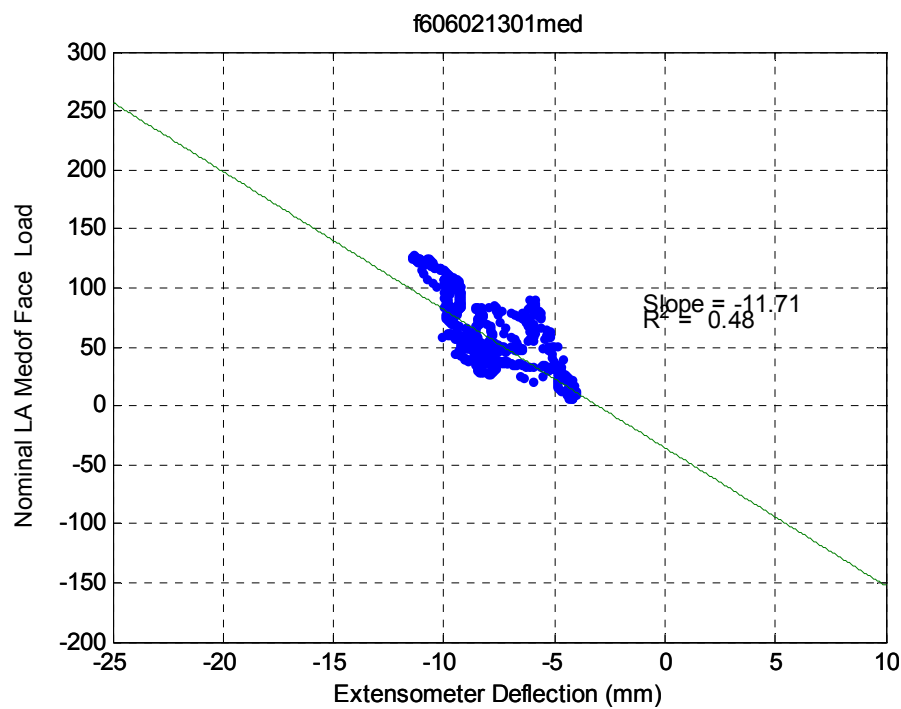


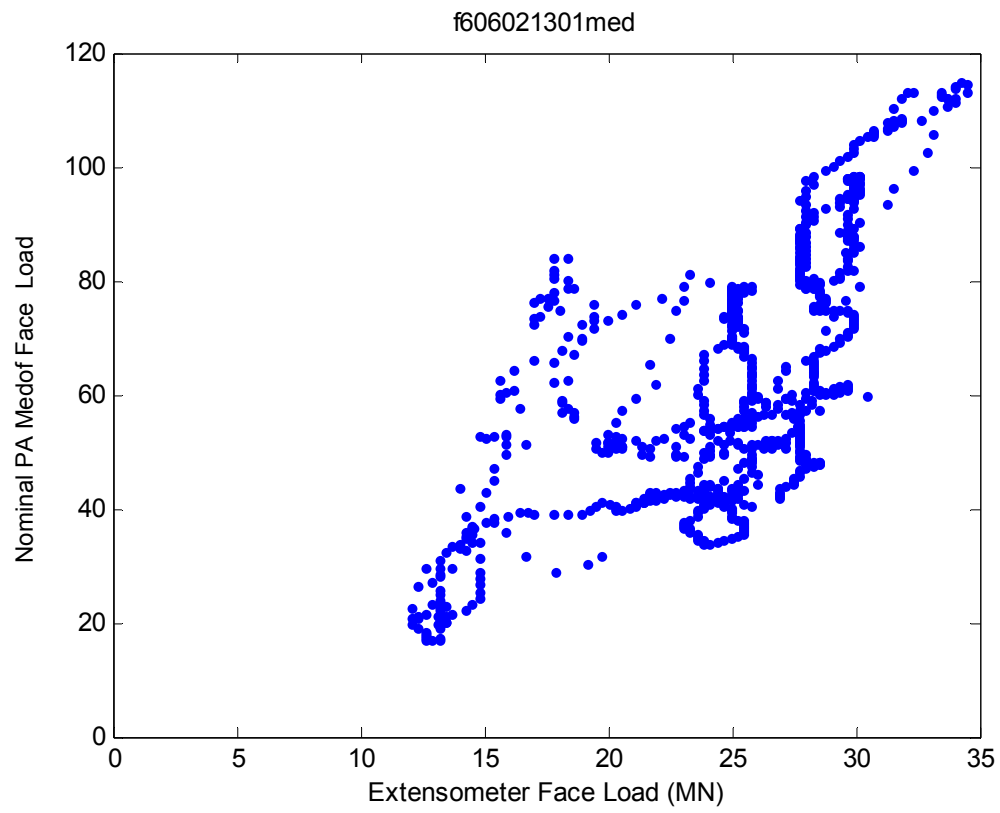
**June 2 – f606021301**

**7.2 Event ID – 19 – 2**

### Crushing

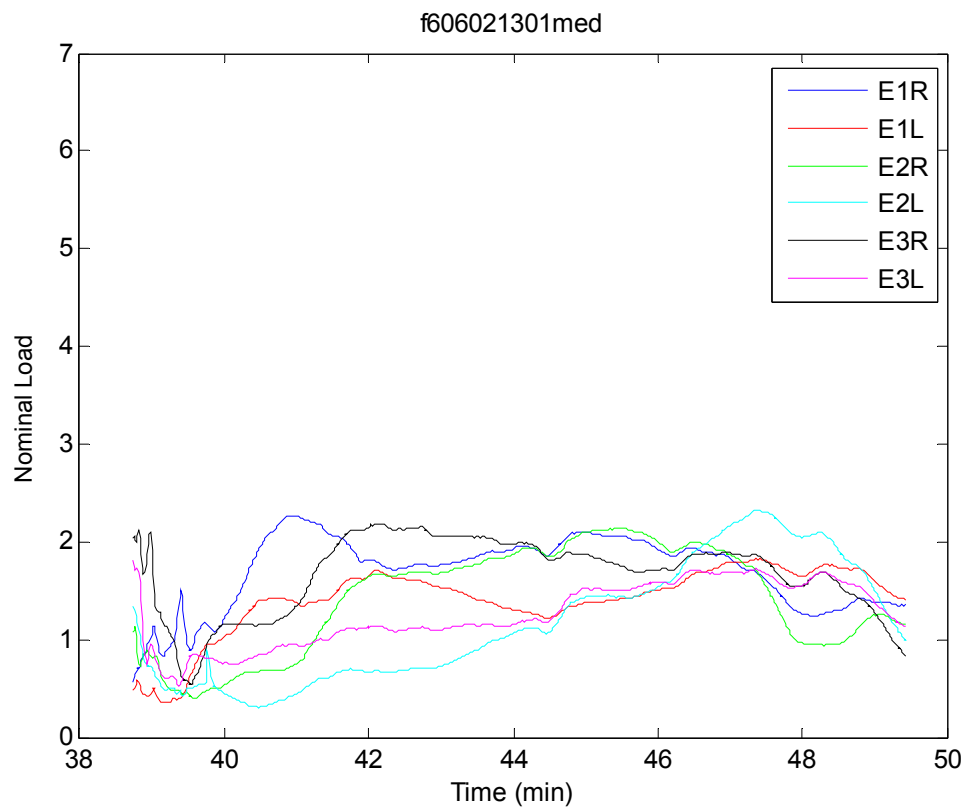


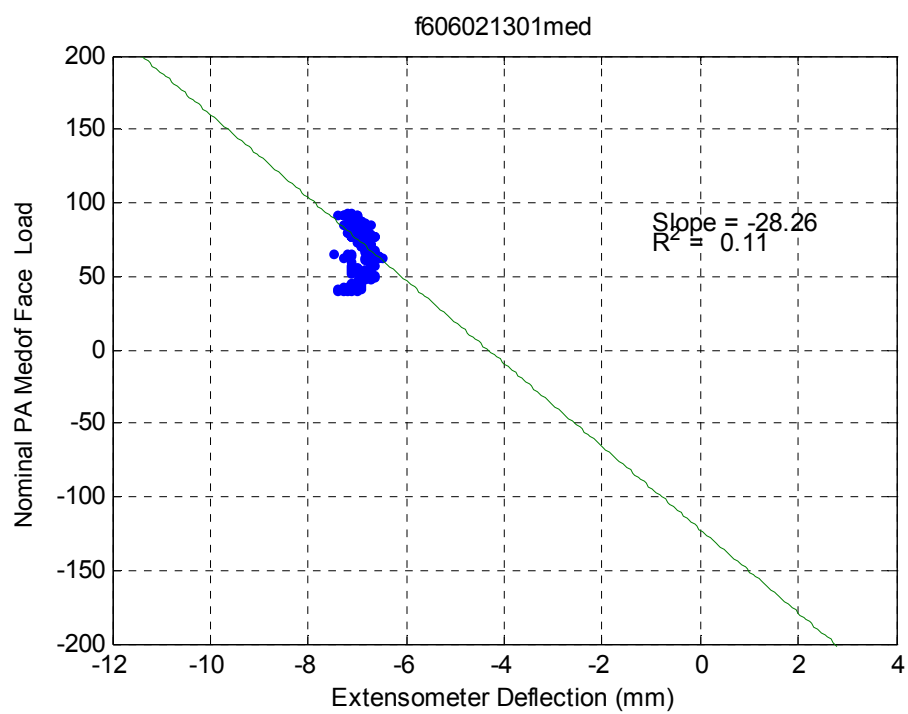
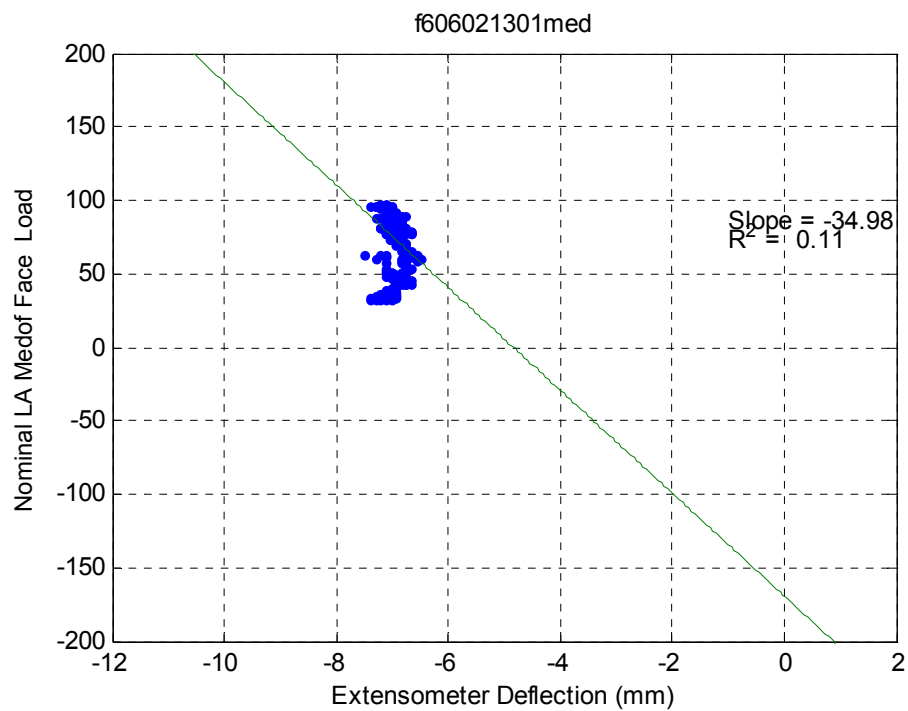


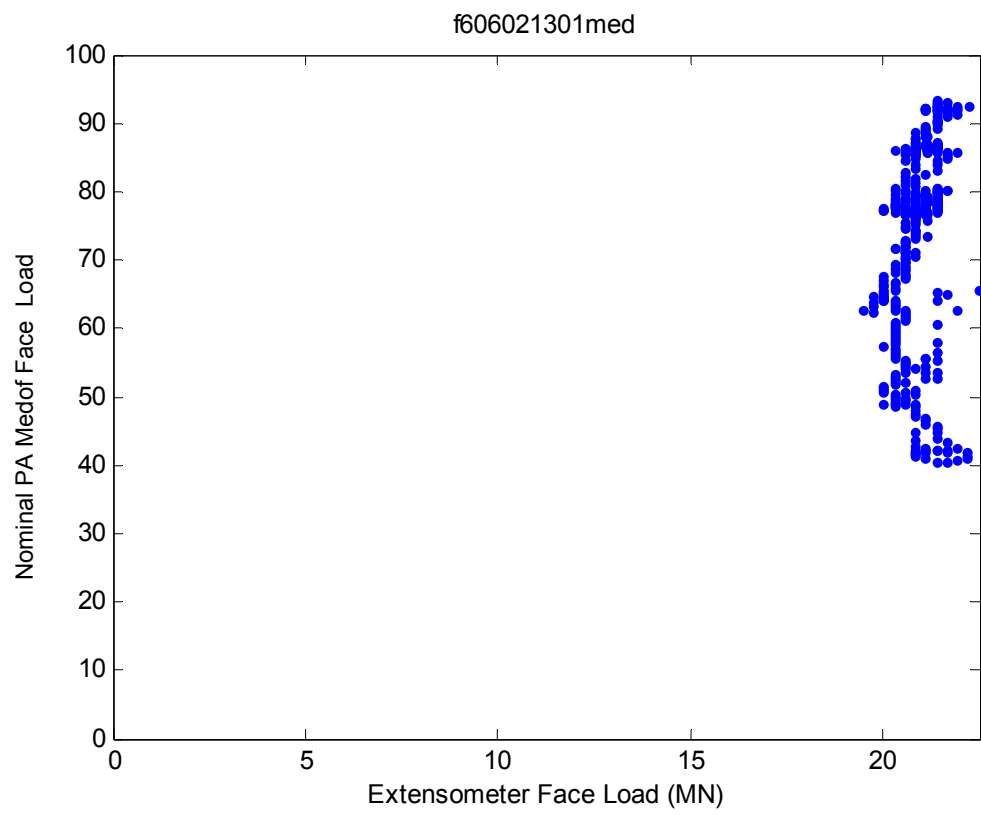


**June 2 – f606021301**  
**7.3 Event ID – 19 – 4**

**Crushing**



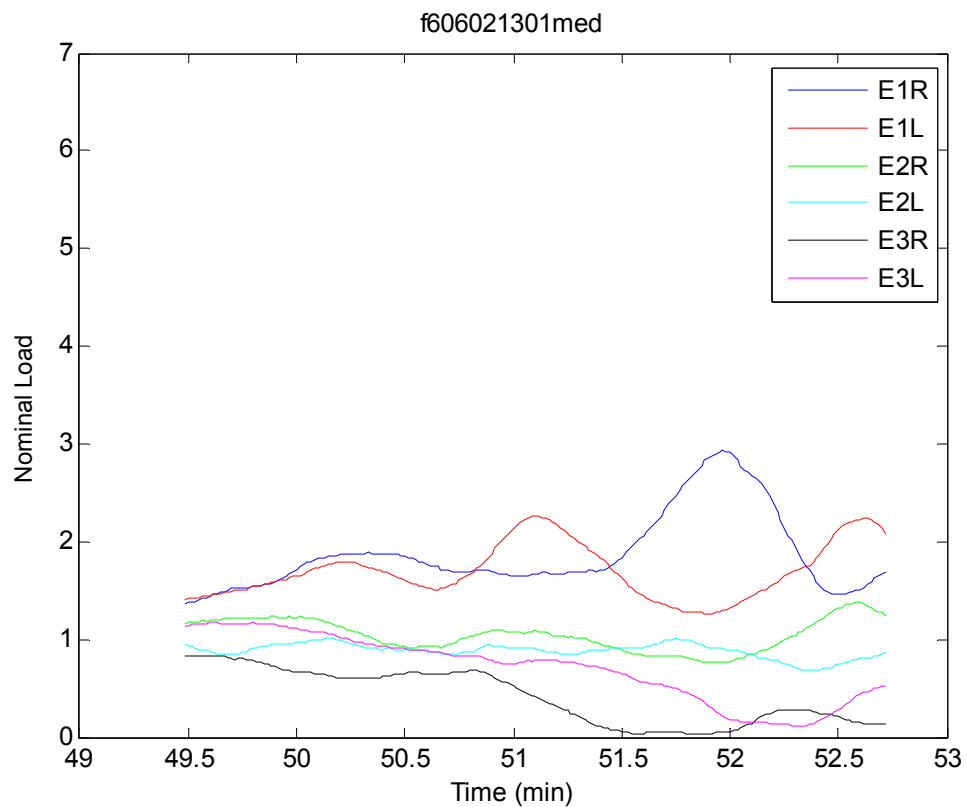


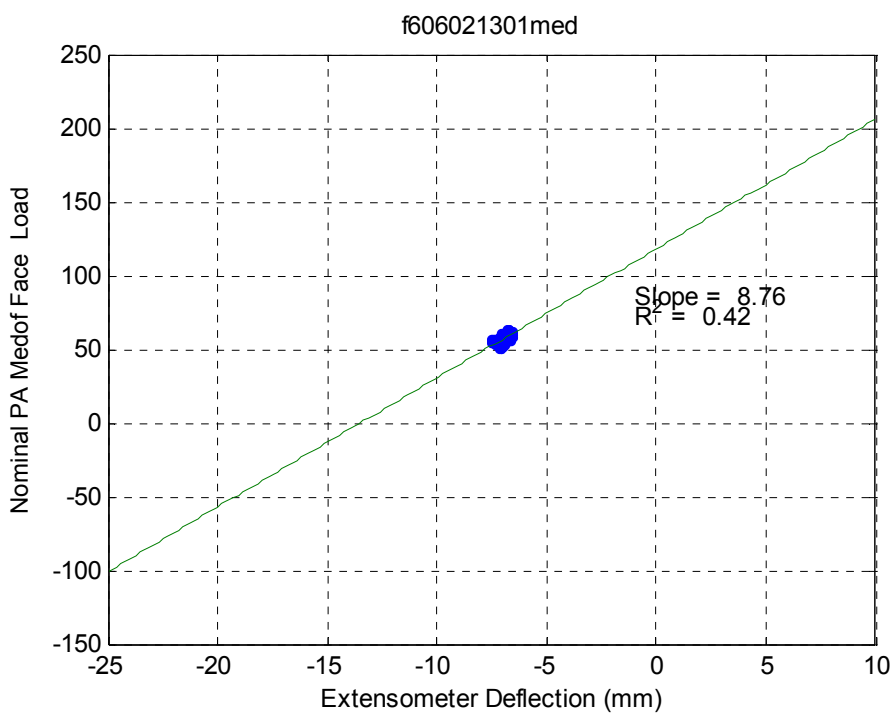
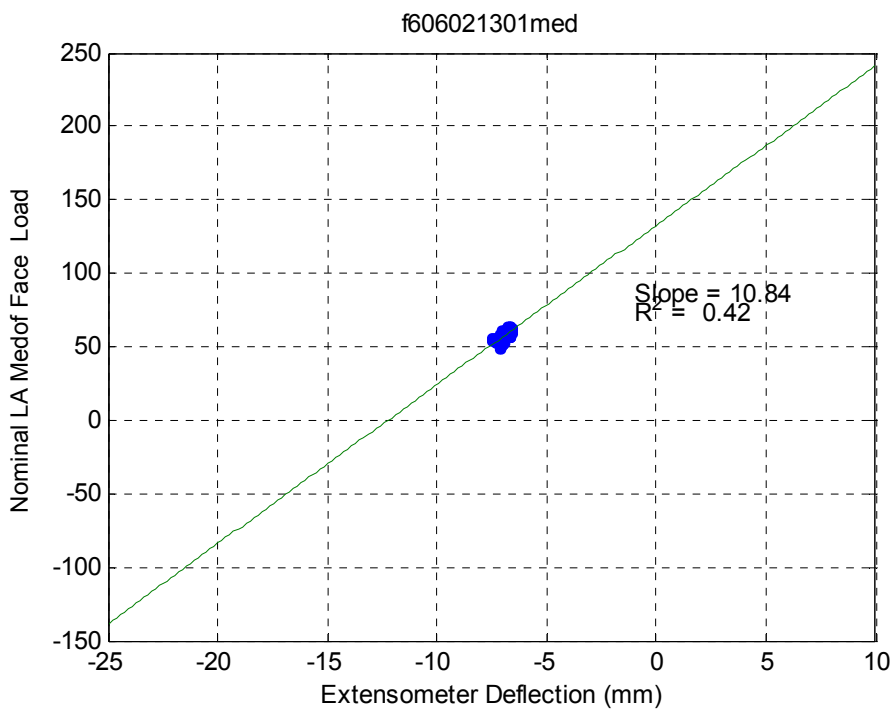


**June 2 – f606021301**

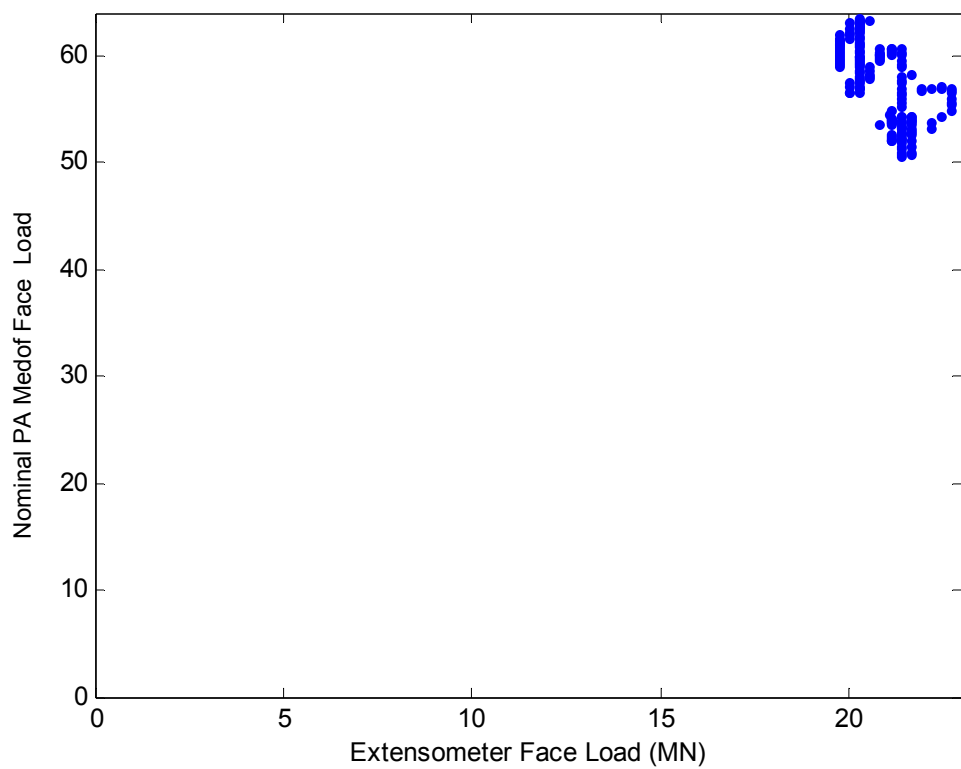
**7.4 Event ID – 19 – 5**

### Crushing



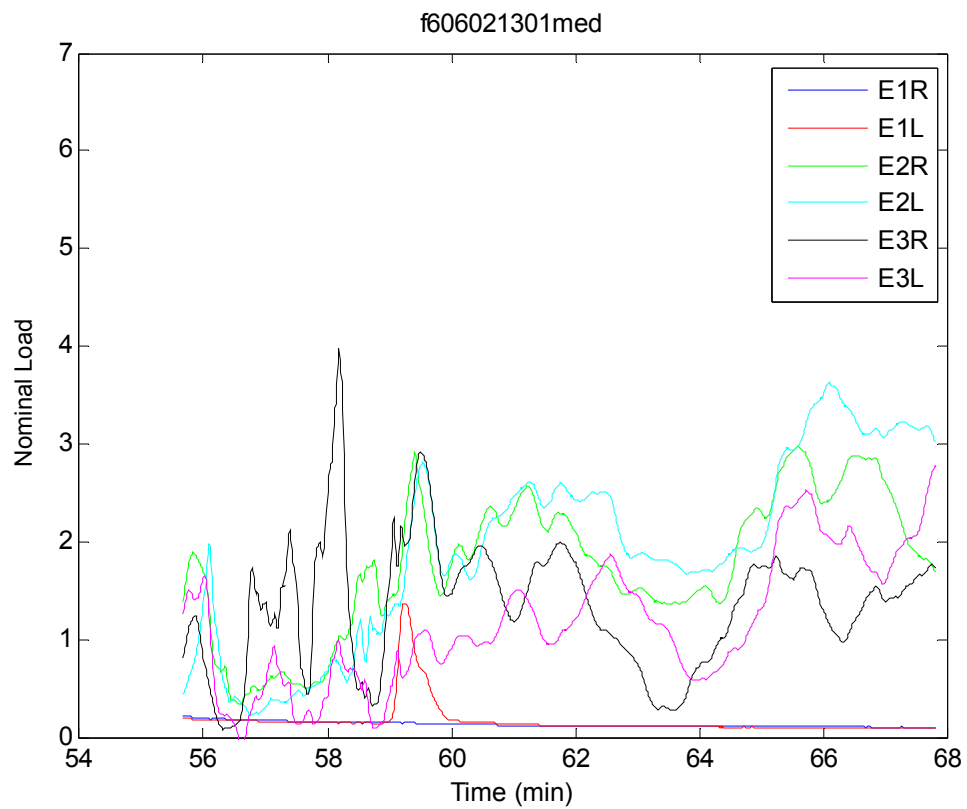


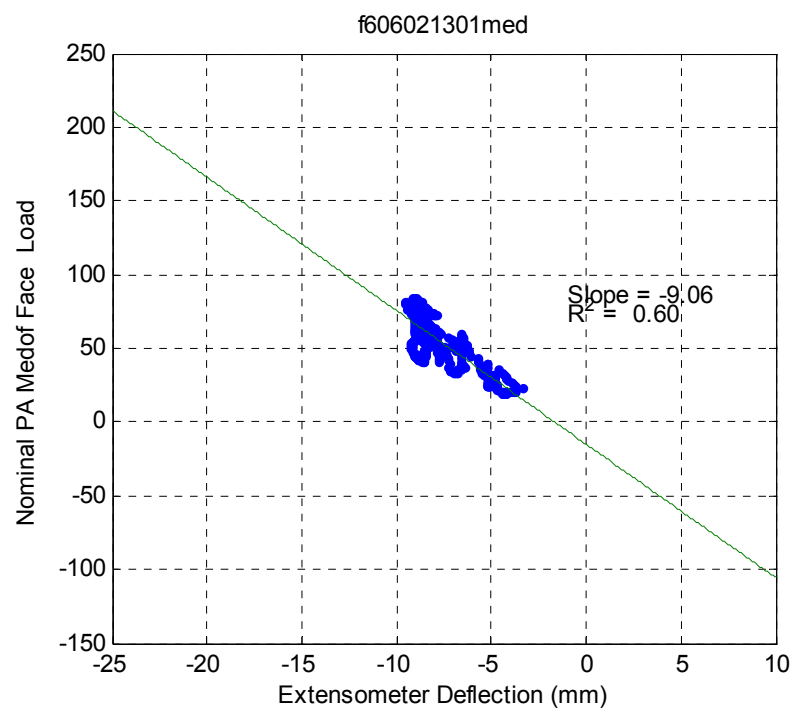
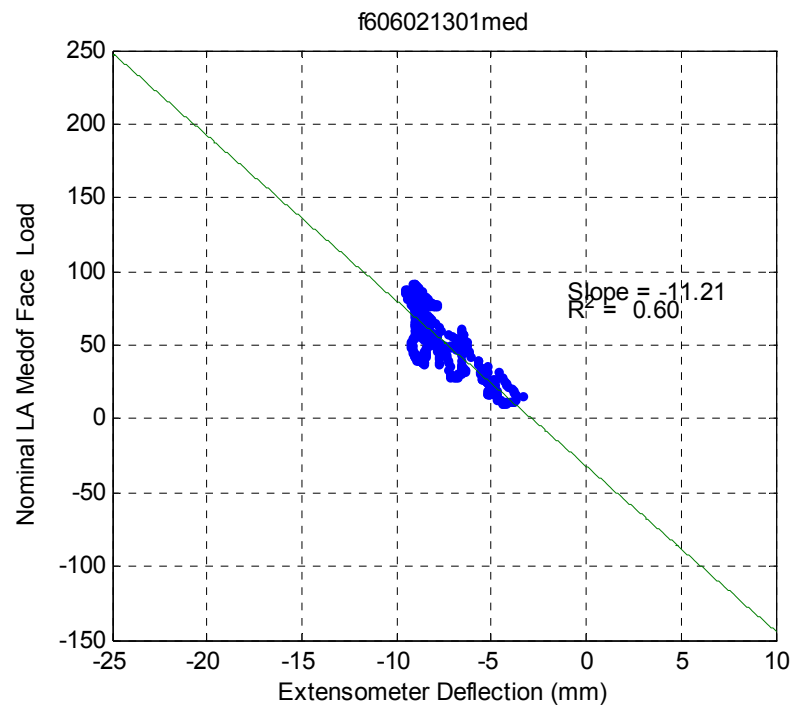
f606021301med

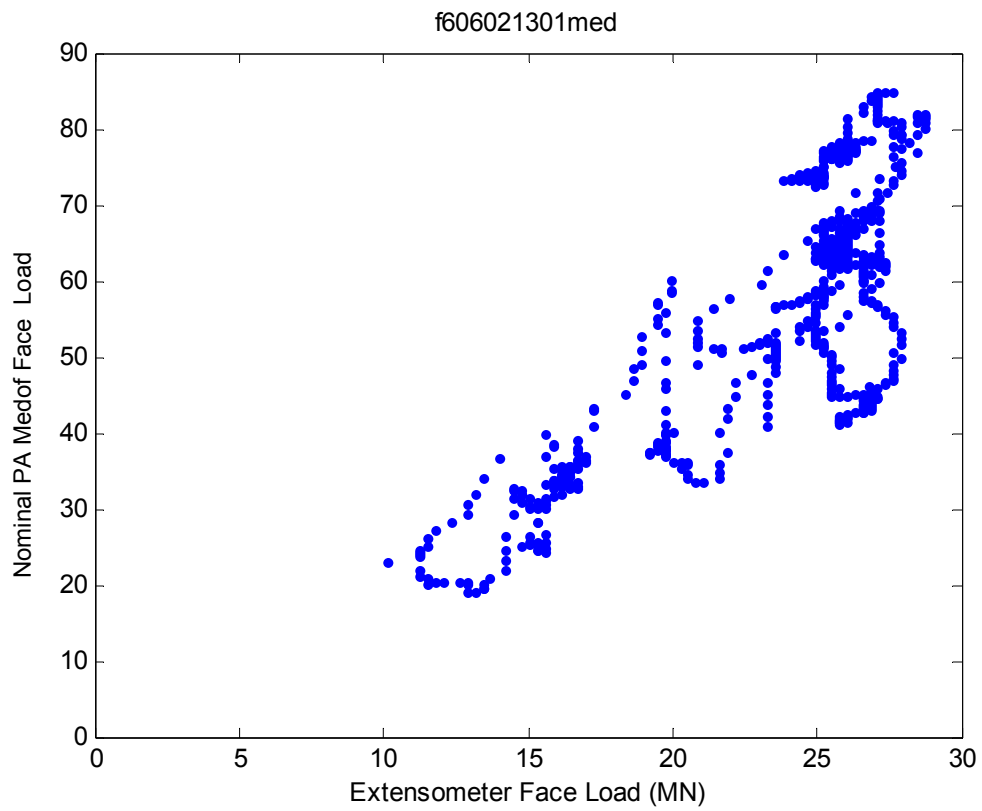


**June 2 – f606021301**  
**7.5 Event ID – 19 – 7**

**Crushing**

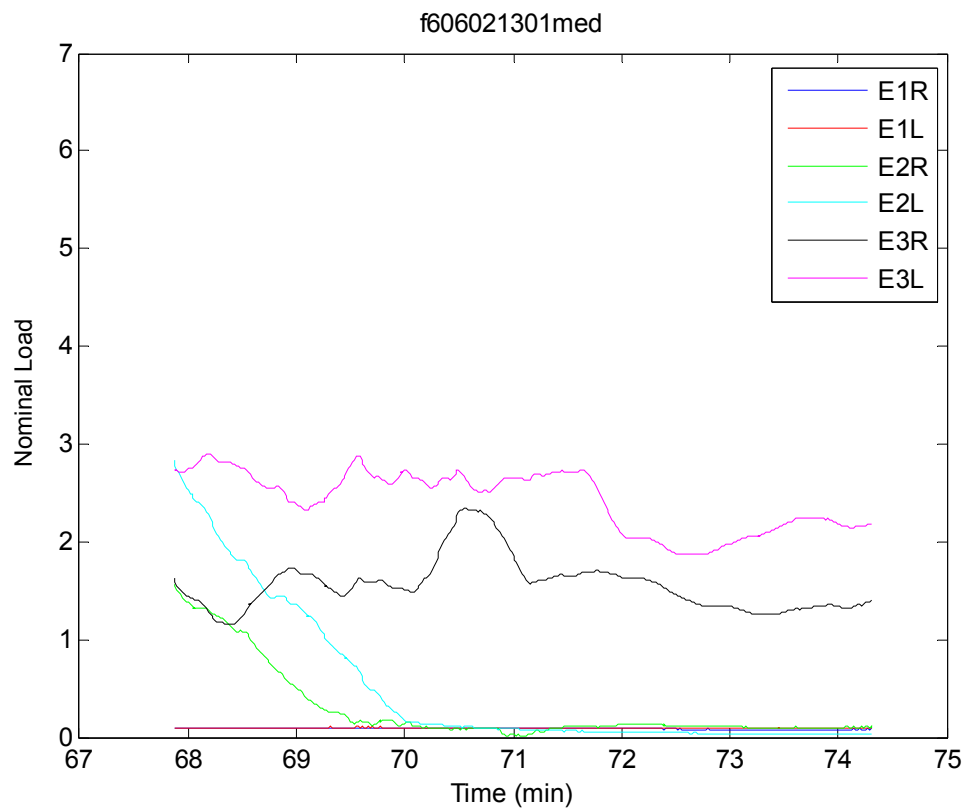


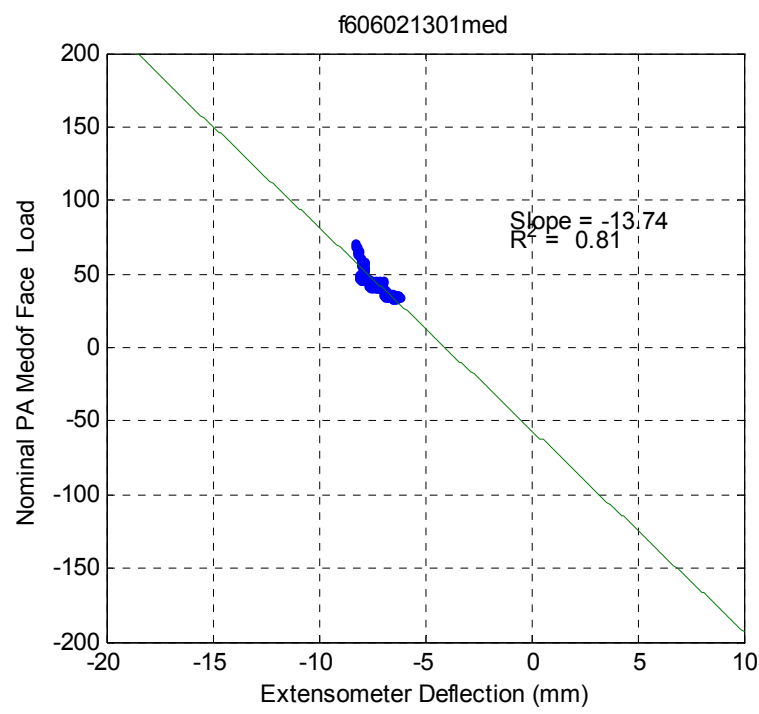
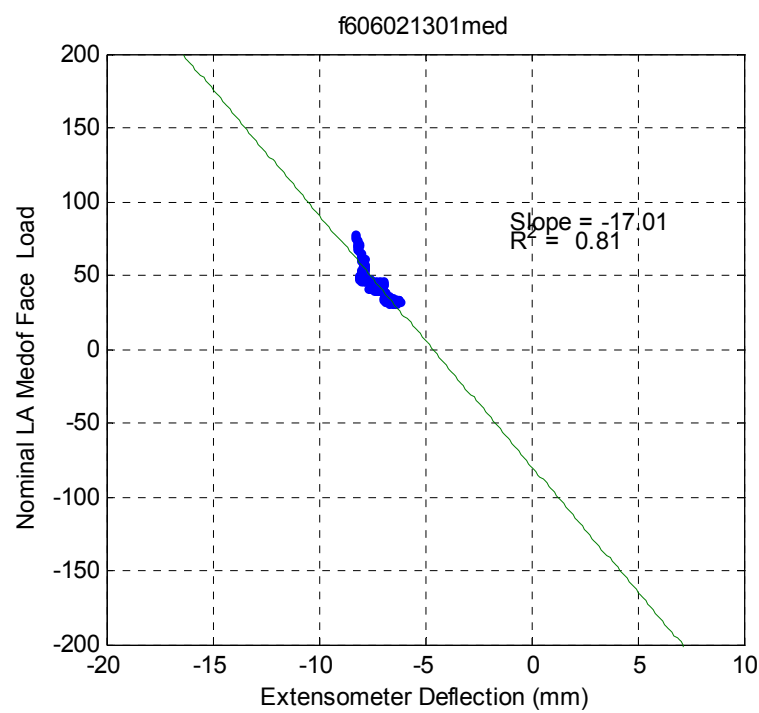


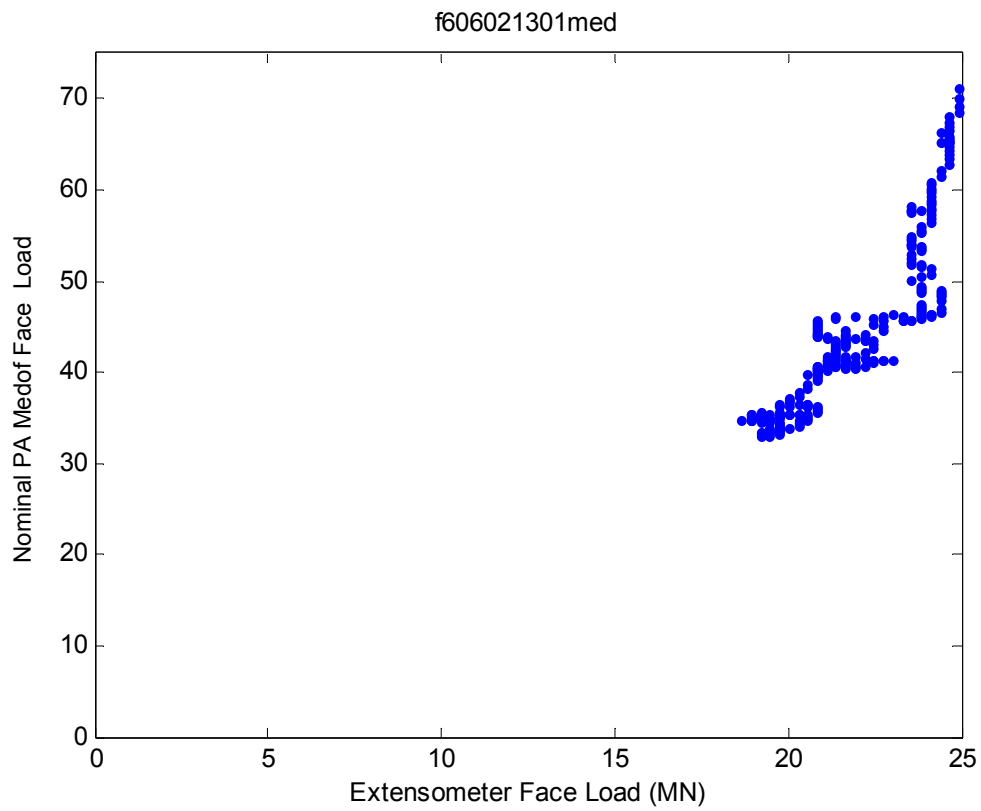


**June 2 – f606021301**  
**7.6 Event ID – 19 – 8**

**Crushing**





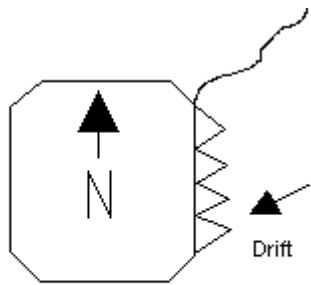


## 8 JUNE 2 – F606022201

**Event ID – 20**

**Creep**

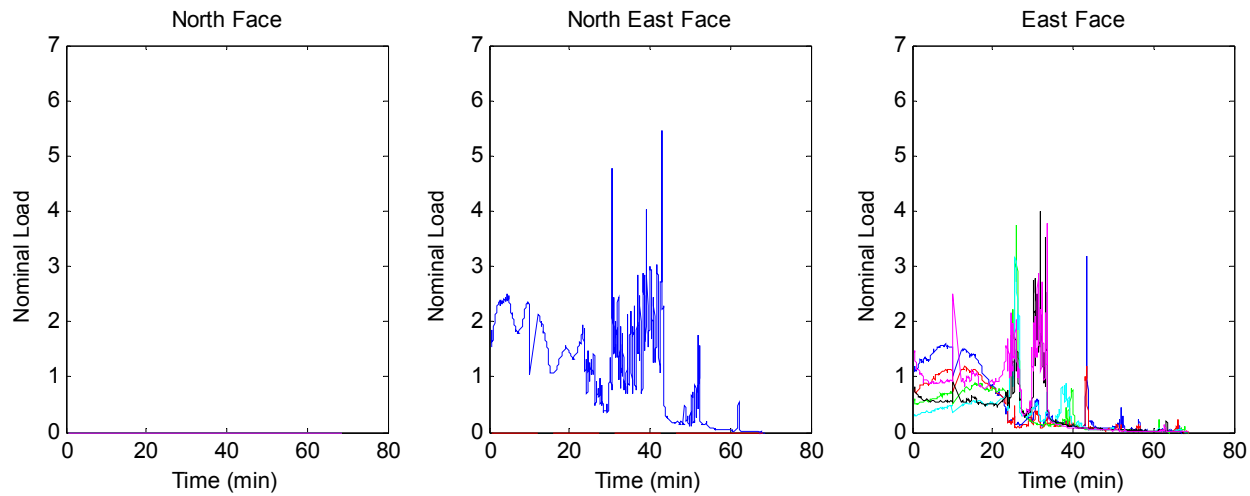
**Ice Thickness: 2m**



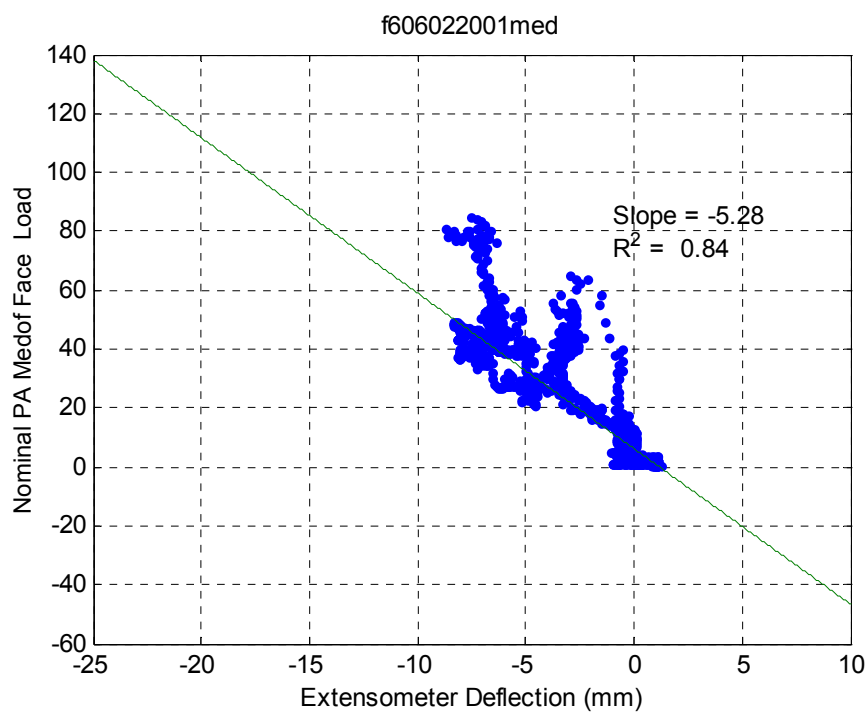
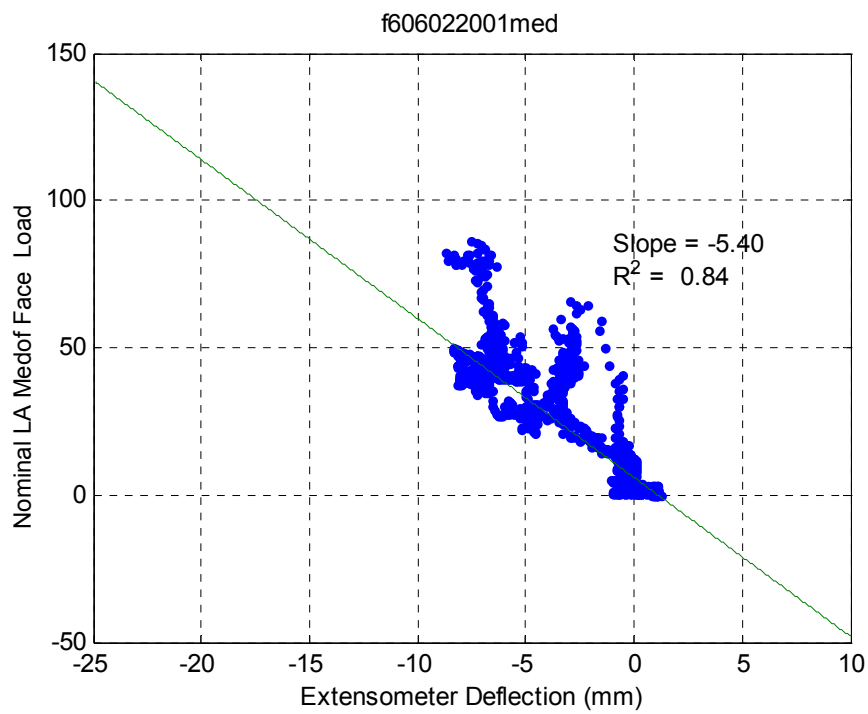
### Dynamac Event Description

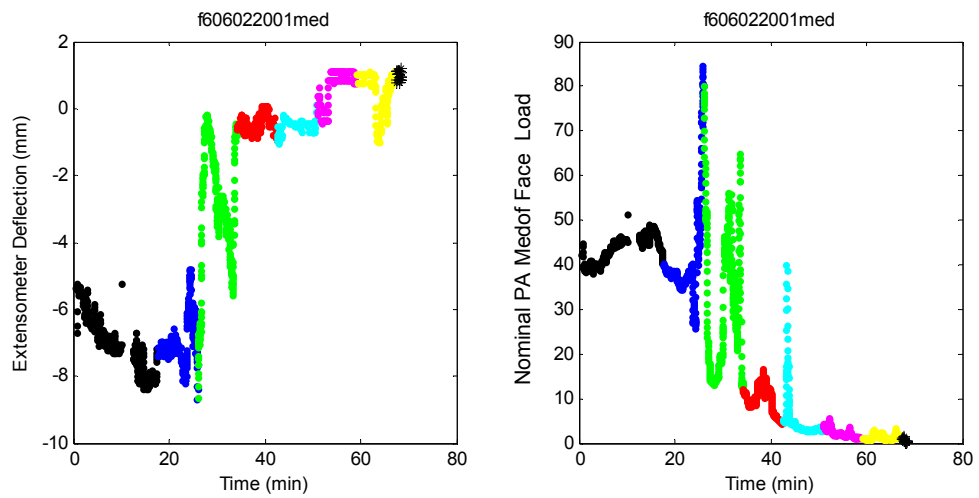
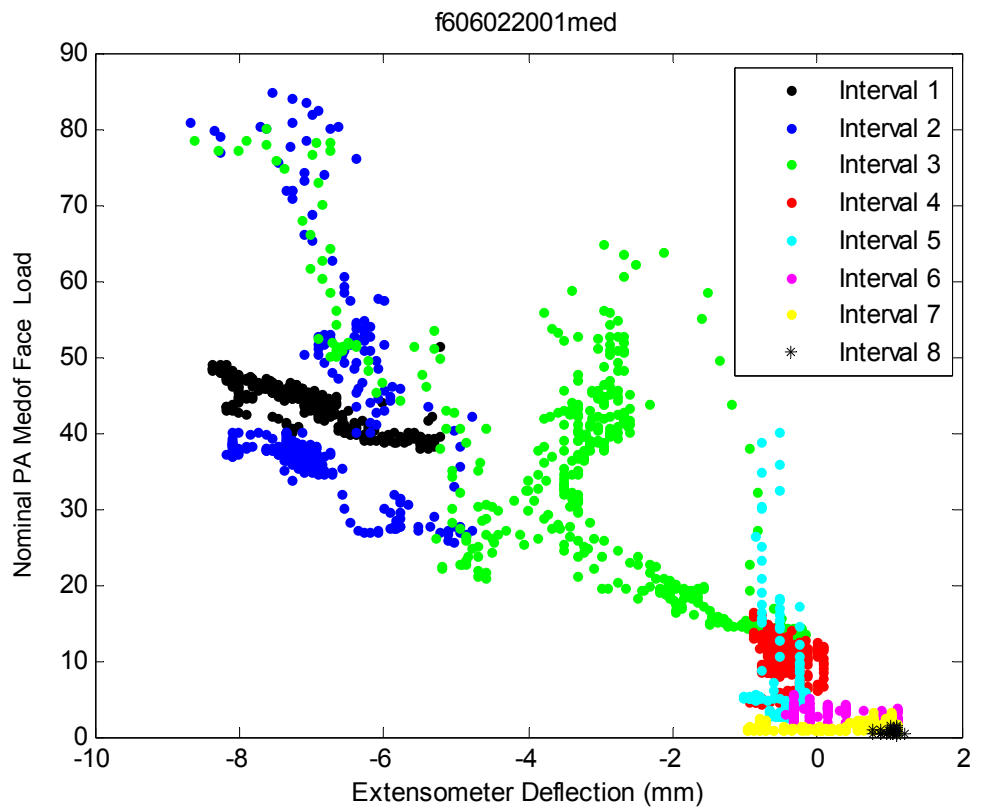
A vast floe comprising 8/10 thick and medium first year ice with 2/10 medium multi-year inclusions impacted the Molikpaq. The interaction involved creep loading, crushing and sliding on the E face.

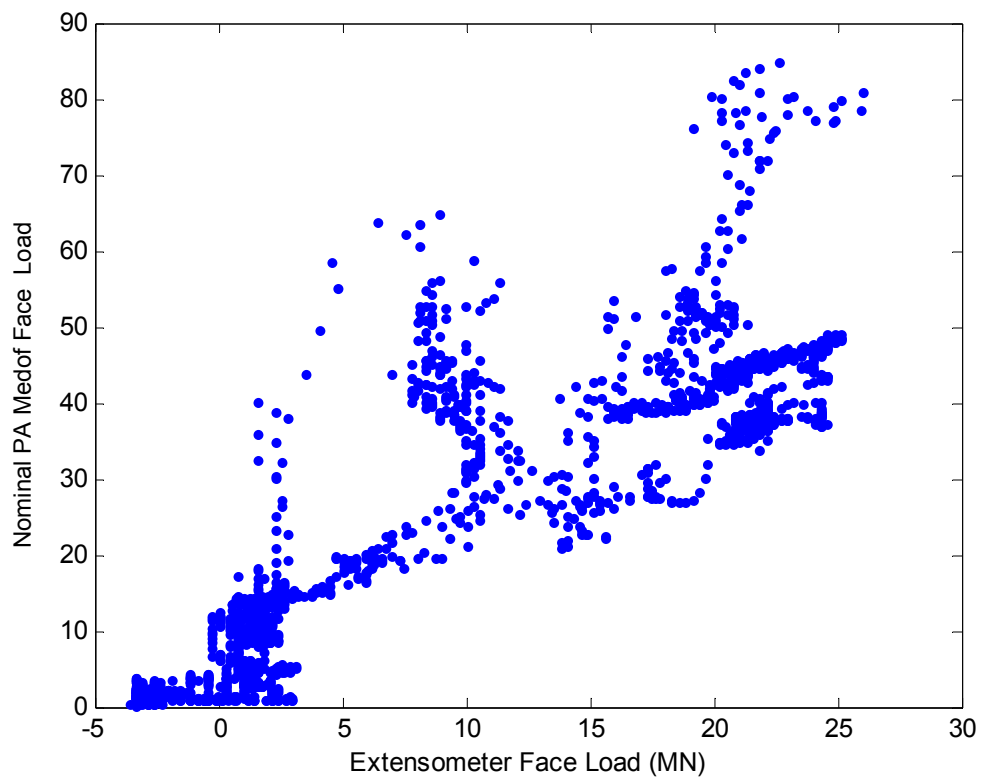
Note: The Bottom panel is loaded during this event. Some modeling of the effect of the bottom panel is required.



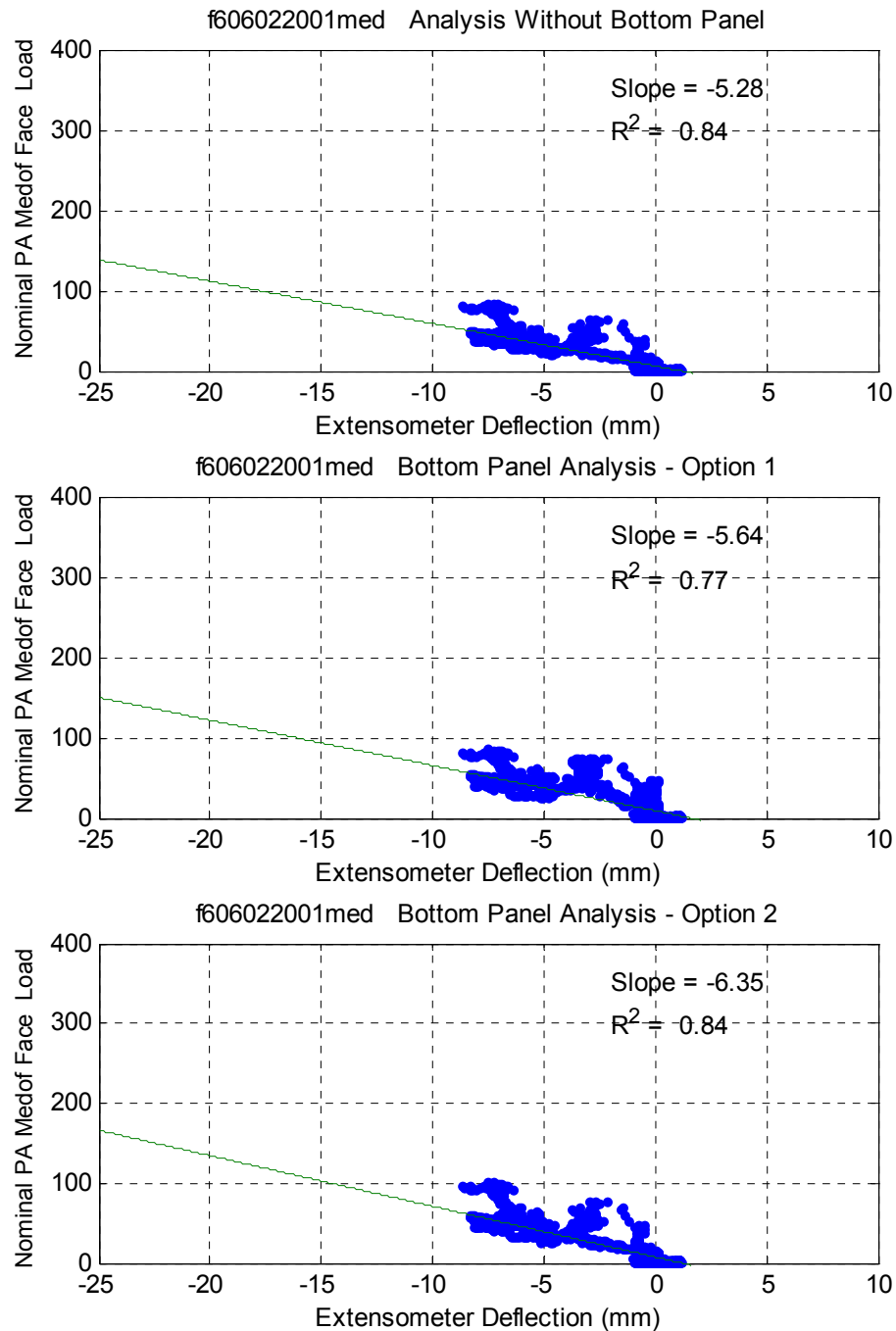
<i>Event ID</i>	<i>Date</i>	<i>Fast File</i>	<i>Segment</i>	<i>Time Period</i>	<i>Failure Mode</i>	<i>Panel Groups</i>	<i>Spacing of Groups</i>
20	2-Jun (C)	F606022201	Full file	20:16:55 – 21:24:33	SLW, CR & MM	E1, E2 & E3	≈ 40m
20-1			1	20:16:55 – 20:40:19	SLW	E1, E2 & E3	≈ 40m
20-2			2	20:40:20 – 20:43:53	CR	E2 & E3	≈ 20m
20-3			3	20:43:54 – 21:00:50	MM	E1, E2 & E3	≈ 40m
20-4			4	21:00:51 – 21:24:33	SLD	E1, E2 & E3	≈ 40m



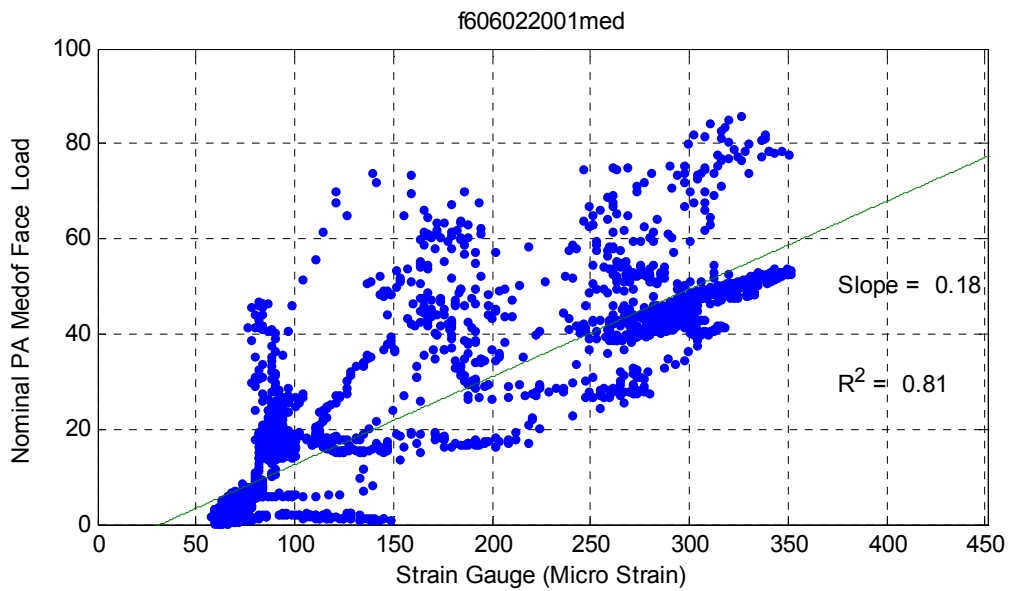
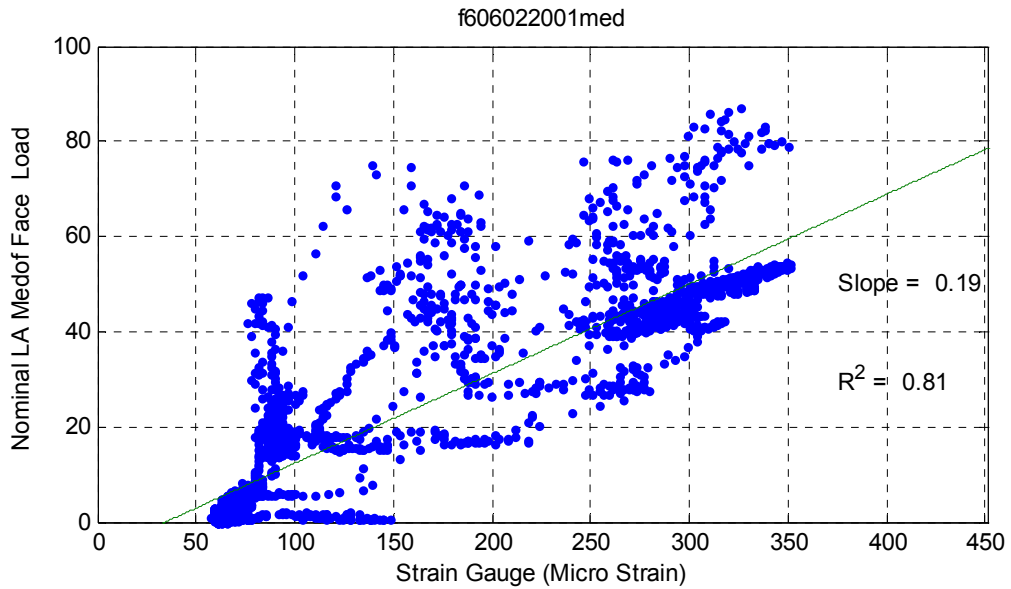




## **Bottom Panel Analysis**



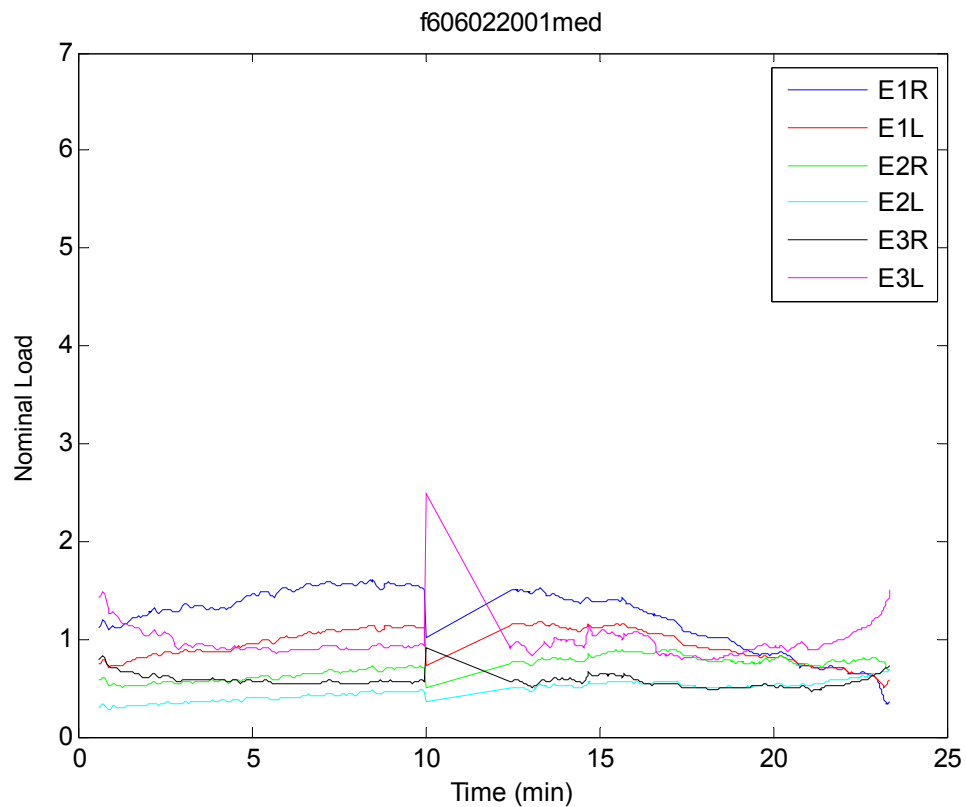
### Strain Gauge Results

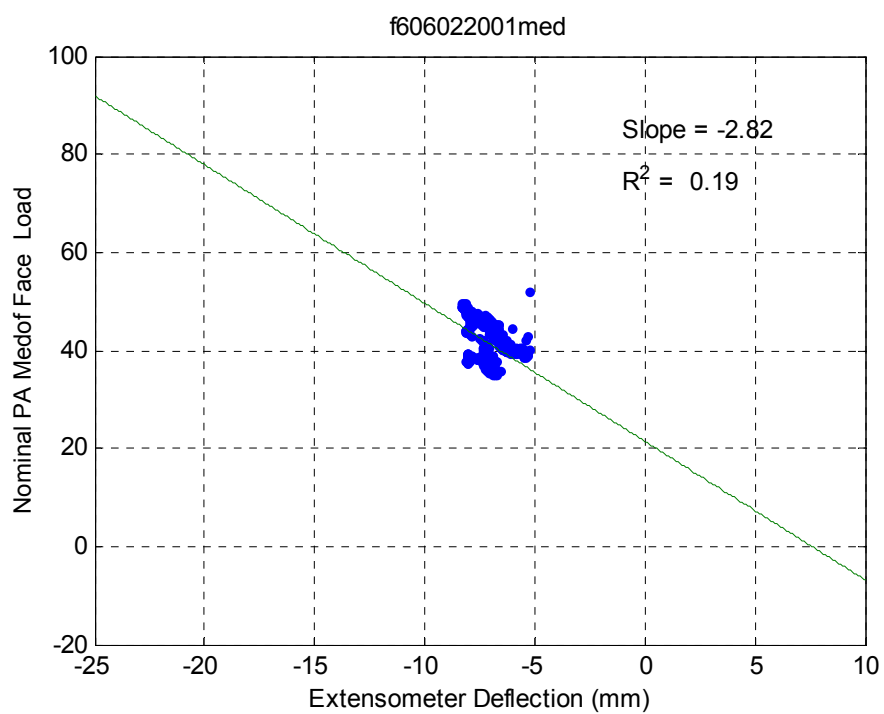
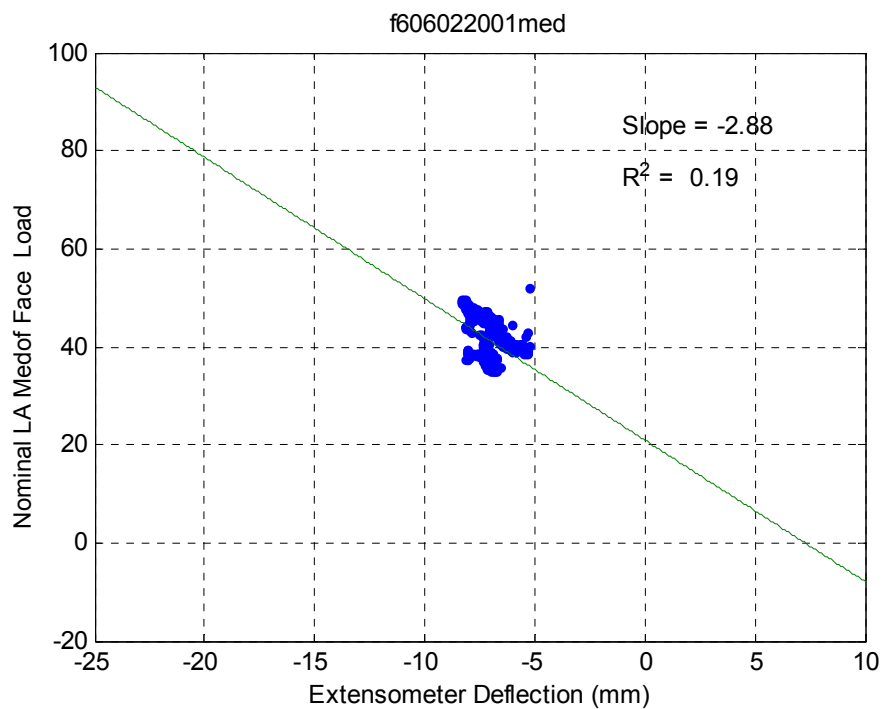


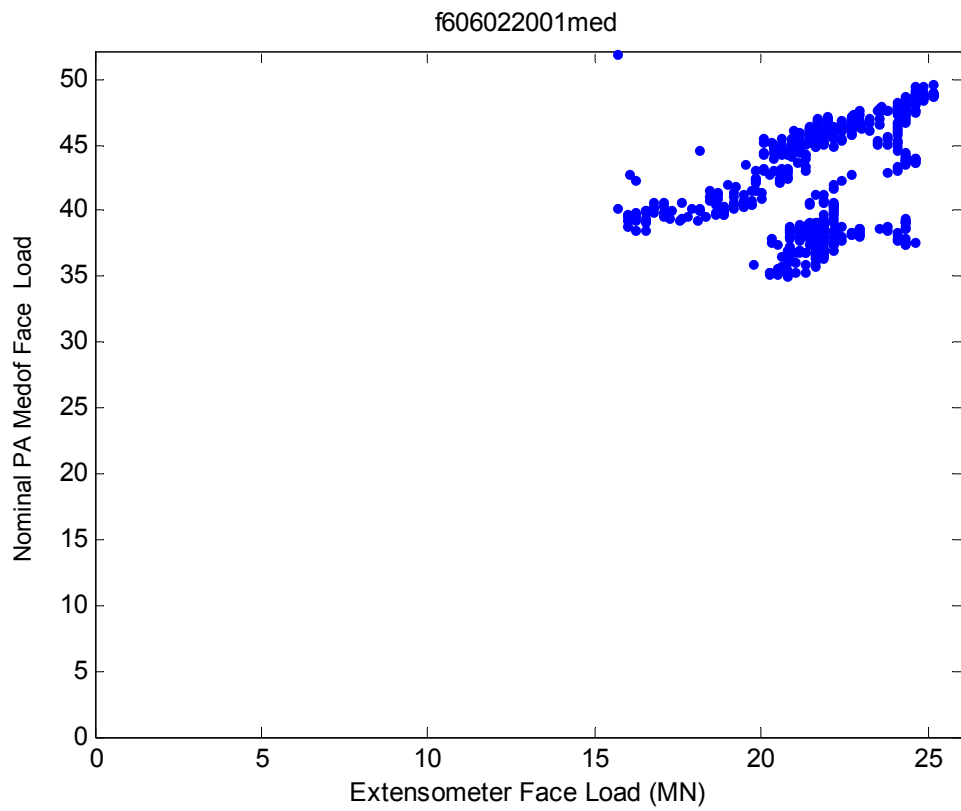
**June 2 – f606022201**

**8.1 Event ID – 20 – 1**

### Creep

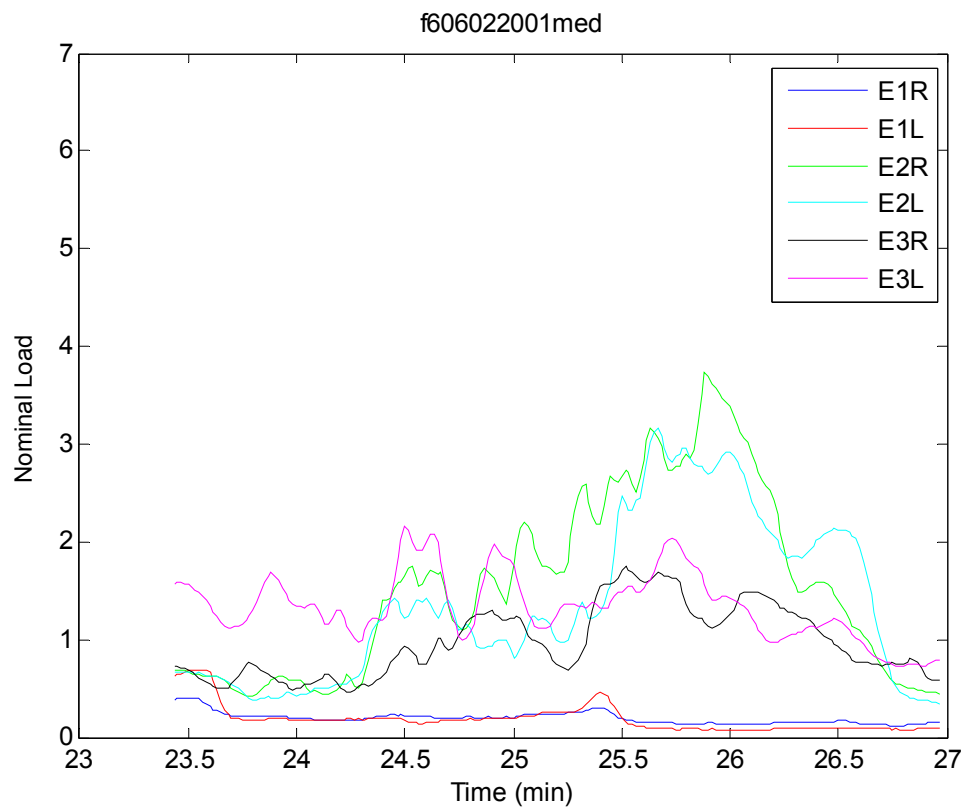


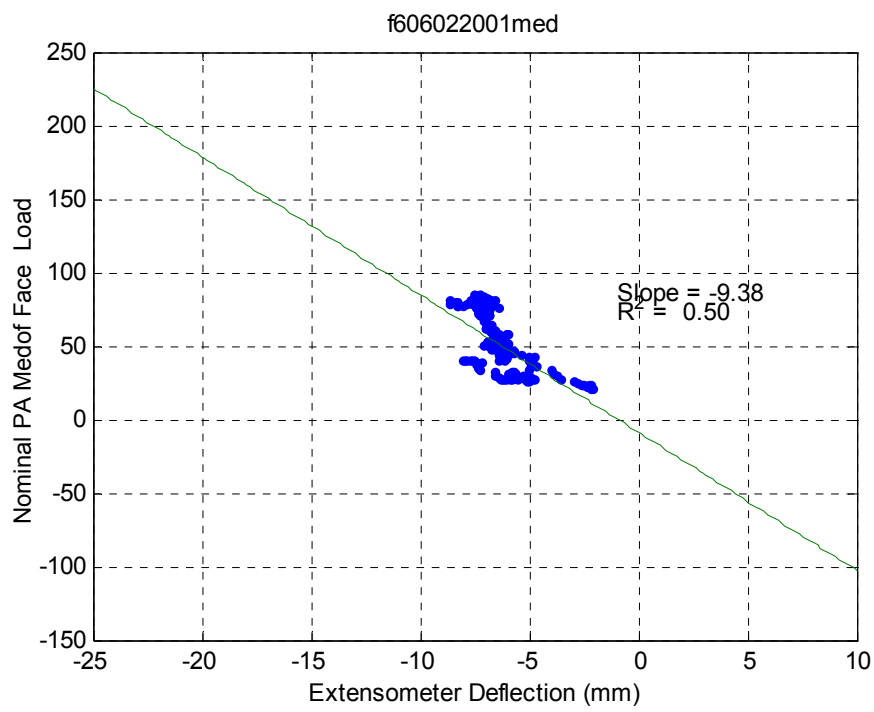
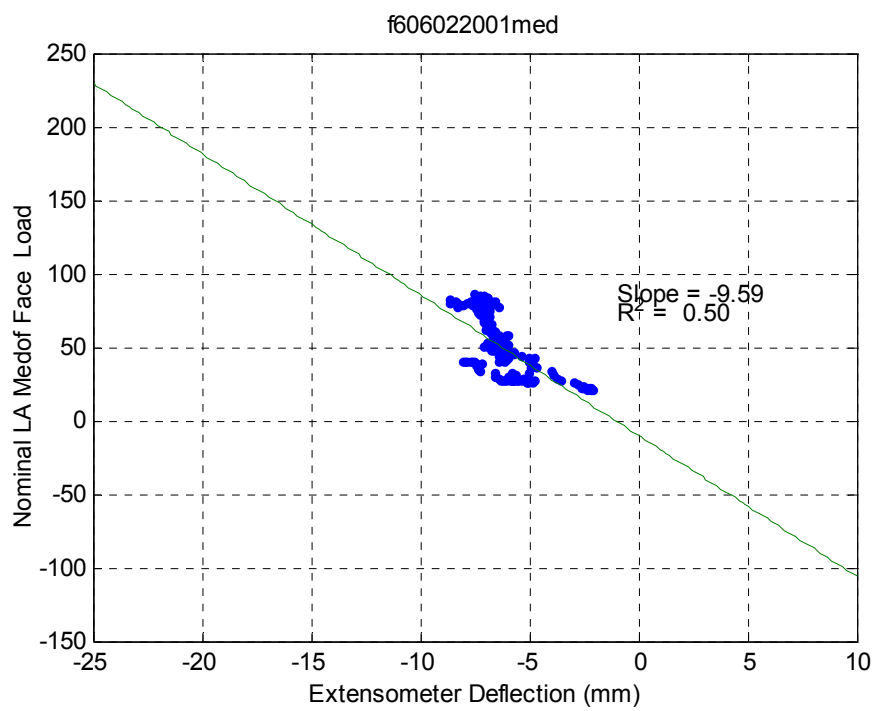


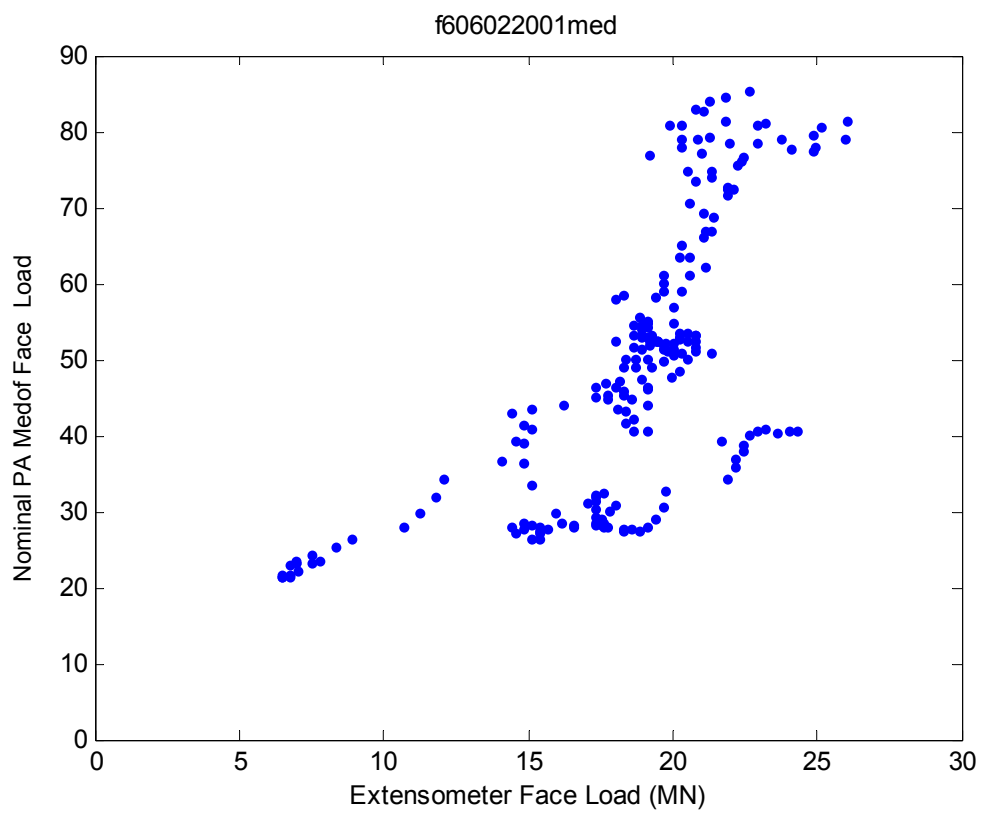


**June 2 – f606022201**  
**8.2 Event ID – 20 – 2**

**Crushing**







## **Appendix IJA - C**

### **Preliminary Geotechnical Overview of 1986 Molikpaq Response**

Submitted by Ryan Phillips of C-CORE.



# Preliminary geotechnical overview of 1986 Molikpaq response

**FINAL REPORT**  
**R-08-044-578v2.0**

**Prepared for:**  
**Ian Jordaan & Associates**

**November 2008**

Captain Robert A. Bartlett Building  
Morrissey Road  
St. John's, NL  
Canada A1B 3X5

T: (709) 737-8354  
F: (709) 737-4706

[Info@c-core.ca](mailto:Info@c-core.ca)  
[www.c-core.ca](http://www.c-core.ca)

*This page is intentionally left blank*

**Preliminary geotechnical  
overview of 1986 Molikpaq  
response**

**FINAL REPORT**

**Version 2**

**Prepared for:**

Ian Jordaan & Associates

**Prepared by:**

C-CORE

**C-CORE Report:**

R-08-044-578v2

November 2008



Captain Robert A. Bartlett Building  
Morrissey Road  
St. John's, NL  
Canada A1B 3X5

T: (709) 737-8354  
F: (709) 737-4706

[Info@c-core.ca](mailto:Info@c-core.ca)  
[www.c-core.ca](http://www.c-core.ca)

**The correct citation for this report is:**

C-CORE (2008). Preliminary geotechnical overview of 1986 Molikpaq response, C-CORE Report R-08-044-578v2, November 2008.

## REVISION HISTORY

VERSION	NAME	COMPANY	DATE OF CHANGES	COMMENTS
1.0	R. Phillips	C-CORE	Oct 2008	Draft Report for Review
2.0	R. Phillips	C-CORE	Nov 2008	Final Report

## DISTRIBUTION LIST

COMPANY	NAME	NUMBER OF COPIES
Ian Jordaan & Associates	Ian Jordaan	1 – pdf

## **EXECUTIVE SUMMARY**

This short technical note was compiled to brief the ice engineering team at Ian Jordaan & Associates and C-CORE on the geotechnical response of the Molikpaq caisson with particular reference to the work of Jeyatharan (1991). This note is not comprehensive and is limited to the references listed being compiled over a short time frame.

The note focuses on the deployment of Molikpaq at Amauligak I-65 site between 1985 and 1986, and on the ice loading events in spring 1986, and especially those of 12 April 1986.

The note reviews the two finite element analyses of Hicks & Smith (1988) and Altaee & Fellenius (1994) to indicate the development of the caisson geotechnical resistance with displacement under static and cyclic loading respectively. Simple resistance interaction diagrams based on the work of Jeyatharan (1991) and his colleagues are discussed.

The displacements required to mobilise these resistances are considered and briefly compared to measured deformation data during the ice loading events in spring 1986.

Most of the significant ice loading events were reacted by caisson basal shear alone requiring no significant caisson global displacement. The 3 larger loading events possibly required more resistance to be provided by the sand core. Permanent core deformations were measured after these 3 events. Permanent global caisson displacements after these 3 large events may be included in the baseline corrections applied to the Dynamac data.

## TABLE OF CONTENTS

<b>1</b>	<b>FINITE ELEMENT ANALYSIS EXAMPLES .....</b>	<b>1-1</b>
1.1	Hicks & Smith (1988).....	1-1
1.2	Altaee & Fellenius (1994).....	1-3
<b>2</b>	<b>CAMBRIDGE UNIVERSITY CONTRIBUTION.....</b>	<b>2-1</b>
2.1	Introduction.....	2-1
2.2	Jeyatharan (1991) thesis summary.....	2-1
2.3	Resistance estimates.....	2-2
<b>3</b>	<b>RESISTANCE MOBILISATION AND CAISSON MOVEMENTS .....</b>	<b>3-1</b>
3.1	Resistance mobilisation .....	3-1
3.2	Caisson movements .....	3-3
<b>4</b>	<b>REFERENCES .....</b>	<b>4-1</b>
A.	SELECT DYNAMAC FAST EVENT DATA RECORDS.....	I

## LIST OF TABLES

Table 3-1	Significant ice loading event summary .....	3-3
Table 3-2	Slope inclinometer permanent lateral displacement event summary, Hardy et al (1996) .....	3-5

## LIST OF FIGURES

Figure 1-1	Artificial island idealization, Hicks & Smith (1988) .....	1-1
Figure 1-2	Caisson load-displacement response, Hicks & Smith (1988) .....	1-2
Figure 1-3	Permanent calculated and measured horizontal deformation following the 5MN/m load event, Hicks & Smith (1988) .....	1-2
Figure 1-4	Typical caisson displacement response, Hicks & Smith (1988) .....	1-3
Figure 1-5	Typical constitutive model calibration, Altaee & Fellenius (1994) .....	1-4
Figure 1-6	Caisson cyclic load-displacement response, Altaee & Fellenius (1994) ..	1-4
Figure 1-7	Cyclic excess pore pressure envelopes near loaded face, after Altaee & Fellenius (1995) .....	1-5
Figure 1-8	Cyclic excess pore pressure envelopes away from loaded face, Altaee & Fellenius (1995) .....	1-5
Figure 2-1	Core lateral resistance contributions, Jeyatharan (1991) .....	2-2
Figure 2-2	Core excess pore pressure considerations, Jeyatharan (1991) .....	2-3
Figure 2-3	Calculated core resistance, Jeyatharan (1991) .....	2-3
Figure 2-4	Measured peak responses to April 12, 1986 ice loads, Hardy et al (1996) 2-4	2-4
Figure 2-5	Measured settlements after April 1986 events, after Jeyatharan (1991) ..	2-5
Figure 2-6	Piping mechanism example, Jeyatharan (1991) .....	2-6
Figure 2-7	Piping development with excess pore pressure, Jeyatharan (1991) .....	2-6
Figure 2-8	Total lateral resistance, after Jeyatharan (1991) .....	2-7
Figure 3-1	Development of compressive axial pile resistance, Davison & Wynford Owens (2003) .....	3-1
Figure 3-2	Development of earth pressure resistance with increasing wall displacements, Potts (1993) .....	3-2
Figure 3-3	Typical relative displacements required to mobilise caisson resistance ..	3-2
Figure 3-4	Caisson face load – displacement summary, after Hardy et al (1996) ....	3-4
Figure 3-5	Dynamac extensometer baseline corrections .....	3-7
Figure 3-6	N Inclinometer – global load: 25 Mar, Frederking (2008a) .....	3-8
Figure A-1	Dynamac calculated ‘fast’ response to 15:20 7 Mar event .....	i
Figure A-2	Dynamac calculated global load–deflection during 15:20 7 Mar event .....	i

Figure A-3	Dynamac calculated ‘fast’ response to 17:31 8 Mar event .....	ii
Figure A-4	Dynamac calculated global load–deflection during 17:31 8 Mar event .....	ii
Figure A-5	Dynamac calculated ‘fast’ response to 08:01 25 Mar event .....	iii
Figure A-6	Dynamac calculated global load–deflection during 08:01 25 Mar event ..	iii
Figure A-7	Dynamac calculated ‘fast’ response to 13:02 25 Mar event .....	iv
Figure A-8	Dynamac calculated global load–deflection during 13:02 25 Mar event ..	iv
Figure A-9	Dynamac calculated ‘fast’ response to 11:01 12 Apr event .....	v
Figure A-10	Dynamac calculated global load–deflection during 11:01 12 Apr event....	v
Figure A-11	Dynamac calculated ‘fast’ response to 12:01 12 Apr event .....	vi
Figure A-12	Dynamac calculated global load–deflection during 12:01 12 Apr event...	vi
Figure A-13	Dynamac calculated ‘fast’ response to 03:01 12 May event .....	vii
Figure A-14	Dynamac calculated global load–deflection during 03:01 12 May event.vii	
Figure A-15	Dynamac calculated ‘fast’ response to 08:01 22 May event .....	viii
Figure A-16	Dynamac calculated global load–deflection during 08:01 22 May eventviii	
Figure A-17	Dynamac calculated ‘fast’ response to 13:01 2 Jun event .....	ix
Figure A-18	Dynamac calculated global load–deflection during 13:01 2 Jun event ....	ix
Figure A-19	Dynamac calculated ‘fast’ response to 20:01 2 Jun event .....	x
Figure A-20	Dynamac calculated global load–deflection during 20:01 2 Jun event .....	x
Figure A-21	Dynamac caisson movements, 15:20 7 Mar event.....	xi
Figure A-22	Dynamac caisson movements, 17:31 8 Mar event.....	xi
Figure A-23	Dynamac caisson movements, 08:01 25 Mar event.....	xii
Figure A-24	Dynamac caisson movements, 13:02 25 Mar event.....	xii
Figure A-25	Dynamac caisson movements, 11:01 12 Apr event.....	xiii
Figure A-26	Dynamac caisson movements, 12:01 12 Apr event.....	xiii
Figure A-27	Dynamac caisson movements, 03:01 12 May event.....	xiv
Figure A-28	Dynamac caisson movements, 08:01 22 May event.....	xiv
Figure A-29	Dynamac caisson movements, 13:01 2 Jun event.....	xv
Figure A-30	Dynamac caisson movements, 20:01 2 Jun event.....	xv
Figure A-31	Dynamac bearing pressures, 15:20 7 Mar event.....	xvi
Figure A-32	Dynamac pore pressures, 15:20 7 Mar event.....	xvii
Figure A-33	Dynamac tilt sensors, 15:20 7 Mar event.....	xviii
Figure A-34	Dynamac bearing pressures, 17:31 8 Mar event.....	xix
Figure A-35	Dynamac pore pressures, 17:31 8 Mar event.....	xx
Figure A-36	Dynamac tilt sensors, 17:31 8 Mar event.....	xxi
Figure A-37	Dynamac bearing pressures, 08:01 25 Mar event.....	xxii
Figure A-38	Dynamac pore pressures, 08:01 25 Mar event.....	xxiii
Figure A-39	Dynamac tilt sensors, 08:01 25 Mar event.....	xxiv
Figure A-40	Dynamac bearing pressures, 13:02 25 Mar event.....	xxv

Figure A-41	Dynamac pore pressures, 13:02 25 Mar event.....	xxvi
Figure A-42	Dynamac tilt sensors, 13:02 25 Mar event.....	xxvii
Figure A-43	Dynamac bearing pressures, 11:01 12 Apr event .....	xxviii
Figure A-44	Dynamac pore pressures, 11:01 12 Apr event .....	xxix
Figure A-45	Dynamac tilt sensors, 11:01 12 Apr event .....	xxx
Figure A-46	Dynamac bearing pressures, 12:01 12 Apr event .....	xxxi
Figure A-47	Dynamac pore pressures, 12:01 12 Apr event .....	xxxii
Figure A-48	Dynamac tilt sensors, 12:01 12 Apr event .....	xxxiii
Figure A-49	Dynamac bearing pressures, 03:01 12 May event .....	xxxiv
Figure A-50	Dynamac pore pressures, 03:01 12 May event .....	xxxv
Figure A-51	Dynamac tilt sensors, 03:01 12 May event.....	xxxvi
Figure A-52	Dynamac bearing pressures, 08:01 22 May event .....	xxxvii
Figure A-53	Dynamac pore pressures, 08:01 22 May event .....	xxxviii
Figure A-54	Dynamac tilt sensors, 08:01 22 May event.....	xxxix
Figure A-55	Dynamac bearing pressures, 13:01 2 Jun event.....	xl
Figure A-56	Dynamac pore pressures, 13:01 2 Jun event.....	xli
Figure A-57	Dynamac tilt sensors 13:01 2 Jun event.....	xlii
Figure A-58	Dynamac bearing pressures, 20:01 2 Jun event .....	xliii
Figure A-59	Dynamac pore pressures, 20:01 2 Jun event .....	xliv
Figure A-60	Dynamac tilt sensors, 20:01 2 Jun event.....	xlv
Figure A-61	Dynamac bearing pressure significant baseline corrections .....	xlvi
Figure A-62	Dynamac bearing pressures, 08:20 12 Apr event .....	xlvi
Figure A-63	Dynamac pore pressures, 08:20 12 Apr event .....	xlvii
Figure A-64	Dynamac tilt sensors, 08:20 12 Apr event .....	xlvii
Figure A-65	Total pressure cell locations.....	xlviii
Figure A-66	Piezometer locations .....	xlix
Figure A-67	Extensometer locations .....	1
Figure A-68	Accelerometer & Tiltmeter locations.....	li
Figure A-69	Slope and digital inclinometer locations.....	lii

## 1 FINITE ELEMENT ANALYSIS EXAMPLES

Many organizations have conducted, mostly proprietary, finite element analyses to back analyse the Molikpaq response to the ice loading events of 12 April 1986. The most commonly referenced public analysis is that of Hicks & Smith (1988).

### 1.1 Hicks & Smith (1988)

Hicks & Smith (1988) conducted a two-dimensional analysis of the geometry shown in Figure 1-1. Their soil constitutive model was calibrated against laboratory data on Kogyuk sand, which was considered similar to that used for caisson infill. No interface elements were used between the soil and the caisson which precluded failure along this interface. The caisson was displaced horizontally at the point of application of the ice load. The caisson load-displacement response under these static conditions are shown in Figure 1-2. They considered their sand density conditions 'A-B' to be the closest to those in the field.

Their analyses shows a load of about 5MN/m causes a total horizontal displacement of about 52 to 71mm depending on the degree of pore pressure dissipation. Field measurements indicate the leading and trailing walls displace by 80 and 50mm respectively for this load estimate. Figure 1-3 shows that upon unloading about 2/3rds of the predicted movement are recovered. The computed profiles are very similar to those measured on site in the sand core. There was however apparently no measured permanent lateral displacement of the caisson structure after the April 12 loading event.

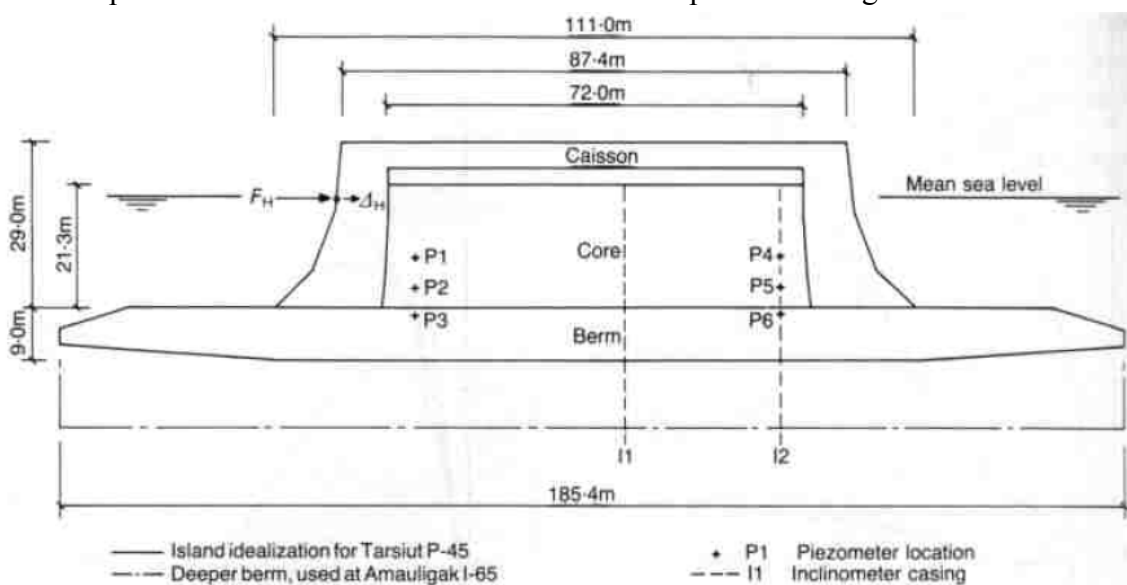


Figure 1-1 Artificial island idealization, Hicks & Smith (1988)

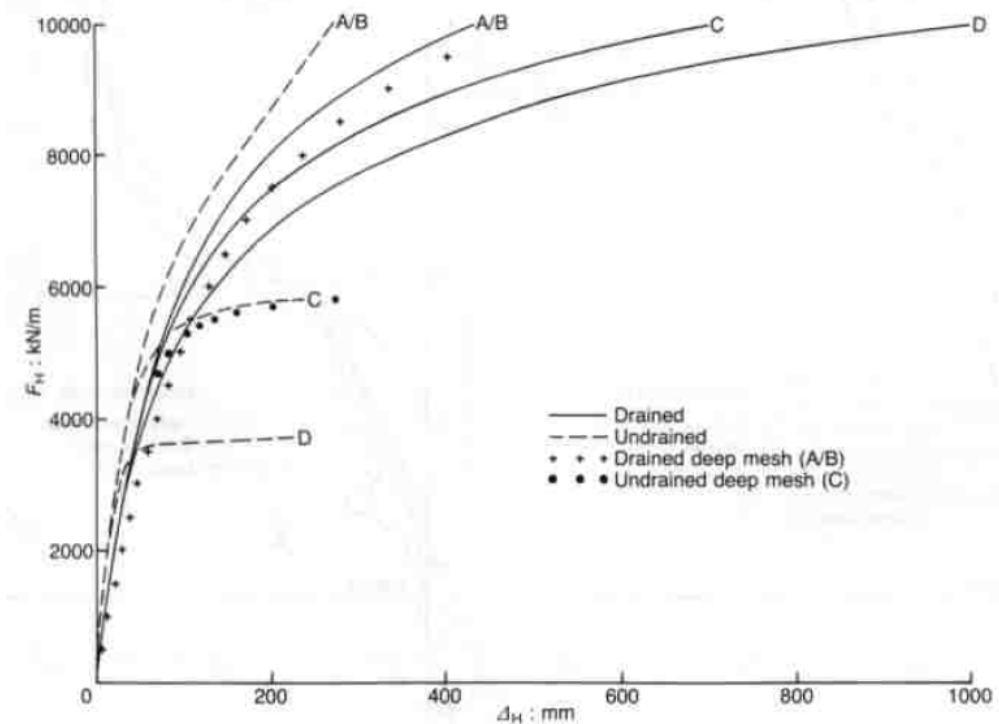


Figure 1-2 Caisson load-displacement response, Hicks &amp; Smith (1988)

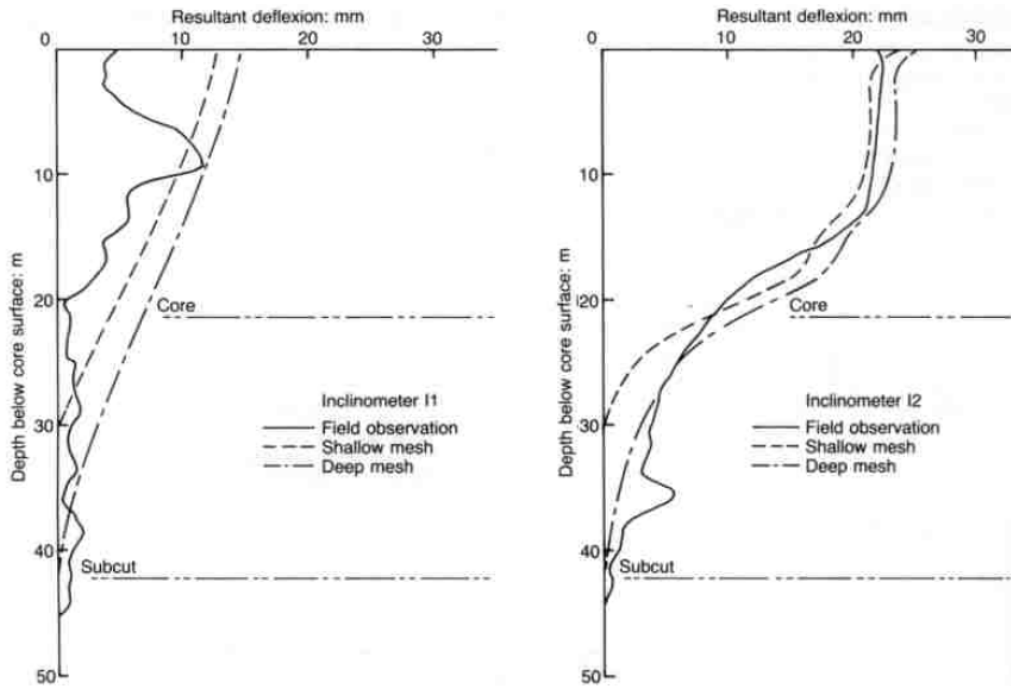


Figure 1-3 Permanent calculated and measured horizontal deformation following the 5MN/m load event, Hicks &amp; Smith (1988)

Typical total predicted deformation vectors within the caisson sand system are shown in Figure 1-4, magnified by 103 times. The development of passive and active failure wedges in the sand against the loaded and trailing caisson faces is noted. There is little movement at the caisson base level within the centre of the sand core. The sand deformations calculated under the caisson bases within the sand berm are probably excessive as failure is more likely to occur along the horizontal caisson sand interfaces.

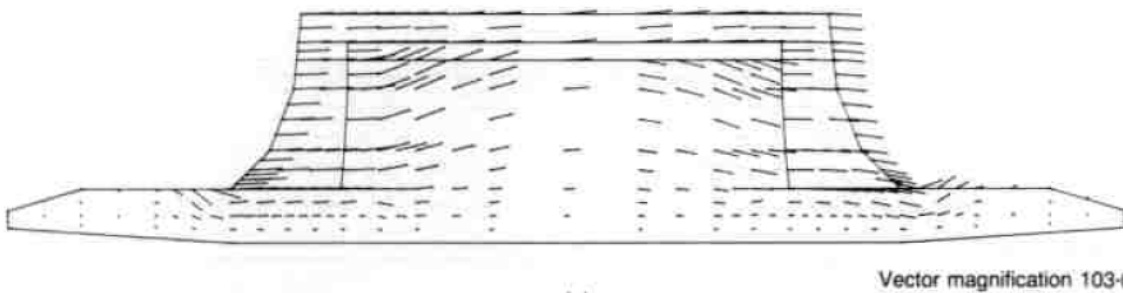


Figure 1-4 Typical caisson displacement response, Hicks & Smith (1988)

## 1.2 Altaee & Fellenius (1994)

Altaee & Fellenius (1994) analysed a similar geometry to Hicks & Smith (1988), and also calibrated their soil model to the same laboratory data, Figure 1-5. They may also have not used interface elements. Their analyses included cyclic, as well as static, loading of the caisson, Figure 1-6. They consider their soil density conditions C5 are the most representative of the field conditions.

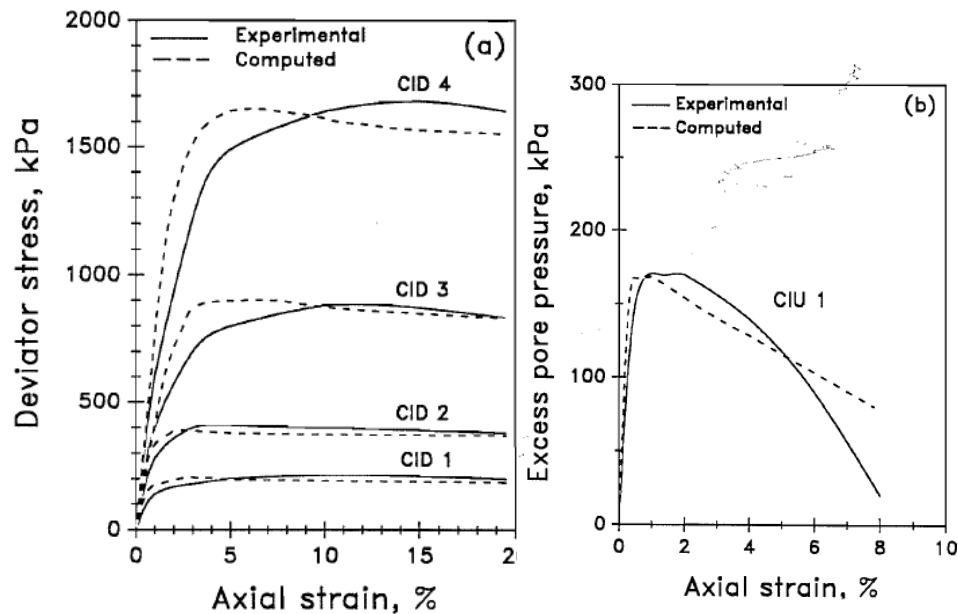


Figure 1-5 Typical constitutive model calibration, Altaee & Fellenius (1994)

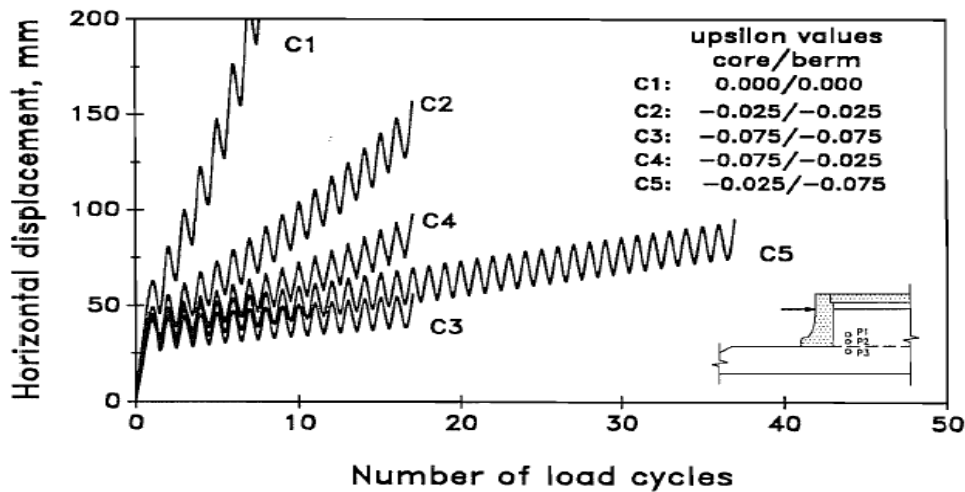


Figure 1-6 Caisson cyclic load-displacement response, Altaee & Fellenius (1994)

Their static caisson load displacement response was similar to that of Hicks & Smith (1988). However, about 40 load cycles between 3 to 5 MN/m accumulated a total caisson displacement up to 80mm, Figure 1-6. Much larger accumulated displacements were predicted for looser sand conditions, (Upsilon is the state parameter for sand).

This paper was discussed by Jefferies (1995) which included reference to pumping in the vicinity of P3, Figure 1-1, during the main April 12 loading event. Altaee & Fellenius (1995) extended their analyses based on this discussion to consider up to 700 load cycles.

Their accumulated displacement stabilized, with the associated pore pressure generation as predicted in Figure 1-7 and Figure 1-8. These predicted values are consistent with the distribution and peak values measured during the loading event, Figure 2-4.

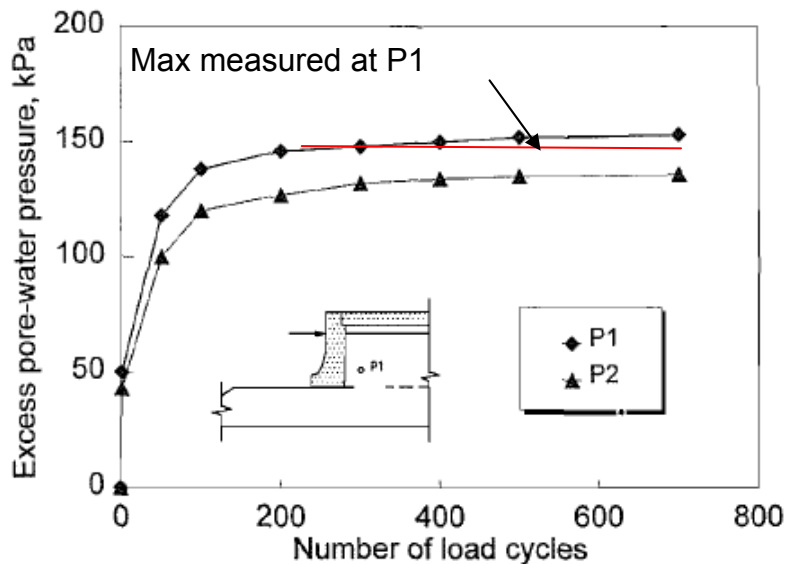


Figure 1-7 Cyclic excess pore pressure envelopes near loaded face, after Altaee & Fellenius (1995)

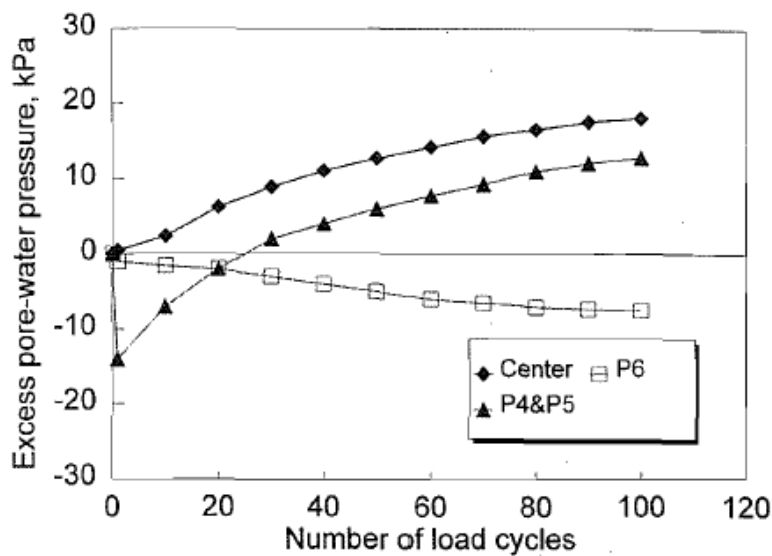


Figure 1-8 Cyclic excess pore pressure envelopes away from loaded face, Altaee & Fellenius (1995)

## 2 CAMBRIDGE UNIVERSITY CONTRIBUTION

### 2.1 Introduction

Between 1988 and 1990 AN Schofield & Associates (ANS&A) were retained by Gulf Resources to critique the centrifuge tests conducted at the University of Manchester by Dr. Rowe. ANS&A was a commercial interface to access facilities at Cambridge University Engineering Department (CUED). The project team was led by Prof Andrew Schofield (retired) and included Richard Dean (now U. West Indies) & K Jeyatharan (now with the Singapore government). Ryan Phillips was CUED centrifuge manager and assisted in the model test programs. The critique comprised a review and interviews with Dr. Rowe, complemented by further more representative physical tests (1g & centrifuge), FE analyses and the development of simple analytical models. The work was presented in three confidential contract reports to Gulf, but its essence is presented in the doctoral thesis of Jeyatharan (1991).

### 2.2 Jeyatharan (1991) thesis summary

Jeyatharan (1991) summary states: “After the April 12th 1986 ice-loading (field) event of about 27 minutes duration in which partial liquefaction and loss of sand were observed, many controversies about excess pore pressure generation within the Molikpaq core and stability of the caisson to horizontal ice loads existed. The response of the core sand fill to horizontal ice loads still remains unclear as some of the field data obtained on that event were considered unreliable. Experiments were conducted at Cambridge to study the response of the core sand fill to horizontal ice loads.

The pattern of excess pore pressure generation and its effect on stability of the caisson were studied in two centrifuge tests using the Cambridge Geotechnical 10m Beam Centrifuge. Although the tests were able to show in a model a pattern of excess pore pressure generation similar to that observed in the field event, they were unable to resolve the controversy about the nature of the loss of sand. In parallel with these experiments, laboratory experiments were carried out to determine the material properties of sand used in the above two centrifuge tests.. These data calibrated a sand constitutive model which was later used in numerical finite element analysis.

Finite element computations were made to back-analyse both the centrifuge test data. The pattern of excess pore pressure generation was well captured by the program: thus it

provides a useful tool to interpret the observed field data and to analyse caissons under ice loads in design stages. In the centrifuge experiments and in the finite element computations, the characteristic state concept of Luong and Sidaner (1981) was found to be an essential element in understanding the response of the core sand fill to horizontal ice loads.

Two different potential failure mechanisms for horizontal sliding and for local core loss were identified by single gravity model testing. These mechanisms together with the excess pore pressure variation obtained from the centrifuge tests and/or the finite element analyses were used to investigate the effect of excess pore pressure within the core and berm on the ice load. This investigation provided a limiting ice load diagram giving the safe region of operation for the Molikpaq caisson.”

### 2.3 Resistance estimates

Jeyatharan (1991) includes some simple calculations to estimate resistance of the caisson and the sand core to lateral movement under varying excess pore pressure regimes. The core lateral resistance, Figure 2-1 will be the minimum of the caisson berm frictional resistance,  $R_b$ , or the sum of the passive,  $R_p$ , and excess pore pressure,  $R_u$ , resistance less the active resistance,  $R_a$ .

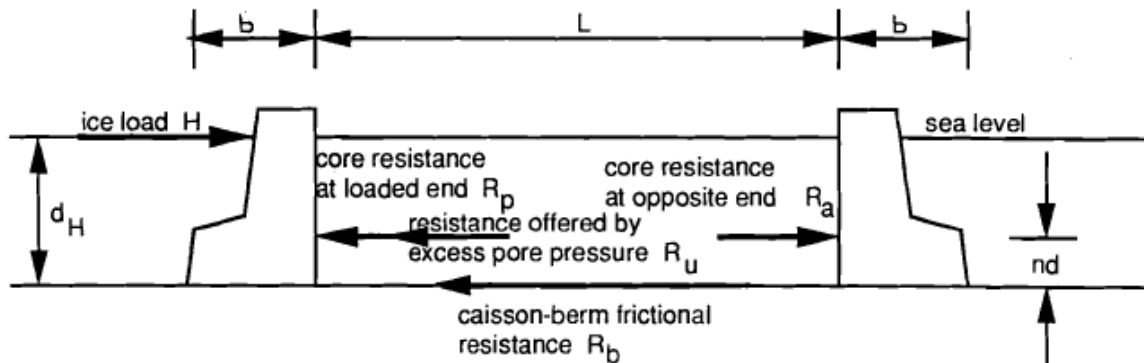


Figure 2-1 Core lateral resistance contributions, Jeyatharan (1991)

The excess pore pressure distribution Figure 2-2 was considered to linearly attenuate along the caisson-berm elevation from the loaded to trailing faces for calculation of  $R_b$ . The passive and excess pore pressure resistances inside the loaded face assumed a linear decay from the base corner, as shown, to zero at the sand surface. No excess pore pressures are considered in the following sections on the active (trailing) face ( $\Psi_a = 0$ ).

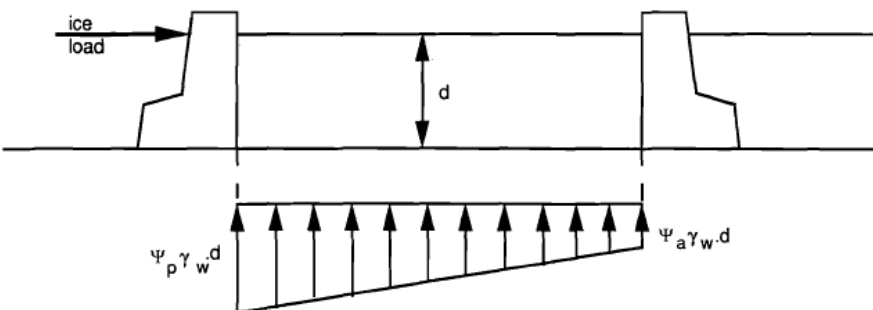


Figure 2-2 Core excess pore pressure considerations, Jeyatharan (1991)

The calculated core resistances are presented in Figure 2-3. The possibility of pore suctions at the caisson base is unlikely ( $\Psi_p < 0$ ). The core resistance is controlled by the passive and active wedge calculation, rather than core base shear. This was confirmed by finite element analysis with prescribed excess pore pressures, and by Hicks and Smith (1988), Figure 1-4. (His stress equilibrium calculation was not rigorous enough to be considered further).

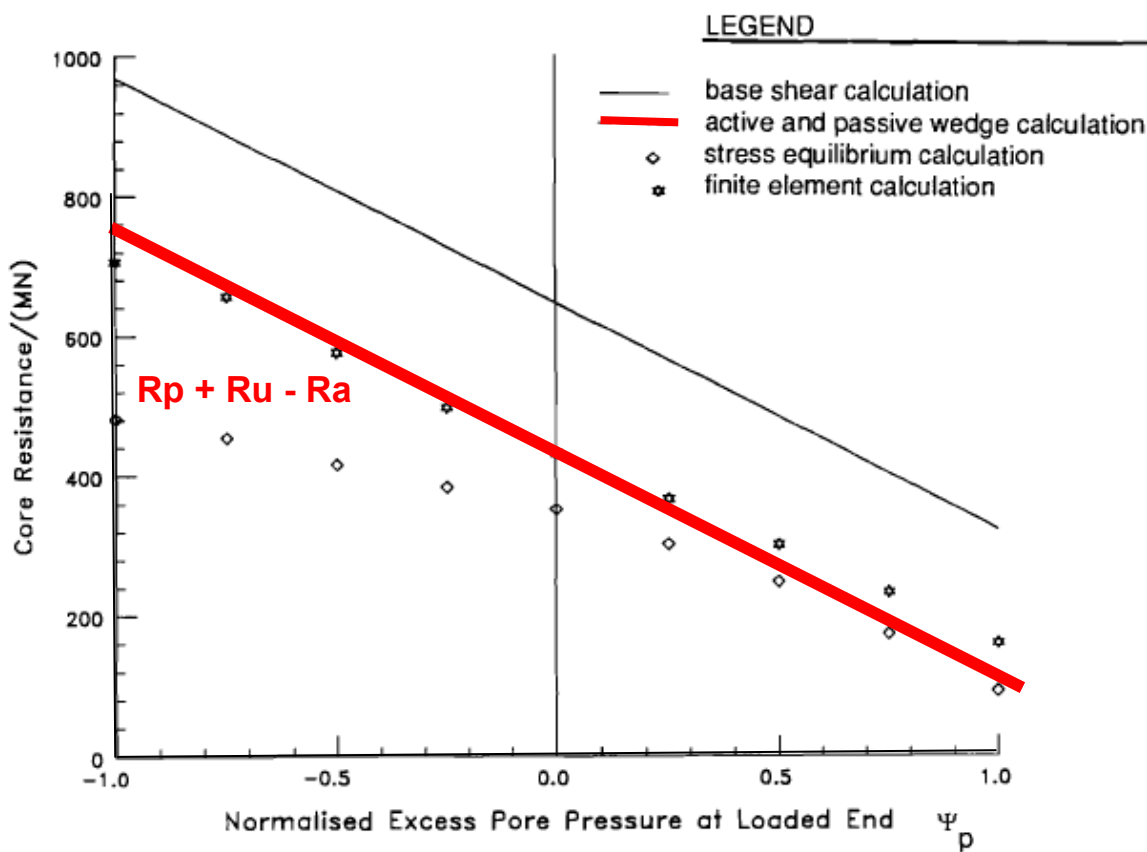


Figure 2-3 Calculated core resistance, Jeyatharan (1991)

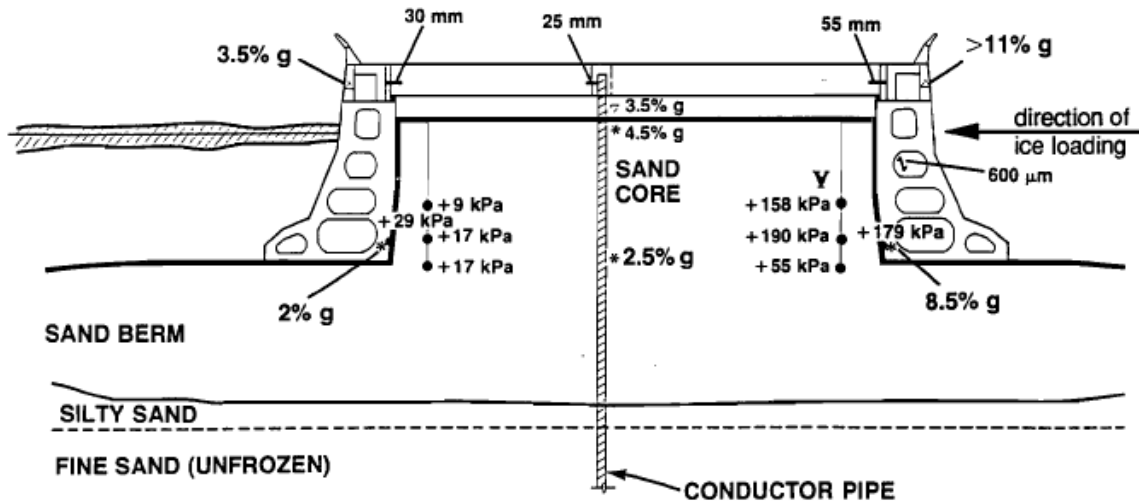


Figure 2-4 Measured peak responses to April 12, 1986 ice loads, Hardy et al (1996)

The maximum excess pore pressures measured at the base of the passive (loading) face, in the vicinity of  $\Psi_p$ , were about 179 kPa, Figure 2-4, giving a  $\Psi_p$  value of around 0.9. Liquefaction is agreed to have occurred at this location and at P2. These two locations, Figure 2-5 suggest that at least sand in the vicinity of the caisson face between the South East corner and the middle of the Eastern side liquefied during the loading event. Jeyatharan (1991) reports a 1,000 tons sand loss from the sand core, equivalent to a 0.3-0.6m thick layer over the 73m x 21m face. This local sand loss is evident from the core surface settlements in millimetres, Figure 2-5.

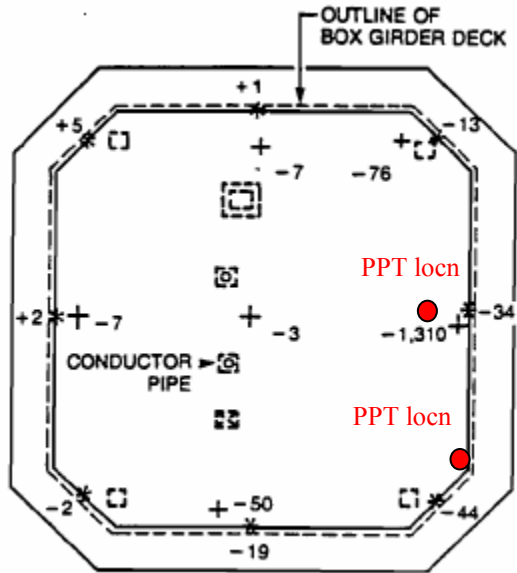


Figure 2-5 Measured settlements after April 1986 events, after Jeyatharan (1991)

The presence of such high pore pressures adjacent to the casing face can initiate a piping failure under the caisson to explain the sand loss. Jeyatharan (1991) considered a range of potential piping mechanisms, Figure 2-6 and calculated the pore pressure magnitude necessary to trigger a mechanism, Figure 2-7. An excess pore pressure index of 0.75 is required which is less than the  $\Psi_p$  measured value of around 0.9, which supports the concept of local core loss through piping.

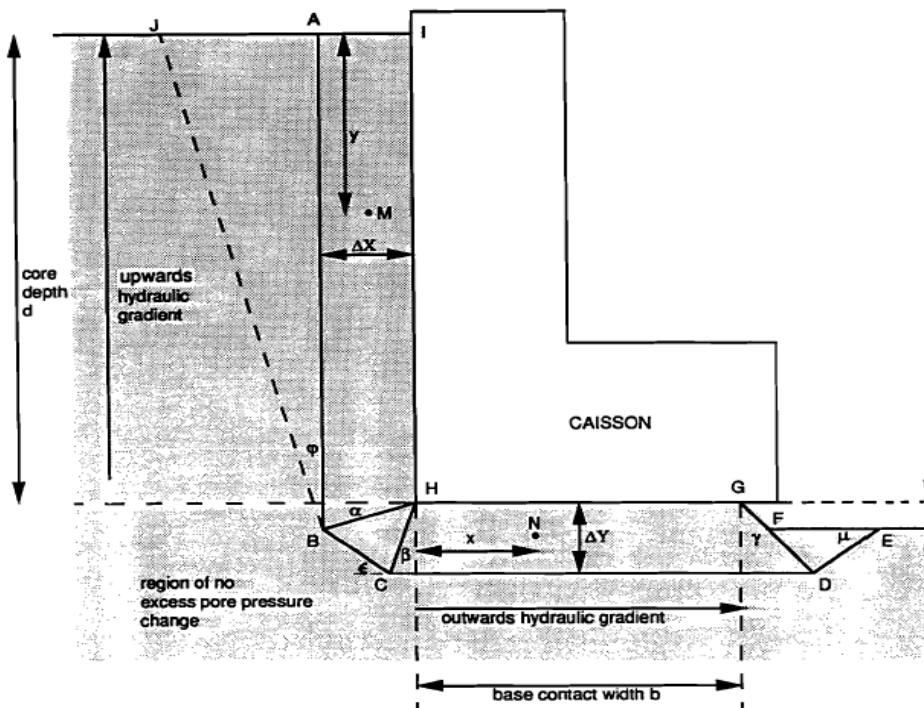


Figure 2-6 Piping mechanism example, Jeyatharan (1991)

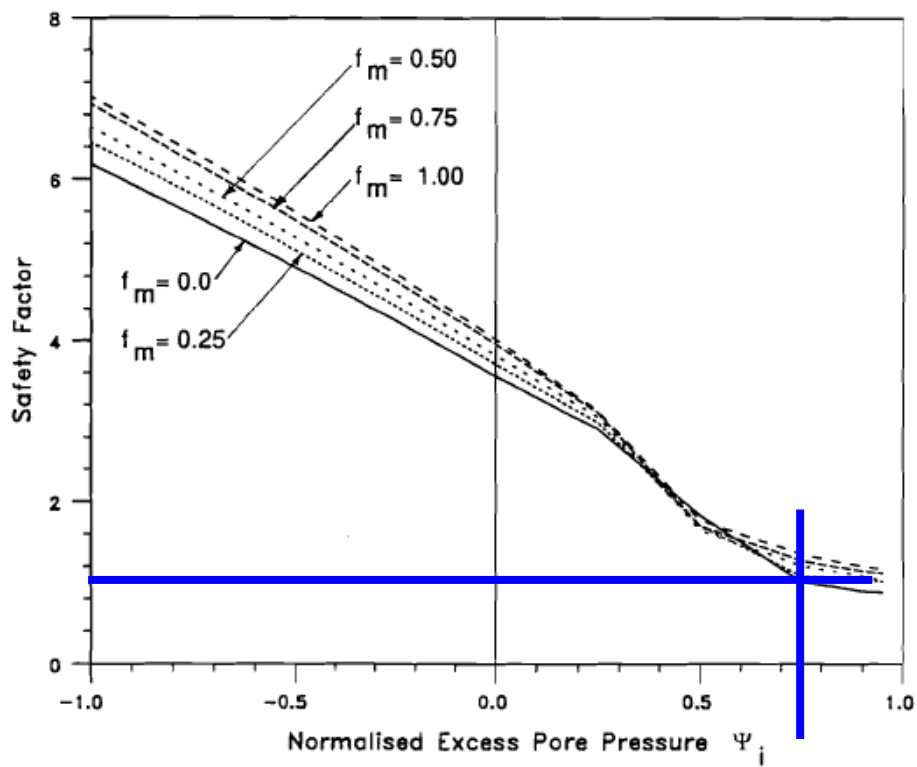


Figure 2-7 Piping development with excess pore pressure, Jeyatharan (1991)

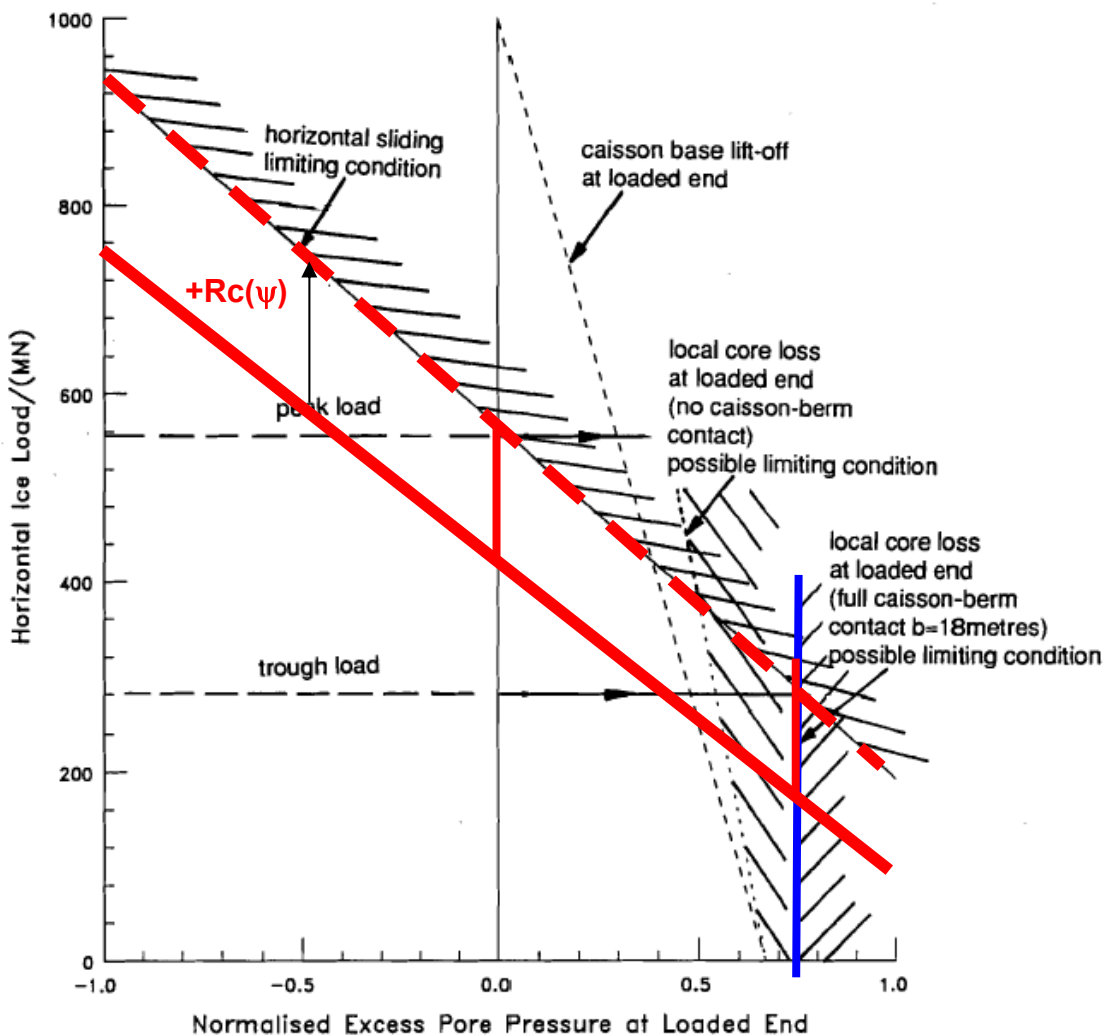


Figure 2-8 Total lateral resistance, after Jeyatharan (1991)

Jeyatharan (1991) reports the unloaded caisson weight to be 324MN increasing to 481MN when fully loaded. He estimates the caisson sliding resistance,  $R_c$  to be +481.  $\tan(15^\circ) = 129$  MN, with  $\Psi_p = 0$ . The 15 degree interface friction angle assumed between the sand and the steel caisson is probably too low, a value of around 25 degrees may be more appropriate. This caisson resistance is additive to the core resistance to define the upper 'horizontal sliding limit' as shown in Figure 2-8. The  $R_c$  value does not change significantly with  $\Psi_p$  when compared with the core resistance. The sliding limit is curtailed under high pore pressures by consideration of the 'local core loss'. Combining these two considerations may cut the corner off the interaction diagram as shown by the two dashed lines.

The maximum total geotechnical resistance to a slowly applied lateral load is about 560MN. This resistance may decrease to about 300MN when significant positive excess pore pressures are generated behind the whole loaded face. However piping under the caisson caused by these excess pore pressures near the face base will also relieve the excess pore pressures acting over the whole face.

Jeyatharan (1991) and the finite element analyses reviewed in section 1 identify the force components of the caisson and core geotechnical resistance. They however present little on how these individual components are mobilised under increasing system displacement. This resistance mobilization is the focus of Section 3.

### 3 RESISTANCE MOBILISATION AND CAISSON MOVEMENTS

#### 3.1 Resistance mobilisation

The total lateral resistance is mainly comprised of the core and caisson lateral resistances. The core resistance is essentially from sand bearing on the inside of the loaded face. The caisson resistance is from basal shear stresses between the caisson and sand berm. This is analogous to the compressive axial resistance of piles in sand. It is accepted that the deformations required to mobilise the bearing (base) resistance is significantly larger than that required to mobilise the shear (shaft) resistance as shown in Figure 3-1.

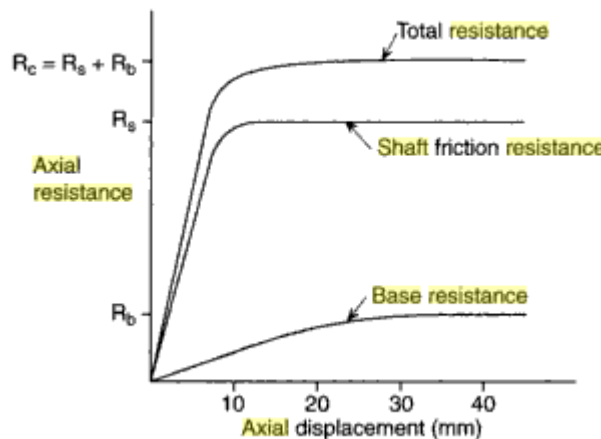


Figure 3-1 Development of compressive axial pile resistance, Davison & Wynford Owens (2003)

In the pile example the base resistance is generally less than the shaft resistance due to the areal ratio of these two sections. The converse is true for Molikpaq, Figure 2-8. The shear resistance can be considered to be fully mobilised before any significant bearing resistance as a starting point.

Potts (1993) analysed a 5m deep retaining rough faced wall in sand under 3 displacement modes, Figure 3-2. The development of the active and passive earth pressures is shown for an initial earth pressure coefficient of 2 for the 3 cases, and for a coefficient of 0.5 for case 1. The passive earth pressure is the main contribution to the core lateral resistance and requires a shear strain over 2% to be fully mobilised. That is equivalent to a lateral caisson wall displacement of tens of millimeters.

Figure 3-3 presents a schematic to understand how the system lateral resistance components are mobilised with relative displacements between the various components.

For example, the caisson basal shear component requires around 5mm of relative displacement to fully mobilise, whereas the passive resistance requires around 50mm.

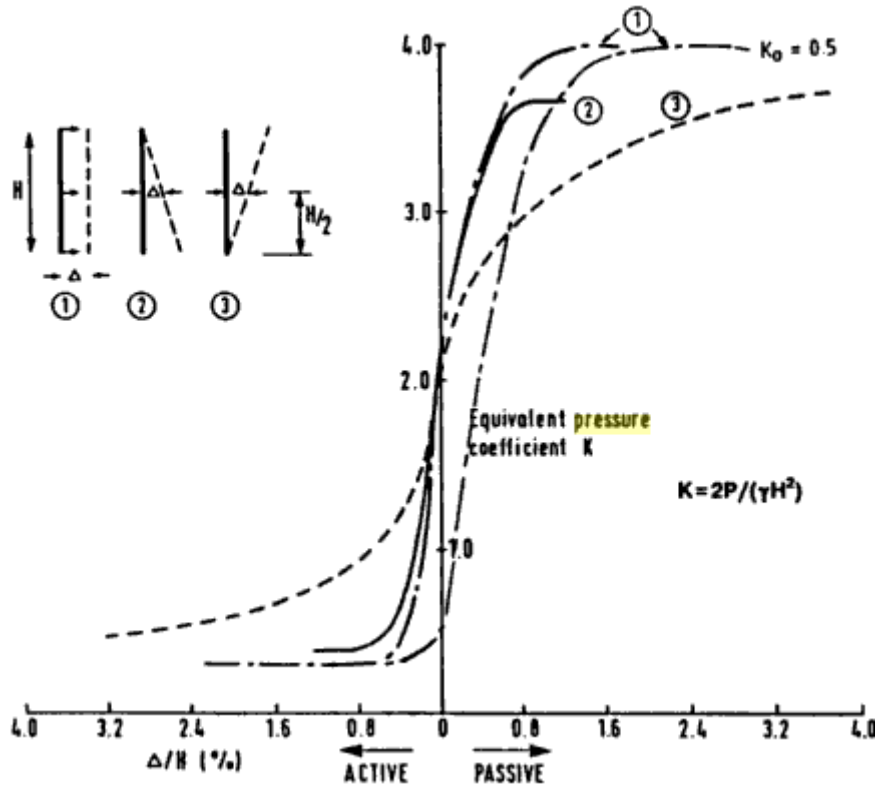


Figure 3-2 Development of earth pressure resistance with increasing wall displacements, Potts (1993)

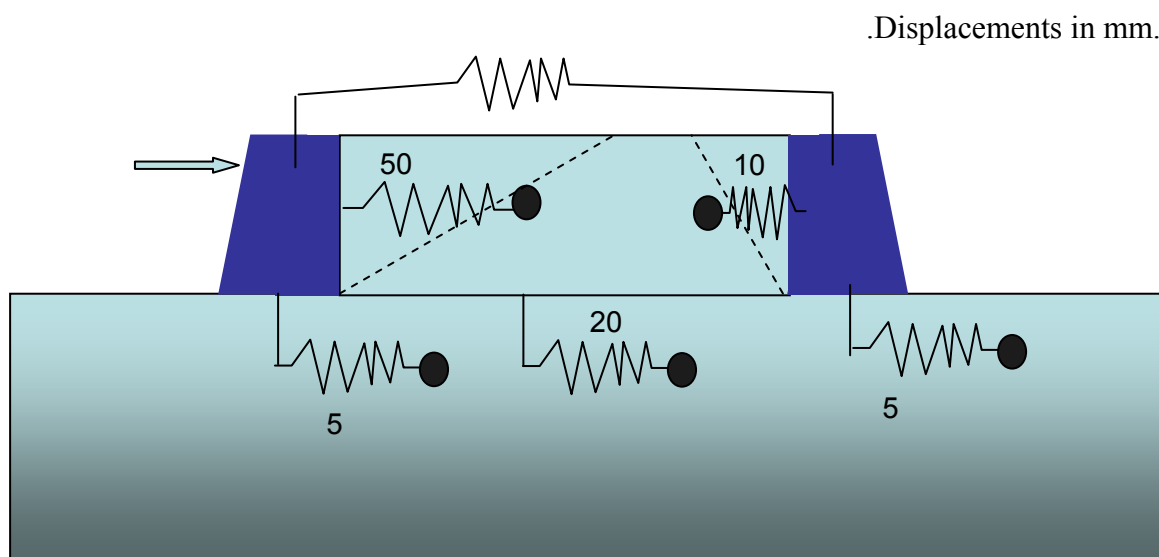


Figure 3-3 Typical relative displacements required to mobilise caisson resistance

### 3.2 Caisson movements

The displacement magnitudes required to mobilise the core and caisson lateral resistances can be compared to those measured. The displacement of the caisson and the core were monitored by extensometers, slope indicators and inclinometers. The locations and measurements from these instrumentation are presented in the Dynamac database prepared by Hardy et al (1996). Significant ice loading events were considered, Table 3-1.

Table 3-1      Significant ice loading event summary

<i>Date</i>	<i>Fast file</i>	<i>Time period</i>	<i>Ice thickness (m)</i>	<i>Ice velocity (m/s)</i>	<i>Failure mode</i>	<i>Face load (MN), Loaded face (N, S, E or W)</i>		
						<i>MEDOF</i>	<i>EXT</i>	<i>SG09</i>
7-Mar	F603071520	15:20:41 – 16:31:01	6.3	0.05	CR, SLD & MM	212 (N)	106 (N), 186 (W)	172 (N)
7-Mar	F603071603	16:38:54 – 17:43:47	6.3	0.05	CR, MM & SLD	142 (N)	132 (N)	175 (N)
8-Mar	F603081603	17:30	3.5* (FY ice at end of time period)	0.1, then slows to creep	CR & SLW	153 (N)	113 (N)	115 (N)
8-Mar	F603081731	18:36	4.3	0.02 – 0.05	CR, CC, SLD & MM	253 (N)	197 (N)	190 (N)
12-Apr	3 BURST files	8:23:30 - 8:29:56	3.3m, with 10m hummock	0.06	CR & CC	–	274 (E)	117 (E)
12-Apr	F604121101	11:16:02 – 12:29:31	3.5	0.1	CC, CR, MM & SLW	182 (E)	82 (E)	85 (E)
12-Apr	F604121201	13:00:07 – 14:01:04	5.9	0.06	CR, M & SLD	179 (E)	103 (E), 154 (S)	158 (E), 215 (S)
12-May	F605120301	03:10:16 – 03:58:24	2.5 (est.)	0.17 to creep	CR, MM & SLW	278 (N)	194 (N)	222 (N)
22-May	F605220801	08:39:23 – 09:50:27	2.5 (est.)	creep	SLW & MM	127 (N), 57 (E)	126 (N), 21 (E)	111 (N), 38 (E)
22-May	F605221301	13:58:07 – 15:11:32	3.5 (est.)	creep to 0.05	CR, SLD & SLW	146 (N), 115 (E)	87 (N), 49 (E)	110 (N), 80 (E)

The Hardy et al (1996) summary of global face load with absolute total caisson face deformation is presented in Figure 3-4. (These global load magnitudes, especially from the Medofs are currently under critical review in the main part of this study. These load are therefore presented only as estimates to aid discussion.) Most of the deformation appears recoverable as evident by comparing two primarily North face loading events. The two May 22 squares around (20,100) have total deformations less than those for the May 12 square at (43,230).

The basis for these data squares was confirmed by processing some of the Dynamac ‘fast’ event files from Hardy et al (1996) for the days presented, Figure A-1 to Figure A-30. There are 3 sets of figures. For example, Figure A-1 presents the time records for a) the Medof global loads and b) the absolute caisson face movements calculated in Dynamac with c) the IPI inclinometer readings. The IPI units are uncertain being shown as ‘%g’ in

Dynamac but as ‘mm’ by Frederking (2008a). Figure A-2 presents the same data of global load with the absolute face movements for both a) the North and b) East faces. From Figure A-21 to Figure A-30, the basis for these Dynamac calculated absolute face movements is checked against the associated extensometer EXT readings. The Dynamac EXT sign convention is consistent, with the opposite polarity, with that proposed by Frederking (2008b).

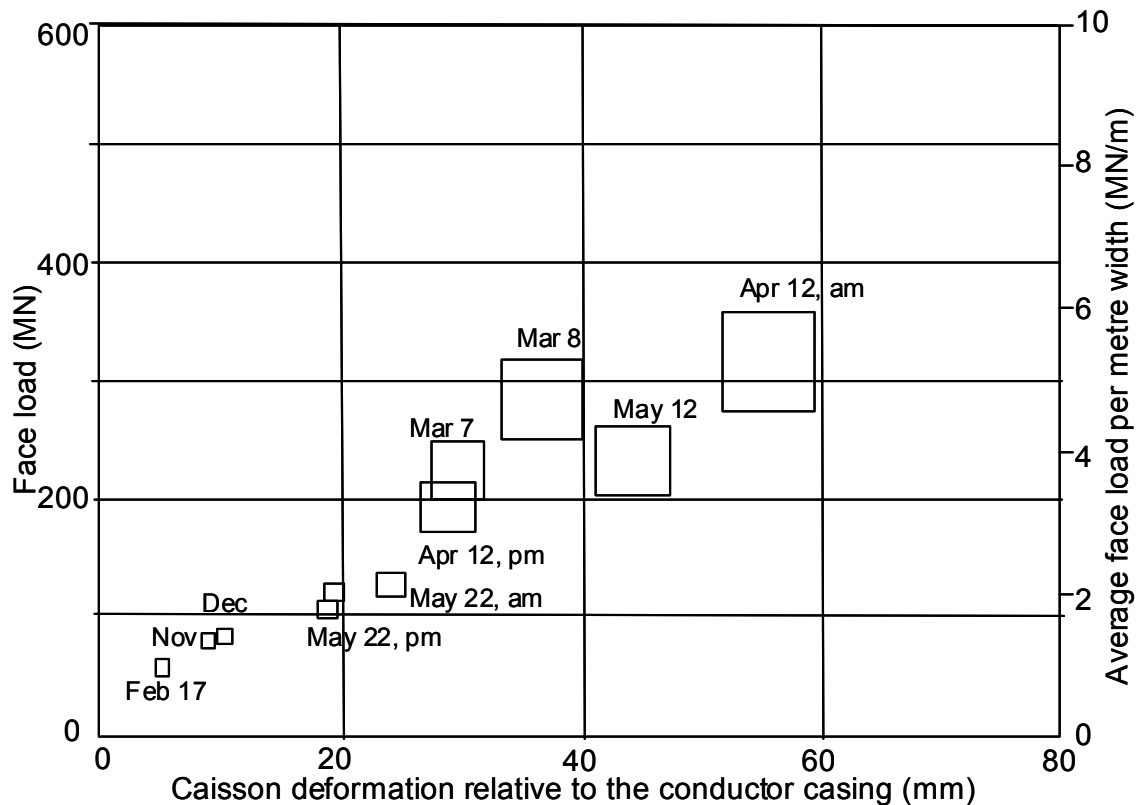


Figure 3-4 Caisson face load – displacement summary, after Hardy et al (1996)

The peak load and displacement values are consistent with the data in Figure A-1 on, see for example Figure A-14a. The time records in Appendix A also show the calculated absolute face movements returning to zero at zero loads irrespective of the load magnitudes. This caisson movement observation is compared to observations made on displacements of the sand core below.

Figure 1-3 showed field observations of 2 slope inclinometers buried in the sand core. There are seven such tubes as shown by Hardy et al (1996) who state: “Deformation monitoring in inclinometers located in the core indicated that these events caused some permanent horizontal sand displacement. *Table 3-2* summarizes the lateral deformations

measured in the seven inclinometer casings. All displacements shown in the table occurred at the interface of the bottom of the core and the berm and within the core itself. Only nominal movement occurred at the subcut/seabed interface and in the berm. No measurable permanent deformation occurred as a result of ice events of less than 150 MN.

The peak load for the season occurred on April 12, 1986... The peak responses for the accelerometer, piezometer and extensometer sensors are shown in *Figure 2-4*. A comparison with the 1985 predictions of Molikpaq response to a 500 MN load ..shows that the piezometers response on April 12 was higher than anticipated. Part of the core sand adjacent to the loaded east face of the caisson liquefied, causing a reduction in the resistance capability of the Molikpaq. However the cyclic loading that caused the increase in pore water pressure in the core landfill reduced as the hummock advanced into the caisson, and pore water pressures started decreasing immediately after the ice sheet experienced a flexural fracture behind the hummock. At this time the liquefied sand was limited to a zone adjacent to the loaded face and above the base of the Molikpaq. Deflections of the caisson face at deck level during the crushing of level ice prior to the hummock were measured at approximately 80 mm during this crushing event. As shown in *Table 3-2* the permanent deformation at the base of the sand core as measured in the centre inclinometer after the event was 12 mm.”

Table 3-2      Slope inclinometer permanent lateral displacement event summary, Hardy et al (1996)

Lateral Displacement (mm)									
Event Date 1986	Load Estimate Tonnes	Direction To:	North	NE	West	Centre	East	South	SW
Mar 7/8	30,000	East, SE, South	12 S	16 SE	8 N	*	20 E	*	12 NW
Apr 12	50,000	West, NW	18 NW	28 N	24 N	12 W	**	30 SW	16 W
May 12	25,000	South	14 S	14 S	0	0	0	0	0

\* casing not profiled for this event

\*\* casing sheared in core during event.

The east inclinometer was probably sheared by the loss of sand adjacent to the east caisson face during the April 12 event. Two statements are of particular interest: 1) No measurable permanent deformation occurred as a result of ice events of less than 150 MN *estimate*. 2) Permanent deformation at the base of the sand core as measured in the centre inclinometer after the event was 12 mm.

The 150 MN load level estimate is comparable to the 129 MN caisson basal shear resistance calculated in the previous section. There will be some increase in the caisson sliding shear resistance from embedment of the caisson under the applied loading. The resistance mobilisation discussion indicates that core movement is required to mobilise resistance above that provided by the basal shear. Therefore total core movement should be expected adjacent to the loaded face to mobilise more resistance. As sand is a plastic material, much of this core movement is expected to be permanent.

The centre and west inclinometers correspond to I1 and I2 in Figure 1-3. The permanent deformations of 12mm and 24mm respectively correspond to the maximum displacements presented in Figure 1-3 around 10m depth in the core. These deformation profiles are indicative of the development of the expected wedge failure mechanisms as shown in Figure 1-4. The 12 April loading was primarily from the east and south, Table 3-1. The 24mm of core displacement over a 10m depth occurred on the opposite side of the caisson to the loaded area. The caisson faces in this vicinity must move to accommodate this permanent core displacement, but the calculated top face movements show no permanent movement.

It would be insightful to review the core movement mechanisms to review the deformation profiles like those presented in Figure 1-3 for events listed in Table 3-2. Further, the face extensometer readings record local movements near the top of the caisson walls. The tiltmeters such as shown on the Extensometer drawing in Hardy et al (1996) could be reviewed to assess how these local top face movements relate to overall caisson movement.

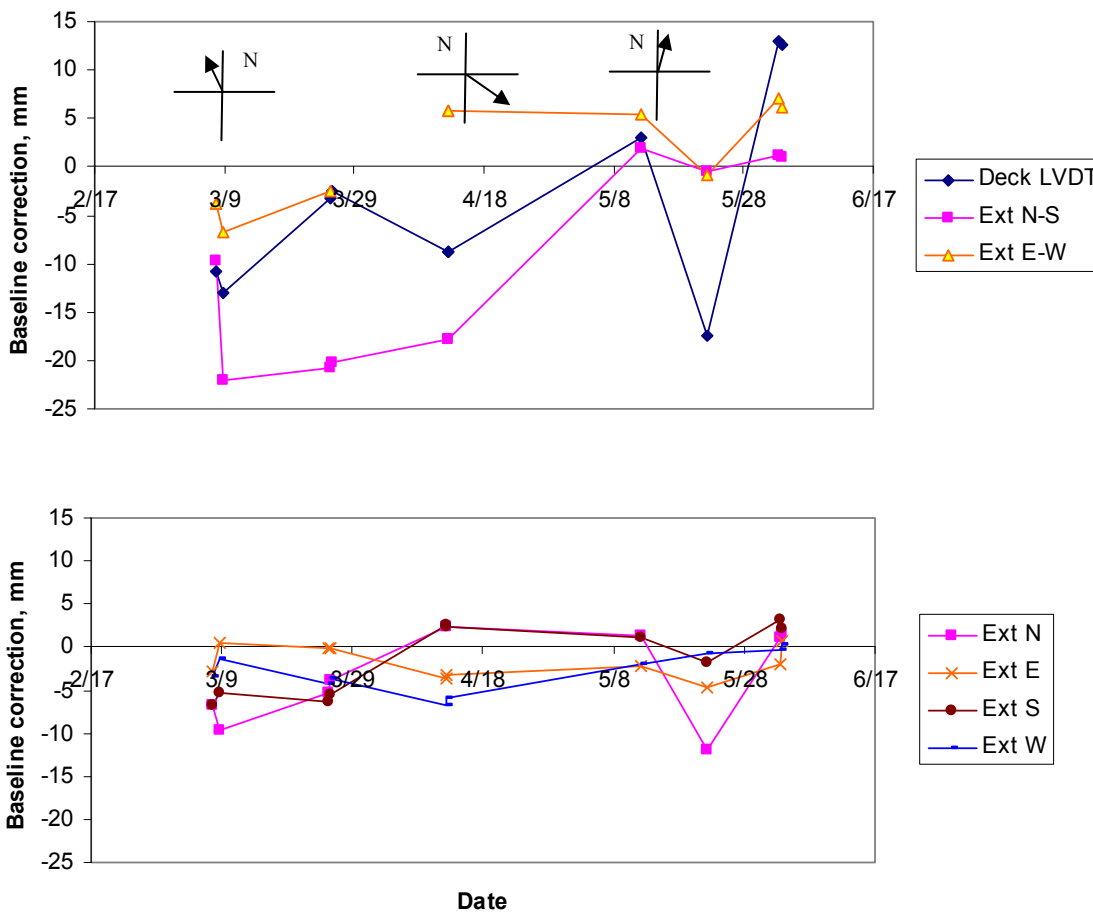


Figure 3-5 Dynamac extensometer baseline corrections

The calculated face displacements include a temporal baseline correction in Dynamac, Figure 3-5. The deck to casing corrections in Figure 3-5a do show some correlation to the direction of the 3 most significant loading events with the depicted load directions. The rational for these baseline corrections may be part of the explanation for the absence of permanent caisson deformations. Figure 3-5b shows the deck to face extensometer corrections to be about half those for the deck to casing. There are also Deck LVDT 965 instrument readings recorded in the Dynamac database, but no other information is provided about its location etc.

The sand core movement may also be assessed only along the N-S centreline through digital inclinometers buried in the sand. These inclinometers can provide indications of the average shear strains induced in the sand core. Frederking (2008a) reports:

"The North face in-place inclinometer (IPI) ...was located 5 m back and 5 m west of the centre of the North face. IPI 807, 809 and 811 are 8.5, 17 and 18 m, respectively, below MSL and measure inclinations in the N-S plane. Time series plots of the MEDOF panel face load and the 3 inclinometers are presented in *Figure 3-6*. They all give a very similar output (linear with depth, at least to the berm) and respond to loading on the North face. The IPI inclinometers have a gauge length of 3 m, so this implies that the location of inclinometer casing, the top of the core would have moved in  $0.4 \text{ mm} \times 21 \text{ m}/3 \text{ m} = 2.8 \text{ mm}$ . The sand core is deforming, but how much resistance did it generate?".

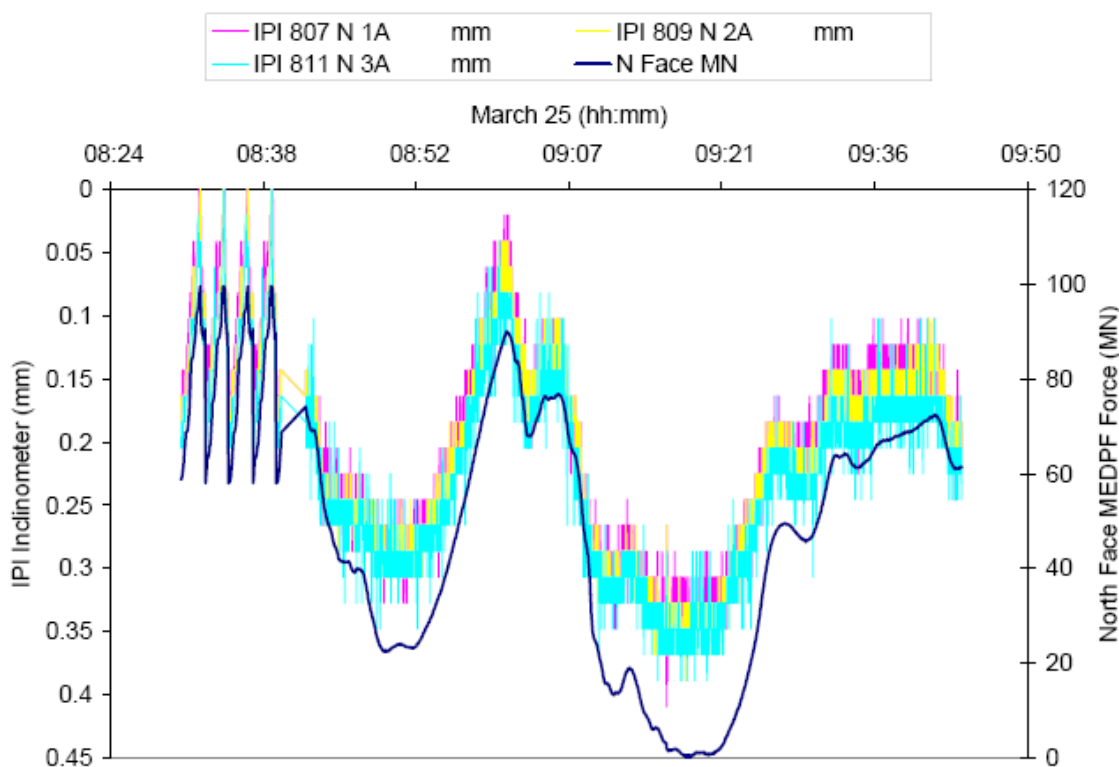


Figure 3-6 N Inclinometer – global load: 25 Mar, Frederking (2008a)

The March 25 event did not require more resistance than that provided by basal shear, so no significant sand core resistance was mobilised. This can be confirmed by the low passive resistance mobilised at the 0.013%  $\Delta/H$  level, Figure 3-2.

There is a good correlation between the IPI inclinometers and the global N face load for the 2 low level May 25 event files. However, there are no Dynamac IPI for the previous events, Figure A-1c and Figure A-3c. The subsequent IPI data, Figure A-9c to Figure

A-19c, no longer show a correlation to the global load but rather a high frequency ‘noisy’ response.

The buried digital inclinometer data do not provide the anticipated indications of shear strains within the sand core during the more significant ice loading events shown in Table 3-1.

It is concluded that most of these ice loading events were reacted by geotechnical resistance mobilised from the caisson basal shear alone. This did not require significant caisson global displacement or significant straining of the sand core. The 3 larger loading events shown in Table 3-2 possibly required more resistance than that provided by the caisson basal shear. This additional resistance was provided by sand core bearing pressures on the inside of the loaded face. This additional resistance requires tens of millimeters of sand core movement to mobilise. This requirement is consistent with permanent core deformations measured after these 3 events, Table 3-2. These large core displacements are associated with top of loaded face total global displacements exceeding 30mm, Figure 3-4. Permanent global caisson displacements after these 3 large events may be included in the baseline corrections applied to the Dynamac data, Figure 3-5.

Further Dynamac datasets for the instrumentation related to the geotechnical response were reviewed while revising this report. This information from total pressure cells, pore pressure sensors and wall tilt meters are included in Appendix A in Figure A-31 to Figure A-60 for completeness. The locations of these and other instrumentation are given in Figure A-65 to Figure A-69. The bearing and pore pressures, for example Figure A-31, are relative as their datum excludes pressures from the caisson and water depth self weight. These data are also baseline corrected, Figure A-61 so do not track changes after significant events such as 12 April. Typically, the bearing pressures under the loaded face reduce under the application of ice load and increase under the trailing face. Persistent excess pore pressure exceeding 15kPa are only observed for the 3 large loading events, Figure A-32, Figure A-50 and Figure A-63. The 3 Dynamac burst files available around 8:30 for 12 April event are concatenated in Figure A-62 to Figure A-64. The offsets and scaling for the first file at 08:25 differ from those in the 2 subsequent files from 08:27. Jeyatharan (1991) presents other complementary burst file data for this period which are not available within Dynamac.

	Preliminary geotechnical overview of 1986 Molikpaq response		
<b>Ian Jordaan &amp; Associates</b>			
Report no:	R-08-044-578v2.0		November 2008

#### 4 REFERENCES

Altaee A & Fellenius BH (1994) Modeling the performance of the Molikpaq, CGJ 31 p649-660

Altaee A & Fellenius BH (1995) Response to Jefferies M (1995) , CGJ 32 p924-926

Davison B & Wynford Owens G (2003) Steel Designers' Manual, Steel Construction Institute (Great Britain)

Frederking, R (2008a) 'March 25 event.pdf' (1Mb file) created 15 Sept 2008

Frederking, R (2008b) Sign Convention March 25 (3).doc of 23 Oct 2008

Hardy M.D., Jefferies M.G., Rogers B.T., & Wright B.D. (1996) DynaMAC: Molikpaq Ice Loading Experience. PERD/CHC Report 14-62 submitted to National Energy Board

Hicks, MA & Smith, IM (1988) Class-A Prediction Of Arctic Caisson Performance, Geotechnique vol 38 :4 p589-612

Jefferies M (1995) Discussion of Altaee A & Fellenius BH (1994), CGJ 32 p922-923

Jeyatharan K (1991) 'Partial liquefaction of sand fill in a mobile arctic caisson under ice loading' Cambridge University Doctoral Thesis

Potts DM (1993). The analysis of earth retaining structures .In: Retaining Structures, C.R.I. Clayton, Institution of Civil Engineers

## A. SELECT DYNAMAC FAST EVENT DATA RECORDS

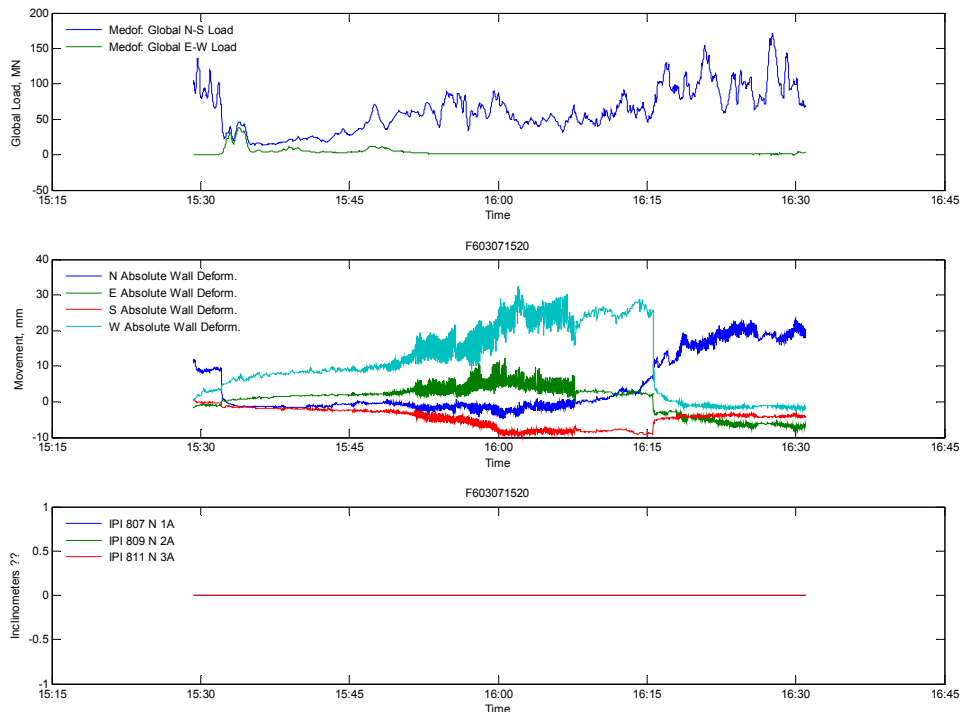


Figure A-1      Dynamac calculated ‘fast’ response to 15:20 7 Mar event

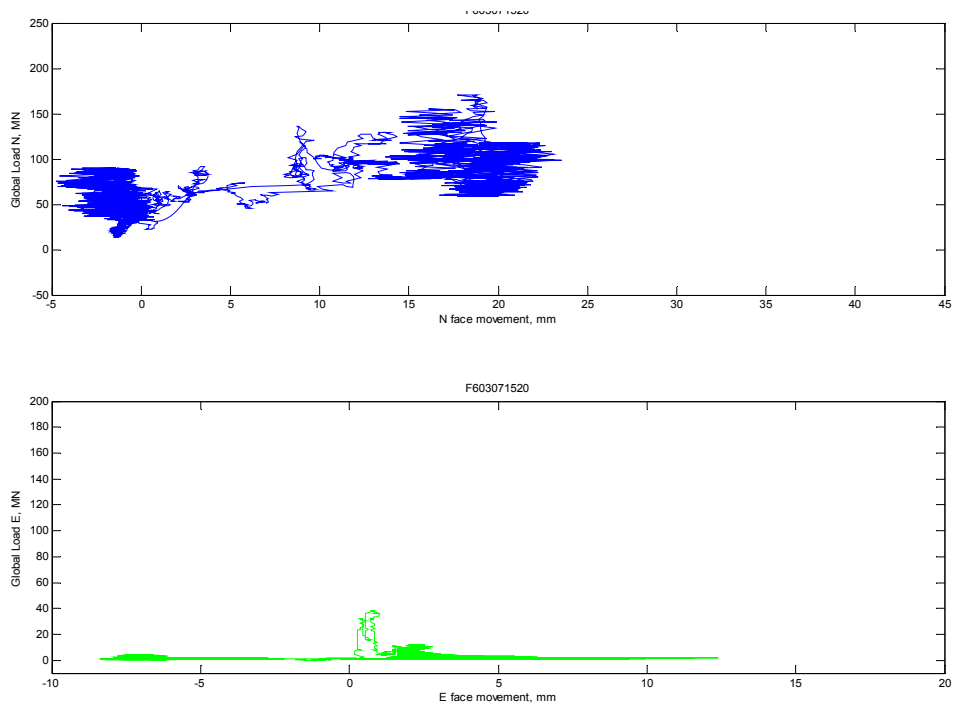


Figure A-2      Dynamac calculated global load–deflection during 15:20 7 Mar event

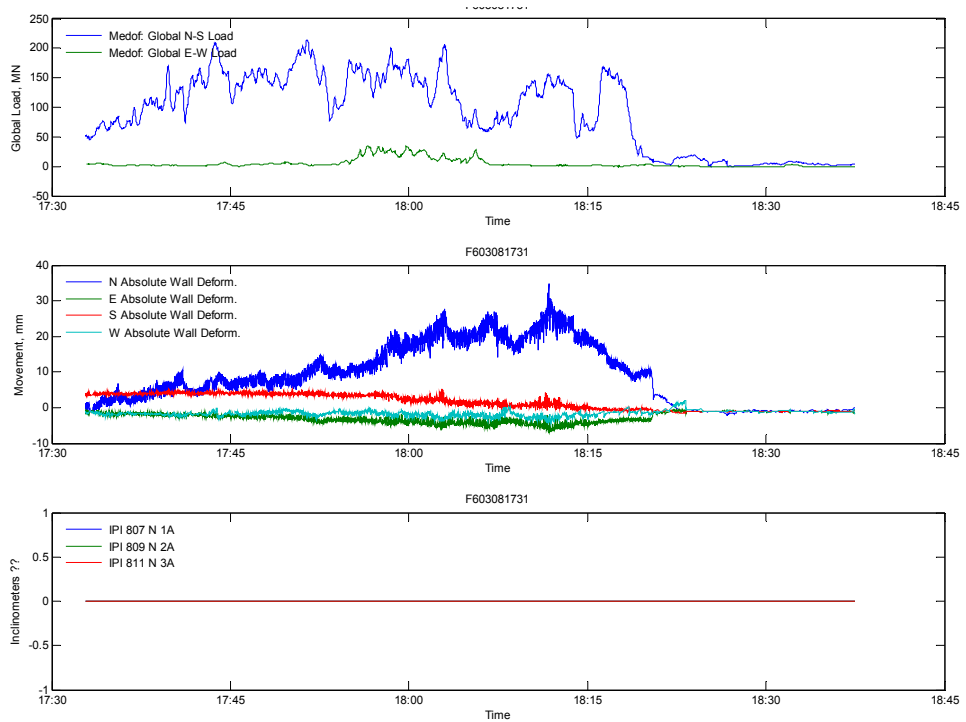


Figure A-3      Dynamac calculated ‘fast’ response to 17:31 8 Mar event

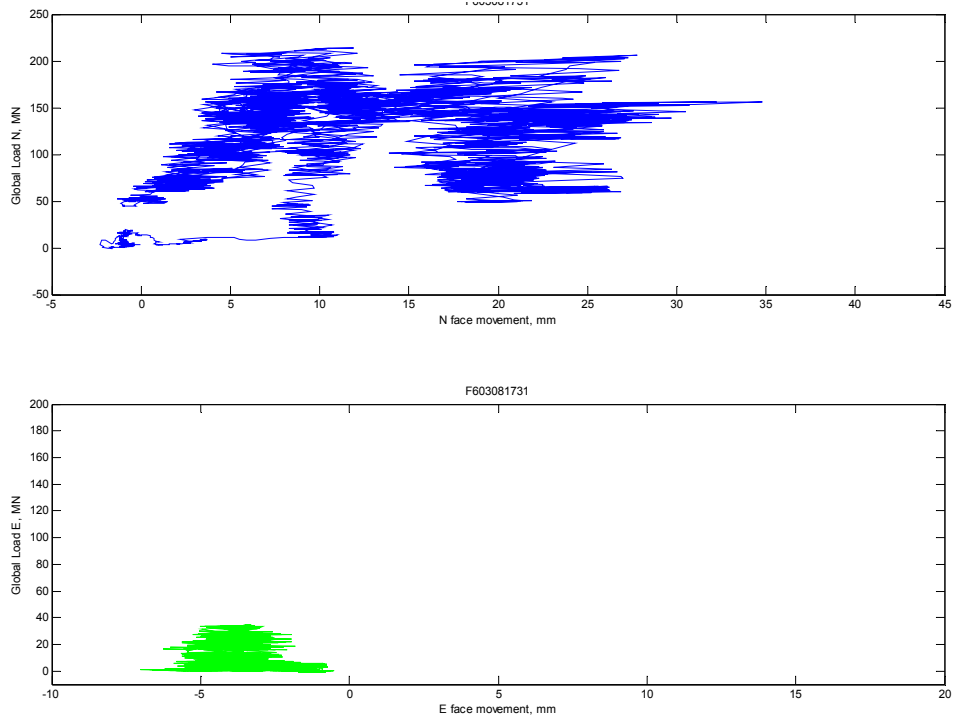
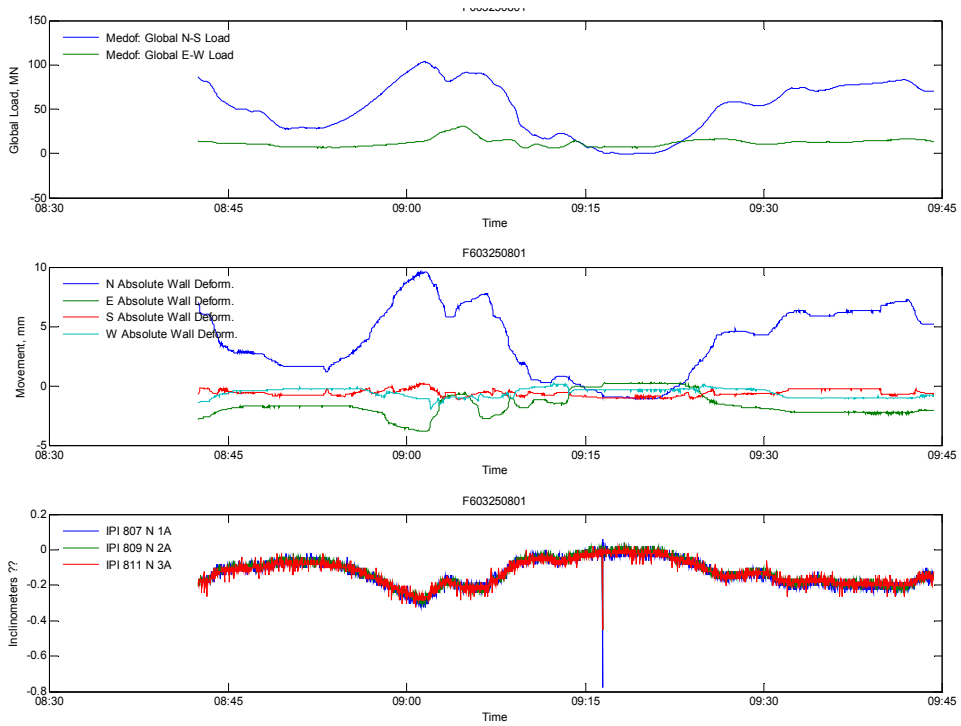
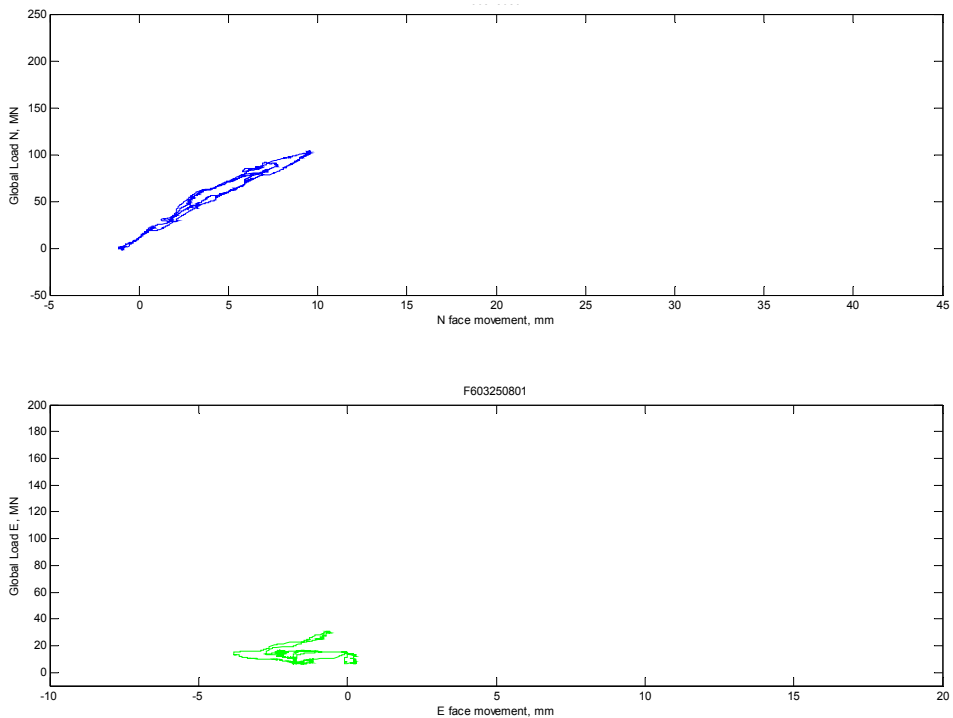


Figure A-4      Dynamac calculated global load–deflection during 17:31 8 Mar event



**Figure A-5**      Dynamac calculated ‘fast’ response to 08:01 25 Mar event



**Figure A-6**      Dynamac calculated global load–deflection during 08:01 25 Mar event

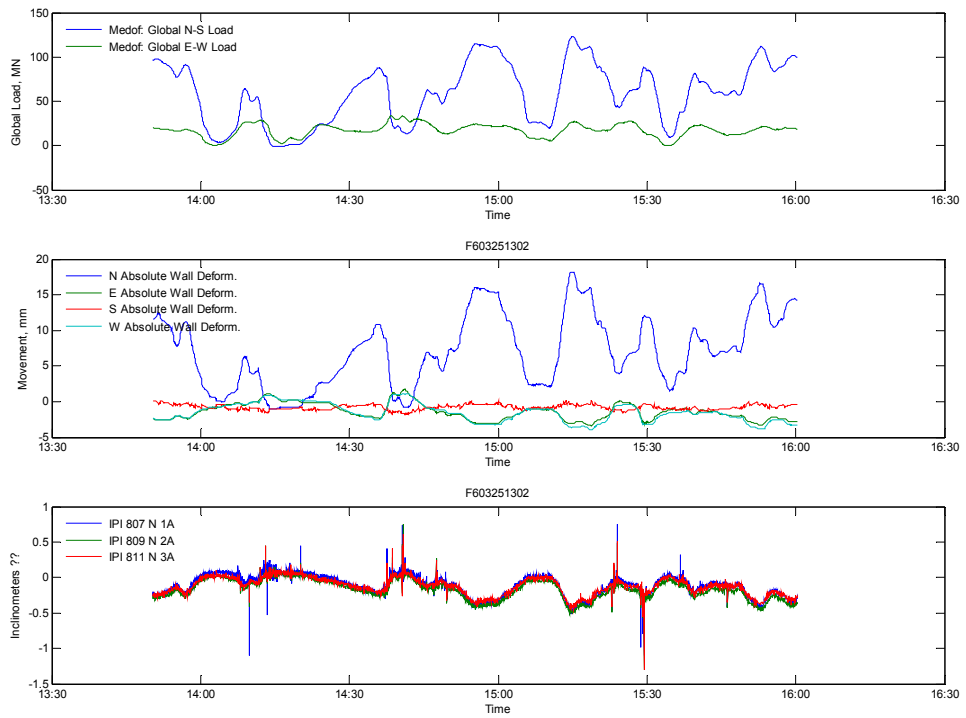


Figure A-7      Dynamac calculated ‘fast’ response to 13:02 25 Mar event

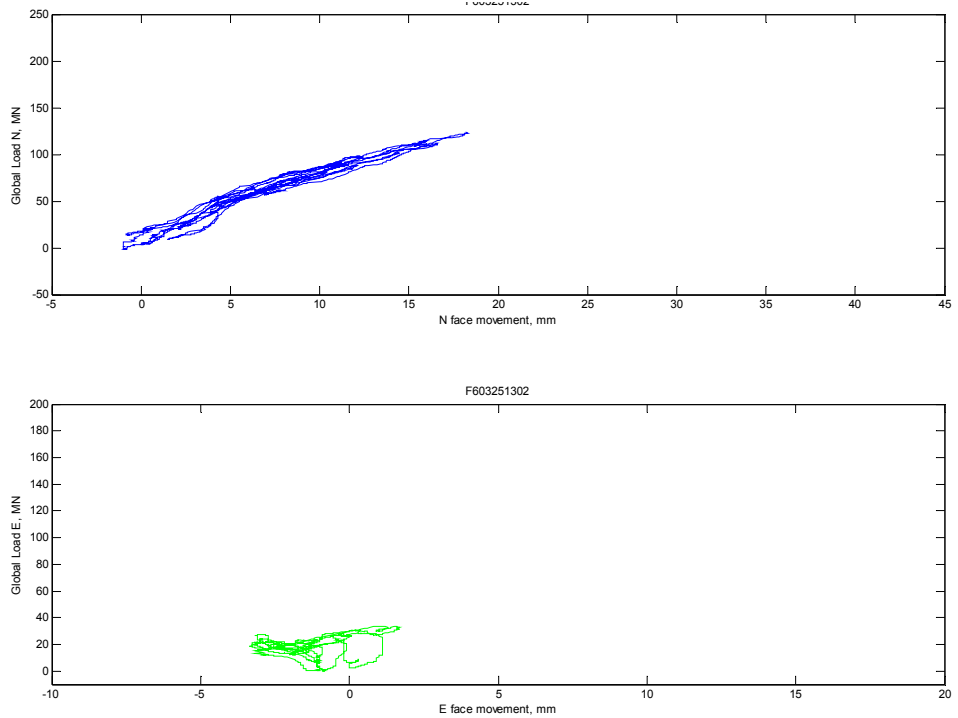
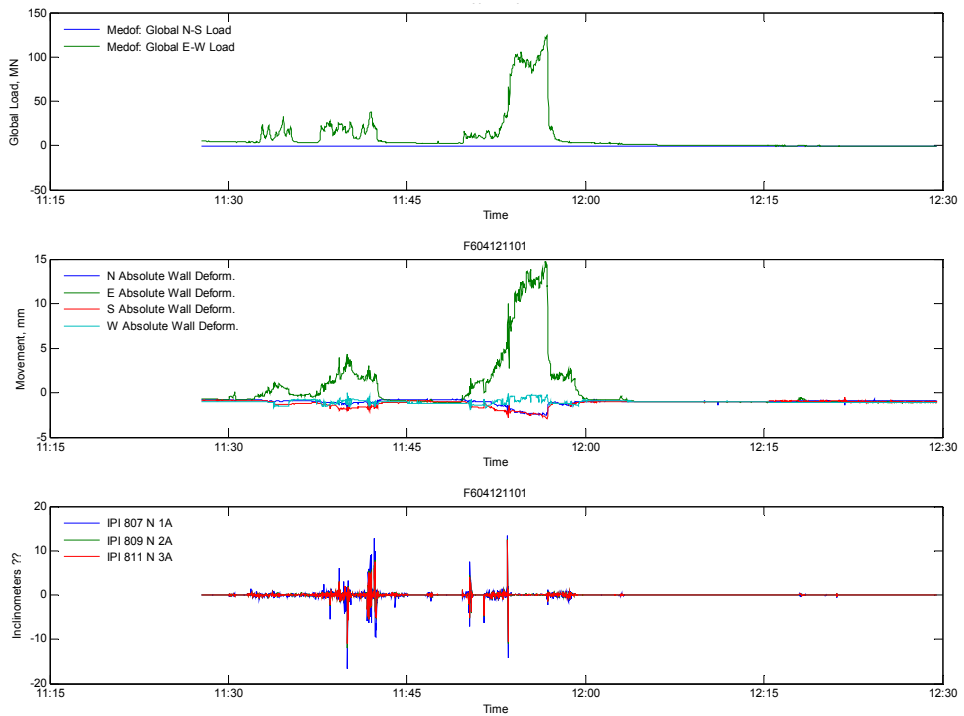
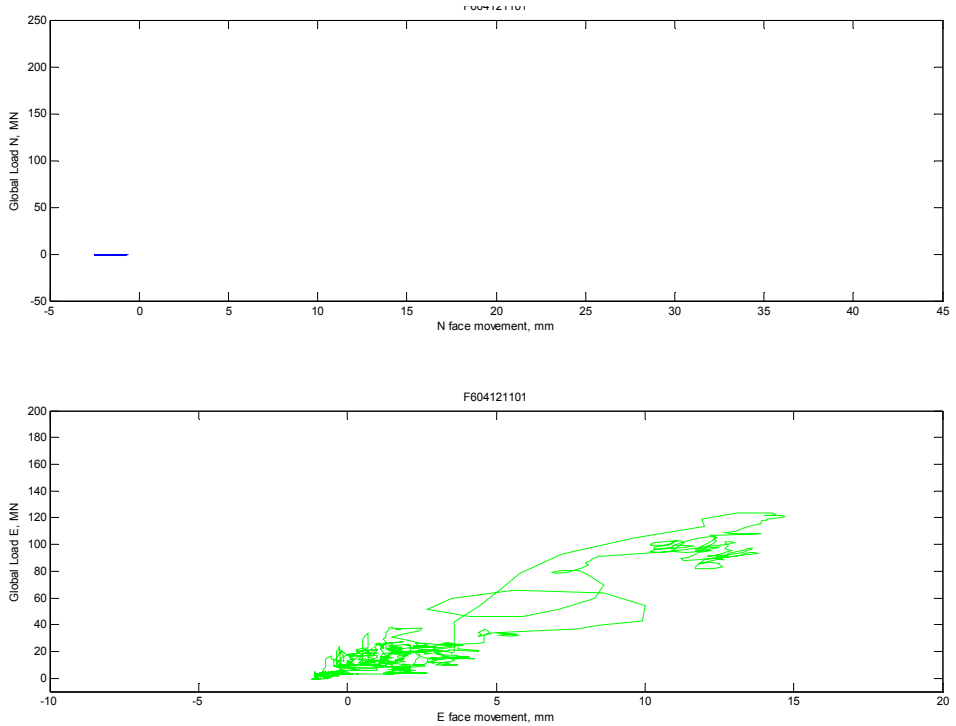


Figure A-8      Dynamac calculated global load–deflection during 13:02 25 Mar event



**Figure A-9**      Dynamac calculated ‘fast’ response to 11:01 12 Apr event



**Figure A-10**      Dynamac calculated global load–deflection during 11:01 12 Apr event

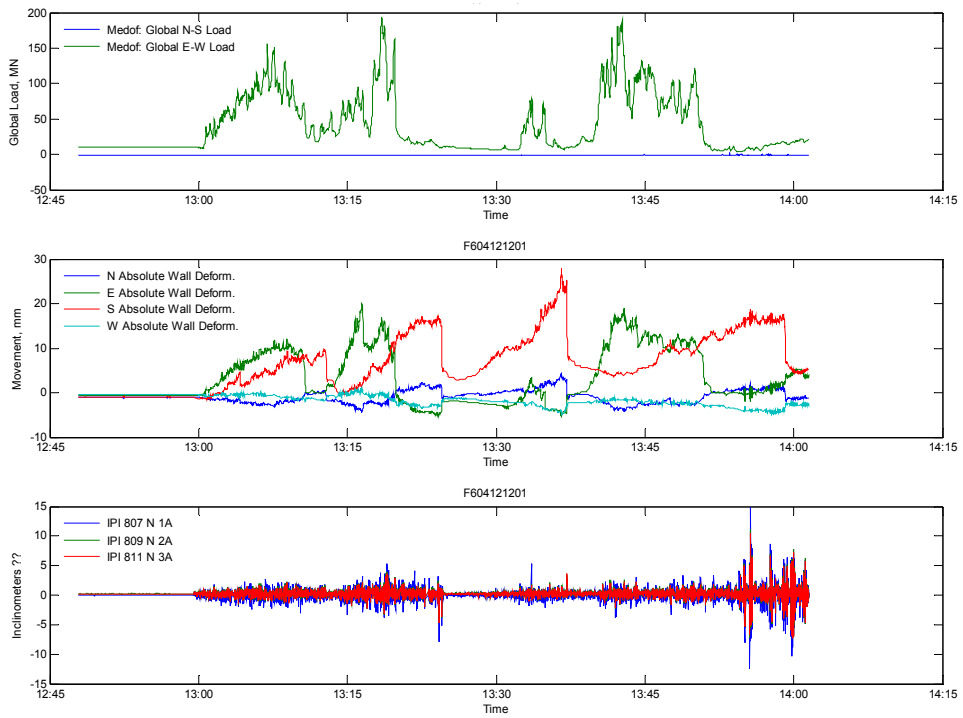


Figure A-11 Dynamac calculated ‘fast’ response to 12:01 12 Apr event

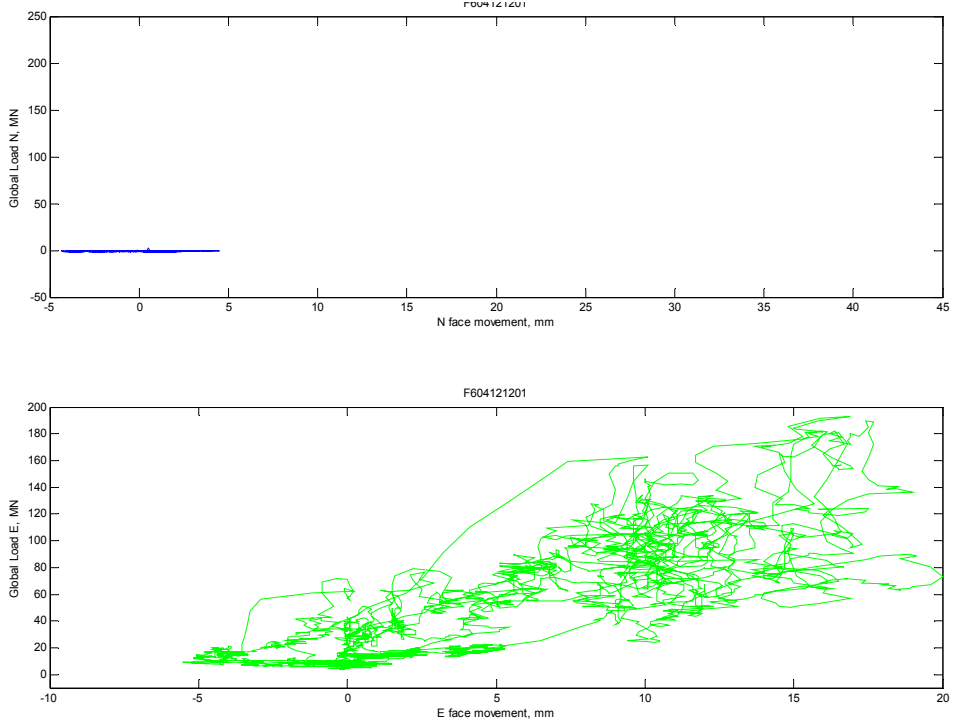
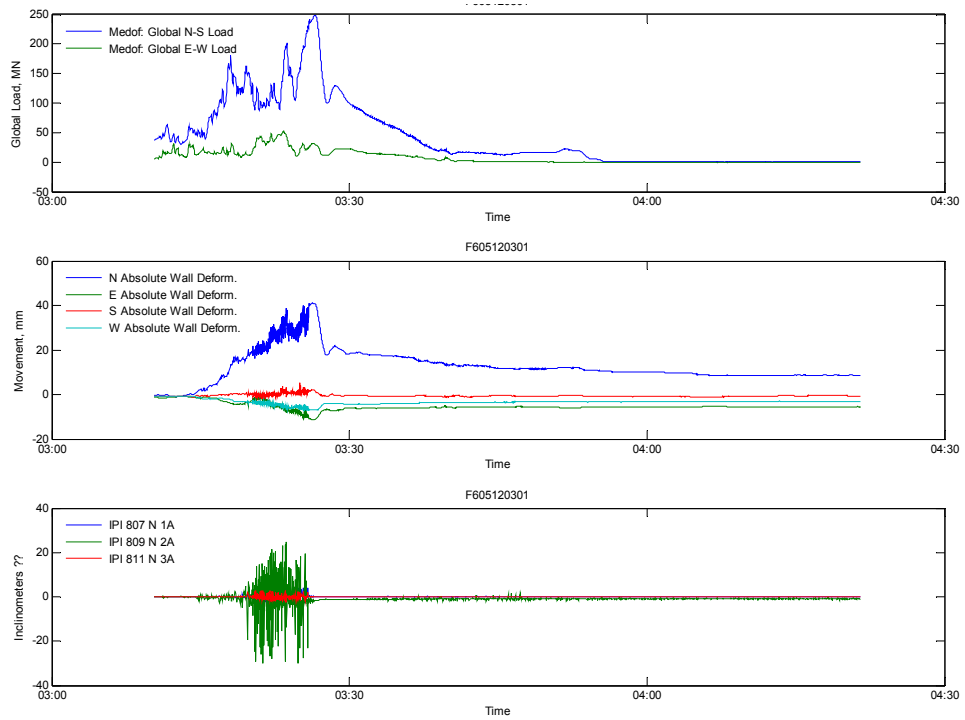
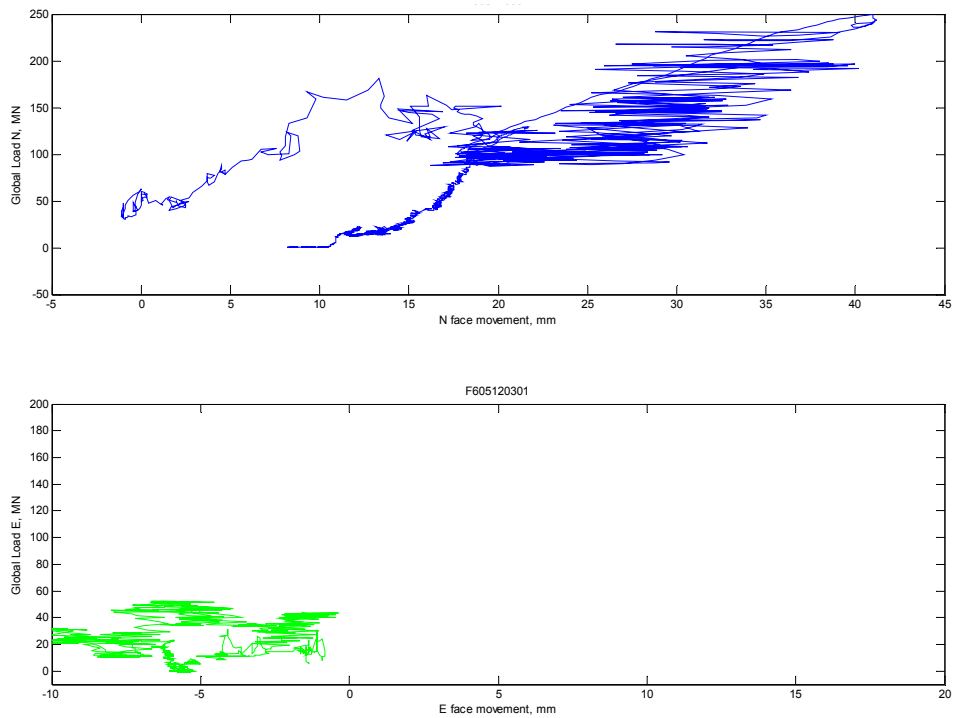


Figure A-12 Dynamac calculated global load-deflection during 12:01 12 Apr event



**Figure A-13** Dynamac calculated ‘fast’ response to 03:01 12 May event



**Figure A-14** Dynamac calculated global load–deflection during 03:01 12 May event

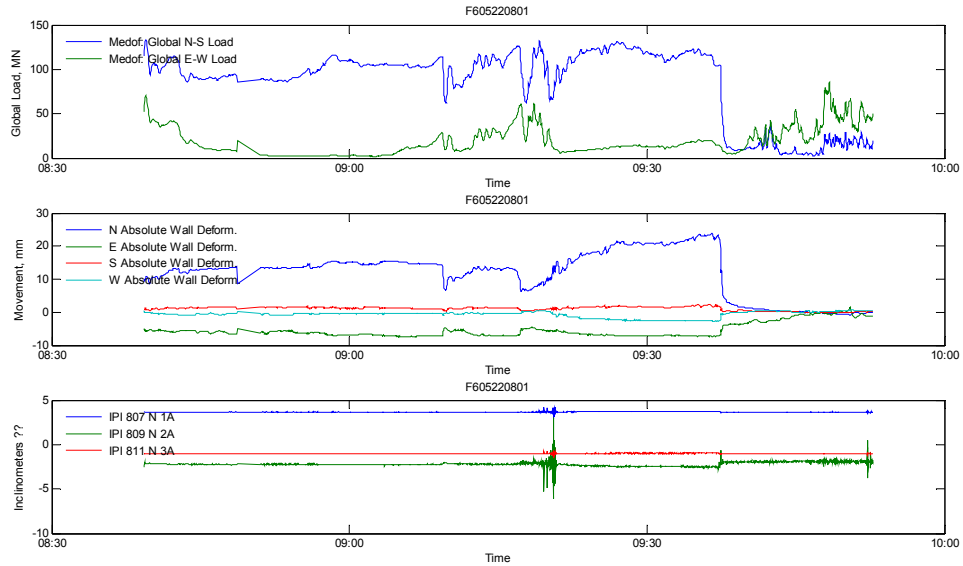


Figure A-15 Dynamac calculated ‘fast’ response to 08:01 22 May event

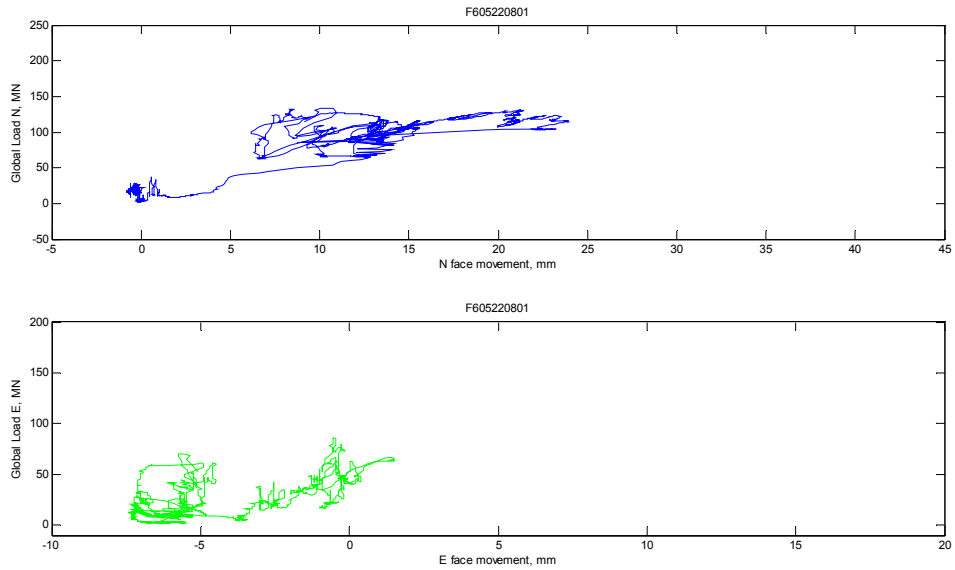


Figure A-16 Dynamac calculated global load–deflection during 08:01 22 May event

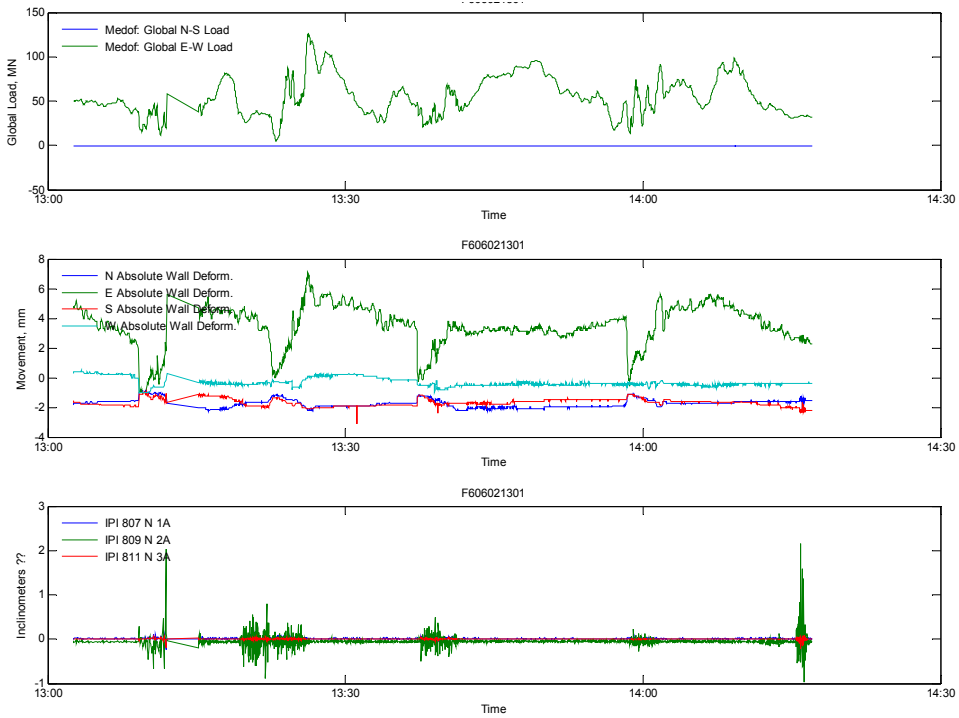


Figure A-17 Dynamac calculated ‘fast’ response to 13:01 2 Jun event

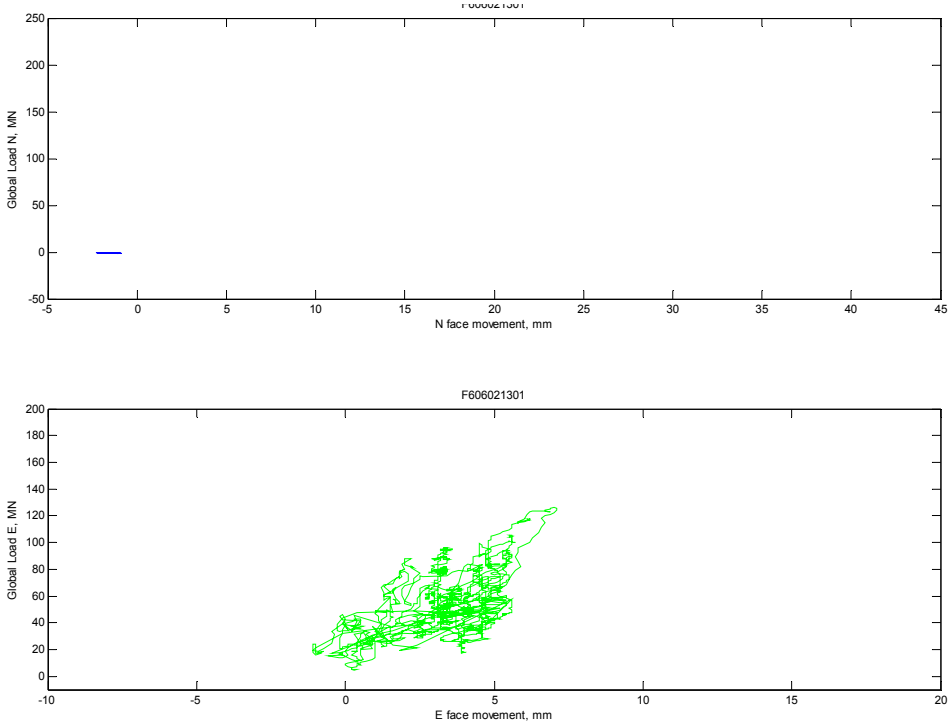
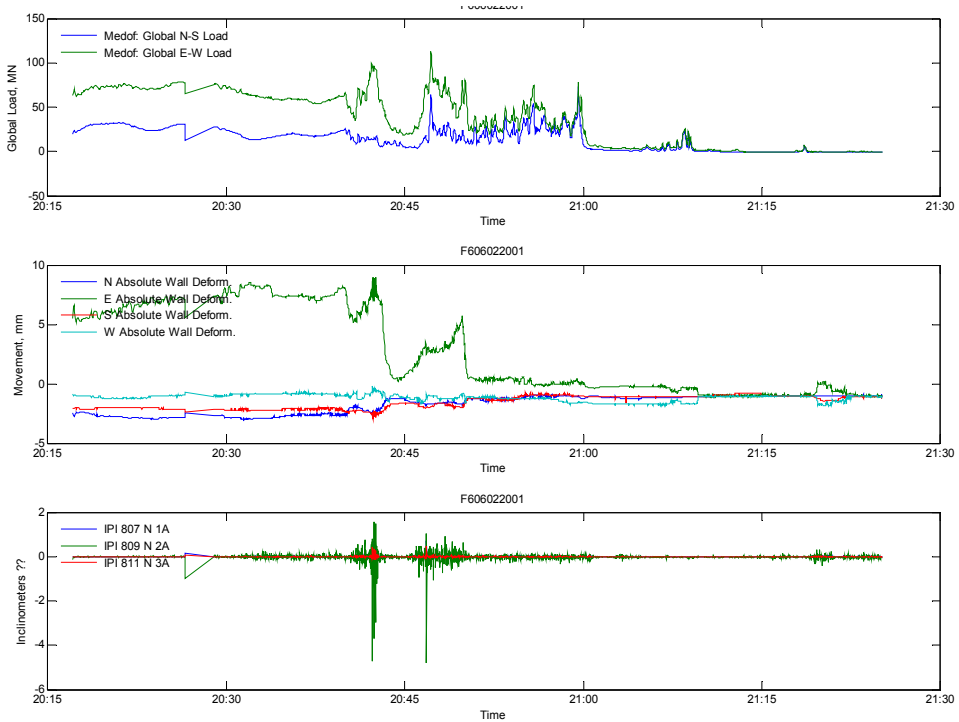
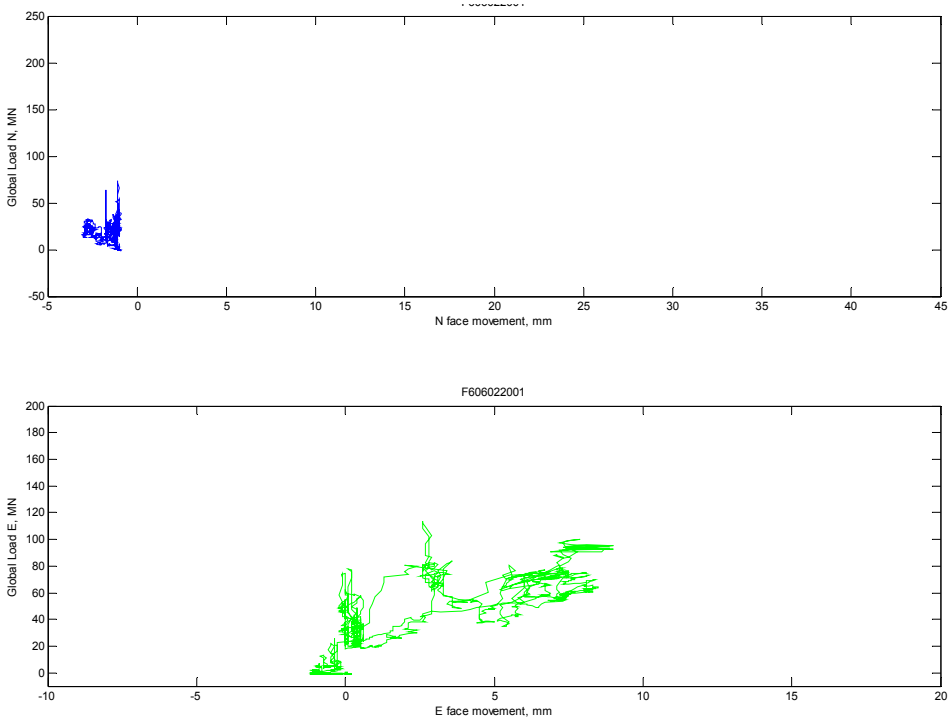


Figure A-18 Dynamac calculated global load–deflection during 13:01 2 Jun event



**Figure A-19** Dynamac calculated ‘fast’ response to 20:01 2 Jun event



**Figure A-20** Dynamac calculated global load–deflection during 20:01 2 Jun event

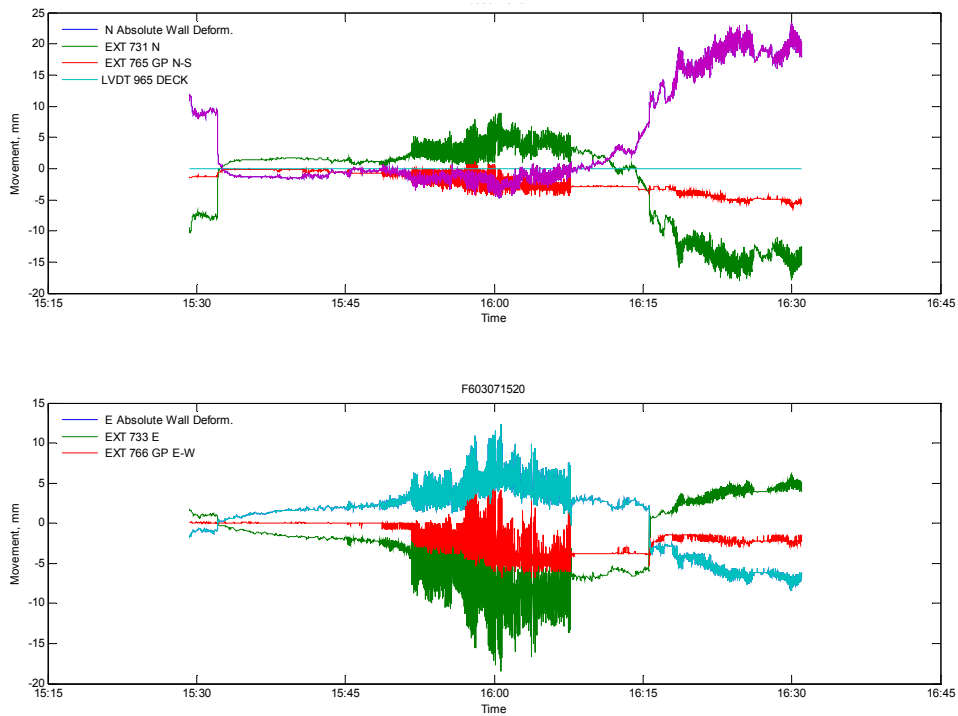


Figure A-21 Dynamac caisson movements, 15:20 7 Mar event

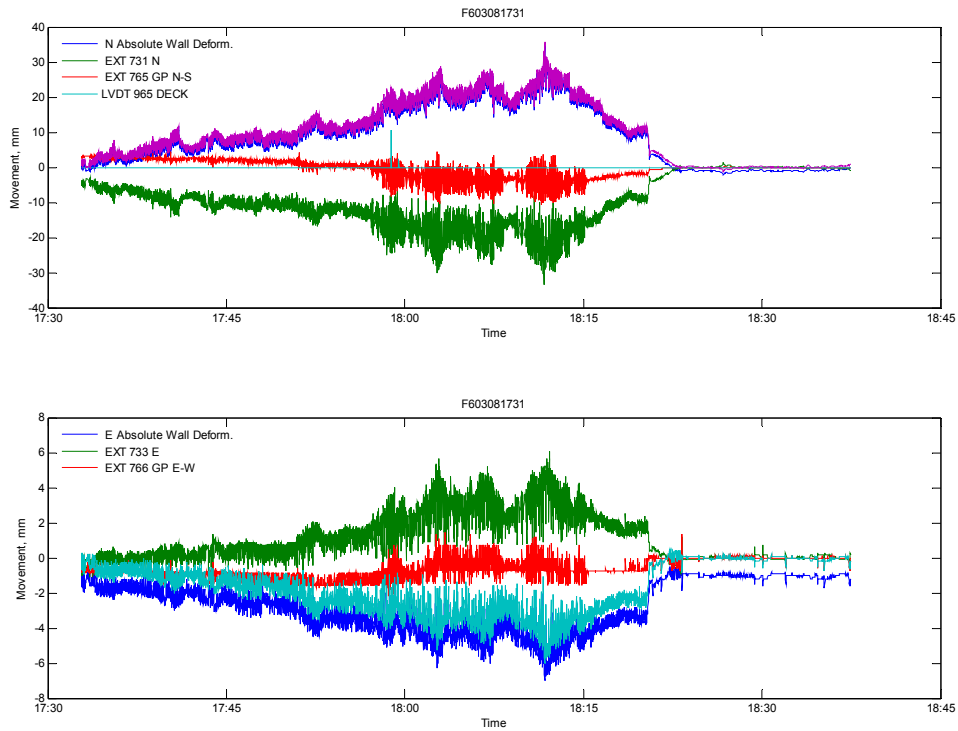
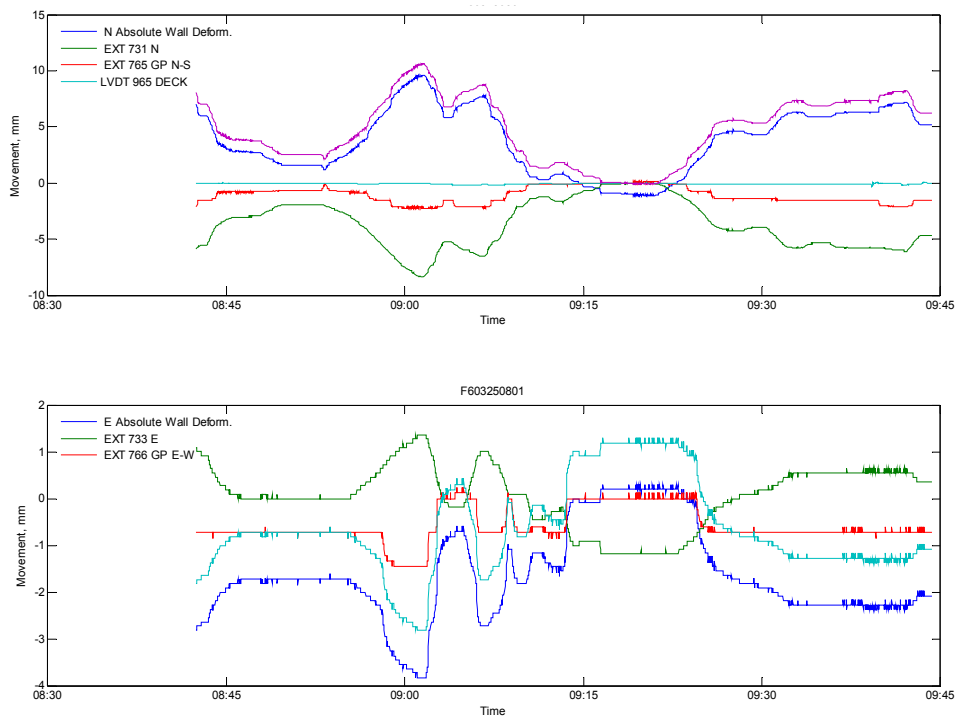
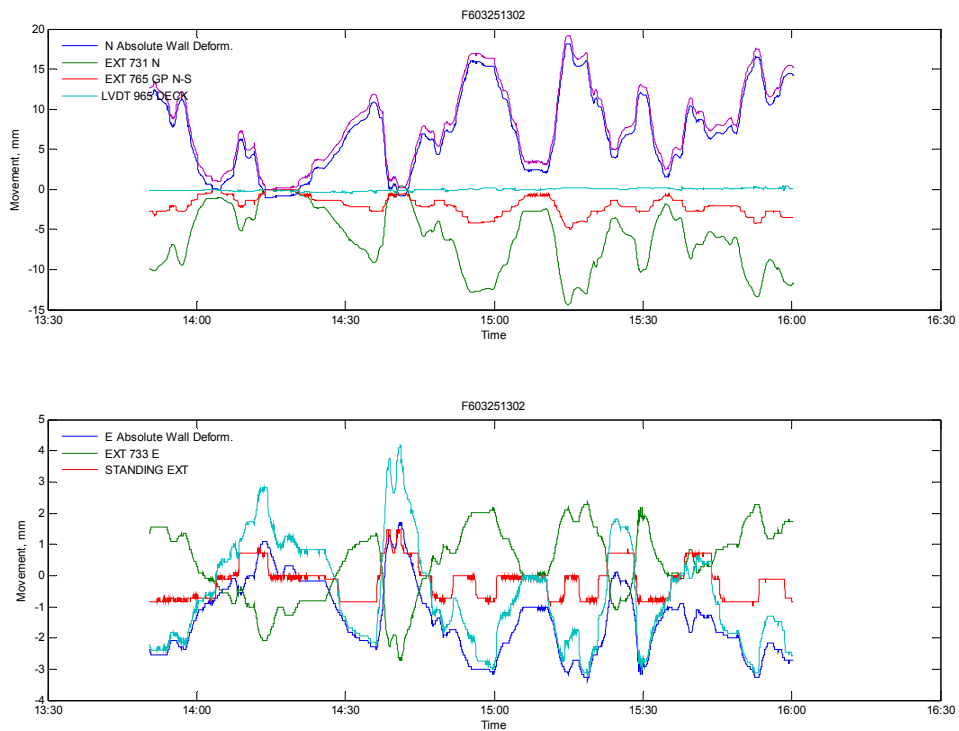


Figure A-22 Dynamac caisson movements, 17:31 8 Mar event



**Figure A-23** Dynamac caisson movements, 08:01 25 Mar event



**Figure A-24** Dynamac caisson movements, 13:02 25 Mar event

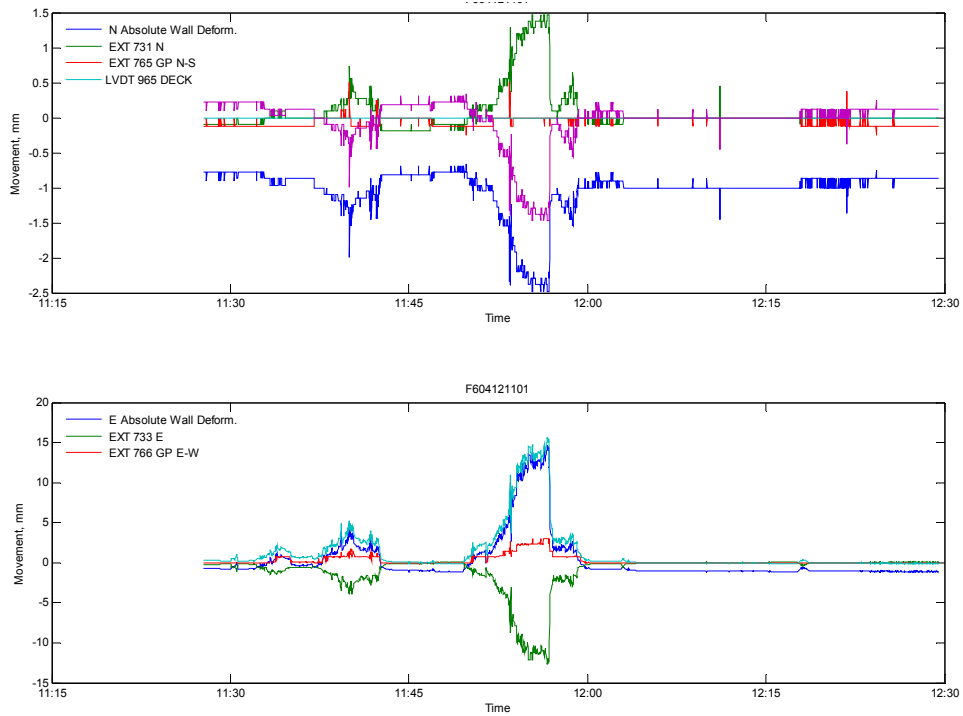


**Figure A-25** Dynamac caisson movements, 11:01 12 Apr event

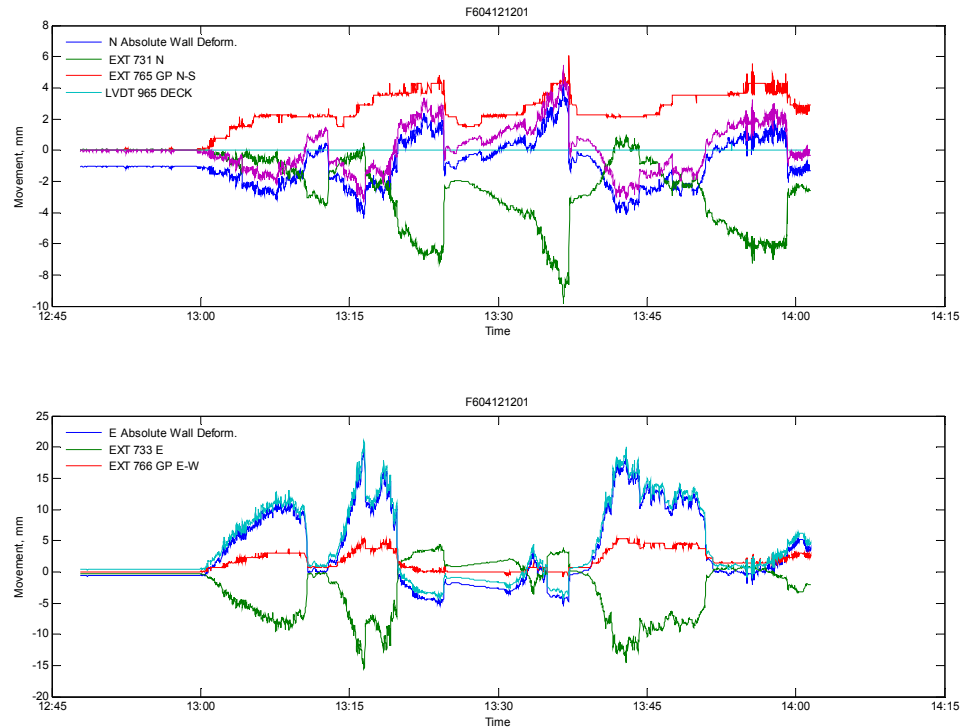


**Figure A-26** Dynamac caisson movements, 12:01 12 Apr event

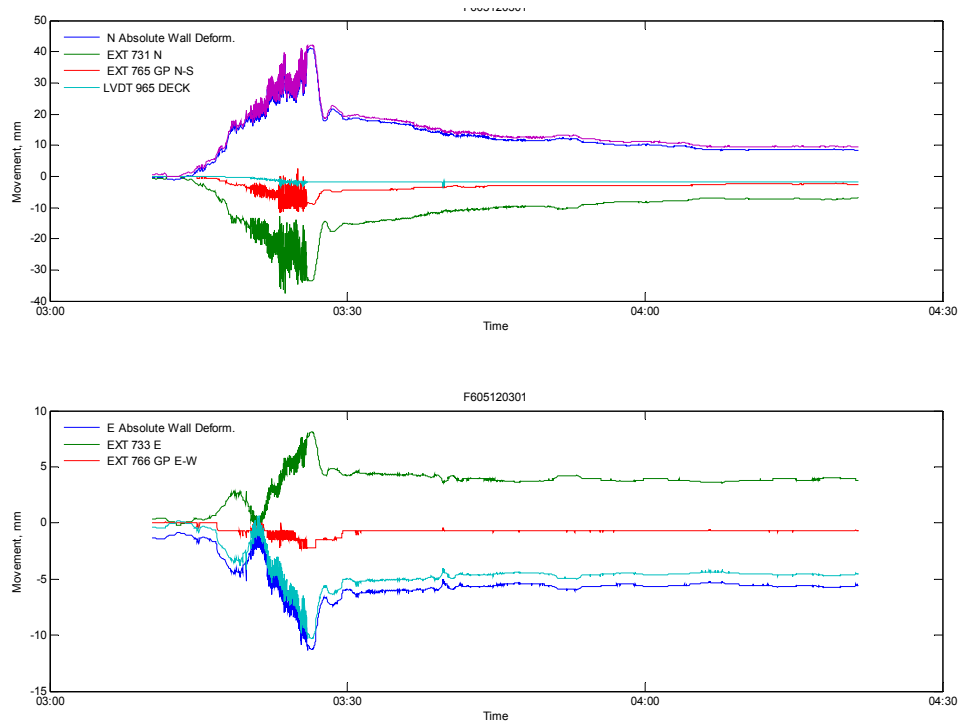


**Figure A-27** Dynamac caisson movements, 03:01 12 May event

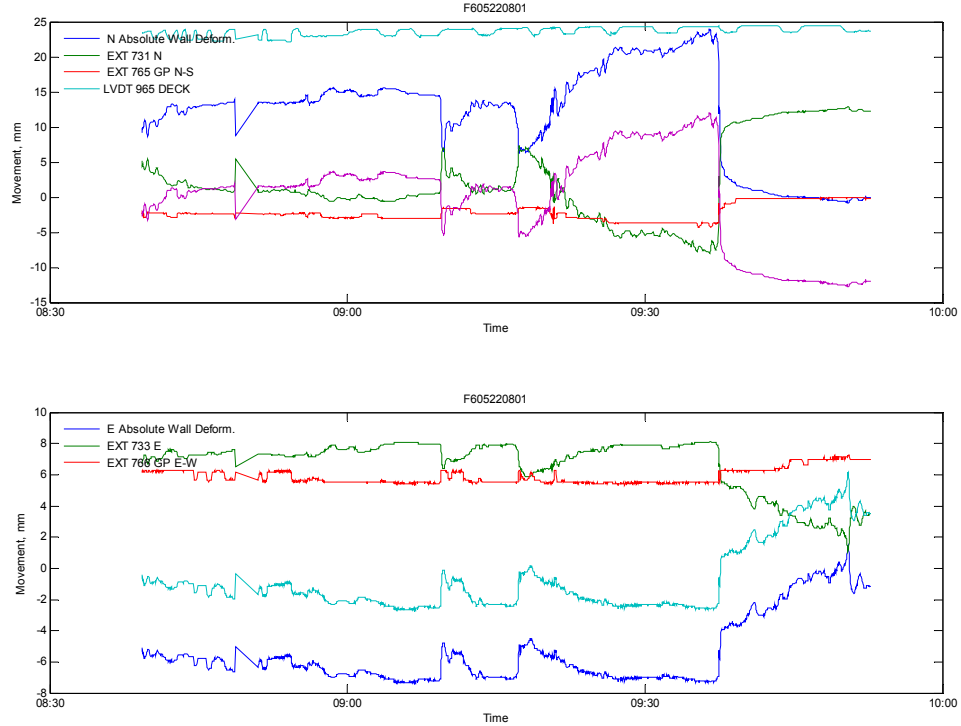


**Figure A-28** Dynamac caisson movements, 08:01 22 May event

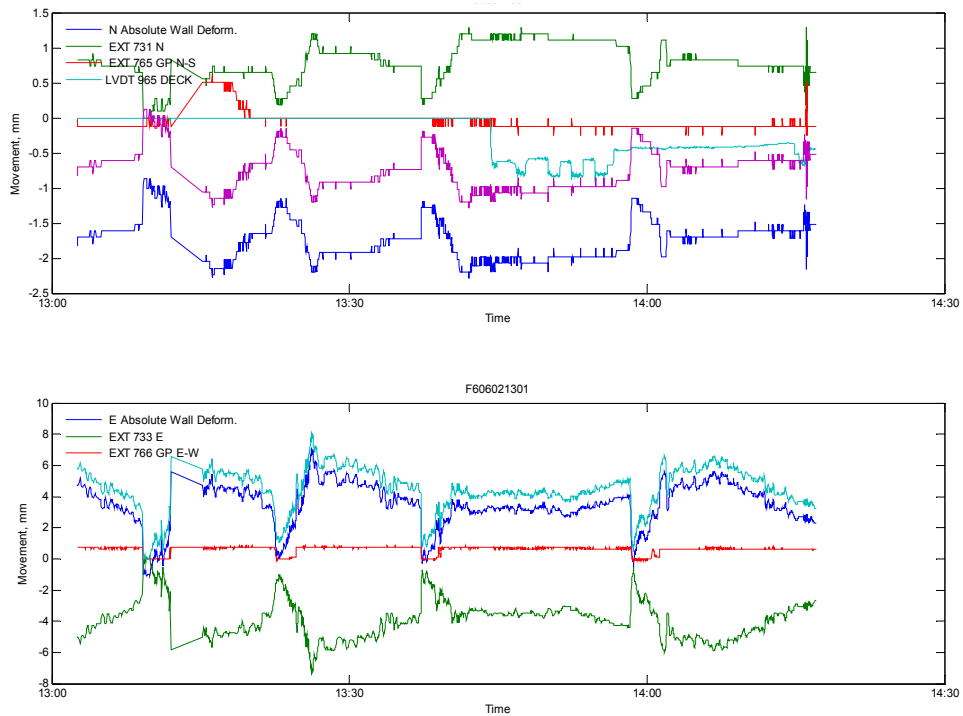


Figure A-29 Dynamac caisson movements, 13:01 2 Jun event

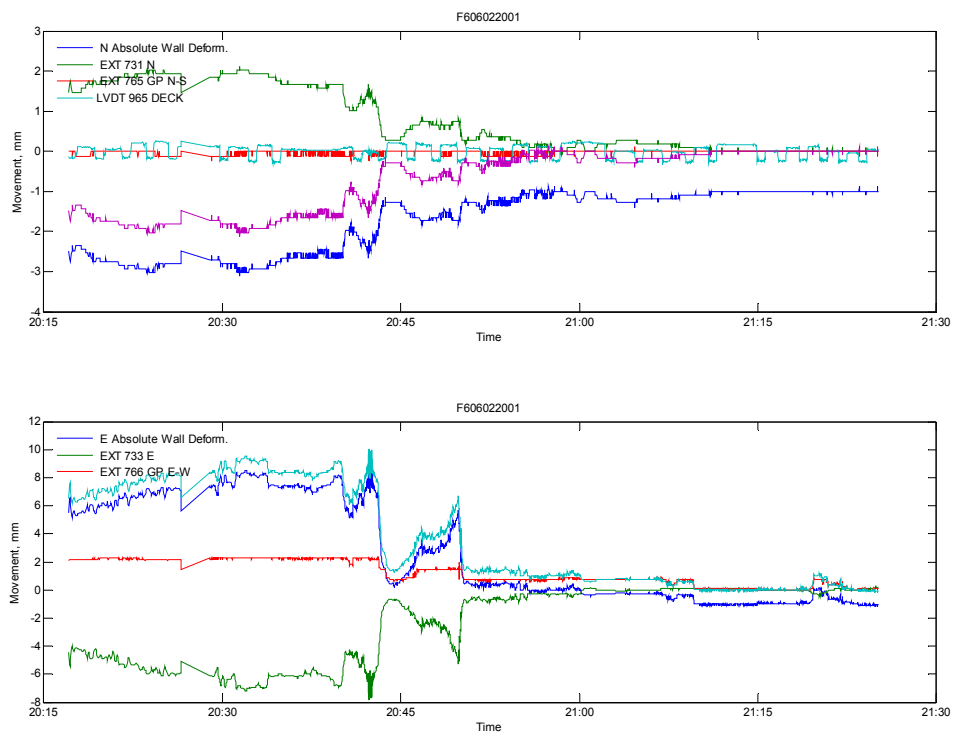


Figure A-30 Dynamac caisson movements, 20:01 2 Jun event

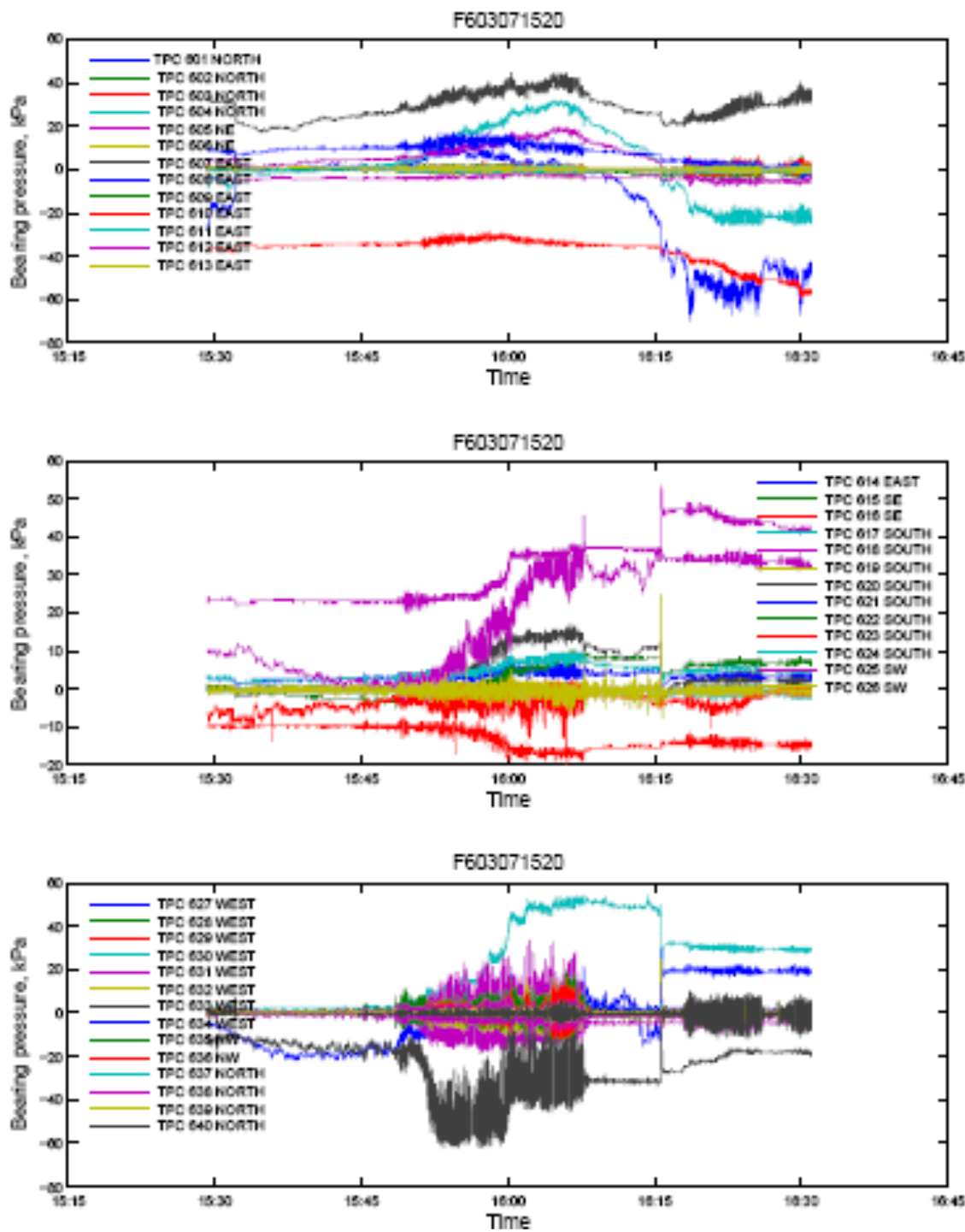


Figure A-31 Dynamac bearing pressures, 15:20 7 Mar event

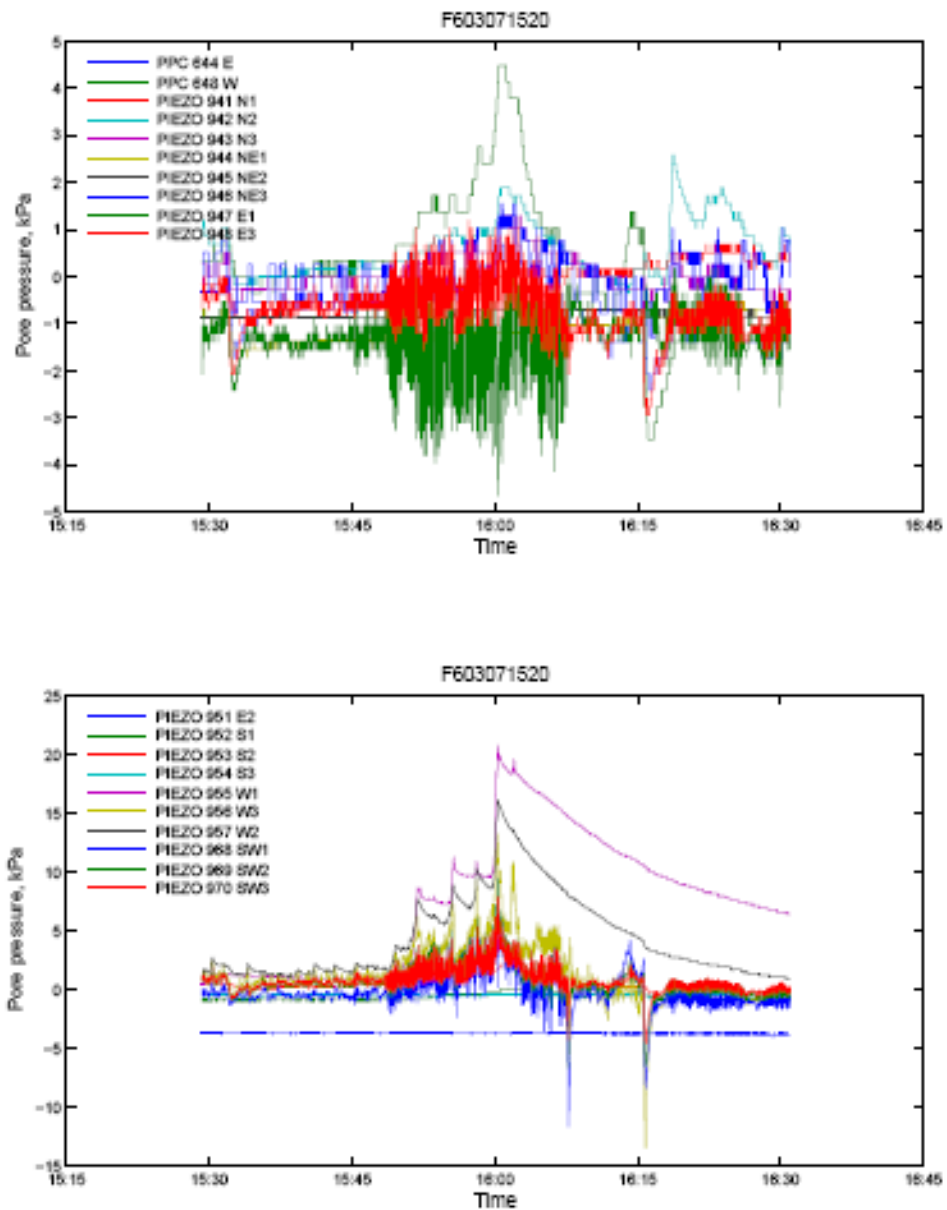


Figure A-32 Dynamac pore pressures, 15:20 7 Mar event

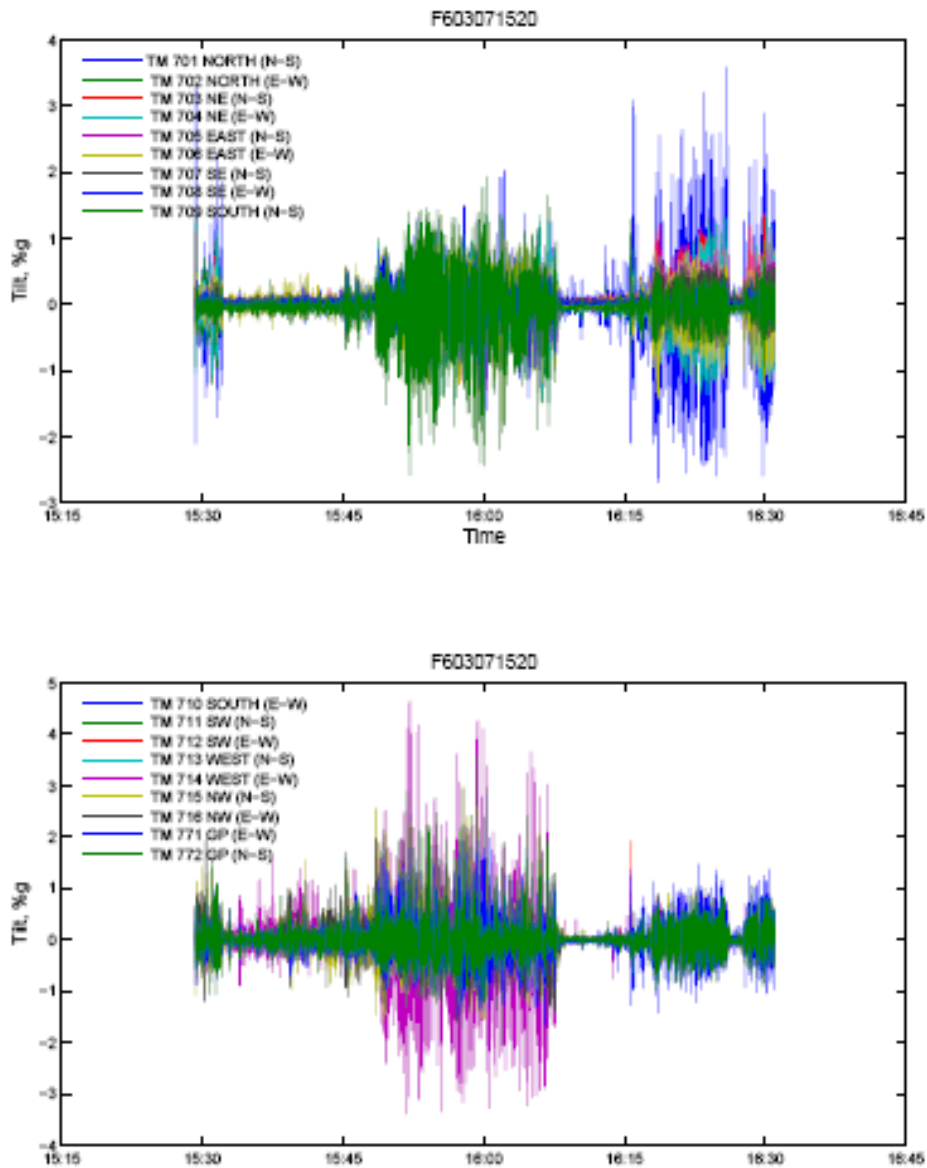


Figure A-33 Dynamac tilt sensors, 15:20 7 Mar event

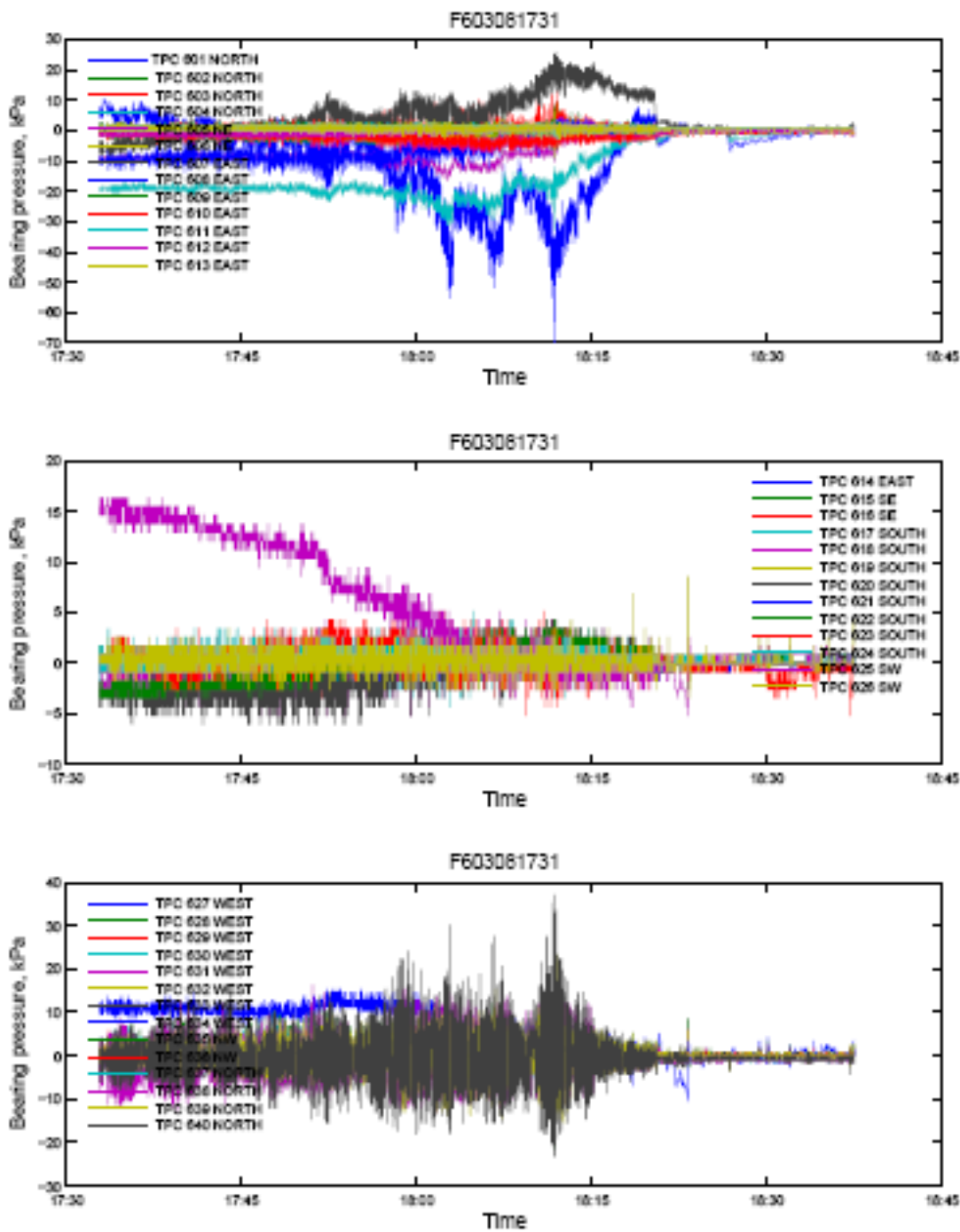


Figure A-34 Dynamac bearing pressures, 17:31 8 Mar event

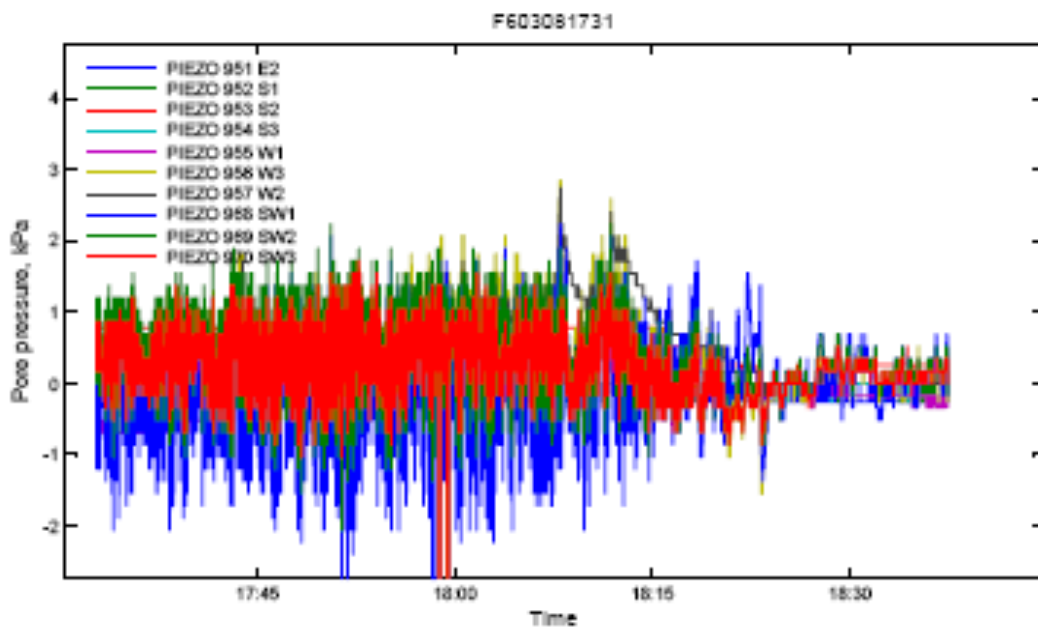
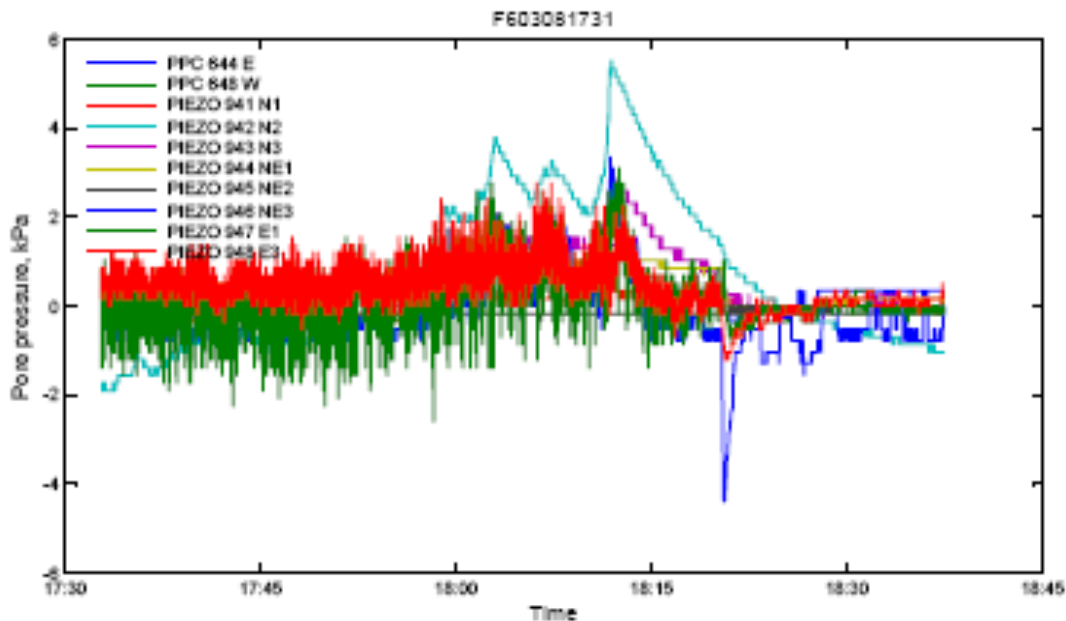


Figure A-35 Dynamac pore pressures, 17:31 8 Mar event

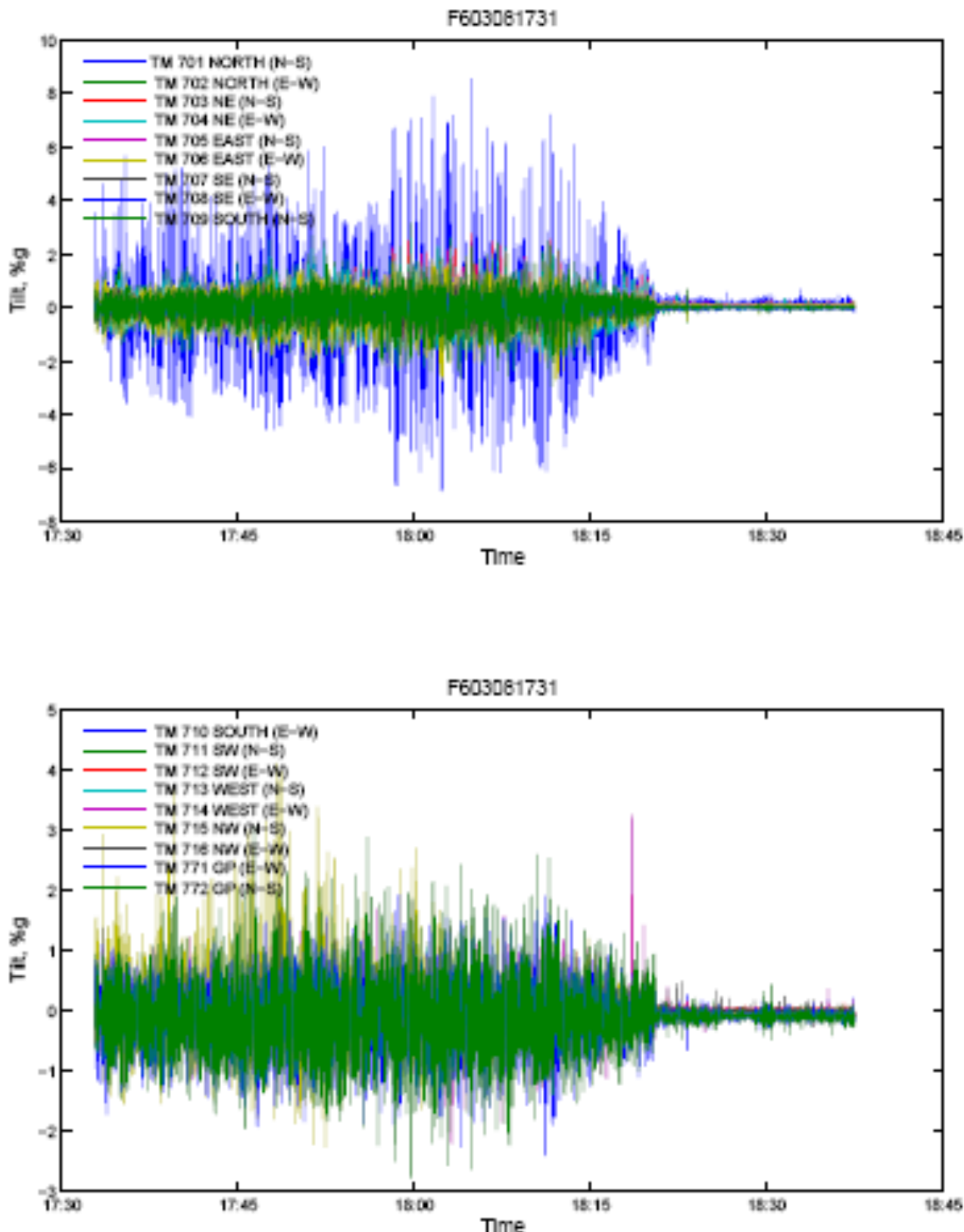


Figure A-36 Dynamac tilt sensors, 17:31 8 Mar event

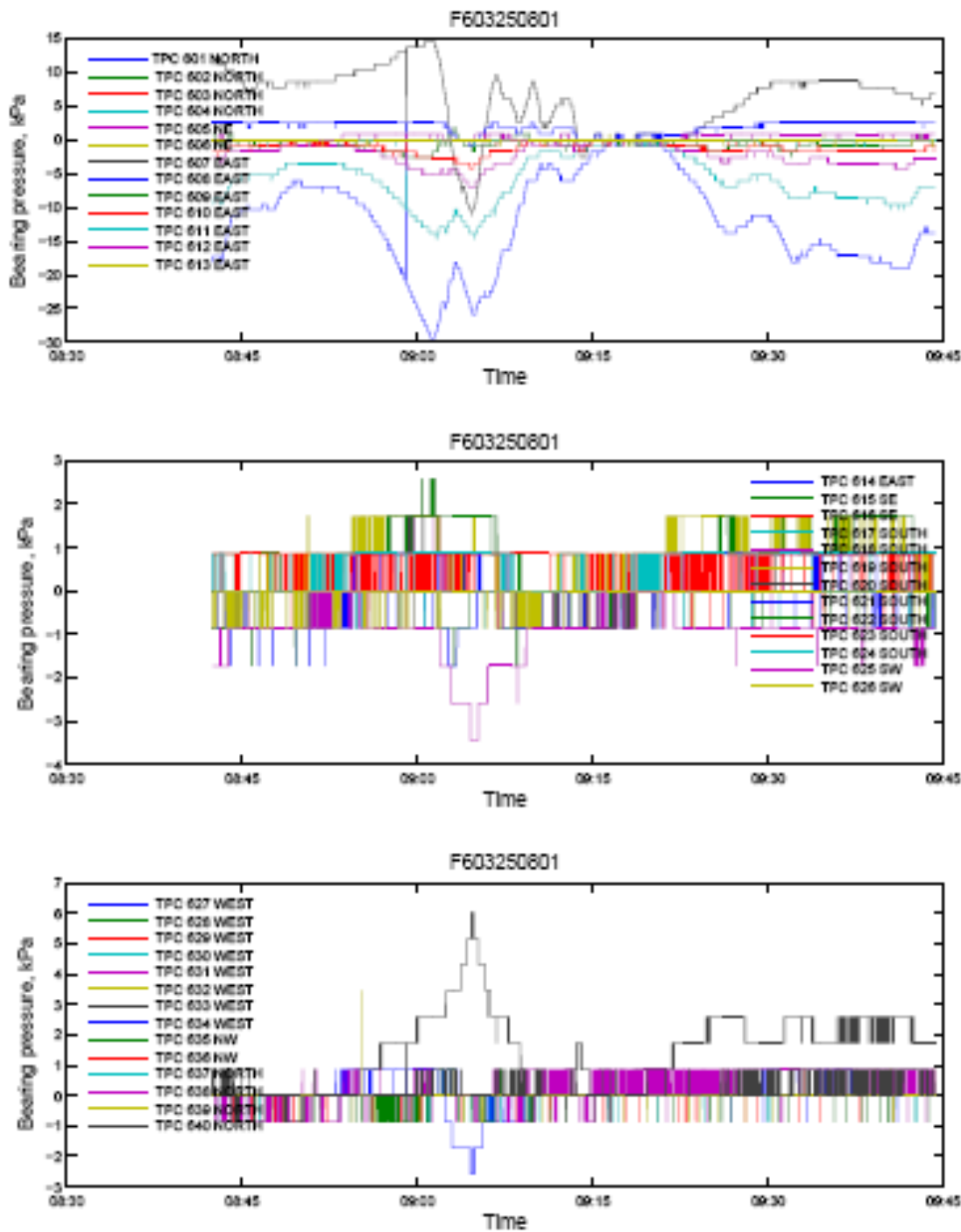


Figure A-37 Dynamac bearing pressures, 08:01 25 Mar event

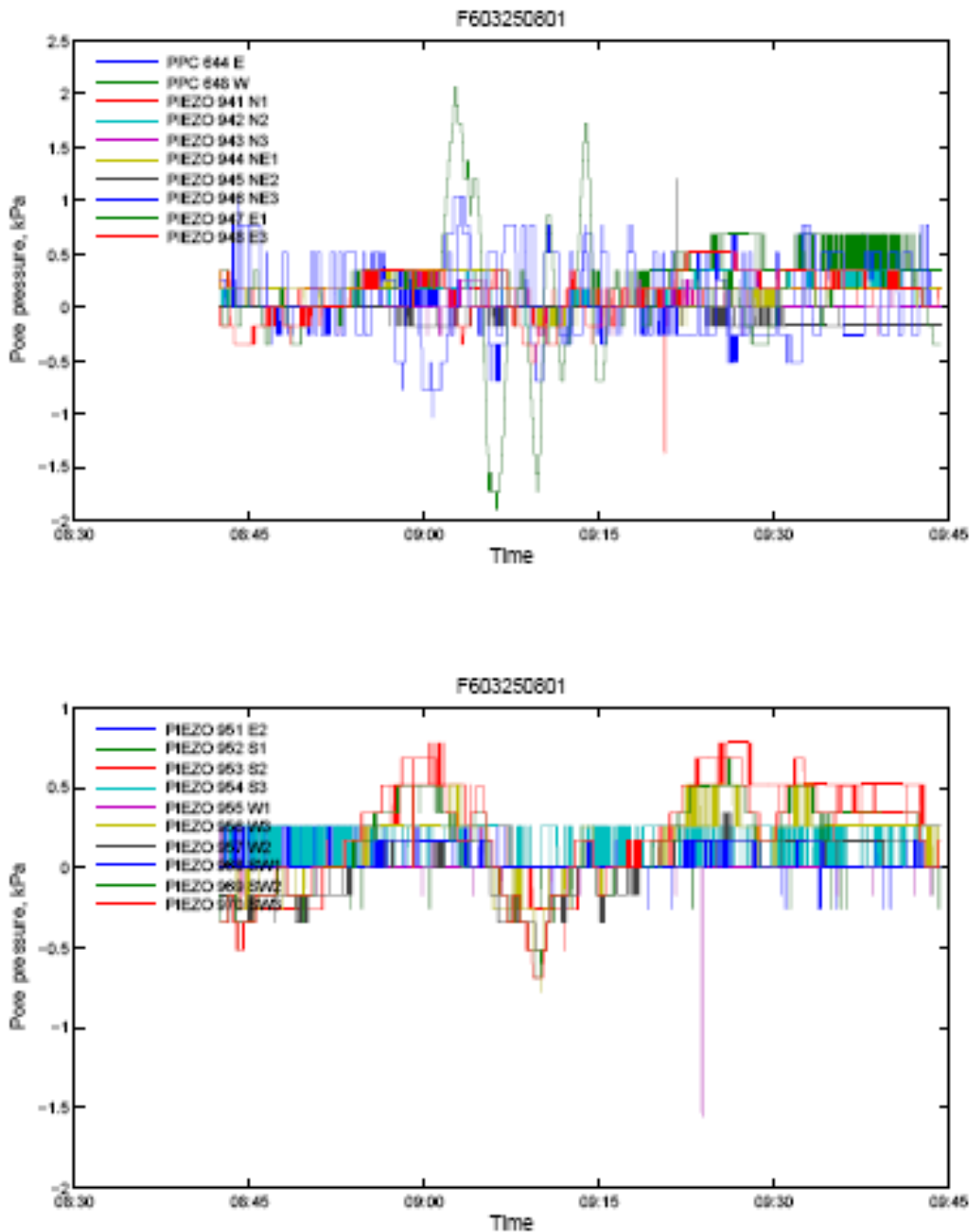


Figure A-38 Dynamac pore pressures, 08:01 25 Mar event

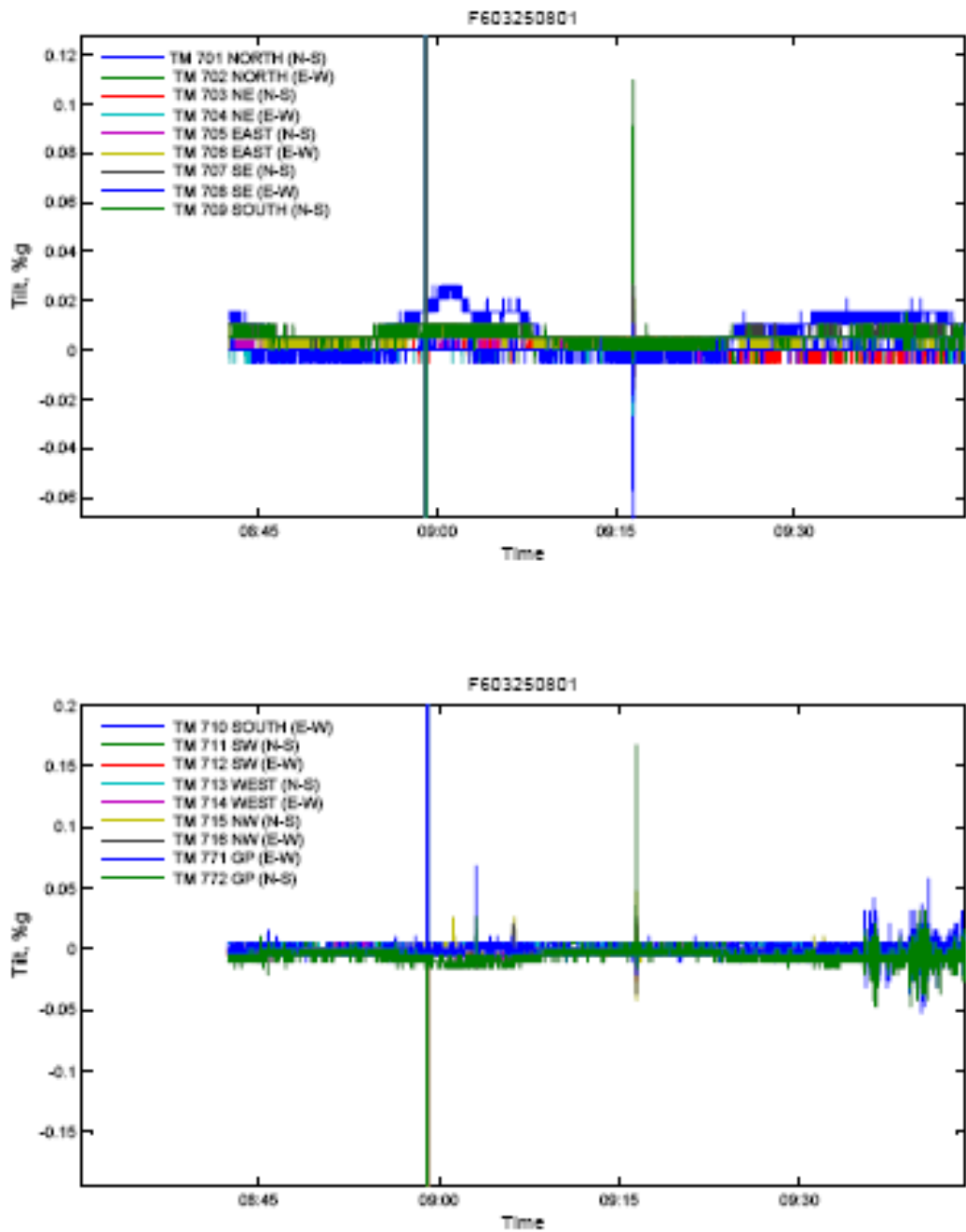


Figure A-39 Dynamac tilt sensors, 08:01 25 Mar event

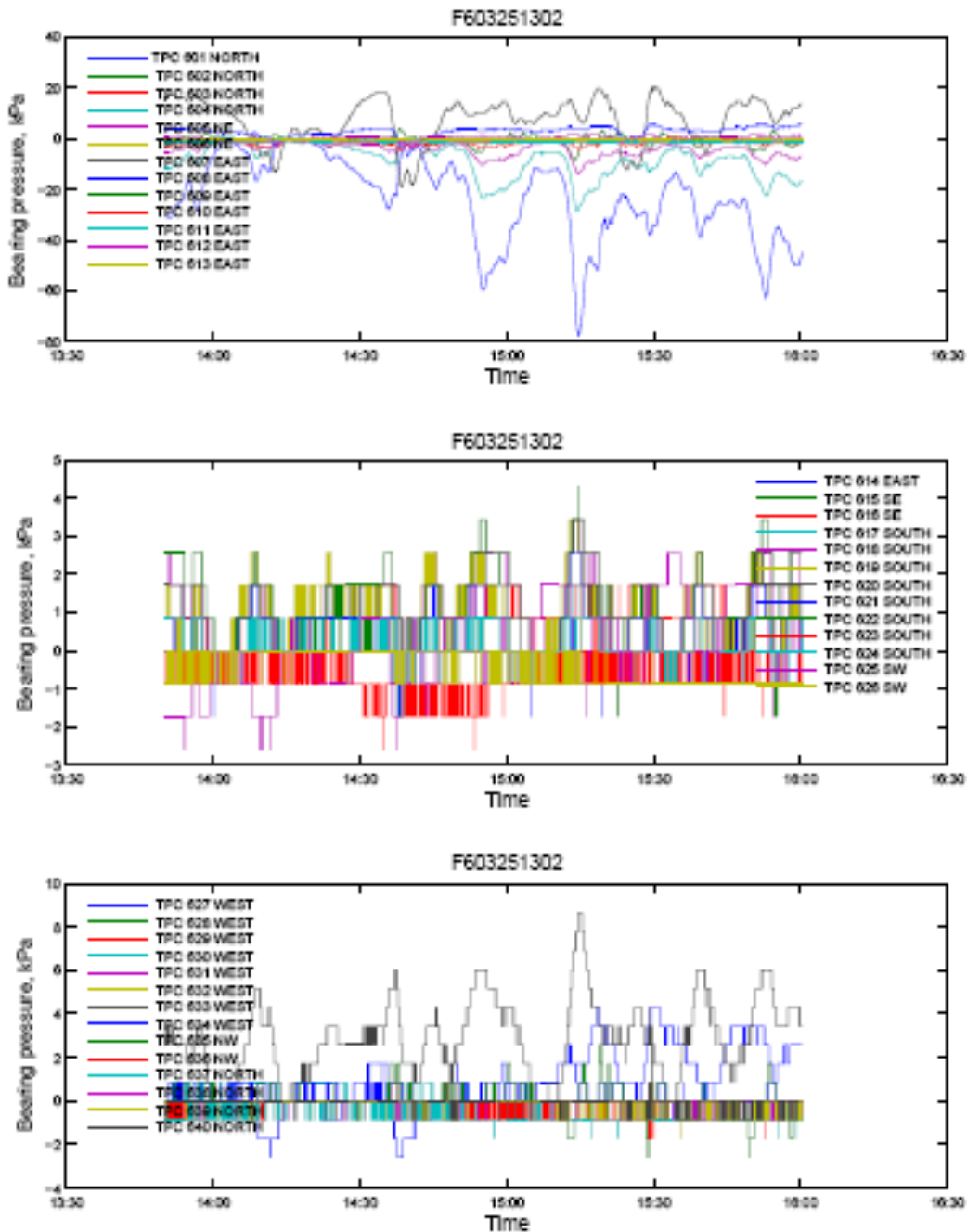


Figure A-40 Dynamac bearing pressures, 13:02 25 Mar event

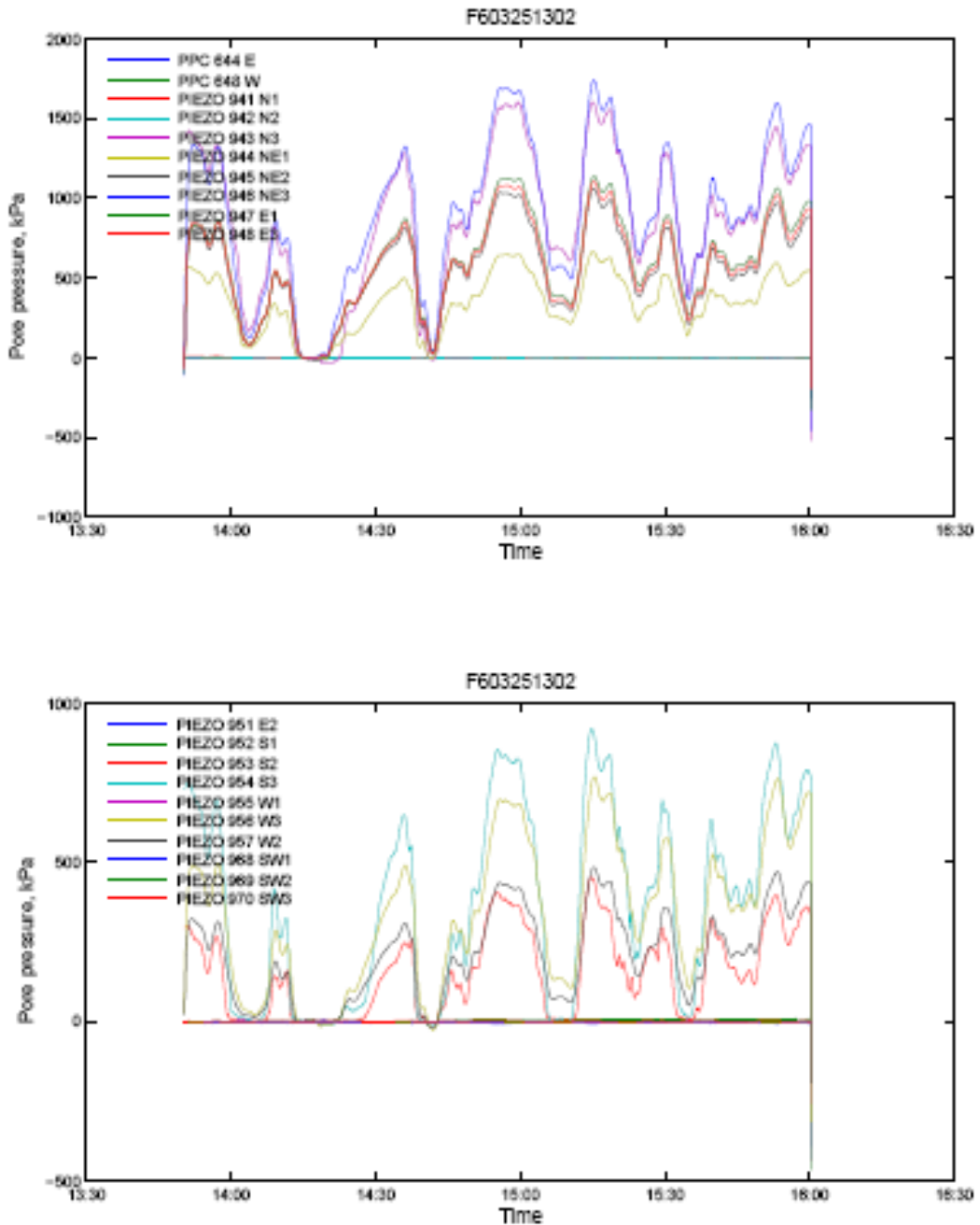


Figure A-41 Dynamac pore pressures, 13:02 25 Mar event

Note: These Dynamac data are NOT pore pressure measurements

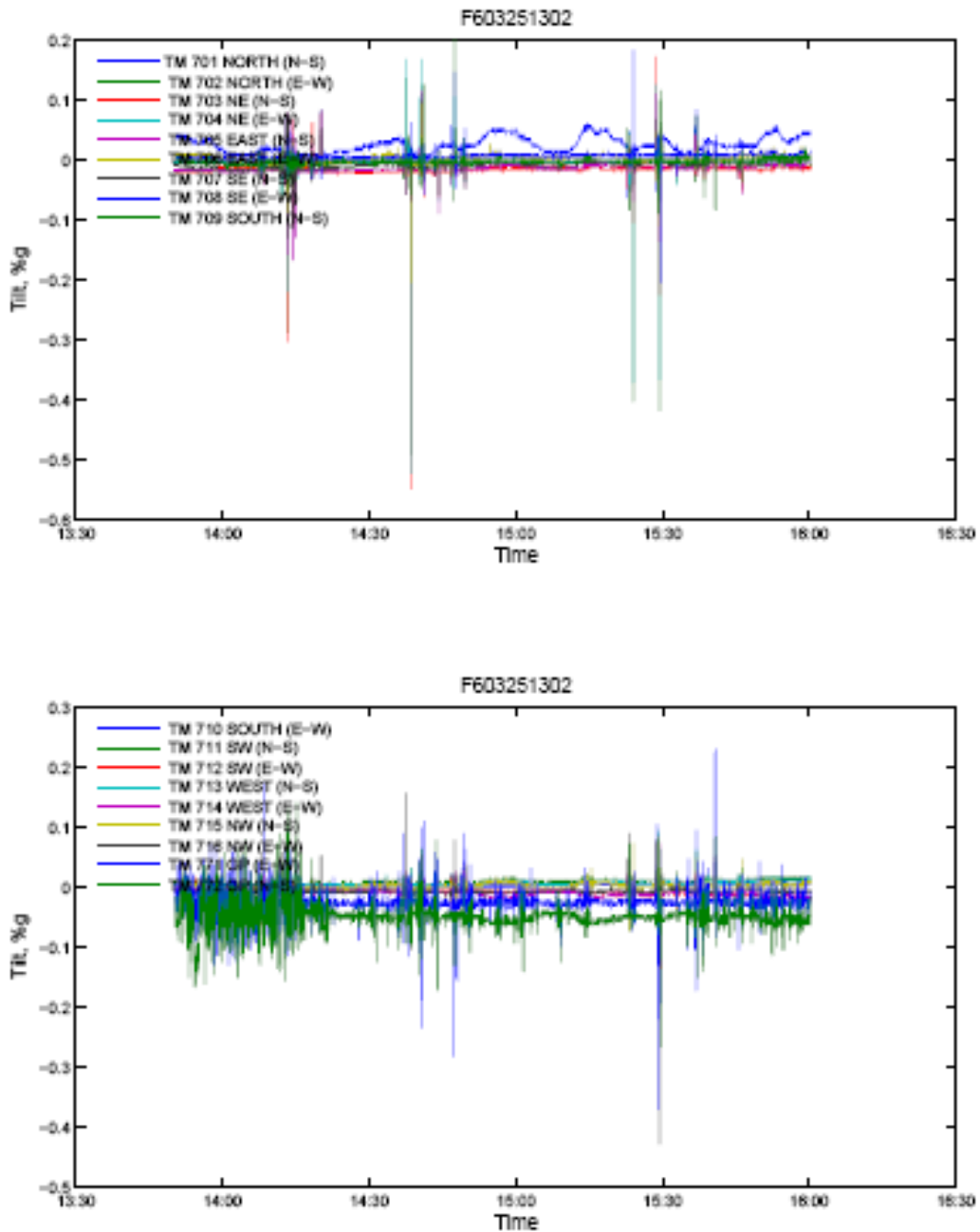


Figure A-42 Dynamac tilt sensors, 13:02 25 Mar event

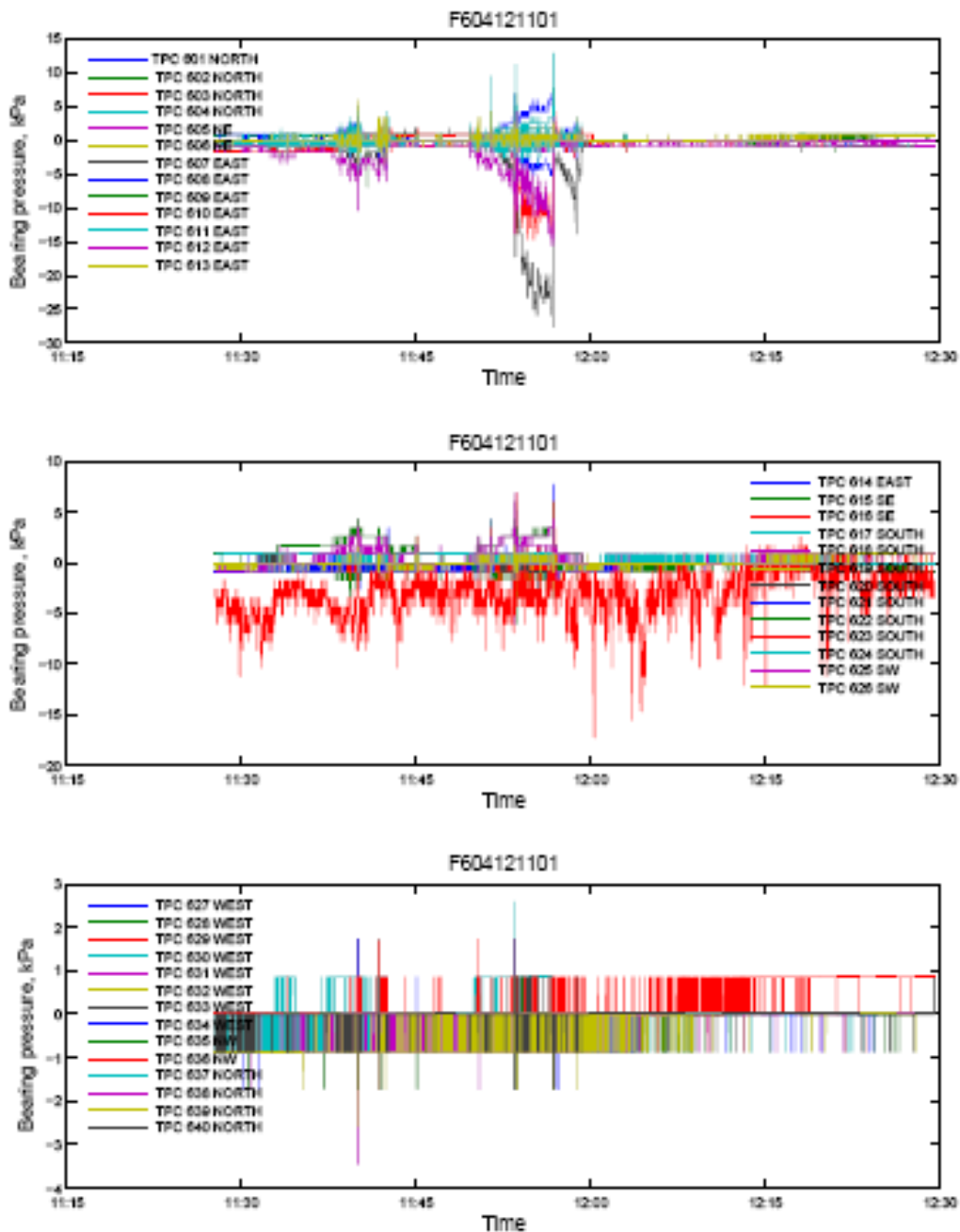


Figure A-43 Dynamac bearing pressures, 11:01 12 Apr event

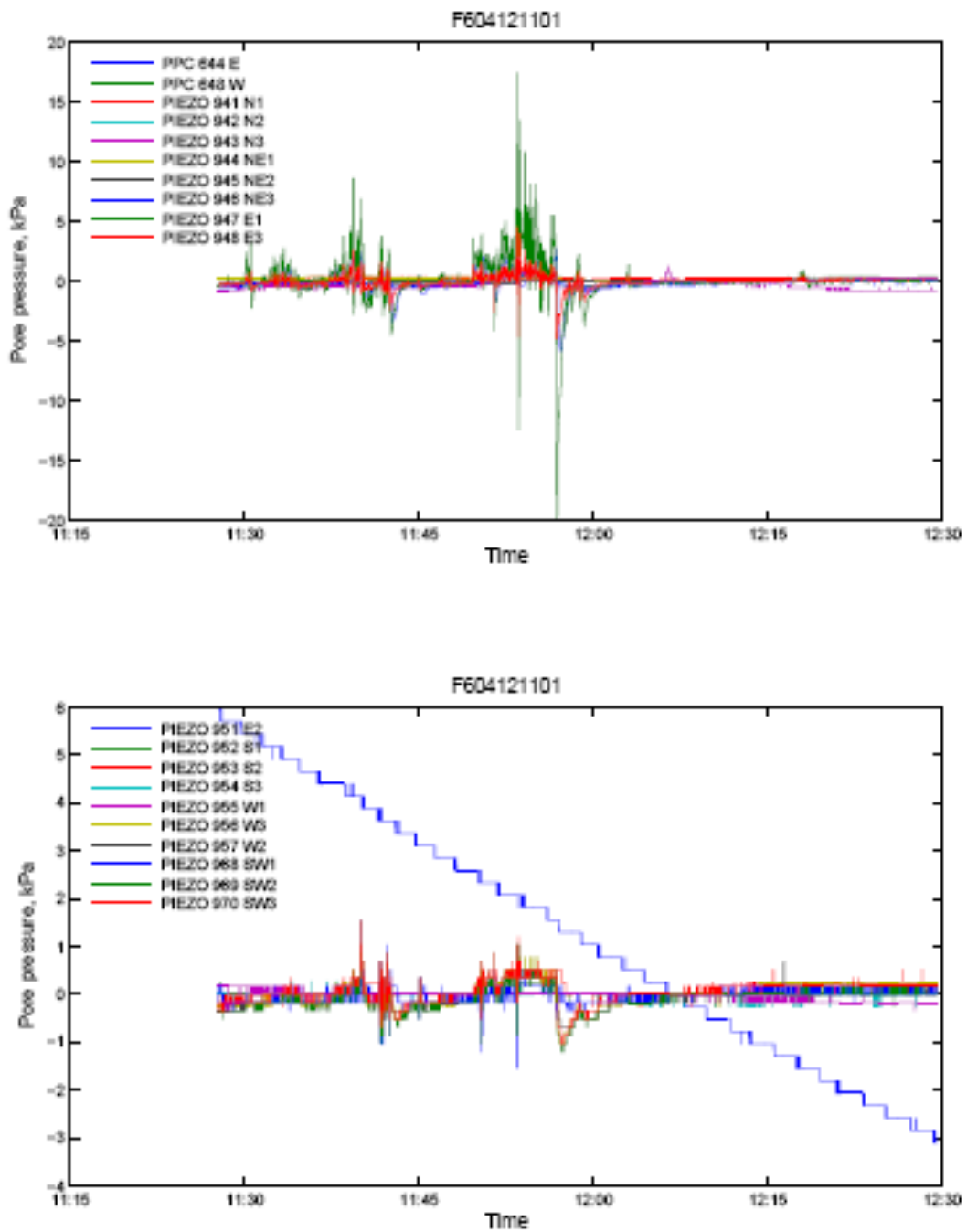


Figure A-44 Dynamac pore pressures, 11:01 12 Apr event

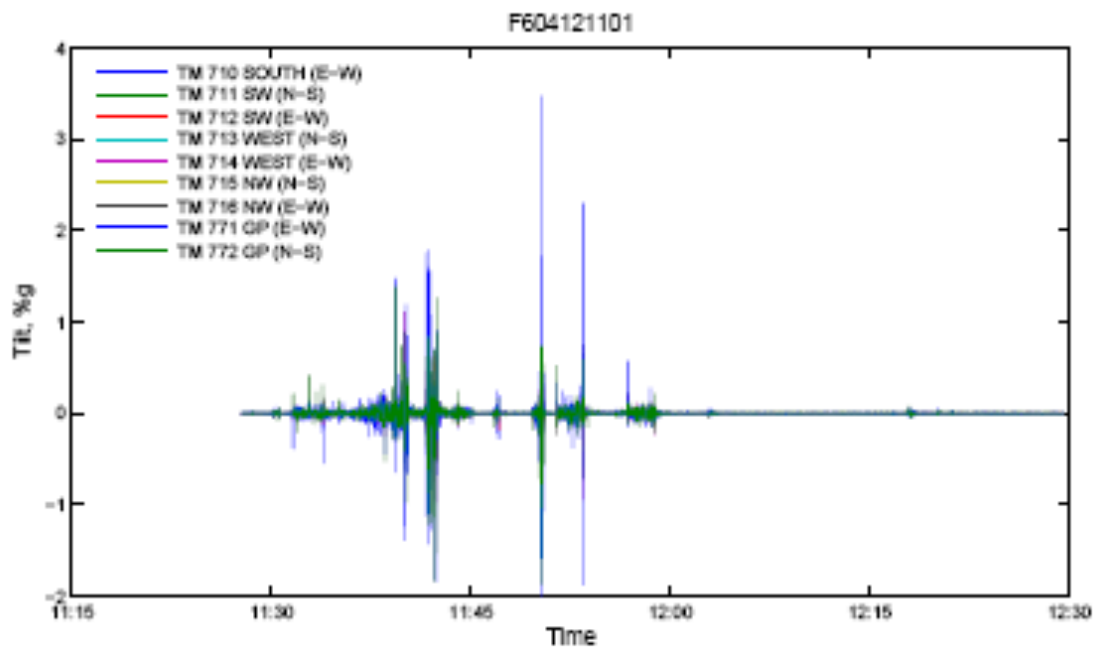
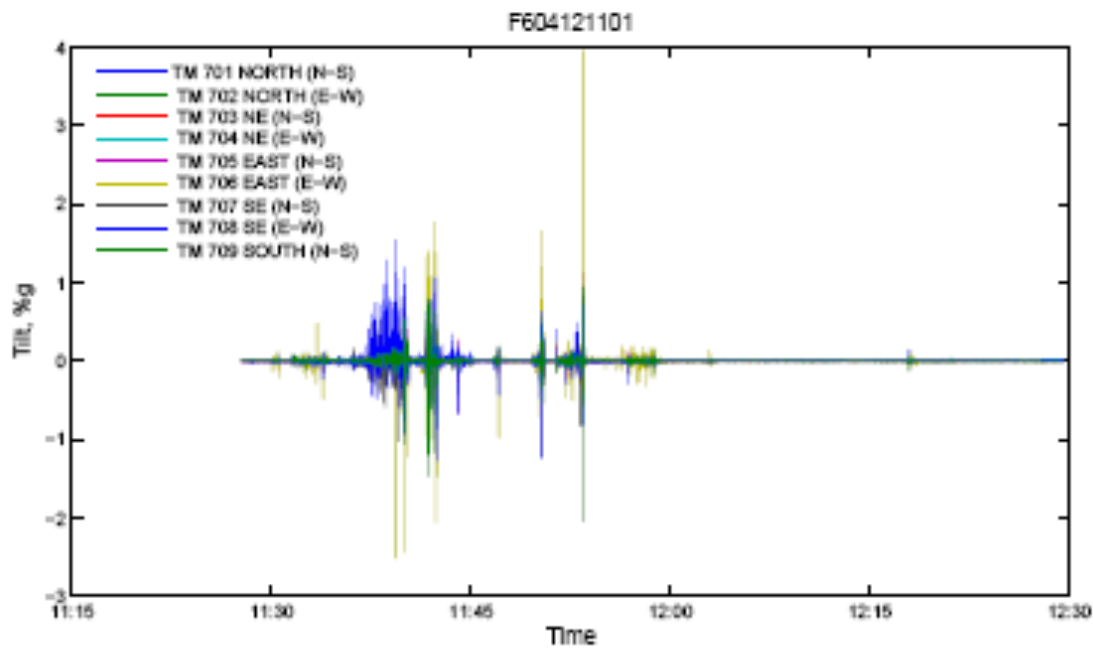


Figure A-45 Dynamac tilt sensors, 11:01 12 Apr event

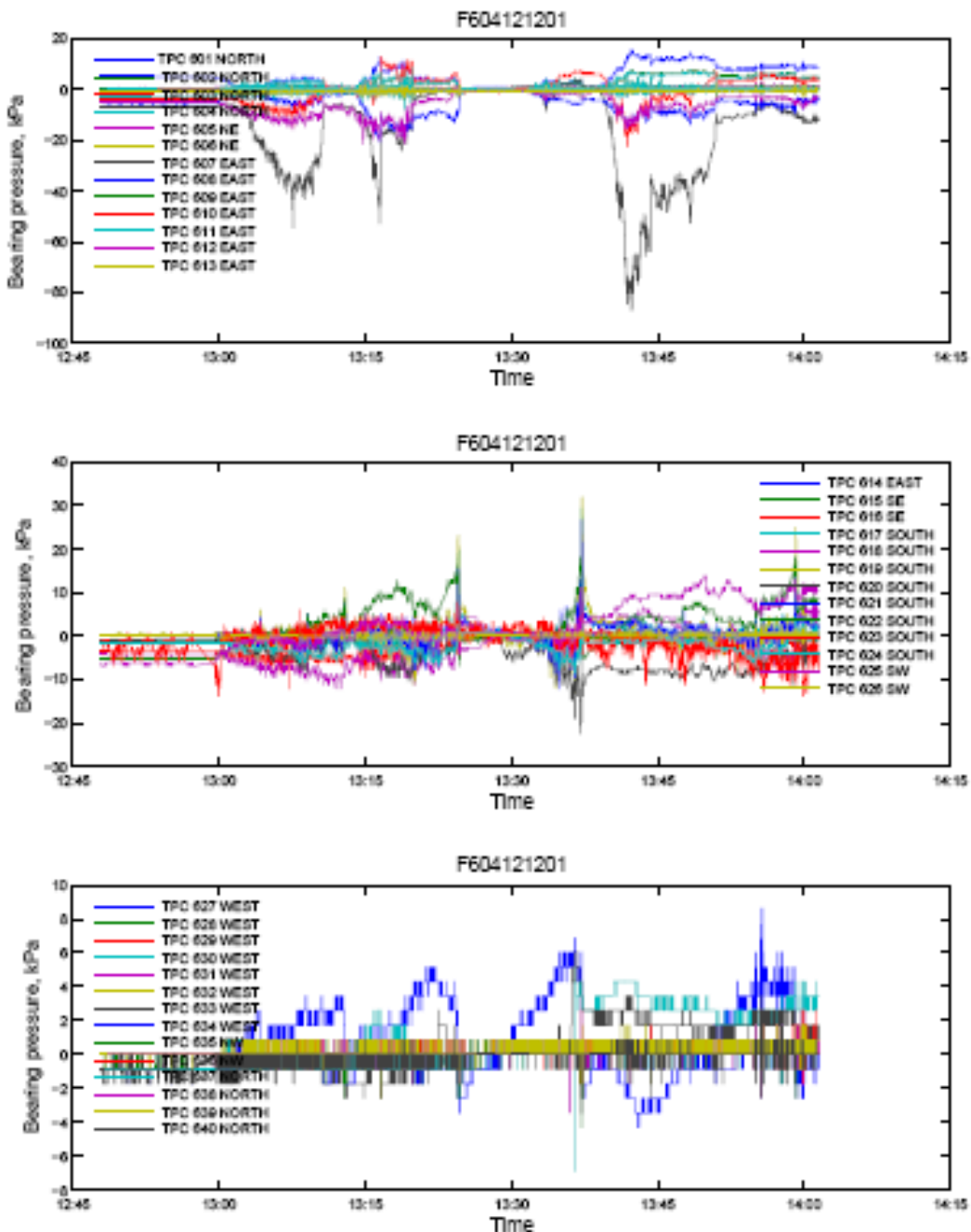


Figure A-46 Dynamac bearing pressures, 12:01 12 Apr event

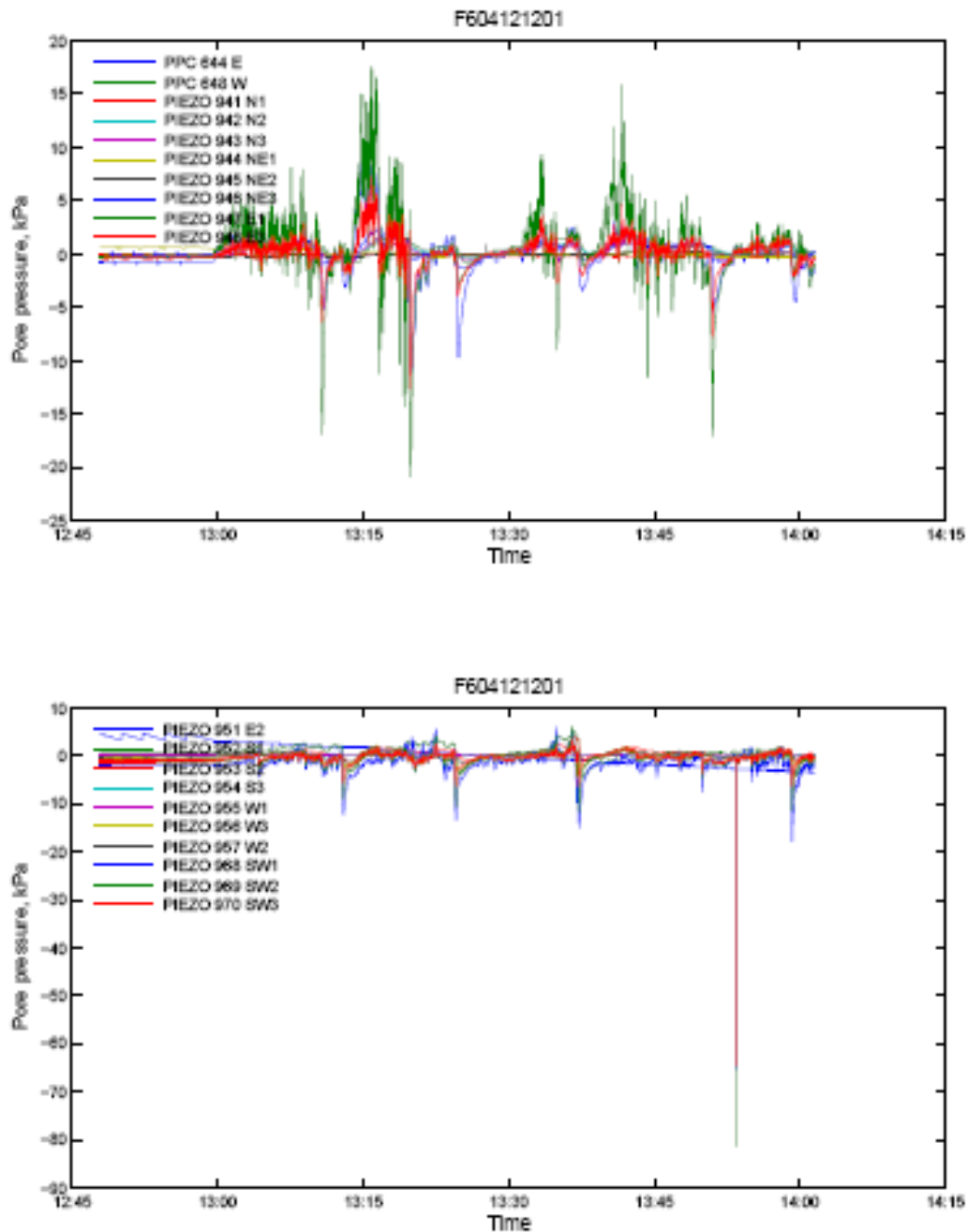


Figure A-47 Dynamac pore pressures, 12:01 12 Apr event

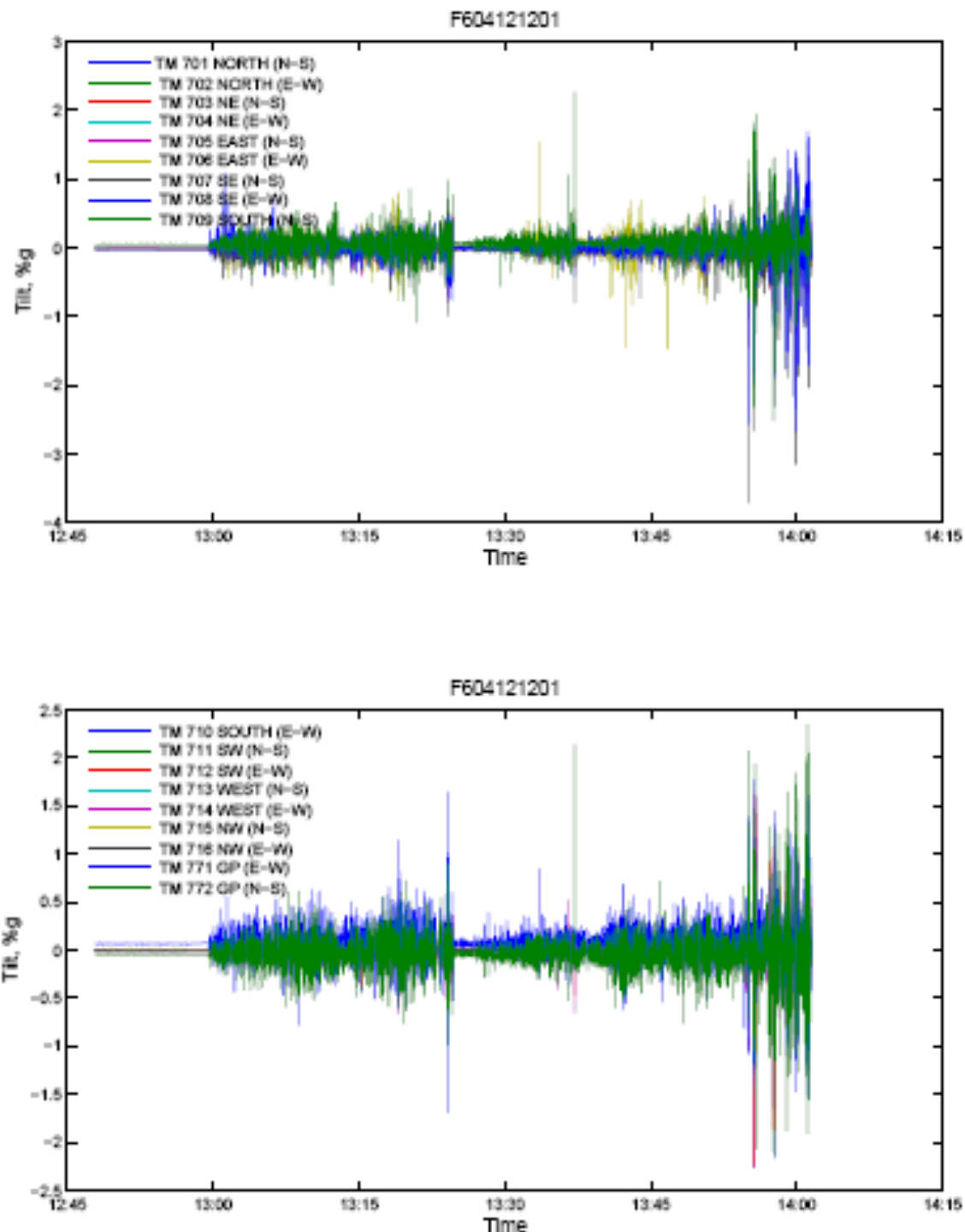


Figure A-48 Dynamac tilt sensors, 12:01 12 Apr event

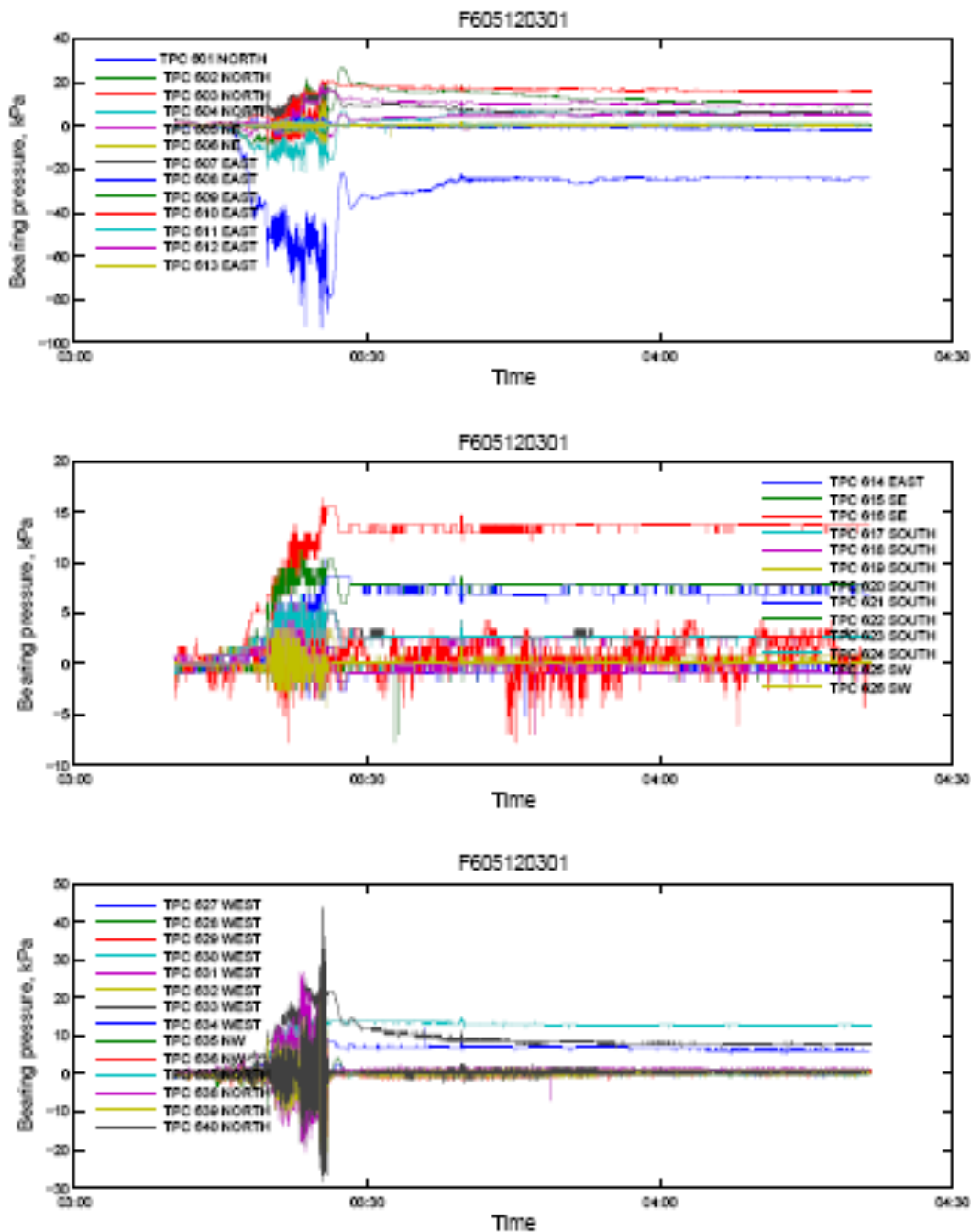


Figure A-49 Dynamac bearing pressures, 03:01 12 May event

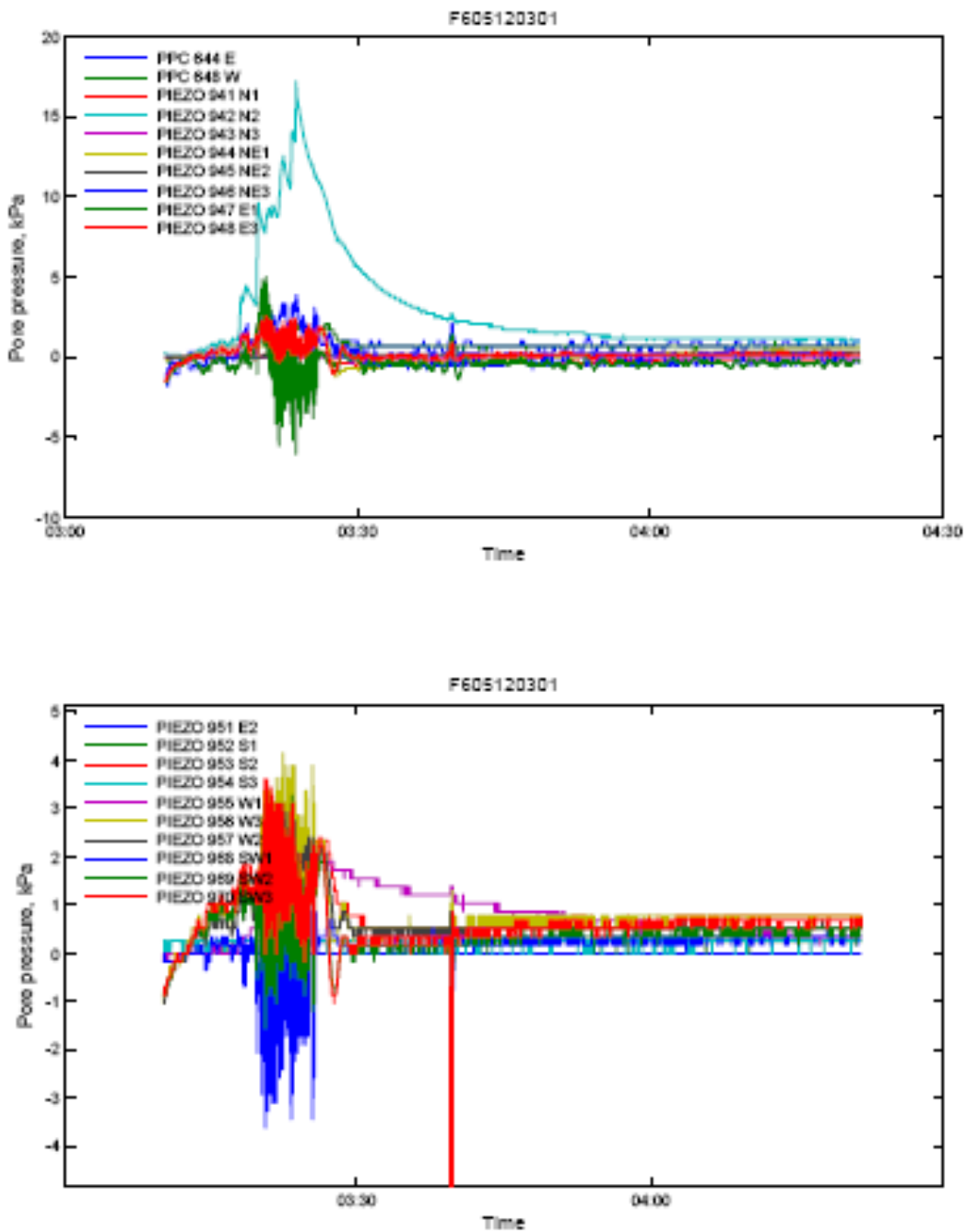


Figure A-50 Dynamac pore pressures, 03:01 12 May event

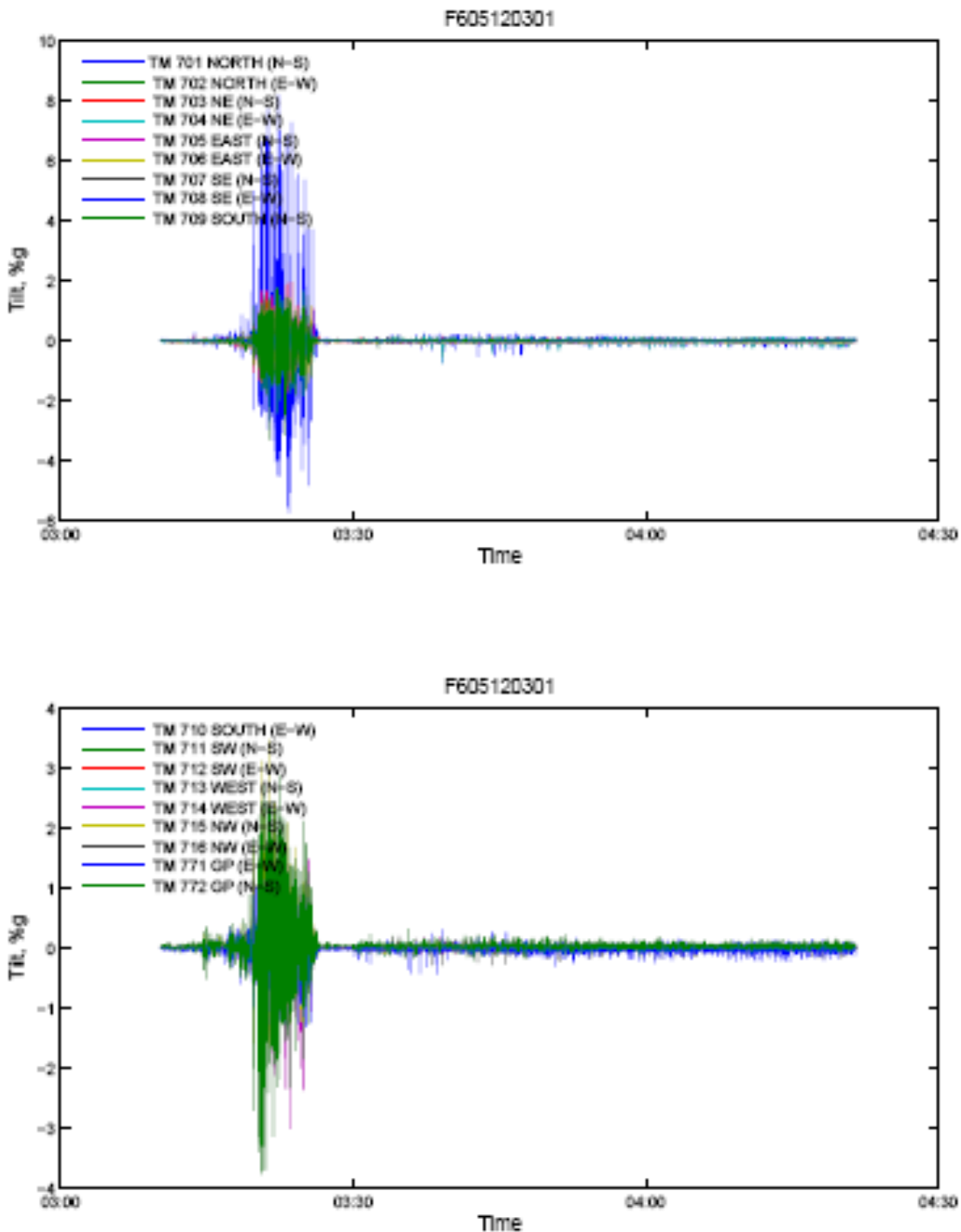


Figure A-51 Dynamac tilt sensors, 03:01 12 May event

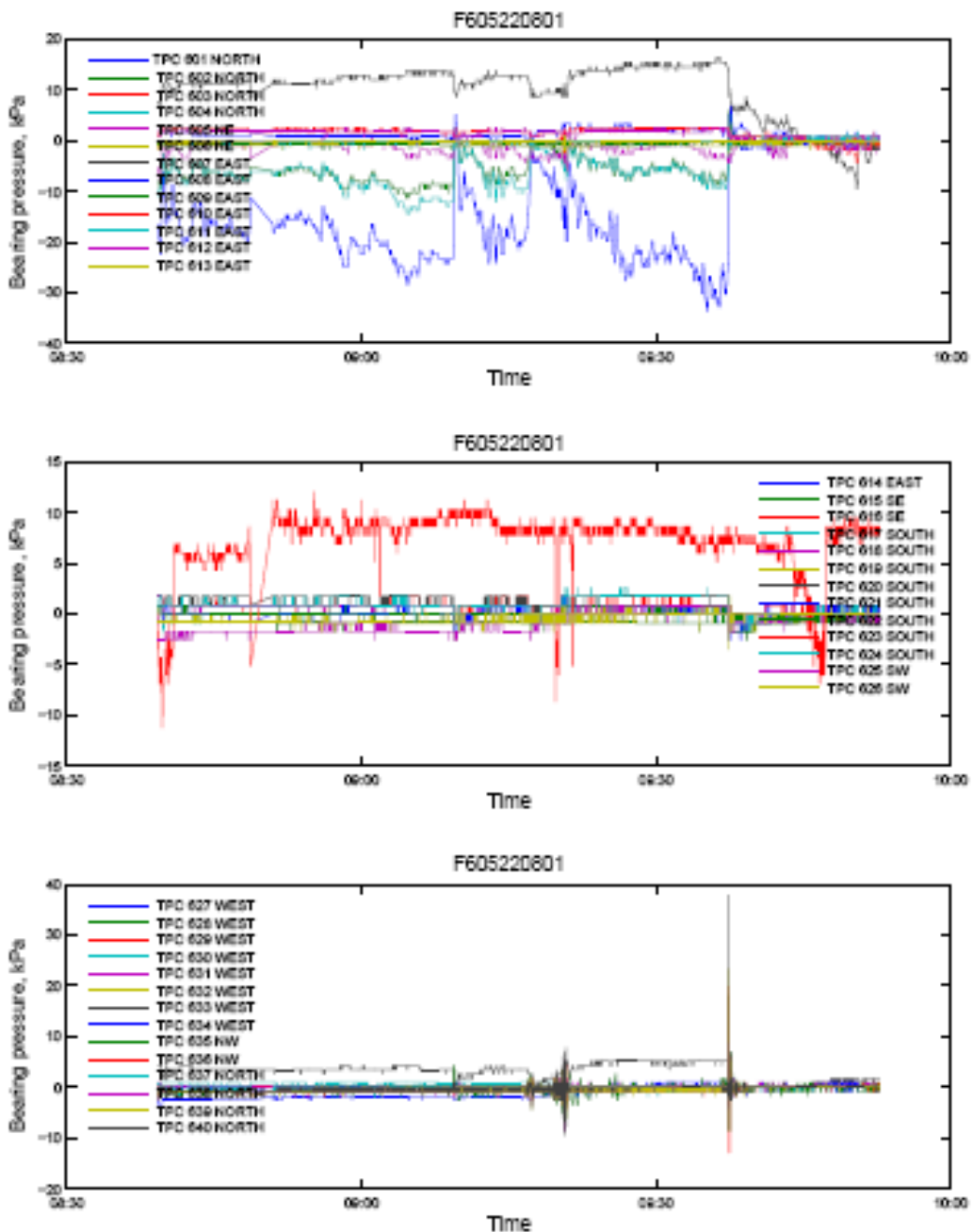


Figure A-52 Dynamac bearing pressures, 08:01 22 May event

Note: These Dynamac data probably exclude the baseline correction

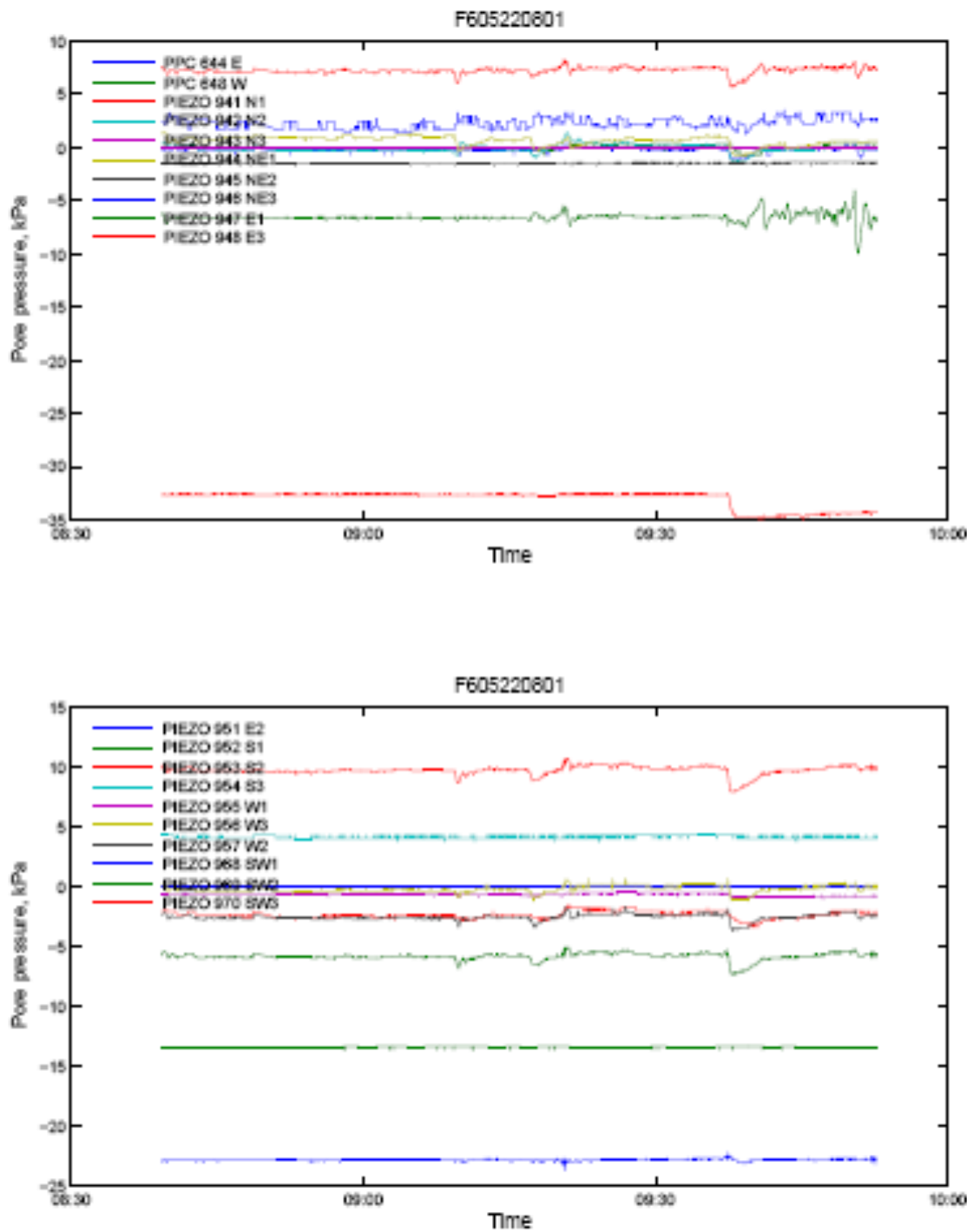


Figure A-53 Dynamac pore pressures, 08:01 22 May event

Note: These Dynamac data probably exclude the baseline correction

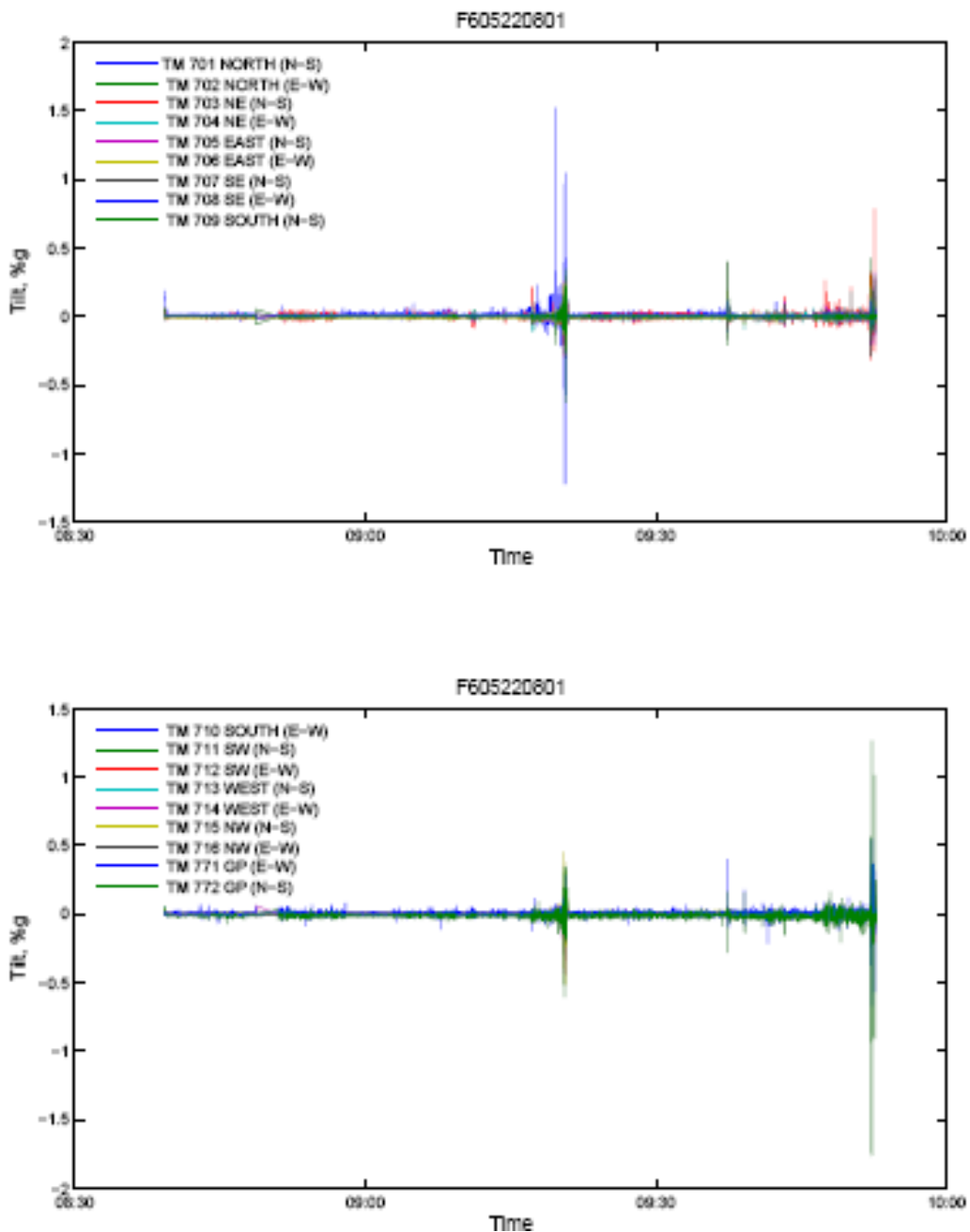


Figure A-54 Dynamac tilt sensors, 08:01 22 May event

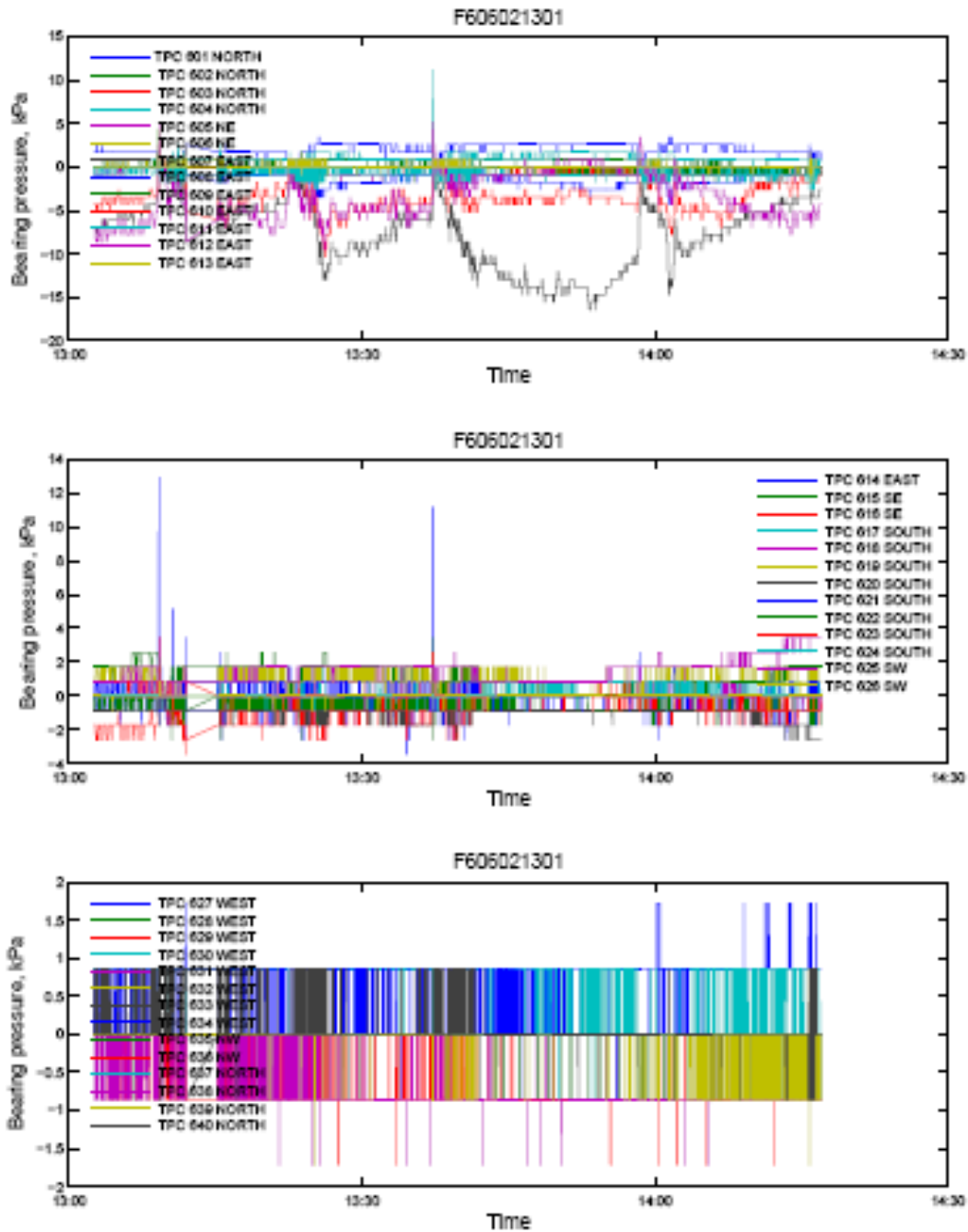


Figure A-55 Dynamac bearing pressures, 13:01 2 Jun event

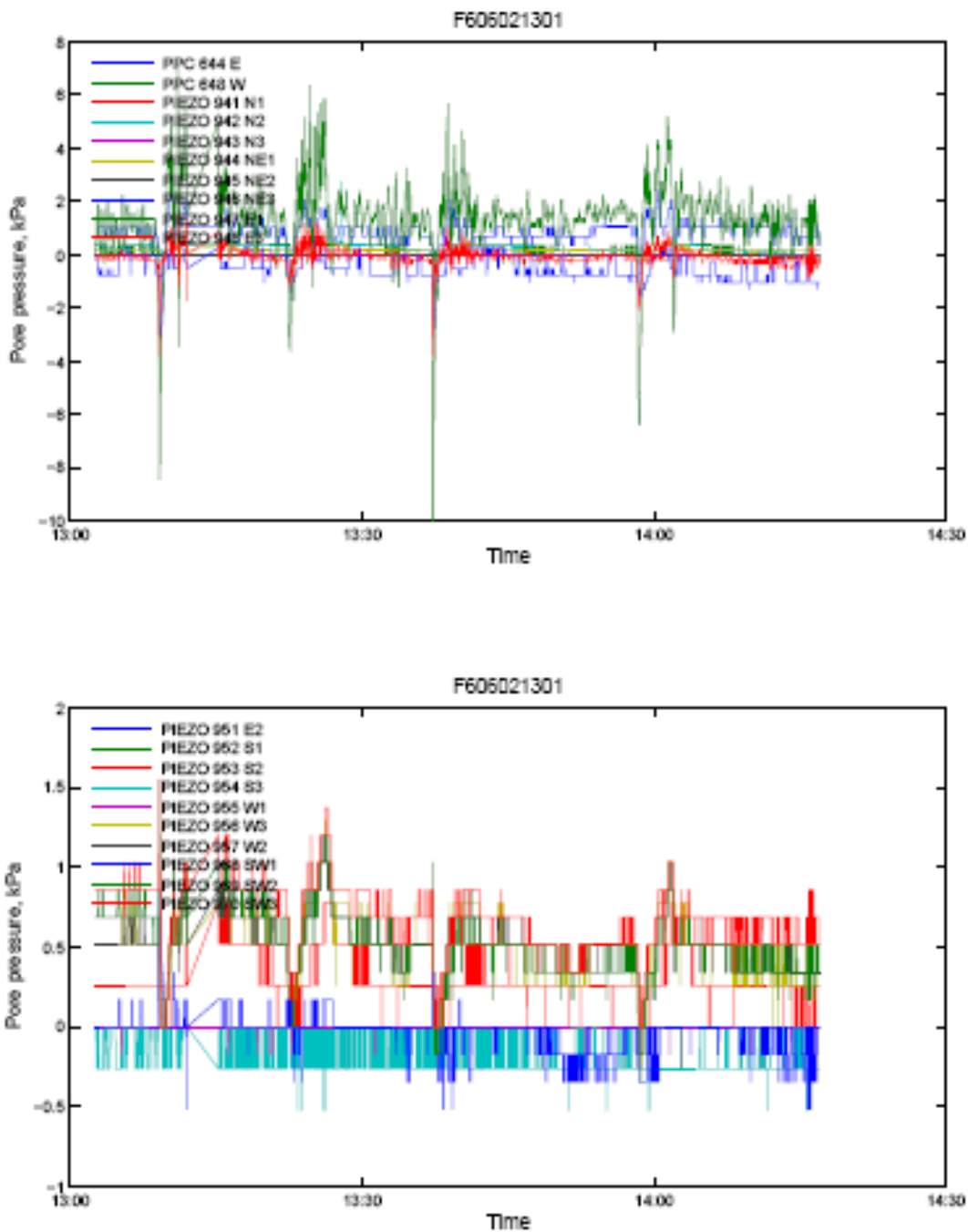


Figure A-56 Dynamac pore pressures, 13:01 2 Jun event

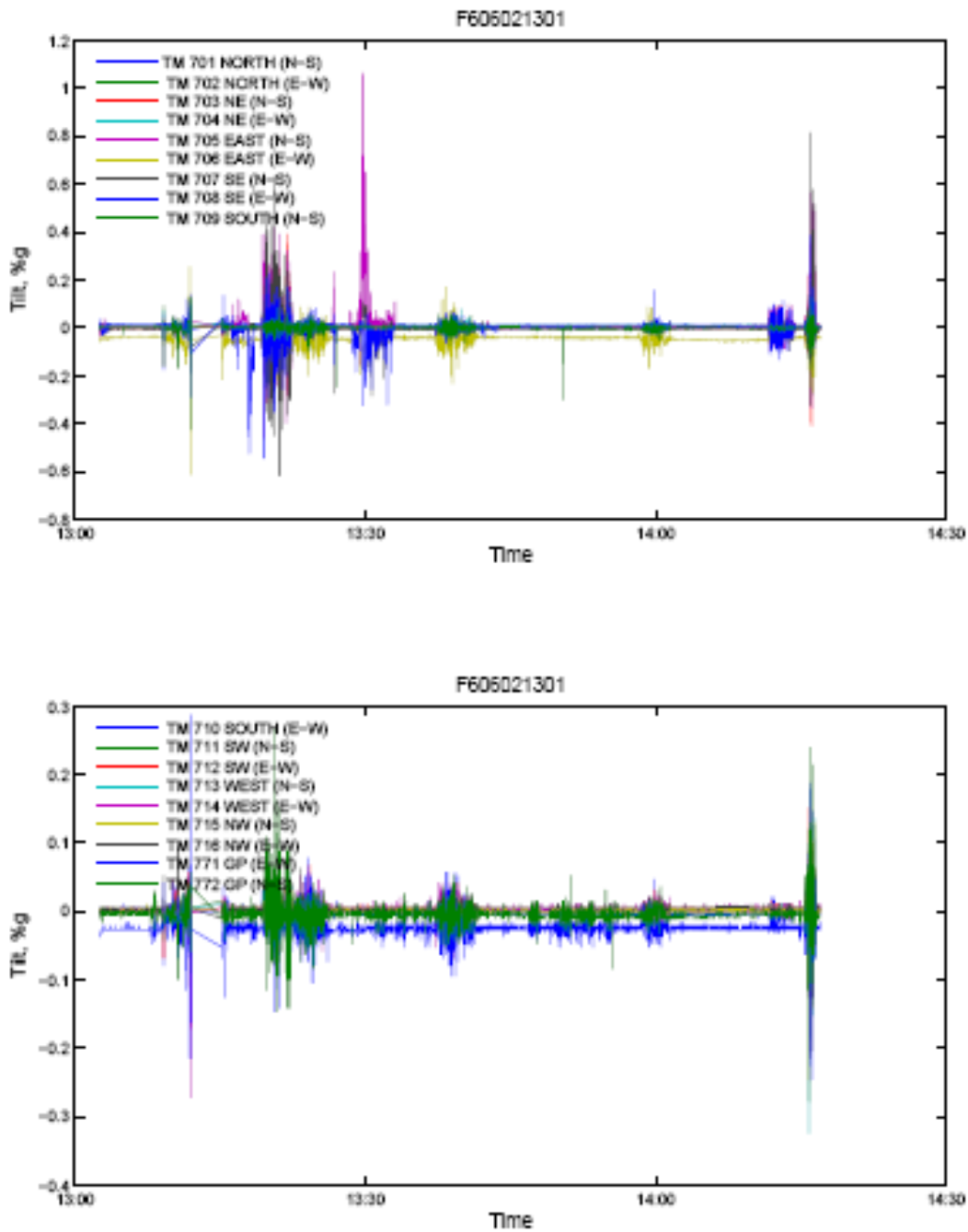


Figure A-57 Dynamac tilt sensors 13:01 2 Jun event

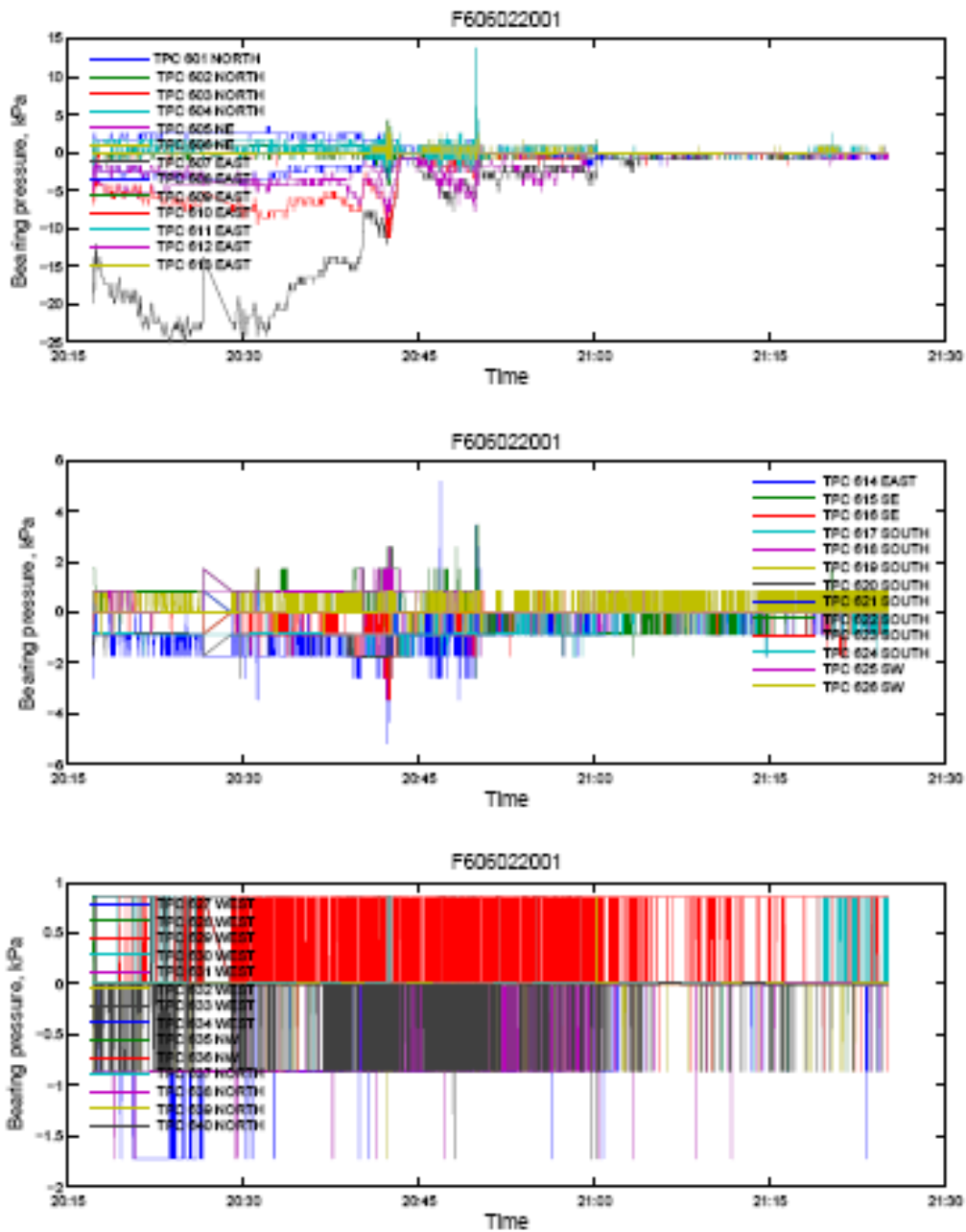


Figure A-58 Dynamac bearing pressures, 20:01 2 Jun event

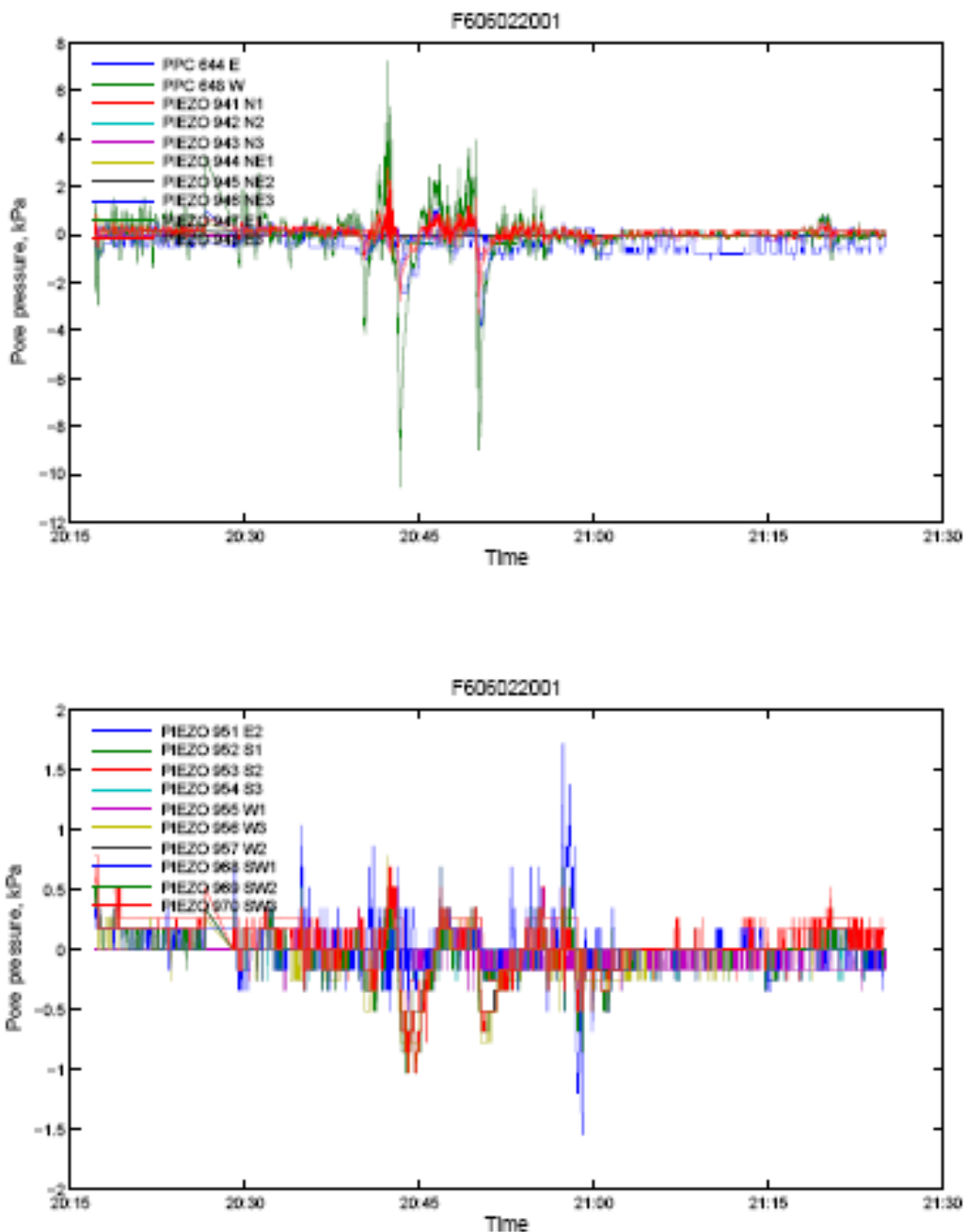


Figure A-59 Dynamac pore pressures, 20:01 2 Jun event

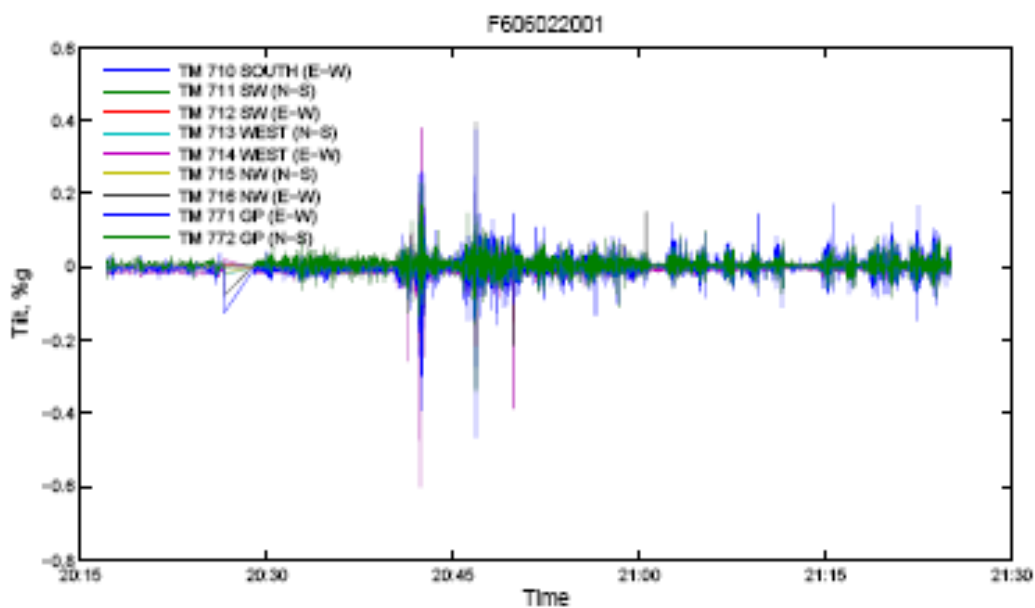
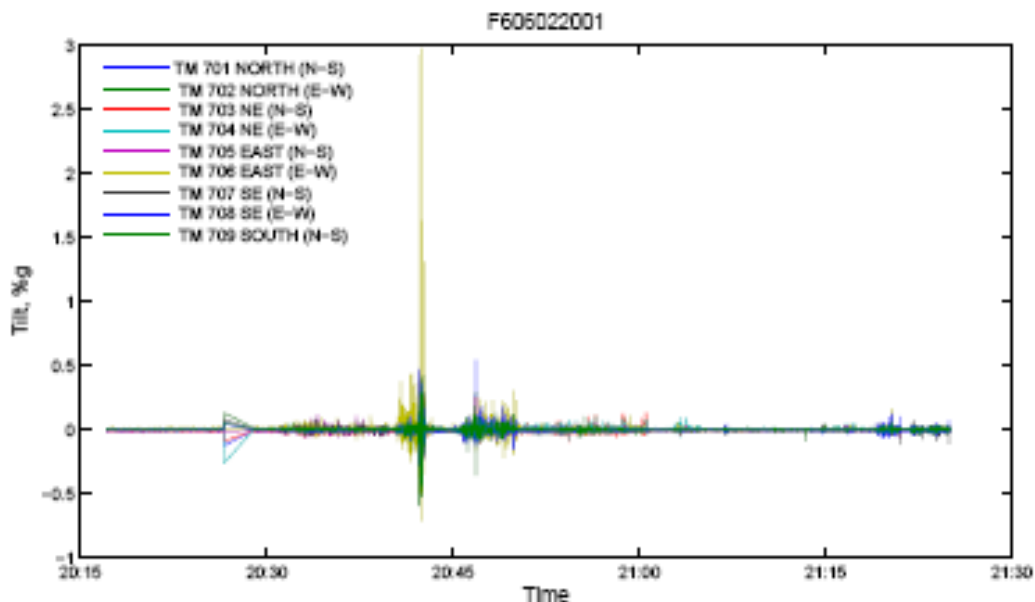


Figure A-60 Dynamac tilt sensors, 20:01 2 Jun event

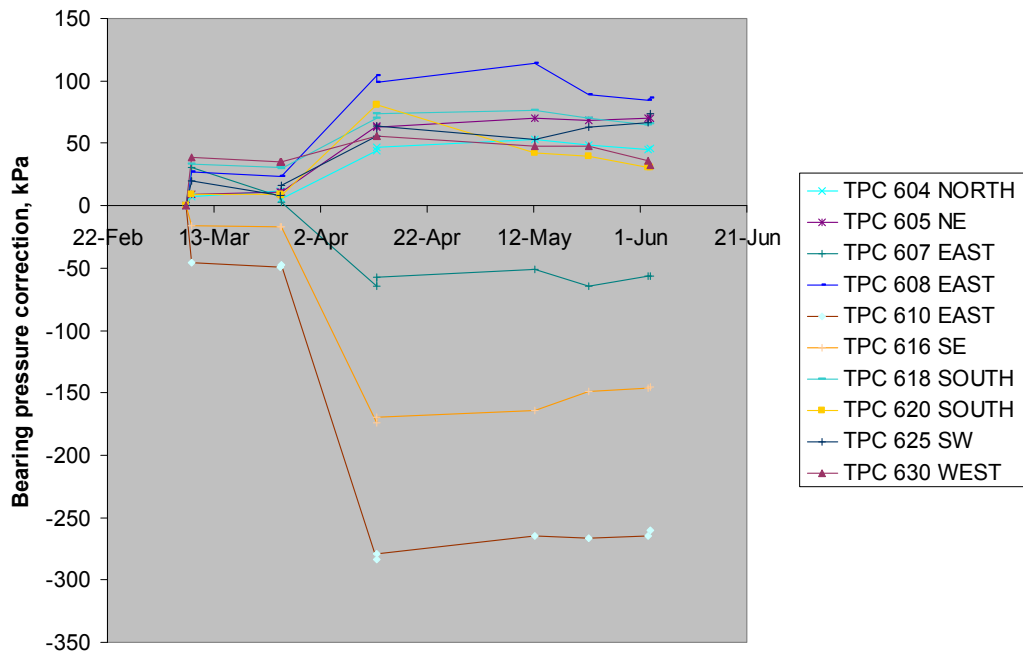


Figure A-61 Dynamac bearing pressure significant baseline corrections

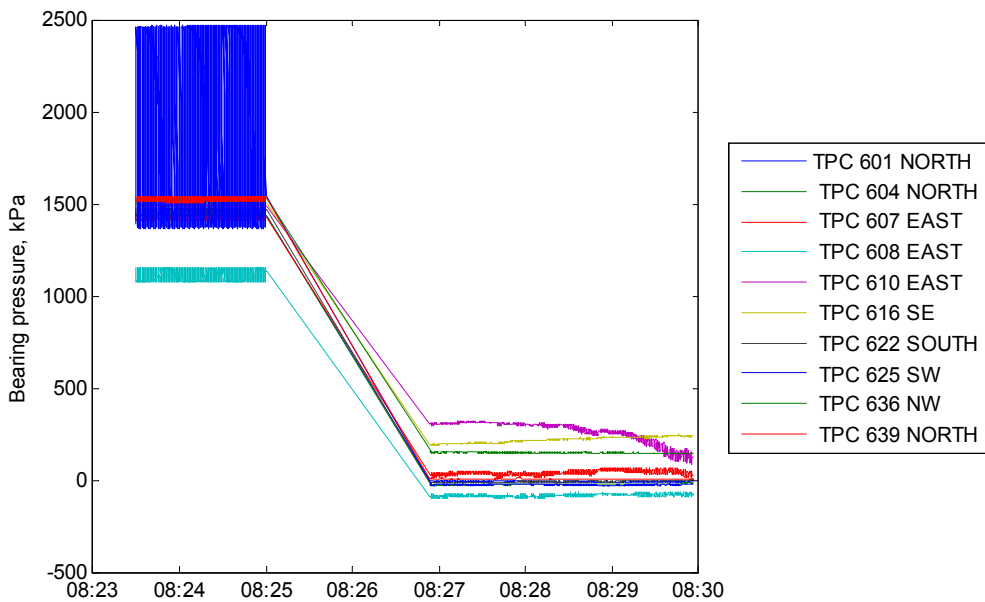


Figure A-62 Dynamac bearing pressures, 08:20 12 Apr event

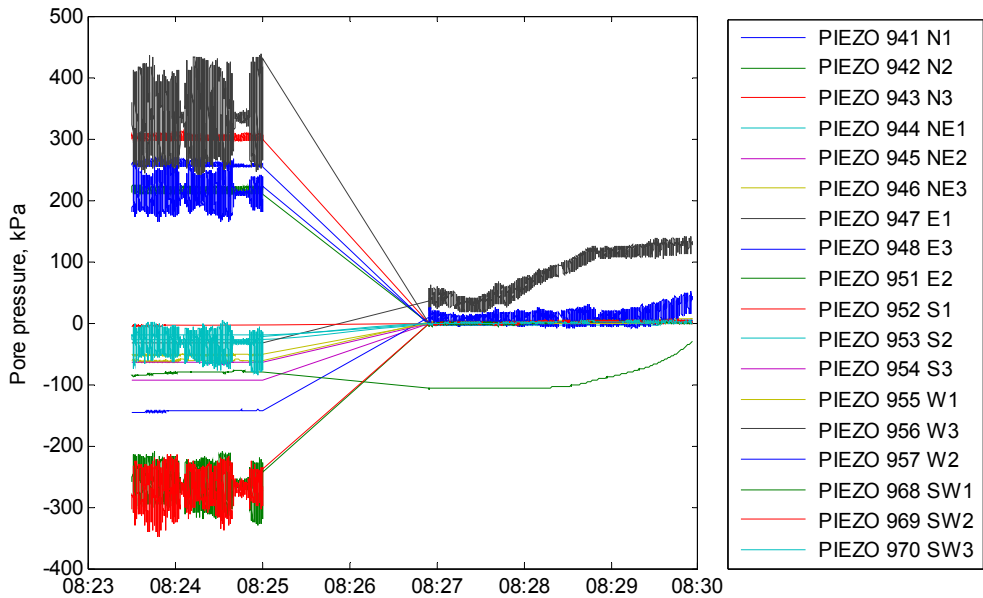


Figure A-63 Dynamac pore pressures, 08:20 12 Apr event

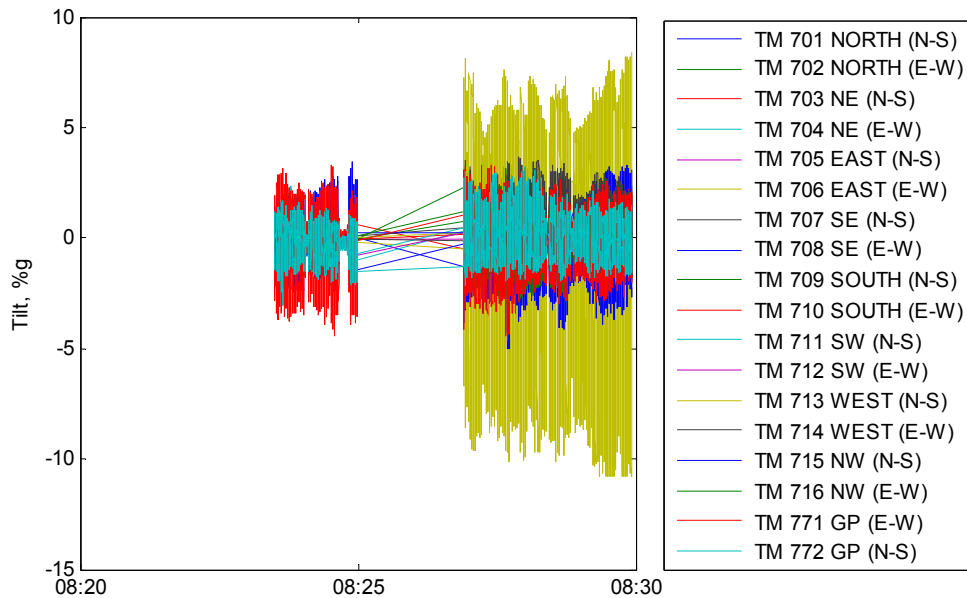


Figure A-64 Dynamac tilt sensors, 08:20 12 Apr event

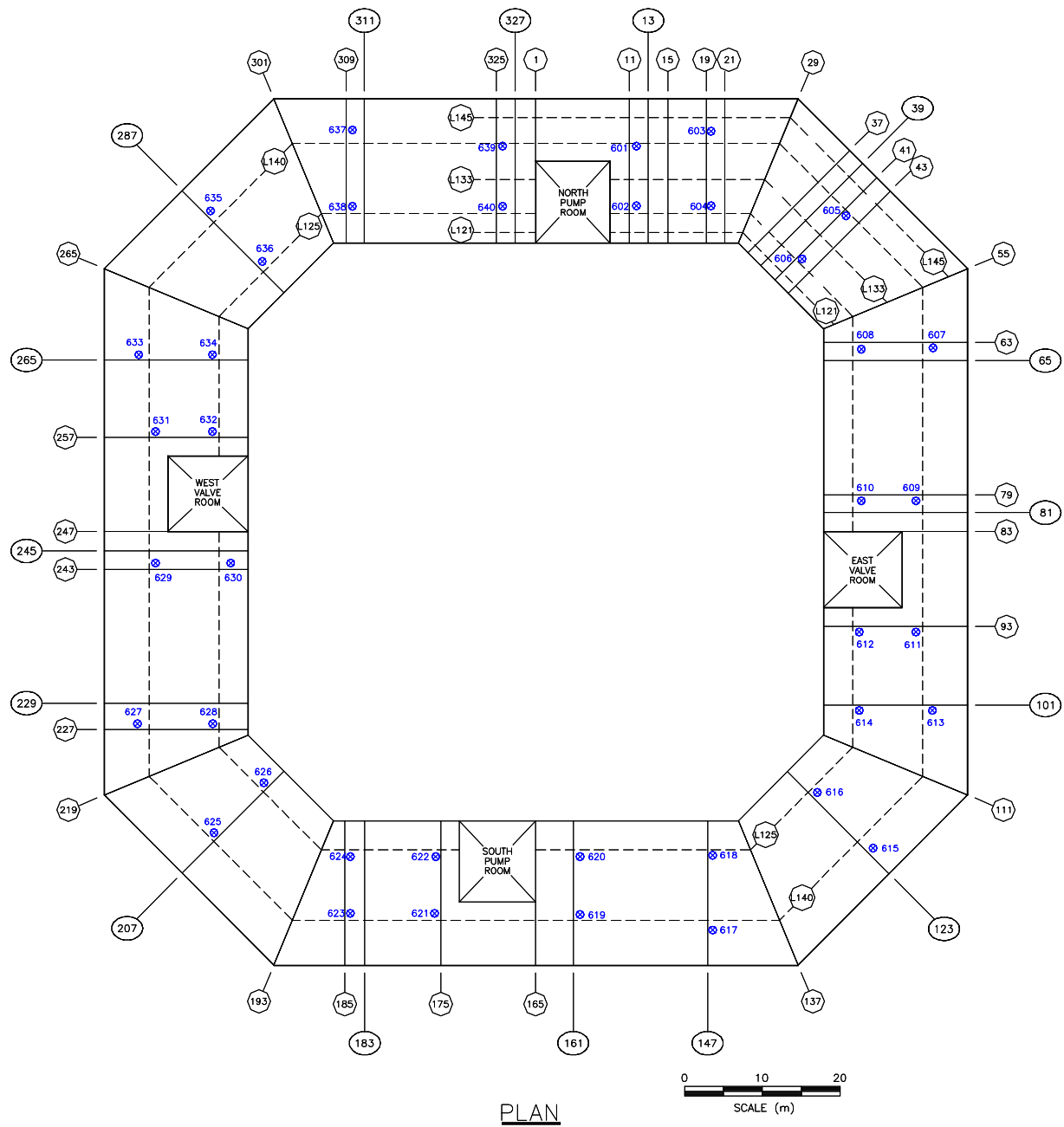


Figure A-65 Total pressure cell locations

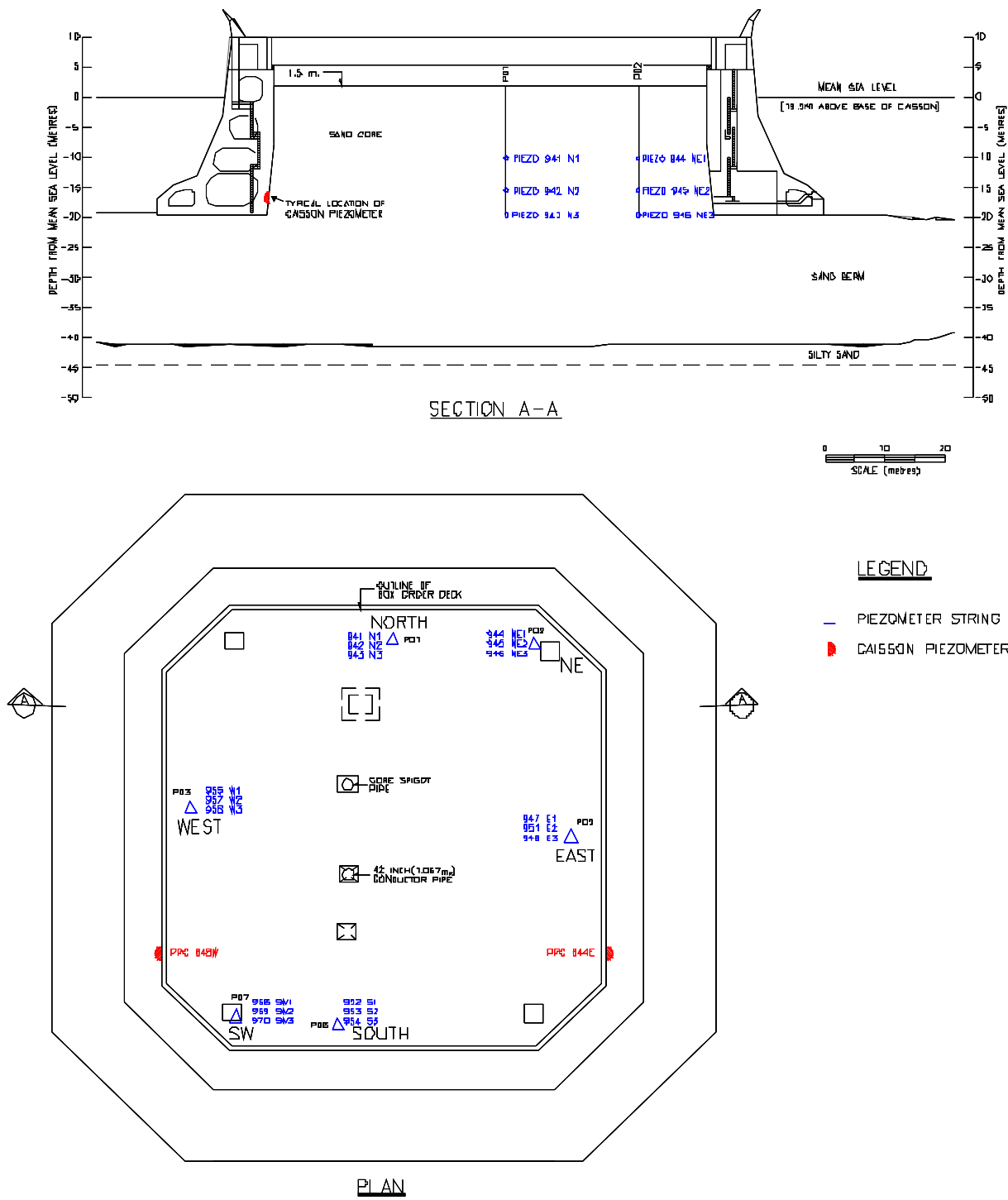


Figure A-66 Piezometer locations

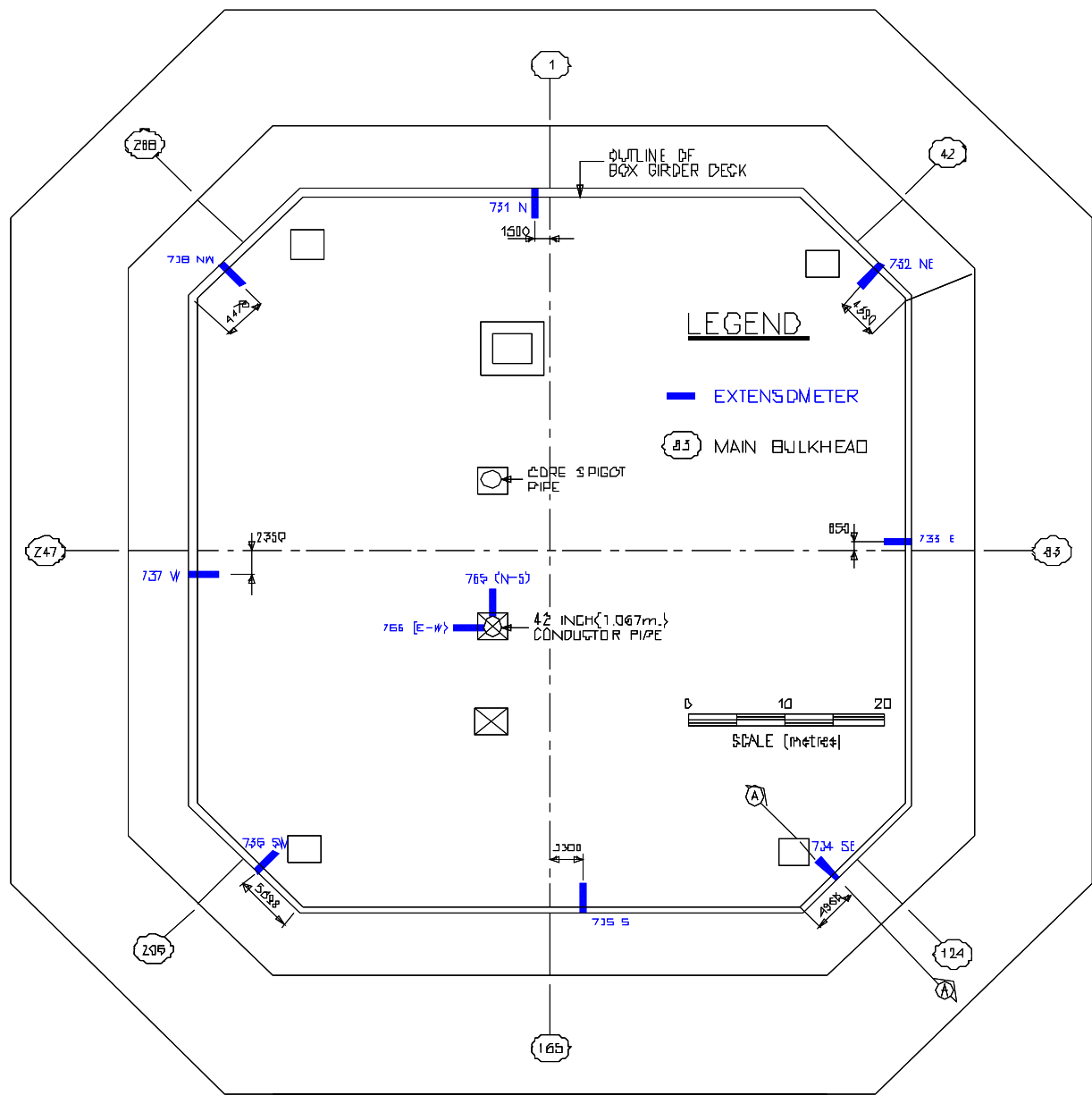


Figure A-67 Extensometer locations

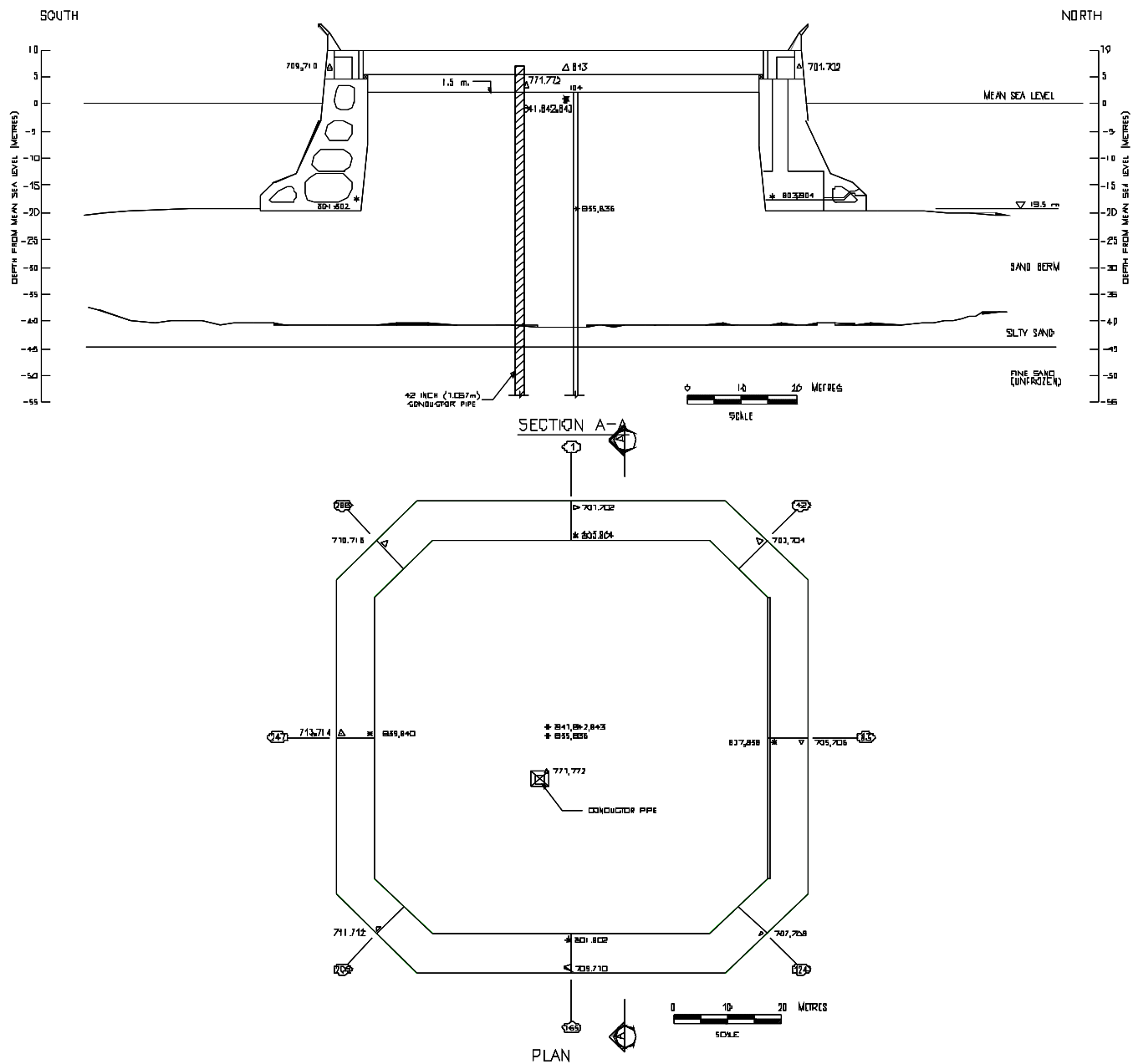


Figure A-68 Accelerometer & Tiltmeter locations

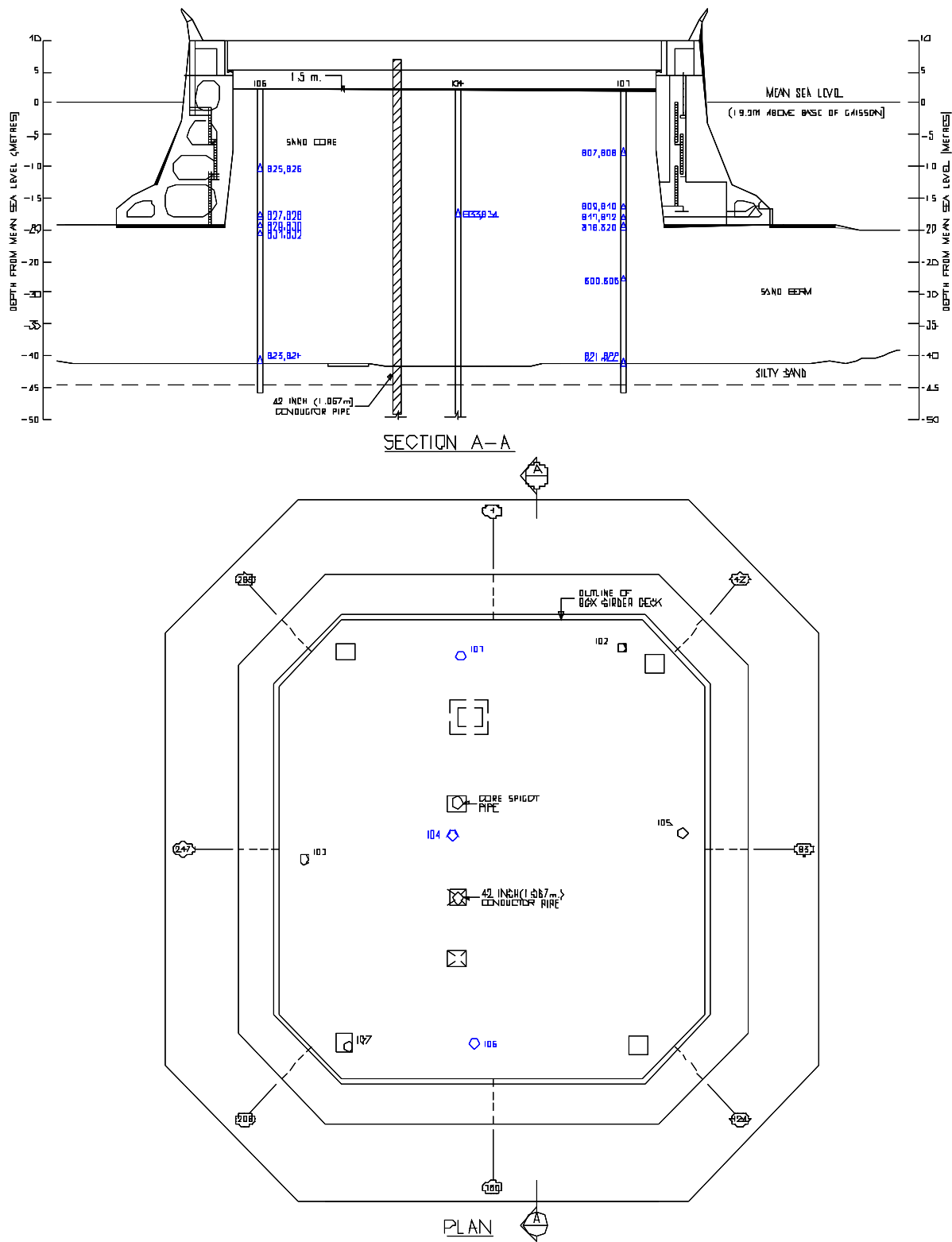


Figure A-69 Slope and digital inclinometer locations



Captain Robert A. Bartlett Building  
Morrissey Road St. John's NL  
Canada A1B 3X5  
T (709) 737-8354  
F (709) 737-4706

[www.c-core.ca](http://www.c-core.ca) [info@c-core.ca](mailto:info@c-core.ca)

400 March Road, Suite 210  
Kanata, On  
Canada K2K 3H4  
T (613) 592-7700 x 221  
F (613) 592-7701

## C-CORE Technical Memorandum

**From:** Ryan Phillips      **Date:** July 14, 2009  
**To:** Ian Jordaan      **Proj. No.** 270578  
**Cc:** Arash Zakeri      **Doc No:** TM-09-001-578  
**RE:** Molikpak – Geotechnical Response of Sand Core

### 1 Overview

Ian Jordaan email of 8 Jul 2009 forwarded the following request from Shell. “In the meeting, Ryan Phillips mentioned that this upper bound of 200 MN might be on the low side. It would be good if his view, his upper bound ice load prediction and accompanying assumptions are also explained in the final report.”

This document summarizes the basis for this comment. My upper bound load exceeding 200MN is based only on the geotechnical response of the sand core. C-CORE (2008) concluded that ‘Most of the significant ice loading events were reacted by caisson basal shear alone requiring no significant caisson global displacement. The 3 larger loading events possibly required more resistance to be provided by the sand core. Permanent core deformations were measured after these 3 events. Permanent global caisson displacements after these 3 large events may be included in the baseline corrections applied to the Dynamac data.’

Hewitt (2008) stated ‘The sliding resistance of the base of the Molikpaq on the berm can be calculated to be in the order of 200MN.’ Hence, if the basal shear resistance is mobilized before the lateral core resistance, then ice loads must exceed the 200MN estimate before significant core response will be observed. I understood that Kevin Hewitt, yourself and I agreed that the April 12 event ice loads exceeded the sliding resistance and mobilised some passive resistance. C-CORE (2008) basis for a core response during the March 7 & 8th, April 12th and May 12th loading events was from

- 1) the manual slope inclinometer readings,
- 2) persistent excess pore pressures in the core over 15kPa and
- 3) changes in the baseline corrections for the global caisson displacements applied to the Dynamac data.

The assumption so far has been that the sliding resistance is mobilised before any passive resistance. A 3D finite element continuum analysis of the compliant caisson, core and berm system to the ice loads may show that some passive resistance is mobilised before all of the sliding resistance, possibly through local caisson wall deflections (ring effects) under the ice load. This may explain the difference between the 'lower bound' ice loads being less than the apparent geotechnical resistance mobilised for loading events other than that of April 12.

## 2 Manual slope inclinometer reading

C-CORE (2008) was based on very limited manual slope inclinometer readings as presented in 2 profiles by Hicks & Smith (1988) and in a table by Hardy et al (1996). The Hardy et al (1996) data are summarized in Figure 1 from Ryan Phillips 24 November 2008 meeting presentation. The '+' symbols indicate the location of the 7 inclinometers with the 'square' caisson outline; North is to top of page. The blue vectors indicate the maximum deformation vectors. The red vectors indicate the direction of ice loading.

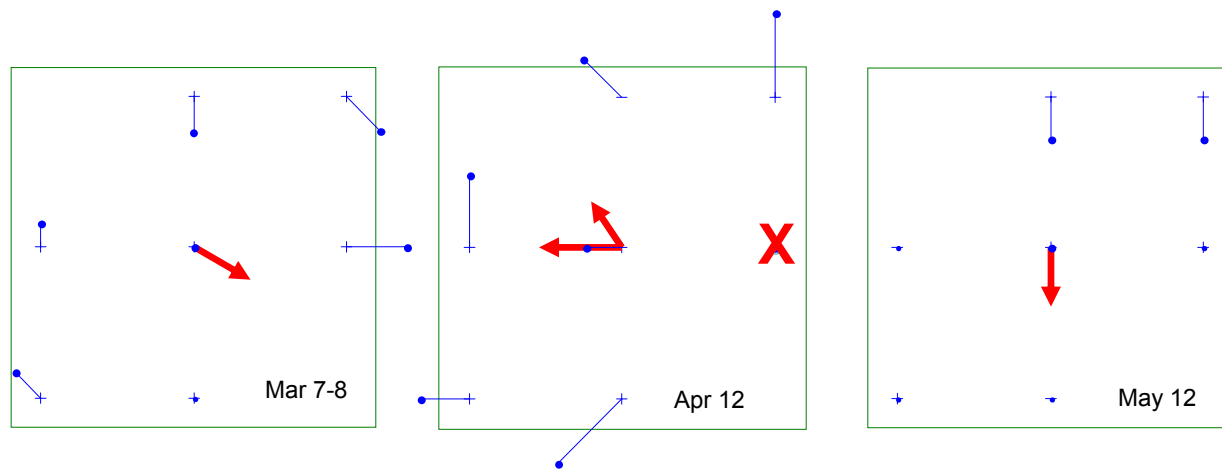


Figure 1: Manual slope inclinometer summary based on Hardy et al (1996)

After the November meeting and submission of the C-CORE (2008) report, 2 reports Gulf (1991a) and Gulf (1991b) were made available for Ryan Phillips review. These reports contain significant information on the vertical and lateral movements of the sand core accumulated during the 3 large load events. Appendix B of Gulf (1991a) contains manual slope inclinometer profiles for most of the inclinometers over many of the loading events. Significant lateral movement accumulations were only recorded associated with the 3 loading events. The profiles associated with the March 7&8 and May 12 events are shown in Figure 2 and Figure 3 and compared with the Hardy et al (1996) summary of Figure 1. The maximum vectors from the Gulf (1991a) profiles are not consistent with the Hardy tabulation. However, Figure 2 shows lateral core translational movements in the NE and E profiles of around 20mm over the core height in an ESE direction, consistent with the direction of ice loading. The W, N and NE profiles also show a secondary movement mechanism of linearly decreasing lateral movement to around 10m depth. This secondary mechanism may be associated with slumping of the core sand towards the caisson walls.

The profiles in Figure 2 and Figure 3 are incremental movements accumulated over a period of typically a few months covering a single loading event. Accumulated total movements could be assessed by summation of these incremental movements.

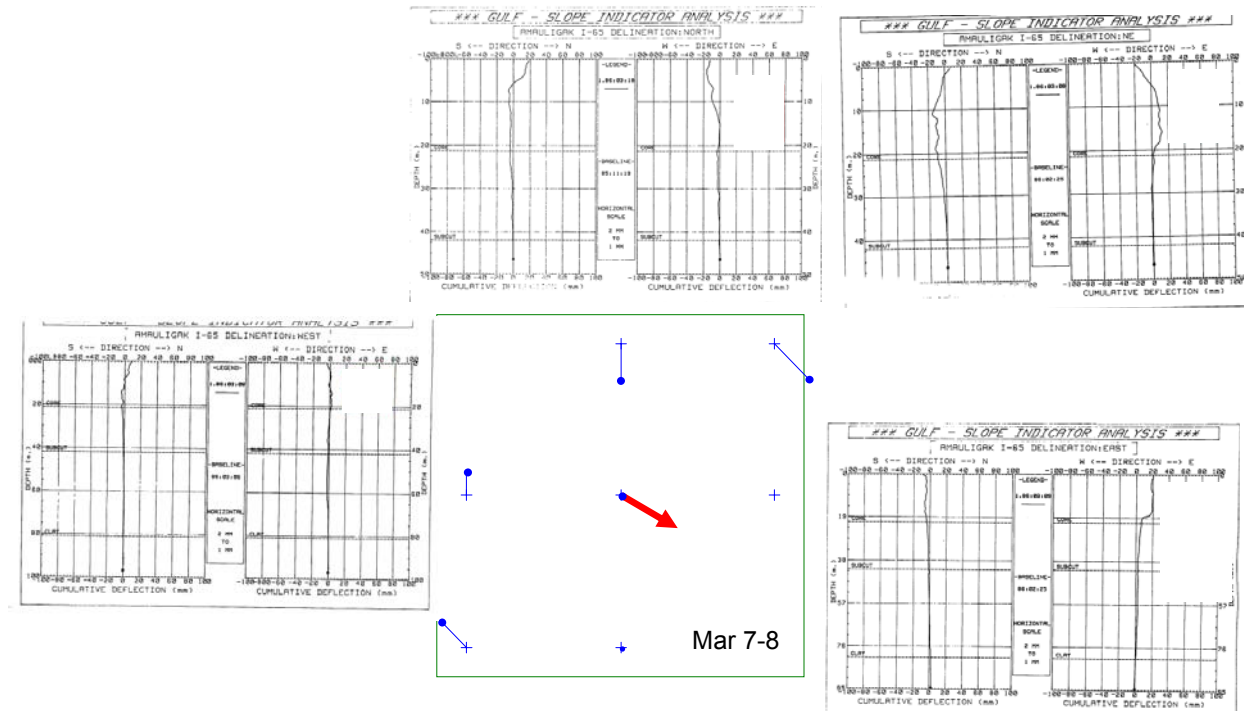


Figure 2: Mar 7-8 manual slope inclinometer data

The profile summary, like Figure 2 for the April 12 event is presented in Fig 3.15 of Gulf (1991b). This summary clearly shows core lateral translation over the 20m depth in the S, W, N and NE profiles, with evidence of a slumping mechanism in the NE and centre profiles. Figure 3 for the May 12 event shows southerly lateral core translation in the N and NE profiles again consistent with the direction of ice loading, which is away from the northerly caisson face. Some surface slumping is apparent in the N profile. The E profile shows no movement over its full depth, but this inclinometer tube was reported as failed during the previous Apr 12 event. This discrepancy is unresolved.

Hewitt (2008) believed the manual inclinometer readings were unreliable due to possible buckling of the inclinometer tubes, and also due to lateral soil movements associated with vertical slumping of the core sand under the cyclic ice loads. Ryan Phillips asked 2 field instrumentation (especially inclinometers) experts independently ‘whether an 80m long inclinometer tube installed in early 1980s would buckle under 50 to 100mm of vertical settlement of the top 20m of loose sand (remaining 80m in competent soil).’ Mikkelsen (2009) responded that ‘A good rule-of-thumb is that ABS inclinometer casing can withstand at least 1% compression under confined conditions without significant damage (1 foot in 100 feet)’. Dunnicliff (2009) provided a similar response.

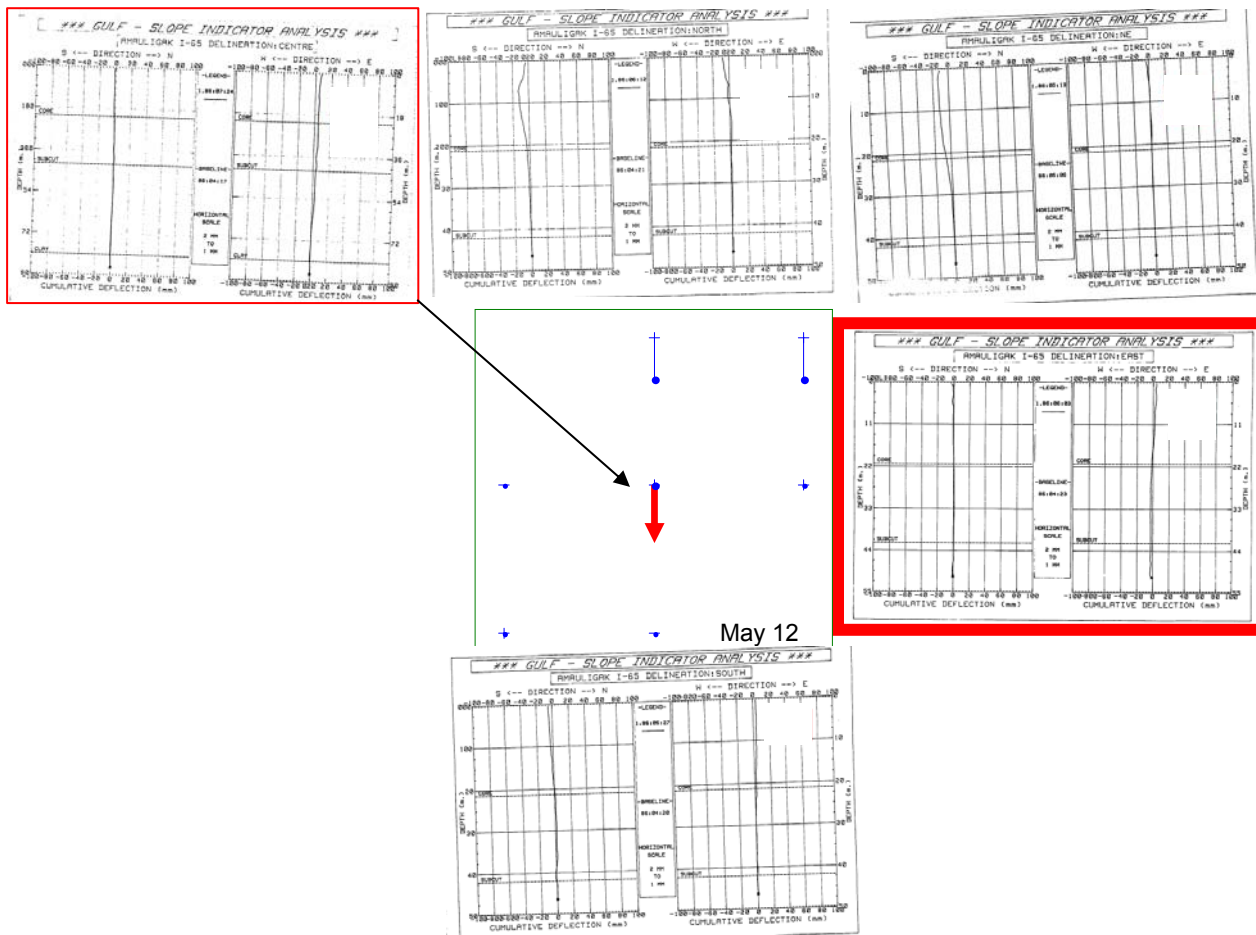


Figure 3: May 12 manual slope inclinometer data

The total core near surface vertical settlements were monitored, Figure 4a from Gulf (1991b). These total settlements include significant contributions (about 40mm) from the underlying clay and foundation sand, below the base of the inclinometers, Figure 4b. Assuming that all the vertical settlement accrued in the 20m deep core, around 200mm of surface settlement would be required to buckle the inclinometer casings. This level was only exceeded in the E, N and NE inclinometers after the April 12<sup>th</sup> event.

There is evidence of a sand slumping mechanism as discussed above. The vertical settlements from a slumping mechanism should exceed the associated lateral core deformations. Comparing Figure 4a and the inclinometer profiles shows that the lateral deformations in the sand core generally exceeded the local vertical settlements, thus core slumping does not explain the measured lateral core deformations.

There then remains a set of measurements for each of the 3 large events showing primarily translational movement at the base of the sand core, with lateral movement greater than

associated vertical settlements. These are believed to indicate the type of core movement patterns one would associate with mobilisation of some active and passive earth pressure mobilisation, that is suggesting ice loads above the sliding resistance level.

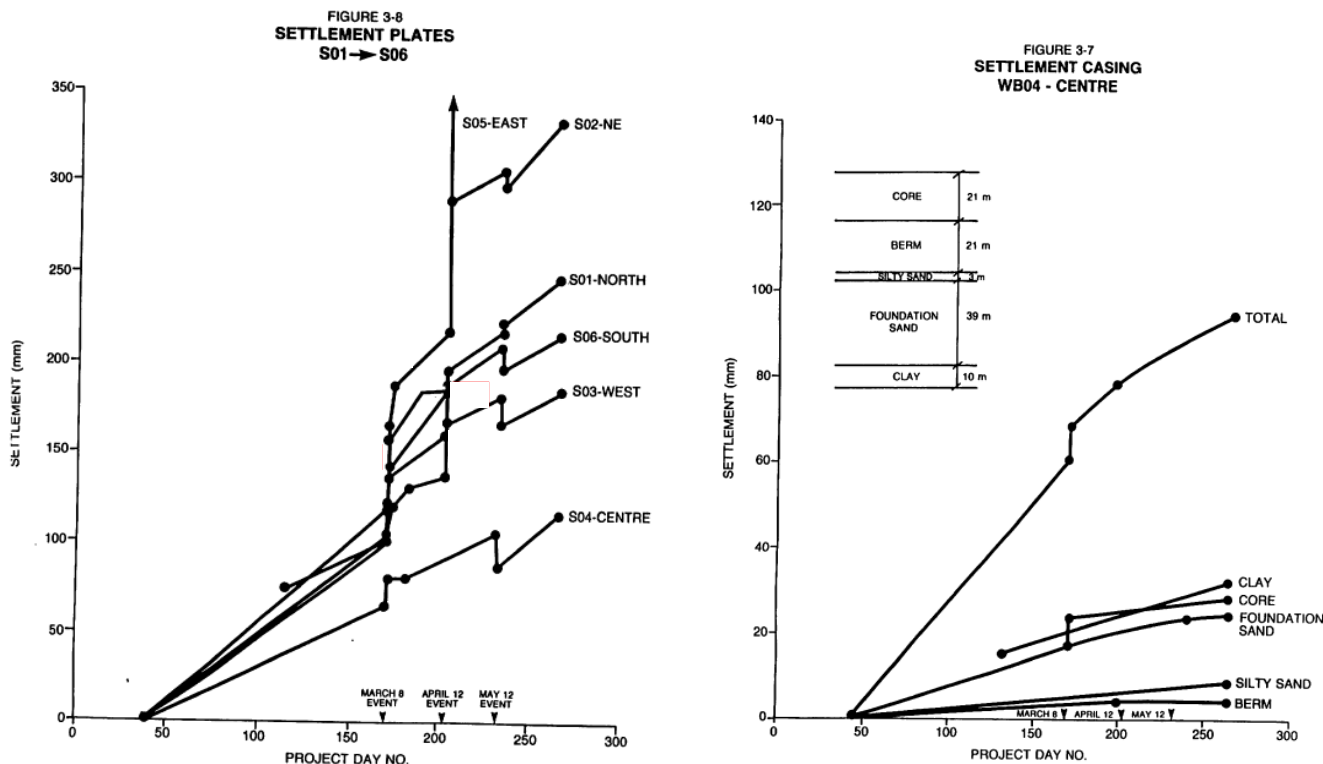


Figure 4: Vertical settlement data

### 3 Persistent excess pore pressure

The persistent excess pore pressures over 15 kPa measured in the sand core may be associated with either a slumping or translational movement of the core.

### 4 Baseline corrections changes

Gulf (1991a) Table 3.7 confirms the association of the deck extensometer baseline correction ‘jumps’ in C-CORE (2008) Fig 3.5 with permanent offsets caused by the significant ice events. The baseline corrections in the Dynamac data are suspect: for example, there are very obviously permanent offsets in some of the TPC sensors after the April 12 event, C-CORE (2008) Fig A-61. These offsets however are ignored by changing the baseline correction in the Dynamac database.

The 20mm offset change over April 12 event is still not enough to mobilise any significant passive resistance, especially as the sand core is probably looser than implied in the C-CORE (2008) report, as

	<b>Technical Memorandum</b>		
<b>Molikpak – Geotechnical Response of Sand Core</b>			
Proj. No. 270578	Doc. No. TM-09-001-578	Date: July 14, 2009	

shown by Hewitt (2008). The implication is still that the 3 significant load events exceeded the ‘200MN’ basal shear resistance, but not by very much.

## REFERENCES:

C-CORE (2008). Preliminary geotechnical overview of 1986 Molikpaq response, C CORE Report R-08-044-578v2, November 2008. Report to Ian Jordaan & Associates.

Dunncliff, John (2009) Email communication, January 2009

Gulf Canada Resources Limited (1991a) Dynamic Horizontal Ice Loading on an Offshore Structure Phase 1a: Molikpaq Performance at Amauligak 1-65. Volume VIII of X: Geotechnical Monitoring (CHC 14-8)

Gulf Canada Resources Limited (1991b) Joint Industry Project, Dynamic Ice/Structure Interaction with the Molikpaq at Amauligak 1-65. Phase 2, Volume 1 of 9: Main Report: Characterization of Sand Core Behaviour on April 12, 1986, and Development of Analysis Methodology. April 1991 (CHC 14-23)

Hardy M.D., Jefferies M.G., Rogers B.T., & Wright B.D. (1996) DynaMAC: Molikpaq Ice Loading Experience. PERD/CHC Report 14-62 submitted to National Energy Board

Hewitt K.J. & Associates Ltd. (2008) Estimates of Ice Loads on the Molikpaq Based on Geotechnical Analyses and Responses. Draft Report. June 2008

Hicks, MA & Smith, IM (1988) Class-A Prediction Of Arctic Caisson Performance, Geotechnique Vol. 38:4 p589-612

Mikkelsen, Erik (2009) Email communication, January 2009

## **Appendix IJA - D**

### **Response to C-CORE report “Preliminary Geotechnical Overview of 1986 Molikpaq Response”**

Submitted by Kevin Hewitt

**Draft Comments on**  
**PRELIMINARY GEOTECHNICAL OVERVIEW OF 1986 MOLIKPAQ  
RESPONSE**

**C-CORE Report R-08-044-578v2, November 2008**

**by K. J. Hewitt, August 9<sup>th</sup>, 2009**

## **SUMMARY**

As discussed in the author's report (K.J. Hewitt & Associates Ltd., August, 2009) the three finite element models discussed in the C-CORE report (Hicks & Smith, 1988; Altaee & Fellenius, 1994; and Jeyatharan, 1991) all appear to be technically sound and the author believes that, within their limits, could be useful tools in predicting field behaviour. However, this would only be true if the input parameters with respect to the insitu state of the sand and/or the ice loads were correct.

However the analyses undertaken using these three models all assumed that the insitu state of the core sand was medium dense. This is in contrast to all basic evidence, as explained in the author's report that the core sand was in a loose state.

With respect to caisson movements, the C-CORE report makes numerous references to the fact that there were no permanent deformations of the core. Based on this observation it is concluded that resistance was primarily provided by caisson basal shear alone and this limits the maximum ice load in 1986 to less than 200MN.

## **SPECIFIC COMMENTS**

The author has discussed the three models in general terms in his report. Based on a review of the C-CORE report the following additional comments are provided. It is also important to note that the three models were developed to back analyze the April 12<sup>th</sup> event.

### Hicks & Smith (1988) Section 1.1

In figure 1-3 C-CORE present two slope indicator plots (inclinometer #11 and #12). One plot shows a resultant deflection of just 5mm and the other around 23mm. The author first assumed these were inclinometers I01 and I02 which were in the north and north east. However on further investigation, when compared with the records of inclinometer plots, the inclinometer #11 profile closely matches with that of I04 (centre) and the inclinometer #12 profile closely

matches that of I03 (west, the non loaded trailing face). However of most interest is that I03 was in, or close to, the zone corresponding to settlement of the core. The direction of movement is not mentioned in the Hicks & Smith plot but it is in the general direction of the ice load, which was basically from the east. However this outward movement would also correspond well to the slumping of the perimeter sand.

Referring to Figure 2-5 in the C-CORE report, massive settlement was recorded on the east side. However some settlement was recorded on the west side - but whether the amount is representative or not is questionable. Evidence would suggest significant slumping occurred. Figure 2-4 in the C-CORE report shows that accelerations of the caisson were measured on the west face of between 2 and 3.5% of gravity. To put this in perspective, reference is made to the Mercalli earthquake intensity scale. A magnitude IV earthquake has ground accelerations of between 1.5 and 2% of G; the values for a magnitude V earthquake are 3 and 4%. A descriptor of a magnitude V earthquake includes "Some dishes and windows broken. Cracked plaster. Unstable objects overturned." It is reasonable to assume that under these conditions a loose sand would experience considerable settlement. Further, the west wall rose up (the whole structure tilted toward the ice load) which would have resulted in a loss of wall support and associated settlement.

The centre I04 deflection is not totally consistent with the direction of the load but on the other hand the deflection is very small and not reliable because of the indicated buckling of the slope indicator casing.

It is implied by the C-CORE report that these two inclinometer profiles in figure 1-3 are representative of the deformation of the sand core. However there were four other inclinometers with data within the core and mention of them is conspicuously absent (a fifth one – SW - has no data in this zone). It is interesting to review the profiles from these four inclinometers. There is no overall trend toward movement in the direction of the load. In fact the general trend is deformation toward the outer walls which is consistent with slumping around the outer walls, which is well documented (Jeyatharan, 1991). Of special note are the north east and east inclinometer profiles. The north east one is consistent with twisting and buckling and the east one sheared off completely just below 6 metres.

Actually based on the author's overall review of the inclinometer data (K.J. Hewitt & Associates Ltd., August, 2009) it is concluded that the quoted deflections (determined by inclinometers) are not representative. This is because they almost invariably indicate buckling, which is associated with settlement, which basically makes the inclinometer readings invalid. In other words, inclinometers are not appropriate measurement devices in loose sand.

In summary, these measured profiles in figure 1-3 are not representative or conclusive and cannot be used to verify the model. If anything, they tend to verify that there was considerable slumping of the core around the perimeter and probably no permanent lateral displacement in the direction of the load. A review of all the inclinometer profiles would indicate that there was no permanent global deformation of the core. This is consistent with the statement in the C-CORE report that 'there was however apparently no measured permanent lateral displacement of the caisson structure after the April 12<sup>th</sup> loading event' (page 1-1). This statement is presumably based on extensometer measurements.

All of this is not to say that the model is not a good one. Based on a review of the original paper (Hicks & Smith, 1988) it is the author's belief that had they assumed a low ice load and loose sand core in their analyses, that their prediction would likely have represented the field behaviour very well.

### Altaee & Fellenius (1994) Section 1.2

It is stated by C-CORE that Altaee & Fellenius's static caisson load displacement response was similar to that of Hicks and Smith which is not surprising as they both assumed a medium dense sand in the core.

Their cyclic analyses are more revealing. As can be seen in figure 1-6, if the core sand were assumed to have an  $\epsilon$  value of 0.000 (C1), which is only slightly less dense than their assumption, then the required number of cycles to produce major deformations drops very significantly! They state in their paper that 'The computation results indicate that Case C1, having the loosest sand, would not have been stable for the imposed ice loading.' Further, had they assumed a more realistic  $\epsilon$  value of +0.025 then a lot lower ice load would produce the same result, which would also result in significant deformations and pore pressure generation.

### Resistance Mobilization Section 3.1

The author generally agrees with the discussion and interpretation presented in this section (summarized in Figure 3-3).

### Caisson Movements

These notes should be read in conjunction with the comments made in the previous Hicks & Smith (1988) section regarding slope indicators.

It should also be pointed out again, that extensometer readings and deformations determined from slope indicators are not directly comparable.

Here are a few general comments on this section:

- Figure 3-4 is interesting as it provides a nice summary of extensometer readings for each event. However the load values on this figure do not directly relate to the values in Table 3-1? But using this figure and the Sandwell extensometer calibration report (Sandwell, 1991) one can quickly estimate the face load for each significant event. Referring to the concluding statement in the Sandwell report: ‘the North-South Face Load distortion ratio was in the range of 2.0 to 4.2 MN/mm’ – let’s say a mean of 3 MN/mm. Hence the maximum face load would be around 180MN and all other loads for other events were proportionally less!
- Several references are made in this section to the fact that there were no measured permanent deformations of the core. (i.e. Page 3-3 ‘Most of the deformation appears recoverable’. Page 3-4 ‘absolute face movements return to zero at zero loads irrespective of the load magnitudes.’). The only potential evidence of permanent deformations is from the manual slope indicators. However the author refers to the previous Hicks & Smith (1988) section where it is stated that a review of all the inclinometer profiles (for the April 12<sup>th</sup> event) would indicate that there was no permanent global deformation of the core. Likewise a review of table 3-2 shows that for the March 7/8 events the interpreted deformations were all small and in no consistent direction! The only potentially plausible interpreted deformations from the slope indicators are those for the May 12<sup>th</sup> event as they are in the direction of the load. But this was a dynamic event and in such cases slope indicators are unreliable, as mentioned previously.
- Regarding the statements on page 3-5 and 3-6 that ‘the permanent deformation at the base of the sand core as measured in the centre inclinometer after the event was 12mm.’ This is not consistent with figure 1-3 which shows a 5mm deflection related to buckling of the slope indicator in the upper portion of the core. It cannot be deduced that this is a real deformation.
- On page 3-9 it is stated that ‘The buried digital inclinometer data (that is the real time IPI’s) do not provide the anticipated indications of shear strains within the sand core during the more significant ice loading events. It is concluded that most of these ice loading events were reacted by geotechnical resistance mobilized from the caisson basal shear alone.’ The author fully agrees with this conclusion.

## REFERENCES

Altaee, A & Fellenius, BH (1994) ‘Modeling the Performance of the Molikpaq.’ CGJ 31, p649-660.

Hicks, MA & Smith, IM (1988) 'Class-A Prediction of Arctic Caisson Performance', *Geotechnique*, vol 38:4 p589-612.

Jeyatharan, K (1991). 'Partial Liquefaction of Sand Fill in a Mobile Arctic Caisson Under Ice Loading.' Cambridge University Doctoral Thesis.

K.J. Hewitt & Associates Ltd., August, 2009. 'Estimates of Ice Loads on the Molikpaq Based on Geotechnical Analyses and Responses.'

Sandwell Inc., 1991. 'Gulf Canada Resources Ltd., Extensometer Calibration for Ice Load Measurement.' Ref #112451, May, 1991.

